Strong Meson-Baryon Interactions

A soft-core model for low- and intermediate-energy π-nucleon and K^+-nucleon scattering

Strong Meson-Baryon Interactions

A soft-core model for low- and intermediate-energy π-nucleon and K^+-nucleon scattering

een wetenschappelijke proeve op het gebied
van de Natuurwetenschappen, Wiskunde en Informatica

Proefschrift

ter verkrijging van de graad van doctor
aan de Katholieke Universiteit Nijmegen
op gezag van de Rector Magnificus Prof. Dr. C. W. P. M. Blom,
volgens besluit van het College van Decanen
in het openbaar te verdedigen
op donderdag 12 februari 2004
des namiddags om 1.30 uur precies
door

Hendrik Polinder

geboren op 29 juli 1975 te Harderwijk

Promotor:	**Prof. Dr. R. H. P. Kleiss**
Co-promotor:	**Dr. Th. A. Rijken**
Manuscriptcommissie:	**Prof. Dr. S. J. de Jong** **Prof. Dr. R. G. E. Timmermans (KVI, Groningen)** **Prof. Dr. P. J. G. Mulders (VU, Amsterdam)**

ISBN 90-9017742-6

Graag wil ik iedereen bedanken die een bijdrage heeft geleverd aan de totstandkoming van dit proefschrift, hierbij wil ik twee personen bij naam noemen. In de eerste plaats ben ik Tom Rijken erkentelijk voor de zeer goede en prettige samenwerking tijdens het onderzoek en het schrijven van het proefschrift. Te allen tijde was hij bereid met groot enthousiasme zijn kennis met mij te delen.

En ten tweede wil ik Joyce heel hartelijk bedanken voor haar belangstelling voor mijn werkzaamheden van de afgelopen jaren, en voor haar voortdurende vertrouwen in mij.

Contents

Chapter 1

Introduction

The strong force acting between mesons and baryons, in particular the pion-nucleon, kaon-nucleon and antikaon-nucleon force, has been the subject of investigation for some decades, experimentally as well as theoretically. Experimentally the strong force can be studied by scattering a meson beam of a nuclear target and measuring the scattering observables, i.e. total cross sections (σ), differential cross sections ($d\sigma/d\Omega$), polarizations (P) etc..

The effect of the interaction on the asymptotic radial wave function is a phase shift with respect to the asymptotic radial wave function in absence of the interaction, for each partial wave. The empirical phase shifts are obtained from an analysis of the scattering observables, such an analysis judges the validity of all scattering data and gives a compact representation of these data. Although in principle an infinite number of phase shifts need to be determined from the data, the strong interaction is short-ranged and only the lower partial wave phase shifts will suffice. In constructing theoretical models for the strong interaction, it is much easier to use a phase shift analysis than the scattering observables themselves. A large number of scattering experiments have been performed to investigate the pion-nucleon interaction and the different pion-nucleon phase shift analyses give quite accurate and consistent results. The most recent pion-nucleon phase shift analysis has been performed by Arndt et al. [1], more information on the pion-nucleon scattering data base is found here.

However, the situation for the kaon-nucleon interaction is different from the pion-nucleon interaction. The kaon-nucleon scattering observables are known to less accuracy, especially at low energies, due to the relatively low flux of the kaon beams. Consequently, the different kaon-nucleon phase shift analyses do not give quite accurate and maybe not totally consistent results. This lack of empirical knowledge makes it more difficult to construct theoretical kaon-nucleon models. The most recent kaon-nucleon phase shift analysis has been performed by Hyslop et al. [2], here more information on the kaon-nucleon scattering data base can be found.

Recently there has been a revival of interest in the kaon-nucleon and antikaon-nucleon interaction. An exotic resonance in the isospin zero kaon-nucleon system has been observed last summer [3], this experiment, however, was not a simple scattering experiment and a resonance has never been seen in the present kaon-nucleon scattering data.

The construction of the *K-factory* at the Japan Proton Accelerator Research Complex (J-

PARC), a joint project of JAERI and KEK, is an interesting prospect. One of the major beams at this complex is a kaon beam, having a much higher intensity (ca. ten times) than the presently available kaon beams, for example at Brookhaven National Laboratory and KEK. In the near future more and accurate experimental data on the kaon-nucleon and antikaon-nucleon interaction will be obtained here. Other new scattering data could be delivered by the DAΦNE facility at Frascati [4], giving stronger constraints on kaon-nucleon models and hopefully a better understanding of the role of $SU_f(3)$ in meson-baryon interactions. Akaishi and Yamazaki [5] have done theoretical research on the possibility of nuclear anti-kaon bound states in nuclei in the framework of the Brueckner-Hartree-Fock theory using a phenomenological antikaon-nucleon model.

In view of these experimental and theoretical developments it would be desirable to have a realistic kaon-nucleon model at one's disposal.

The subject of this thesis is the construction of a dynamical model for the pion-nucleon and kaon-nucleon (K^+N) interactions. First a soft-core meson- and baryon-exchange model for the pion-nucleon interaction is derived, showing that the soft-core approach of the Nijmegen group is not only successful for baryon-baryon (NN and YN) interactions but also for meson-baryon interactions. The rich and accurate pion-nucleon scattering data base is used to determine the nonstrange coupling constants. Several other pion-nucleon models already exist and our soft-core pion-nucleon model, besides the value in its own right, mainly serves as a natural starting point for the construction of a soft-core kaon-nucleon model. This model is an $SU_f(3)$ extension of the soft-core pion-nucleon model, similar to the successful Nijmegen soft-core one-boson-exchange nucleon-nucleon and hyperon-nucleon models [6] and [7]. In this way several parameters in the kaon-nucleon model are determined by the pion-nucleon model.

The approach for the strong low- and intermediate-energy hadron-hadron interactions [8, 9, 10], used by the Nijmegen group, is schematically outlined in Figure 1.1. The starting point is the Standard Model, in which strong interactions occur between the six quarks and the gluons, and integrating out the heavier quarks to arrive at an effective Quantum Chromo Dynamics (QCD) for the light quarks (u,d,s) only. Generally accepted, the vacuum of QCD becomes unstable for momenta transfer $q^2 \leq \Lambda^2_{\chi SB} \simeq 1\text{GeV}^2$ and the chiral symmetry is broken spontaneously (χSB). The vacuum goes through a phase transition and generates constituent quark masses ($m_q \approx 300$ MeV) and reduces the strong coupling constant α_s. The pseudoscalar mesons are viewed as the Nambu-Goldstone bosons originating from the χSB, which makes it natural to assume the presence of a meson-cloud around the constituent quarks.

This provides a natural basis for an approach to the interaction between mesons and baryons using effective baryon-meson Lagrangians. At low- and intermediate-energies we do not consider a mixed phase of hadrons and quarks using the resonating-group method (RGM) [11, 12, 13, 14, 15], but restrict our selves to the hadronic phase only. Furthermore heavy baryons and mesons can be integrated out, using for example the renormalization method in the manner of Wilson [16], and an effective field theory, with meson and baryon masses with M$\leq$ 1.5 GeV, is used to construct a soft-core meson-baryon model for low- and intermediate-energy interactions.

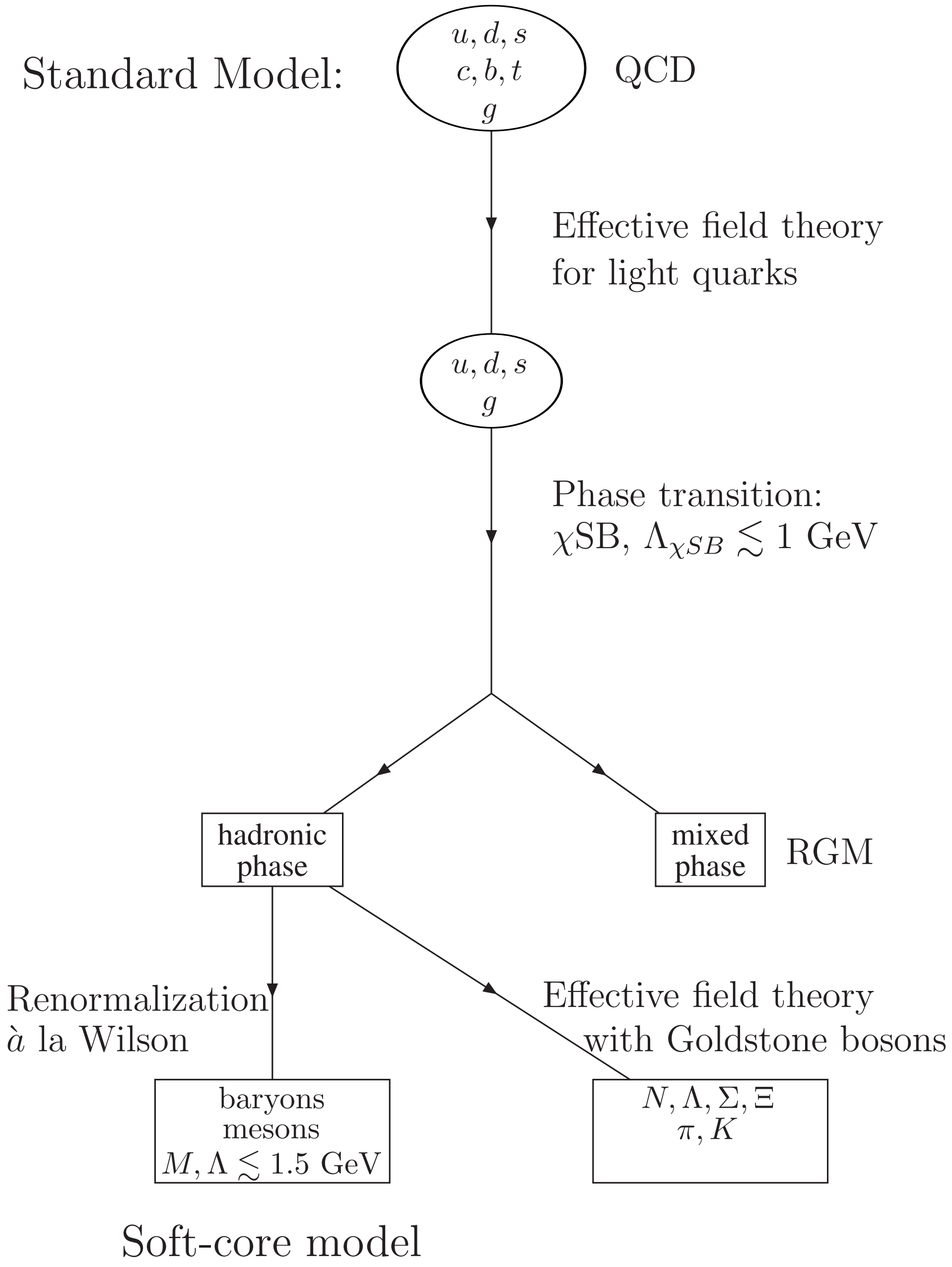

Figure 1.1: Overview of the theoretical basis for the soft-core meson-baryon interactions.

In the soft-core meson-baryon model the one-meson-exchange and one-baryon-exchange potentials are obtained from field theoretical Feynman diagrams in momentum space using effective interaction Hamiltonians, together with the meson-baryon Green function they constitute the kernel of the two-particle integral equation for the amplitude, which is a three-dimensional reduction of the fully covariant (four-dimensional) Bethe-Salpeter equation [17]. Form factors are introduced to take into account the extended size of the hadrons and to make the integral equation of the Fredholm type. The Coulomb interaction, playing a role at very low energies only and which is important in charge symmetry breaking (CSB) studies, will be neglected in this thesis. The integral equation for the amplitude is solved on the partial wave basis, in this way only one-dimensional integrals need to be performed to find the amplitude and the corresponding scattering observables or phase shifts for each partial wave.

The major differences between the existing pion-nucleon and kaon-nucleon models and the soft-core meson-baryon model presented in this thesis are briefly discussed below. Form factors of the Gaussian type are used in the soft-core approach in this thesis, while monopole type form factors and other form factors are used for the pion-nucleon model by Pascalutsa and Tjon [18] and the kaon-nucleon model by Hoffmann et al. [19]. The Roper resonance in the pion-nucleon system is, at least partially, considered as a three-quark state and treated in the same way as the nucleon and is included explicitly in the potential. However, we renormalize the Roper contribution at its pole, while Pascalutsa and Tjon [18] renormalize it at the nucleon pole.

An other difference is our treatment of the scalar meson σ, we consider it to belong to an $SU_f(3)$ nonet, while in all other models it is considered to effectively represent correlated two-pion exchange. Also we include Pomeron exchange, where the physical nature of the Pomeron can be seen in the light of QCD as a two-gluon exchange effect [20, 21], in order to comply with the soft-pion theorems for low-energy pion-nucleon scattering [22, 23].

Furthermore the exchange of tensor mesons is included in the soft-core meson-baryon model to find a good description of the kaon-nucleon scattering data, we use only one-particle exchanges to find this description while Hoffmann et al. [19] need to consider two-particle exchanges in their kaon-nucleon model.

The contents of this thesis are as follows. The definition of the field theoretical one-meson-exchange and one-baryon-exchange potentials in the context of a three-dimensional integral equation, a relativistic generalization of the Lippmann-Schwinger equation, is reviewed in Chapter 2. We introduce the usual potential forms in Pauli-spinor space, where we include the central (C) and the spin-orbit (SO) potentials, which are the only relevant potentials in case of spin-1 spin-$\frac{1}{2}$ interactions. And the relations between the relativistic and center-of-mass amplitudes are given.

The integral equation for the amplitude is solved on the partial wave basis in order to find the partial wave phase shifts, which are compared with the empirical phase shifts. Therefore we perform the basic partial wave projections, in particular those for the spinor invariants, in Chapter 3. And the relations between the partial wave amplitudes, the phase shifts and the scattering observables, σ, $d\sigma/d\Omega$ and P, for spin-1 spin$\frac{1}{2}$ scattering are given. The partial wave basis is chosen according to the convention of [24].

The effective baryon-baryon-meson and meson-meson-meson interaction Hamiltonians from which the one-meson-exchange and one-baryon-exchange Feynman diagrams are derived, are given in Chapter 4. The explicit expressions for the momentum space Feynman diagrams for scalar meson-, vector meson-, tensor meson- and baryon-exchanges as well as their partial wave projections are also listed in this chapter and the $SU_f(3)$ relations between the coupling constants used in the pion-nucleon and kaon-nucleon interactions are shown.

The pion-nucleon total cross section shows several resonances, the $\Delta(1232)$, Roper(1440), etc. in the considered energy range. These resonances are considered as, at least partially, genuine three-quark states and are therefore treated in the same way as the nucleon and explicitly included in our potential. The renormalization procedure we use to include the s-channel Feynman diagrams for the resonances in the pion-nucleon potential is described in Chapter 5.

An overview of the recent theoretical investigation of the pion-nucleon interaction is given in Chapter 6. Here also our soft-core pion-nucleon model is discussed and the results of the fit to the empirical phase shifts of the lower partial waves are presented.

The soft-core pion-nucleon model is, via $SU_f(3)$-symmetry, extended to the soft-core kaon-nucleon model in Chapter 7. Some other kaon-nucleon models are discussed and compared with our model. The results of the fit to the empirical phase shifts are given, since the different phase shift analyses are not always consistent, also the model calculation of some scattering observables is given. The soft-core kaon-nucleon model is used to give a theoretical estimate for the upper limit of the decay width of the recently discovered exotic resonance in the isospin zero kaon-nucleon system.

Finally the summary gives an overview of the research in this thesis and its main results. Also, some suggestions for improvement and extension of the present soft-core meson-baryon model are given. In the appendices added, details are given on the calculation of the partial wave matrix elements (Appendix A), the isospin factors for pion-nucleon and kaon-nucleon interactions (Appendix B), the one-particle exchange Feynman diagrams (Appendix C), the expansion coefficients, X, Y and Z, of the partial wave potentials in $x = \cos\theta$ for the different exchanges (Appendix D) and finally the Haftel-Tabakin method used to deal numerically with singularities in the Green function (Appendix E).

Chapter 2

The meson-baryon potential and amplitude

The field theoretical one-particle-exchange meson-baryon potentials in the context of a two-particle equation are defined in this chapter. We approximate the Bethe-Salpeter equation by assuming ”dynamical pair suppression”, hence neglecting the propagation of negative-energy states and by integrating out the time variable, we end up with a three-dimensional integral equation for the meson-baryon amplitude in the center of mass system. The relations between the center of mass and the relativistic amplitudes are given in the last section of this chapter.

2.1 Kinematics and relativistic amplitudes

In this thesis we consider the meson-baryon or more specific the pion-nucleon and kaon-nucleon reactions

$$P_i(q) + B_i(p,s) \rightarrow P_f(q') + B_f(p',s') \ , \tag{2.1}$$

where P stands for the pseudoscalar mesons, and B stands for the baryons. We will refer to P_i and P_f as particles 1 and 3 and to B_i and B_f as particles 2 and 4. The four momentum of particle i is $p_i = (E_i, \mathbf{p}_i)$ where $E_i = \sqrt{\mathbf{p}_i^2 + M_i^2}$ is the energy and M_i is the mass of particle i. In our convention the transition amplitude matrix M is related to the S-matrix via

$$\langle f|S|i\rangle = \langle f|i\rangle - i(2\pi)^4\delta^4(P_f - P_i)\langle f|M|i\rangle \ , \tag{2.2}$$

in this convention a negative potential corresponds with attraction and a positive potential with repulsion. Here $P_i = p+q$ and $P_f = p'+q'$ represent the total four momentum for the initial state $|i\rangle$ and the final state $|f\rangle$. The latter refer to the two-particle states, which we normalize in the following way, see e.g. [25, 26],

$$\langle \mathbf{p'}_1, \mathbf{p'}_2|\mathbf{p}_1, \mathbf{p}_2\rangle = (2\pi)^3 2E(\mathbf{p}_1)\delta^3(\mathbf{p}'_1 - \mathbf{p}_1)\cdot(2\pi)^3 2E(\mathbf{p}_2)\delta^3(\mathbf{p}'_2 - \mathbf{p}_2) \ . \tag{2.3}$$

With this normalization, the unpolarized differential cross section in the center of mass (CM) system is given by

$$\left(\frac{d\sigma}{d\Omega}\right)_{CM} = \frac{p_f}{p_i}\frac{1}{2}\sum\left|\frac{\langle f|M|i\rangle}{8\pi\sqrt{s}}\right|^2 \ , \tag{2.4}$$

where $\sum$ stands for the summation over the spin of the final baryon.

Since in this work, the scattering particles are always on the mass-shell, i.e. $p_i^2 = m_i^2$, parity conservation and Lorentz invariance implies that the matrix elements of the M-operator for meson-baryon interactions, which is a 4×4-matrix sandwiched between Dirac spinors, can be written in terms of two independent amplitudes

$$\langle f|M|i\rangle = \bar{u}_{B'}(\mathbf{p}', s_f)\left[A_{fi}(s,t,u) + \frac{1}{2}\left(\not{q}' + \not{q}\right) B_{fi}(s,t,u)\right] u_B(\mathbf{p}, s_i) \ , \tag{2.5}$$

where f and i stand for the two-particle channels $\pi N, KN, \pi Y, \eta Y$, and $\eta' Y$. In the Dirac spinors s_f, s_i are the magnetic spin variables, which will be specified later. The functions $A_{fi}(s,t,u)$ and $B_{fi}(s,t,u)$ are Lorentz scalars, and depend on the Mandelstam invariants

$$\begin{aligned} s &= (p+q)^2 = (p'+q')^2 \ , \\ t &= (q'-q)^2 = (p-p')^2 \ , \\ u &= (p-q')^2 = (p'-q)^2 \ , \end{aligned} \tag{2.6}$$

which satisfy the well-known (on-mass-shell) relation $s+t+u = \sum_{i=1}^{4} m_i^2$. The total and relative four-momenta (P_c and k_c) of the initial, final, and intermediate channel ($c = i, f, n$) are defined by

$$P_c = p_c + q_c \ , \ k_c = \mu_{c,2}\, p_c - \mu_{c,1}\, q_c \ , \tag{2.7}$$

where the weights are arbitrary besides the condition $\mu_{c,1} + \mu_{c,2} = 1$. For each channel the four-momenta of the baryons and pseudoscalar mesons (p_c and q_c) in terms of P_c and k_c are

$$p_c = \mu_{c,1} P_c + k_c \ , \ \ q_c = \mu_{c,2}\, P_c - k_c \ . \tag{2.8}$$

In this work we will use $\mu_{c,1} = \mu_{c,2} = \frac{1}{2}$. In the center-of-mass system (CM-system) we have for on-mass-shell momenta

$$\begin{aligned} p_c &= (E(\mathbf{p}_c), \mathbf{p}_c) \ , \quad q_c = (\mathcal{E}(\mathbf{p}_c), -\mathbf{p}_c) \ , \\ P_c &= (W_c, \mathbf{0}) \ , \qquad k_c = (\mu_2 E(\mathbf{p}_c) - \mu_1 \mathcal{E}(\mathbf{p}_c), \mathbf{p}_c) \ , \end{aligned} \tag{2.9}$$

where the total energy is $W_c = \sqrt{s} = E(\mathbf{p}_c) + \mathcal{E}(\mathbf{p}_c)$. Obviously the relative three-momentum is equal to the center-of-mass three-momentum of the baryon.

In general Feynman diagrams, in particular in the Green functions, the particles are off-mass-shell. In the following the three-momenta for the initial and the final states are denoted respectively by $\mathbf{q}_i$ and $\mathbf{q}_f$. Because of translation invariance $P_i = P_f$ and so $\sqrt{s} = W_i = W_f$. As introduced here, the total energies in the CM-system are $W_i = E(\mathbf{q}_i) + \mathcal{E}(\mathbf{q}_i)$, and $W_f = E(\mathbf{q}_f) + \mathcal{E}(\mathbf{q}_f)$.

Often it is convenient to express energies and momenta in terms of the Mandelstam variables. Useful relations for the baryon and meson energies and the the CM three-momentum squared are

$$E = \frac{s+M-\mu}{2\sqrt{s}} \ , \quad \mathcal{E} = \frac{s-M+\mu}{2\sqrt{s}} \ , \tag{2.10}$$

$$p^2 = \frac{1}{4s}\left[\left(s-M^2-\mu^2\right)^2-4M^2\mu^2\right], \tag{2.11}$$

where M denotes the baryon mass and μ denotes the meson mass. The CM scattering angle is given by

$$\cos(\theta) = \frac{1}{2pp'}\left[t+p^2+p'^2-\left(E-E'\right)^2\right], \tag{2.12}$$

and the laboratory kinetic energy of the meson beam is

$$T_{\rm lab} = \frac{s-(M+\mu)^2}{2M}. \tag{2.13}$$

2.2 Relativistic two-particle equations

The Bethe-Salpeter equation, a full two-particle relativistic scattering equation, for the M-amplitudes reads

$$\begin{aligned} M_{fi}(q_f,q_i;P) &= M^{irr}_{fi}(q_f,q_i;P)+\sum_n\int d^4k_n \\ &\times M^{irr}_{fn}(q_f,k_n;P)\; G(k_n;P)\; M_{ni}(k_n,q_i;P)\,, \end{aligned} \tag{2.14}$$

where the interaction kernel is denoted by M^{irr}, and G is the two-particle Green function. The contributions to the kernel M^{irr} come from the meson-baryon irreducible Feynman diagrams. The reducible diagrams are generated by the integral equation. In deriving Eq. (2.14) the integration over the momenta of the intermediate particles can be replaced by an integration over the total and relative momenta $\int\int d^4p_n d^4q_n \to \int\int d^4P_n d^4k_n$. Then, using the conservation of the total four-momentum, one can perform $\int d^4P_c$ and separate an overall $(2\pi)^4\delta^4(P_f-P_i)$ factor. The meson-baryon Green function is given in terms of the one-particle Green functions

$$G(k_n;P) = \frac{i}{(2\pi)^4}\left[\frac{1}{\gamma\left(\mu_{n,1}P+k\right)-M_n}\right]^{(a)}\left[\frac{1}{\left(\mu_{n,2}P-k\right)^2-m_n}\right]^{(b)}. \tag{2.15}$$

It is instructive to separate the positive and the negative energy components of the propagator. For that purpose, we rewrite the one-particle propagators as follows. For the spin-$\frac{1}{2}$ baryons the off-mass-shell propagator can be written in terms of the Dirac spinors as

$$\frac{\not p+M}{p^2-M^2+i\delta} = \frac{M}{E(\mathbf{p})}\left[\frac{\Lambda_+(\mathbf{p})}{p^0-E(\mathbf{p})+i\delta}-\frac{\Lambda_-(-\mathbf{p})}{p^0+E(\mathbf{p})-i\delta}\right], \tag{2.16}$$

where the projection operators $\Lambda_+(\mathbf{p})$ and $\Lambda_-(\mathbf{p})$ on the positive- and negative-energy states are [27]

$$\begin{aligned} 2M\Lambda_+(\mathbf{p}) &= \sum_s u(\mathbf{p},s)\otimes\bar u(\mathbf{p},s) = \not p+M\,, \\ 2M\Lambda_-(\mathbf{p}) &= -\sum_s v(\mathbf{p},s)\otimes\bar v(\mathbf{p},s) = -\not p+M\,, \end{aligned} \tag{2.17}$$

and $u(\mathbf{p},s)$ and $v(\mathbf{p},s)$ are the (on-mass-shell) Dirac spinors for spin-$\frac{1}{2}$ particles. For the meson propagator similar to Eq. (2.16) one has the identity

$$\frac{1}{q^2-m^2+i\delta} = \frac{1}{2\mathcal{E}(\mathbf{q})}\left[\frac{1}{q^0-\mathcal{E}(\mathbf{q})+i\delta} - \frac{1}{q^0+\mathcal{E}(\mathbf{q})-i\delta}\right] . \tag{2.18}$$

Then, in the CM-system, where $\mathbf{P}=0$ and $P_0=W$, the meson-baryon Green function can be written as

$$\begin{aligned} G(k_n;P) \;&=\; \frac{i}{(2\pi)^4}\left[\frac{M}{2E(\mathbf{k}_n)\mathcal{E}(\mathbf{k}_n)}\right] \\ &\times\left[\frac{\Lambda_+(\mathbf{k}_n)}{\mu_{n,1}W+k_n^0-E(\mathbf{k}_n)+i\delta} - \frac{\Lambda_-(-\mathbf{k}_n)}{\mu_{n,1}W+k_n^0+E(\mathbf{k}_n)-i\delta}\right] \\ &\times\left[\frac{1}{\mu_{n,2}W-k_n^0-\mathcal{E}(\mathbf{k}_n)+i\delta} - \frac{1}{\mu_{n,2}W-k_n^0+\mathcal{E}(\mathbf{k}_n)-i\delta}\right] . \end{aligned} \tag{2.19}$$

Multiplying out Eq. (2.19), writing the ensuing terms using an obvious short hand notation, the contribution of the different propagating components is displayed fully

$$\begin{aligned} G(k_n;P) \;&=\; G^{++}(k_n;W)+G^{+-}(k_n;W)+G^{-+}(k_n;W) \\ &\quad +G^{--}(k_n;W) , \end{aligned} \tag{2.20}$$

where the subscripts indicate the positive $(+)$ and negative $(-)$ energy single particle states. For example the first term in the Green function only connects positive energy states with each other. Considering similarly the amplitudes

$$M_{ij}^{\beta,\alpha} \;:\; M_{ij}^{++,++} ,\; M_{ij}^{++,+-} ,\; M_{ij}^{++,-+} ,\; M_{ij}^{++,--} , \tag{2.21}$$

where the subscripts i and j refer to the different two-particle channels, one obtains from Eqs. (2.14), (2.20) and (2.21), the full relativistic scattering equation

$$\begin{aligned} M_{fi}^{\beta,\alpha}(q_f,q_i;P) \;&=\; (M^{irr})_{fi}^{\beta,\alpha}(q_f,q_i;P)+\sum_n\int d^4k_n (M^{irr})_{fn}^{\beta,\gamma}(q_f,k_n;P) \\ &\quad \times G_n^{\gamma}(k_n;P)\; M_{ni}^{\gamma,\alpha}(k_n,q_i;P) . \end{aligned} \tag{2.22}$$

For the calculation of experimental data we need the scattering amplitude sandwiched between positive energy states. Written explicitly for $\alpha=++$ and $\beta=++$, Eq. (2.22) reads

$$\begin{aligned} & M_{f,i}^{++,++}(q_f,q_i;P) = (M^{irr})_{fi}^{++,++}(q_f,q_i;P)+\sum_n\int d^4k_n \\ & \times\Big\{(M^{irr})_{fn}^{++,++}(q_f,k_n;P)\; G_n^{++}(k_n;P)\; M_{ni}^{++,++}(k_n,q_i;P) \\ & \quad +(M^{irr})_{fn}^{++,+-}(q_f,k_n;P)\; G_n^{+-}(k_n;P)\; M_{ni}^{+-,++}(k_n,q_i;P) \\ & \quad +(M^{irr})_{fn}^{++,-+}(q_f,k_n;P)\; G_n^{-+}(k_n;P)\; M_{ni}^{-+,++}(k_n,q_i;P) \\ & \quad +(M^{irr})_{fn}^{++,--}(q_f,k_n;P)\; G_n^{--}(k_n;P)\; M_{ni}^{--,++}(k_n,q_i;P)\Big\} . \end{aligned} \tag{2.23}$$

Similar coupled equations hold for the other amplitudes. In all we have $2^4 = 16$ amplitudes, which are coupled as illustrated in Eq. (2.23).

The complexity of the previous equation can be reduced considerably if we assume "dynamical pair-suppression", i.e. if we neglect the contribution of negative energy states. Then the full scattering equation Eq. (2.23) reduces to the four-dimensional integral equation

$$
\begin{aligned}
& M_{fi}^{++,++}(q_f, q_i; P) = (M^{irr})_{fi}^{++,++}(q_f, q_i; P) + \sum_n \int d^4 k_n \\
& \times (M^{irr})_{fn}^{++,++}(q_f, k_n; P)\ G_n^{++}(k_n; P)\ M_{ni}^{++,++}(k_n, q_i; P)\ ,
\end{aligned} \tag{2.24}
$$

with the positive energy Green function

$$
\begin{aligned}
G^{++}(k_n; P) \quad = \quad & \frac{i}{(2\pi)^4}\left[\frac{M}{2E(\mathbf{k}_n)\mathcal{E}(\mathbf{k}_n)}\right]\frac{\Lambda_+(\mathbf{k}_n)}{\left[\mu_1 W + k_n^0 - E(\mathbf{k}_n) + i\delta\right]} \\
& \times \frac{1}{\left[\mu_2 W - k_n^0 - \mathcal{E}(\mathbf{k}_n) + i\delta\right]}\ .
\end{aligned} \tag{2.25}
$$

We note that this simplification in principle brings about a hopefully tolerable breach of relativistic invariance. On the other hand in Feynman diagrams particles go off-mass-shell, and the off-mass-shell behavior is not really known for mesons and baryons, certainly not if a truncated kernel is used, which is always the case. Then it might be better to allow positive energy states only.

2.3 Three-dimensional two-particle equations

Three-dimensional integral equations for the amplitudes can be derived in various ways. The methods assume 2-particle unitarity as a basic ingredient. The derivation for the meson-baryon systems follows the same procedure as that for the baryon-baryon channels. For the latter see e.g. references [28, 29, 30, 31, 32, 33, 34]. In [35] the derivation is based entirely on two-particle unitarity and the analyticity properties of the amplitudes, using the N/D-formalism. In the latter approach the in essence Regge pole nature of meson-exchange can be apprehended most easily.

2.3.1 On-mass-shell approximation

The simplest way to reduce the four-dimensional integral equation, Eq. (2.23), to a three-dimensional one is to put the intermediate particles on the mass-shell, i.e. $p_n^0 = E(\mathbf{k}_n) = \sqrt{\mathbf{k}_n^2 + M_n^2}$, $q_n^0 = \mathcal{E}(\mathbf{k}_n) = \sqrt{\mathbf{k}_n^2 + m_n^2}$. It can readily be shown from Eq. (2.8) that the zero components of the relative and total momenta k_n and P_n are given by

$$
\begin{aligned}
k_n^0 &= \mu_{n,2} E(\mathbf{k}_n) - \mu_{n,1}\mathcal{E}(\mathbf{k}_n)\ , \\
P_n^0 &= E(\mathbf{k}_n) + \mathcal{E}(\mathbf{k}_n)\ .
\end{aligned} \tag{2.26}
$$

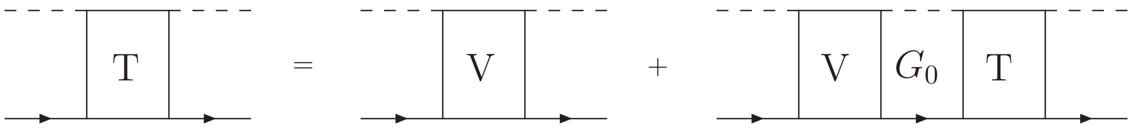

Figure 2.1: Diagrammatic representation of the meson-baryon scattering equation Eq. (2.29). The solid line denotes the baryon and the dashed line denotes the meson.

If we neglect the k_n^0-dependence of the amplitudes, and evaluate them at the value given by Eq. (2.26), the dependence of the four-dimensional equation on k_n^0 only occurs in the Green function, and the k_n^0-integration of the Green function can be done. We can define the k_n^0-independent amplitudes

$$\begin{aligned} M_{ni}(\mathbf{k}_n, \mathbf{q}_i; W) &= M_{ni}(\tilde{k}_n, q_i; P) , \\ W_{fn}(\mathbf{q}_f, \mathbf{k}_n; W) &= M_{fn}^{irr}(q_f, \tilde{k}_n; P) , \end{aligned} \tag{2.27}$$

where $\tilde{k}_n^0 = \mu_{n,2}E(\mathbf{k}_n) - \mu_{n,1}\mathcal{E}(\mathbf{k}_n)$. Now, the k_n^0-integration in Eq. (2.23) can be carried through, this leads to

$$\int_{-\infty}^{\infty} dk_{n0}\, G_n^{++}(k_n; P) = \frac{1}{(2\pi)^3} \frac{2M\Lambda_+(\mathbf{k}_n)}{4E_n(\mathbf{k}_n)\mathcal{E}_n(\mathbf{k}_n)} \cdot \frac{1}{W - E(\mathbf{k}_n) - \mathcal{E}(\mathbf{k}_n) + i\delta} . \tag{2.28}$$

The four-dimensional integral equation, Eq. (2.24), now results in the three-dimensional integral equation for the amplitudes sandwiched between Dirac spinors, which is also derived in [34],

$$\begin{aligned} T_{fi}(\mathbf{q}_f, \mathbf{q}_i; W) &= V_{fi}(\mathbf{q}_f, \mathbf{q}_i; W) + \sum_n \int \frac{d^3k_n}{(2\pi)^3} V_{fn}(\mathbf{q}_f, \mathbf{k}_n; W) \\ &\quad \times G_0(\mathbf{k}_n, W) T_{ni}(\mathbf{k}_n, \mathbf{q}_i; W) , \end{aligned} \tag{2.29}$$

where the T-matrix, the potential and the Green function are defined by

$$\begin{aligned} T_{fi}(\mathbf{q}_f, \mathbf{q}_i; W) &= \bar{u}(\mathbf{q}_f) M_{fi}(\mathbf{q}_f, \mathbf{q}_i; W) u(\mathbf{q}_i) , \\ V_{fi}(\mathbf{q}_f, \mathbf{q}_i; W) &= \bar{u}(\mathbf{q}_f)\, W_{fi}(\mathbf{q}_f, \mathbf{q}_i; W) u(\mathbf{q}_i) , \\ G_0(\mathbf{k}_n; W) &= \frac{1}{4E(\mathbf{k}_n)\mathcal{E}(\mathbf{k}_n)} [W - (E(\mathbf{k}_n) + \mathcal{E}(\mathbf{k}_n)) + i\delta]^{-1} , \end{aligned} \tag{2.30}$$

with the total energy in the CM system $W = E(\mathbf{q}) + \mathcal{E}(\mathbf{q})$. The integral equation for the T-matrix, Eq. (2.29), is schematically given in Figure 2.1.

We remark that the three-dimensional integral equation for the amplitude, Eq. (2.29), is here obtained as an approximation of the Bethe-Salpeter equation, but in the formulation of Quantum Field Theory (QFT) as developed by Kadyshevski [36, 37, 38, 39] this integral equation is obtained without making any approximation. In this formulation of QFT all particles, in particular the intermediate particles, are always on the mass-shell in contrast to the formalism of Feynman. Hence a covariant form of pair-suppression can be introduced phenomenologically.

Until this section the intermediate particles were in principle off mass-shell and the total four momentum was conserved. Now we have put the intermediate particles on mass-shell, but now in principle they are off energy-shell, which means that $\sqrt{s} \neq E(\mathbf{k}_n) + \mathcal{E}(\mathbf{k}_n)$. And the total four momentum in not conserved, but the total three momentum is conserved.

Note that if the intermediate state is on energy-shell, i.e. $W = E(\mathbf{k}_n) + \mathcal{E}(\mathbf{k}_n)$, the two poles of the Green function, Eq. (2.25), coincide. The value of k_n^0 at which this "pinching" occurs is given by the on mass-shell value, Eq. (2.26),

$$k_n^0 = \mu_{n,2} E(\mathbf{k}_n) - \mu_{n,1} \mathcal{E}(\mathbf{k}_n) \pm i\delta \ . \tag{2.31}$$

The contribution to the integral around this value of k_n^0 will be dominant, due to the pinching of the poles. This is the rationale for the "*on-mass-shell approximation*".

2.3.2 Potentials for the 3-d integral equation

In order to calculate cross sections or phase shifts we need to solve Eq. (2.29), which is a complex integral equation for the T-matrix, even for physical momenta. It is possible to transform Eq. (2.29) into a Lippmann-Schwinger equation (which can be Fourier-transformed into coordinate space) as will be seen in the next section. However we do our calculations always in momentum space, so we do not need to solve the Lippmann-Schwinger equation but we will always solve Eq. (2.29).

In the OBEP-approximation only second-order irreducible Feynman diagrams contributing to the kernel *i.e.* $W = M^{\mathrm{irr}(2)}$ are included. Which we employ here.

Using rotational invariance and parity conservation we expand the T-matrix, which is a 2×2-matrix in Pauli-spinor space, into a complete set of Pauli-spinor invariants. Introducing the momentum vectors

$$\mathbf{q} = \frac{1}{2}(\mathbf{q}_f + \mathbf{q}_i) \ , \qquad \mathbf{k} = \mathbf{q}_f - \mathbf{q}_i \ , \qquad \hat{\mathbf{n}} = \hat{\mathbf{q}}_i \times \hat{\mathbf{q}}_f = \frac{\mathbf{q}\times\mathbf{k}}{|\mathbf{q}\times\mathbf{k}|} \ , \tag{2.32}$$

where $\mathbf{q}_f$ and $\mathbf{q}_i$ are the final and initial CM-three-momenta respectively, there are only two independent spinor invariants P_α, rotational invariant and invariant under parity transformations. We choose for the operators P_α in spin-space

$$P_1 = 1 \ \ , \ \ P_2 = \boldsymbol{\sigma}\cdot\mathbf{q}_i \times \mathbf{q}_f \ , \tag{2.33}$$

corresponding to the central and spin-orbit piece of the amplitude, now the expansion of the T-matrix in spinor invariants reads

$$\begin{aligned} T &= \sum_1^2 T_\alpha(\mathbf{q}_f^2, \mathbf{q}_i^2, \mathbf{q}_f\cdot\mathbf{q}_i)\ P_\alpha \\ &= f(\mathbf{q}_f,\mathbf{q}_i) + i\ g(\mathbf{q}_f,\mathbf{q}_i)\ \left(\boldsymbol{\sigma}\cdot\hat{\mathbf{n}}\right) \ . \end{aligned} \tag{2.34}$$

For the partial wave projection we found it convenient to rewrite the T-matrix in terms of the amplitudes F and G

$$T = F\left(\mathbf{q}_f, \mathbf{q}_i\right) + (\boldsymbol{\sigma}\cdot\hat{\mathbf{q}}_f)\; G\left(\mathbf{q}_f, \mathbf{q}_i\right)\; (\boldsymbol{\sigma}\cdot\hat{\mathbf{q}}_i)\ . \tag{2.35}$$

The relation between the "spin-nonflip" and "spin-flip" amplitudes f, g and the amplitudes F, G is readily found to be

$$F = f + (\hat{\mathbf{q}}_f\cdot\hat{\mathbf{q}}_i)\; g\ \ ,\ \ G = -g\ . \tag{2.36}$$

The connection between the non-relativistic amplitudes F and G defined in Eq. (2.35) and the relativistic amplitudes A and B defined in Eq. (2.5) can be obtained in a straightforward way using the explicit representation of the Dirac spinors, as will be shown in Section 2.4. Similar to Eq. (2.34) we expand the potentials V. We neglect the dependence of the potentials on $\mathbf{k}\cdot\mathbf{q}$. Then, the expansion in Eq. (2.34) applies also to the potentials, i.e.

$$\begin{aligned} V &= \sum_1^2 V_\alpha(\mathbf{q}_f^2, \mathbf{q}_i^2, \mathbf{q}_f\cdot\mathbf{q}_i)\; P_\alpha \\ &= V_C(\mathbf{q}_f, \mathbf{q}_i) + i\; V_{SO}(\mathbf{q}_f, \mathbf{q}_i)\; (\boldsymbol{\sigma}\cdot\mathbf{n})\ . \end{aligned} \tag{2.37}$$

2.3.3 Lippmann-Schwinger equation

In order to arrive at a Lippmann-Schwinger equation, one chooses a new Green function $g(\mathbf{k}; s)$ which satisfies a dispersion relation in $\mathbf{p}^2(s)$ rather than in s [28]. Then one obtains

$$g(\mathbf{k}_n; s) = \frac{-1}{2[E(\mathbf{k}_n) + \mathcal{E}(\mathbf{k}_n)]}(\mathbf{k}_n^2 - \mathbf{q}_n^2 - i\delta)^{-1}\ , \tag{2.38}$$

where $\mathbf{q}_n$ is the on-energy-shell momentum. This Green function is then used in the integral equation Eq. (2.29) instead of the Green function $G_0(\mathbf{k}_n; s)$. So the corrections to $\langle f|W|i\rangle$ due to the transformation of the Green functions are neglected here, they are of higher order in the couplings and are usually discarded in an OBE-approach. With the substitution of g for G_0, Eq. (2.28) becomes identical to Eq. (2.19) of [28]. From now on we follow Section II of [28] in detail, the transformation to the non-relativistic normalization of the two-particle states leads to states with

$$(\mathbf{p}_1', s_1'; \mathbf{p}_2', s_2'|\mathbf{p}_1, s_1; \mathbf{p}_2, s_2) = (2\pi)^6\delta^3(\mathbf{p}_1' - \mathbf{p}_1)\delta^3(\mathbf{p}_2' - \mathbf{p}_2)\delta_{s_1', s_1}\delta_{s_2', s_1}\ . \tag{2.39}$$

For these states we define the non-relativistic $\mathcal{T}$-matrix by

$$\begin{aligned} (f|\mathcal{T}|i) &= \{4\mu_{34}(E_3 + E_4)\}^{-\frac{1}{2}}\langle f|M|i\rangle\{4\mu_{12}(E_1 + E_2)\}^{-\frac{1}{2}} \\ &\equiv N_f(\mathbf{q}_f)\; \langle f|M|i\rangle\; N_i(\mathbf{q}_i)\ , \end{aligned} \tag{2.40}$$

where μ_{12} and μ_{34} are the reduced masses for respectively the initial and final state. Then we get from Eq. (2.29) the Lippmann-Schwinger equation

$$\begin{aligned} &(3,4|\mathcal{T}|1,2) = (3,4|\mathcal{V}|1,2) + \\ &\quad + \sum_n \int \frac{d^3k_n}{(2\pi)^3}(3,4|\mathcal{V}|n_1, n_2)\frac{2\mu_{n_1,n_2}}{\mathbf{q}_n^2 - \mathbf{k}_n^2 + i\delta}(n_1, n_2|\mathcal{T}|1,2)\ , \end{aligned} \tag{2.41}$$

where analogously to the $\mathcal{T}$-matrix, Eq. (2.40), the potential $\mathcal{V}$ is defined as

$$\begin{aligned}(f|\mathcal{V}|i) &= \{4\mu_{34}(E_3+E_4)\}^{-\frac{1}{2}}\langle f|W|i\rangle\{4\mu_{12}(E_1+E_2)\}^{-\frac{1}{2}} \\ &\equiv N_f(\mathbf{q}_f)\,\langle f|W|i\rangle\,N_i(\mathbf{q}_i)\,. \end{aligned} \tag{2.42}$$

If in the low-energy approximation, the energies are expanded in terms of the momenta squared, the Lippmann-Schwinger equation in momentum space can in principle be Fourier-transformed into the equivalent Schrödinger equation in configuration space. However our calculations are always in momentum space, so we always solve Eq. (2.29).

2.4 Relation between relativistic- and CM-amplitudes

The relation between the relativistic amplitudes A and B and the non-relativistic amplitudes F and G is found making use of the representation of the Dirac spinors [27]. Since in the three-dimensional integral equation, Eq. (2.29), off-energy shell amplitudes appear, we now distinguish between the CM-energies of the final and initial states, defined by

$$W_f^2 \equiv s_f = (p'+q')^2\ \ ,\ \ W_i^2 \equiv s_i = (p+q)^2\,. \tag{2.43}$$

Then, a straightforward calculation of the operators 1 and $\not{Q}$ between Dirac spinors gives the corresponding operators between Pauli spinors.

$$\begin{aligned}\bar{u}(\mathbf{p}',s')\,u(\mathbf{p},s) &= \sqrt{(E'+M')(E+M)}\,\chi'^{\,\dagger}\left\{1-\frac{\boldsymbol{\sigma}\cdot\mathbf{p}'\,\boldsymbol{\sigma}\cdot\mathbf{p}}{(E'+M')(E+M)}\right\}\chi\,, \\ \bar{u}(\mathbf{p}',s')\,\not{Q}\,u(\mathbf{p},s) &= \sqrt{(E'+M')(E+M)}\,\chi'^{\,\dagger}\left\{\frac{1}{2}\left[(W'-M')+(W-M)\right]\right. \\ &\left. +\frac{1}{2}\left[(W'+M')+(W+M)\right]\,\frac{\boldsymbol{\sigma}\cdot\mathbf{p}'\,\boldsymbol{\sigma}\cdot\mathbf{p}}{(E'+M')(E+M)}\right\}\chi\,, \end{aligned} \tag{2.44}$$

with

$$Q^\mu = \frac{1}{2}\,(q'+q)^\mu\ . \tag{2.45}$$

In Eq. (2.44) we used the shorthand notations $E' = E(\mathbf{p}')$ etc. for the baryon variables. The meson variables were eliminated using $q^0 = W-E$ etc. From the expressions in Eqs. (2.44), (2.5) and (2.35) we immediately obtain the relations between the amplitudes F, G and A,B

$$\begin{aligned}F(\mathbf{p}',\mathbf{p}) &= \sqrt{(E'+M')(E+M)}\,\left\{A(s,t,u)+\right. \\ &\left.\frac{1}{2}\left[(W'-M')+(W-M)\right]\,B(s,t,u)\right\}\,, \\ G(\mathbf{p}',\mathbf{p}) &= \sqrt{(E'-M')(E-M)}\,\left\{-A(s,t,u)+\right. \\ &\left.\frac{1}{2}\left[(W'+M')+(W+M)\right]\,B(s,t,u)\right\}\,. \end{aligned} \tag{2.46}$$

Chapter 3

The partial wave equation

The meson-baryon model is fitted to the partial wave analyses of the pion-nucleon and kaon-nucleon scattering data, for this purpose the integral equation for the meson-baryon amplitude must be solved on the partial wave basis. This chapter deals with the transformation of the integral equation on the plane wave basis to the integral equation on the partial wave (LSJ) basis. From the unitarity of the scattering matrix, the relation between the partial wave amplitude and the partial wave phase shifts is derived.

3.1 Partial wave analysis

[1] The states for the meson-baryon system are characterized by J, L, where J is the total angular momentum and L the orbital angular momentum. The latter, for fixed J-value, can assume the values $L = J \mp \frac{1}{2}$, since the spin of the baryons is $S = \frac{1}{2}$. Distinguishing between the partial waves with parity $P = (-)^{J-1/2}$ and $P = (-)^{J+1/2}$, using rotational invariance, we can write the potential matrix elements on the LSJ-basis in the following way

(i) $P = (-)^{J-1/2}, L_+ = J - 1/2$:

$$(q_f; L'J'M'|\ V\ |q_i; LJM) = 4\pi\ V^{J,L_+}(L', L)\delta_{J'J}\ \delta_{M'M}\ \delta_{L'L}\ , \tag{3.1}$$

(ii) $P = (-)^{J+1/2}, L_- = J + 1/2$:

$$(q_f; L'J'M'|\ V\ |q_i; LJM) = 4\pi\ V^{J,L_-}(L', L)\delta_{J'J}\ \delta_{M'M}\ \delta_{L'L}\ . \tag{3.2}$$

Because of parity conservation in strong interactions, the $L_+ = J - 1/2$ and the $L_- = J + 1/2$ waves obviously are decoupled. So mixing between states with different angular momentum never occurs.

The spherical wave functions in momentum space with quantum numbers $J, M, L, S = 1/2$ are

$$\mathcal{Y}^M_{J,L}(\hat{p}, s) = \big(\hat{p}, s|JM; L\ 1/2\big) = \sum_{m,\mu} C^{L\ 1/2\ J}_{m\ \mu\ M}\ Y^L_m(\hat{p})\ \chi^{(1/2)}_\mu(s)\ , \tag{3.3}$$

[1] In this chapter we use the non-relativistic normalization Eq. (2.39) of the one-particle states.

where s is a spin variable for the baryons. For example, s denotes the helicity of the baryon, or the projection of the spin along the normal $\hat{\mathbf{n}}$ to the scattering plane, or the projection of the spin along the z-axis. The latter spin variable we will use in this thesis. Then, in Eq. (3.3) we have $\chi_\mu^{(1/2)}(s) = \delta_{s,\mu}$. The central and non-central potential matrix elements on the LSJ-basis are derived in detail in Appendix A.1, the results are

1. *Central* $P_1 = 1$:

$$\left(q_f; L'J'M'|F(\mathbf{q}_f,\mathbf{q}_i)|q_i; LJM\right) = \sum_{s_f,s_i} \int \frac{d^3q'_f}{(2\pi)^3} \int \frac{d^3q'_i}{(2\pi)^3} \left(q_f; L'J'M'|\mathbf{q}'_f, s_f\right)$$
$$\times \left(\mathbf{q}'_f, s_f|F_{op}|\mathbf{q}'_i, s_i\right) \left(\mathbf{q}'_i, s_i|q_i, LJM\right) = 4\pi\, F_L\left(q_f, q_i\right)\, \delta_{L'L}\delta_{J',J}\, \delta_{M',M}\ , \tag{3.4}$$

2. *Non-central* $P'_2 = (\boldsymbol{\sigma}\cdot\hat{\mathbf{q}}_f)(\boldsymbol{\sigma}\cdot\hat{\mathbf{q}}_i)$:

$$\left(q_f; L'J'M'|G(\mathbf{q}_f,\mathbf{q}_i)|q_i; LJM\right) = \sum_{s_f,s_i} \int \frac{d^3q'_f}{(2\pi)^3} \int \frac{d^3q'_i}{(2\pi)^3} \left(q'_f; L'J'M'|\mathbf{q}_f, s_f\right)$$
$$\times \left(\mathbf{q}'_f, s_f|G_{op}|\mathbf{q}'_i, s_i\right) \left(\mathbf{q}'_i, s_i|q_i, LJM\right) = 4\pi \sum_{L'} a_{L_f,L'} G_{L'}\left(q_f, q_i\right)\, a_{L',L_i}$$
$$\times \delta_{J',J}\delta_{M',M}\ , \tag{3.5}$$

where the partial wave projections F_L and G_L as well as the matrix $a_{L',L}$ are defined in Appendix A. The partial wave potentials V^{J,L_+} and V^{J,L_-} in Eqs. (3.1) and (3.2) can be expressed in terms of the partial wave expansions of F and G. For this purpose we write the results of Eqs. (3.4) and (3.5) in matrix form in $L = (J \pm 1/2)$-space, as expected from parity conservation, we find the diagonal matrix

$$\begin{pmatrix} V^{J,L_+} & 0 \\ 0 & V^{J,L_-} \end{pmatrix} = \begin{pmatrix} F_{J-1/2} + G_{J+1/2} & 0 \\ 0 & F_{J+1/2} + G_{J-1/2} \end{pmatrix}, \tag{3.6}$$

which is equivalent to the compact expression

$$V^{J,L_\pm} = F_{L_\pm} + G_{L_\pm \pm 1}\ . \tag{3.7}$$

The partial wave potentials can also be expressed in terms of the partial wave projections of the central and spin-orbit potential. The relation between F and G and the central and spin-orbit potentials is given by Eq. (2.36),

$$F = V^C + \cos\theta\, V^{SO}\ ,\ G = -V^{SO}\ . \tag{3.8}$$

Knowing from Appendix A.1 that the partial wave projections of F and G are given by

$$\begin{aligned} F_L(q_f, q_i) &= \frac{1}{2}\int_{-1}^{1} d\cos\theta\, F(\mathbf{q}_f,\mathbf{q}_i) P_L(\cos\theta)\ , \\ G_L(q_f, q_i) &= \frac{1}{2}\int_{-1}^{1} d\cos\theta\, G(\mathbf{q}_f,\mathbf{q}_i) P_L(\cos\theta)\ , \end{aligned} \tag{3.9}$$

we find the partial wave potentials in terms of the partial wave projections of the central and spin-orbit potentials

$$\begin{aligned} L_+ = 0 \ : \quad & V^{J,L_+} = V^C_{L_+} \ , \\ L_\pm \geq 1 \ : \quad & V^{J,L_\pm} = V^C_{L_\pm} + \frac{L_\pm + 1}{2L_\pm + 1} V^{SO}_{L_\pm+1} + \frac{L_\pm}{2L_\pm + 1} V^{SO}_{L_\pm-1} - V^{SO}_{L_\pm \pm 1} \ . \end{aligned} \tag{3.10}$$

3.2 Partial wave integral equations and the unitarity relations

3.2.1 Partial wave integral equations

The integral equation Eq. (2.29) we write first explicitly in terms of the plane wave states

$$\begin{aligned} \big(\mathbf{q}_f, s_f|T(\sqrt{s})|\mathbf{q}_i, s_i\big) \ &= \ \big(\mathbf{q}_f, s_f|V|\mathbf{q}_i, s\big) + \sum_n \int \frac{d^3k_n}{(2\pi)^3} \big(\mathbf{q}_f, s_f|V|\mathbf{k}_n, s_n\big) \\ & \times\ G_0(\mathbf{k}_n, \sqrt{s})\, \big(\mathbf{k}_n, s_n|T(\sqrt{s})|\mathbf{q}_i, s_i\big) \ , \end{aligned} \tag{3.11}$$

where, apart from spin-space, the amplitude T, the Green function G_0 and the potential V are matrices in the two-particle channel space. The partial wave T-matrix defined by

$$T_{J,L}(q_f, q_i) = \langle q_f, L_f; JM|T(\sqrt{s})|q_i, L_i; JM\rangle \ , \ \text{ with } L = L_i = L_f \ , \tag{3.12}$$

which is independent of $J_z = M$ due to rotation invariance, is related to the T-matrix on the plane wave basis by

$$\begin{aligned} T_{J,L}(q_f, q_i) \ &= \ \sum_{s_f, s_i} \int \frac{d^3q'_f}{(2\pi)^3} \int \frac{d^3q'_i}{(2\pi)^3} \langle q_f, L; JM|\mathbf{q}'_f, s_f\rangle \\ & \times \langle \mathbf{q'}_f, s_f|T(\sqrt{s})|\mathbf{q'}_i, s_i\rangle\ \langle \mathbf{q}'_i, s_i|q_i, L; JM\rangle \ . \end{aligned} \tag{3.13}$$

Now, using the completeness relation for the spherical wave functions $\mathcal{Y}^M_{LJ}(\hat{p}, s)$, defined by Eq. (3.3),

$$\sum_{L,J,M} \mathcal{Y}^M_{LJ}(\hat{\mathbf{q}}_f, s_f) \mathcal{Y}^{M\,*}_{LJ}(\hat{\mathbf{q}}_i, s_i) = \delta(\hat{\mathbf{q}}_f - \hat{\mathbf{q}}_i)\ \delta_{s_f, s_i} \ , \tag{3.14}$$

the completeness relation for the $|q, L; JM\rangle$-states reads

$$\sum_{L,J,M} \int_0^\infty \frac{q^2 dq}{(2\pi)^3}\ |q, L; JM)\ (q, L; JM| = 1 \ . \tag{3.15}$$

It is straightforward to derive that

$$\begin{aligned} & \sum_{s_n} \int \frac{d^3k_n}{(2\pi)^3}\ |\mathbf{k}_n, s_n\rangle\ G_0(k_n, \sqrt{s})\ \langle \mathbf{k}_n, s_n| = \\ & = \sum_{L,J,M} \int_0^\infty \frac{k_n^2 dk_n}{(2\pi)^3}\ |k_n, L; JM)\, G_0(k_n, \sqrt{s})\ (k_n, L; JM| \ , \end{aligned} \tag{3.16}$$

due to the fact that the Green function is diagonal in the spins and invariant under rotations, i.e. also diagonal in L and J. Using these results, the integral equation for the partial wave amplitude follows, i.e.

$$T_{J,L}(q_f,q_i;\sqrt{s}) = V_{J,L}(q_f,q_i;\sqrt{s}) + \sum_n \int_0^\infty \frac{k_n^2 dk_n}{(2\pi)^3} V_{J,L}(q_f,q_n;\sqrt{s})\; G_0(\mathbf{k}_n,\sqrt{s}) T_{J,L}(q_n,q_i;\sqrt{s}) \;. \tag{3.17}$$

3.2.2 Partial wave unitarity relations, phase shifts

From the unitarity of the S-matrix, $S^\dagger\; S = 1$, the M-matrix in Eq. (2.2) satisfies the condition

$$2\Im\langle f|M|i\rangle \;=\; -(2\pi)^4 \sum_n \delta^4(q_f - k_n)\; \langle f|M^\dagger|n\rangle\langle n|M|i\rangle \;. \tag{3.18}$$

In deriving Eq. (3.18) one factors out a $\delta^4(q_f - q_i)$, so that $q_f = k_n = q_i$, where $q_i = (E_i, \mathbf{q}_i)$ etc., is always understood. The previous equation for the CM-amplitudes can be written more explicitly, see for example Eq. (II.1.14) of [34], as

$$\begin{aligned} 2\Im\left(\mathbf{q}_f, s_f|M|\mathbf{q}_i, s_i\right) \;&=\; -i\left(\mathbf{q}_f, s_f|M - M^\dagger|\mathbf{q}_i, s_i\right) \\ &=\; -\frac{1}{(2\pi)^2}\sum_n \int \frac{d^3k_n}{4E(\mathbf{k}_n)\mathcal{E}(\mathbf{k}_n)} \left(\mathbf{q}_f, s_f|M^\dagger|\mathbf{k}_n, s_n\right) \\ &\quad \times \delta(\sqrt{s} - E(\mathbf{k}_n) - \mathcal{E}(\mathbf{k}_n))\left(\mathbf{k}_n, s_n|M|\mathbf{q}_i, s_i\right) \;, \end{aligned} \tag{3.19}$$

where the summation $\sum_n$ is over all intermediate two-particle channels coupled to the initial and final state. Here, s_i, s_f, and s_n are the spin labels for the initial, final, and intermediate states. The momentum of the intermediate state k_n is such that $E(\mathbf{k}_n) + \mathcal{E}(\mathbf{k}_n) = \sqrt{s}$. The partial wave amplitudes then satisfy the relation

$$\begin{aligned} 2\Im M_{L,J}(q_f,q_i) = \left(q_f, L; JM|M - M^\dagger|q_i, L; JM\right) = \sum_{s_f,s_i} \int \frac{d^3q'_f}{(2\pi)^3} \int \frac{d^3q'_i}{(2\pi)^3} \\ \times \left(q_f, L; JM|\mathbf{q}'_f, s_f\right)\left(\mathbf{q}'_f, s_f|M - M^\dagger|\mathbf{q}'_i, s_i\right)\left(\mathbf{q}'_i, s_i|q_i, L; JM\right) \;. \end{aligned}$$

Inserting Eq. (3.19) and doing the momentum integrations gives

$$\begin{aligned} 2\Im M_{L,J}(q_f,q_i) \;&=\; -\frac{1}{(2\pi)^2}\sum_n \int d^3k_n \frac{1}{4E(\mathbf{k}_n)\mathcal{E}(\mathbf{k}_n)}\left(q_f, L; JM|M^\dagger|\mathbf{k}_n, s_n\right) \\ &\quad \times\delta(\sqrt{s} - E(\mathbf{k}_n) - \mathcal{E}(\mathbf{k}_n))\,(\mathbf{k}_n, s_n|M|q_i, L; JM) \\ &=\; -\frac{1}{(2\pi)^2}\sum_n \int \frac{dk_n k_n^2}{4E(\mathbf{k}_n)\mathcal{E}(\mathbf{k}_n)} \sum_{L',J',M'} \\ &\quad \times\left(q_f, L; JM|M^\dagger|k_n, L'; J'M'\right)\frac{E(\mathbf{q}_n)\mathcal{E}(\mathbf{q}_n)}{q_n\sqrt{s}}\delta(k_n - q_n) \\ &\quad \times\left(k_n, L'; J'M'|M|q_i, L; JM\right), \end{aligned} \tag{3.20}$$

in the last line we used Eq. (3.16), and q_n is the on energy-shell momentum of the intermediate state. Finally performing the integral and knowing that L, J, M are conserved we find the unitarity relation for the partial wave amplitude

$$\begin{aligned} 2\Im M_{L,J}(q_f, q_i) &= -\sum_n \frac{q_n}{16\pi^2\sqrt{s}} \left(q_f, L; JM|M^\dagger|k_n, L; JM\right) \\ &\quad \times (k_n, L; JM|M|q_i, L; JM) \ . \end{aligned} \tag{3.21}$$

Introducing the partial wave amplitudes $F_{L,J}$ by the definition

$$M_{L,J}(\sqrt{s}) = -32\pi^2\sqrt{s}\ F_{L,J}(\sqrt{s}) \ , \tag{3.22}$$

we find the simple unitarity relation for these amplitudes

$$\Im F_{L,J} = \sum_c k_c\ F_{L,J}(q_f, q_c)^\dagger F_{L,J}(q_c, q_i) \ . \tag{3.23}$$

For the single channel case $K_c = q_i = q_f = q$, phase shifts can be defined for the partial wave amplitude $F_{L,J}$ in the usual way

$$F_{L,J} = \frac{1}{q}\ \sin\delta_{L,J}(q)\exp\left(i\delta_{L,J}(q)\right) \ . \tag{3.24}$$

The relation of $F_{L,J}$ with the partial wave S-matrix is

$$S_{L,J} = e^{2i\delta_{L,J}} = 1 + 2iq\ F_{L,J} \ . \tag{3.25}$$

We note that the partial wave projection of the M-matrix is related to the partial wave amplitude $F_{L,J}$ by

$$M_L = \frac{1}{2}\int_{-1}^{1} dx\, P_L(x) M = \frac{1}{4\pi} M_{L,J} = -8\pi\sqrt{s} F_{L,J} \ . \tag{3.26}$$

Now the expression for the differential cross section becomes

$$\frac{d\sigma}{d\Omega} = \left|\tilde{f}\right|^2 + |\tilde{g}|^2 \ , \tag{3.27}$$

where the spin-nonflip and spin-flip amplitudes $\tilde{f}$ and $\tilde{g}$ are given by

$$\begin{aligned} \tilde{f} &= \frac{f}{8\pi\sqrt{s}} = \sum_L \left[(L+1)\, F_{L_+,J} + L F_{L_-,J}\right] P_L(\cos\theta) \ , \\ \tilde{g} &= \frac{g}{8\pi\sqrt{s}} = \sum_L \left[F_{L_+,J} - F_{L_-,J}\right] \sin\theta\ \frac{dP_L(\cos\theta)}{d\cos\theta} \ . \end{aligned} \tag{3.28}$$

The expressions for the total cross section, which is found by integrating the differential cross section, and the polarization are

$$\begin{aligned} \sigma &= 4\pi \sum_J \frac{2J+1}{2} \left(\left|F_{L_+,J}\right|^2 + \left|F_{L_-,J}\right|^2\right) \ , \\ P(\theta) &= \frac{2\Im\left(\tilde{f}\tilde{g}^*\right)}{\left|\tilde{f}\right|^2 + |\tilde{g}|^2} \ . \end{aligned} \tag{3.29}$$

Chapter 4

Baryon- and meson-exchange potentials

The effective local interaction Hamiltonians that are used to calculate the one-hadron-exchange potentials are defined in this chapter. The Lorentz structure of the interaction is given and the $SU_f(3)$ structure is reviewed , since we extend the soft-core pion-nucleon model to the soft-core kaon-nucleon model. The amplitudes of the one-hadron-exchange Feynman diagrams are derived in detail and a partial wave projection is made to find the partial wave potentials.

4.1 Meson-baryon channels and $SU_f(3)$

We consider in this thesis the pion-nucleon and kaon-nucleon interactions, they make up only a subset of all meson-baryon interactions. Because the soft-core kaon-nucleon model is derived from the soft-core pion-nucleon model, using $SU_f(3)$ symmetry, we define an $SU_f(3)$ invariant interaction Hamiltonian describing the baryon-baryon-meson and meson-meson-meson vertices. The Lorentz structure of the baryon-baryon-meson interaction is analyzed in the next section, here we deal with its $SU_f(3)$ structure. In order to find the interaction Hamiltonian we define the octet irreducible representation (irrep) of $SU_f(3)$ for the $J^P = \frac{1}{2}^+$ baryons and the octet and singlet irreducible representations of $SU_f(3)$ for the mesons. Using the phase convention of [40], the $J^P = \frac{1}{2}^+$ baryon octet irrep can be written as traceless 3×3 matrix

$$\mathcal{B} = \begin{pmatrix} \frac{\Sigma^0}{\sqrt{2}} + \frac{\Lambda}{\sqrt{6}} & \Sigma^+ & p \\ \Sigma^- & \frac{\Sigma^0}{\sqrt{2}} + \frac{\Lambda}{\sqrt{6}} & n \\ -\Xi^- & \Xi^0 & -\frac{2\Lambda}{\sqrt{6}} \end{pmatrix}, \tag{4.1}$$

similarly the pseudoscalar meson octet irrep can be written as

$$\mathcal{P}_8 = \begin{pmatrix} \frac{\pi^0}{\sqrt{2}} + \frac{\eta_8}{\sqrt{6}} & \pi^+ & K^+ \\ \pi^- & \frac{\pi^0}{\sqrt{2}} + \frac{\eta_8}{\sqrt{6}} & K^0 \\ K^- & K^0 & -\frac{2\eta_8}{\sqrt{6}} \end{pmatrix}, \tag{4.2}$$

while the pseudoscalar meson singlet irrep is the 3×3 diagonal matrix $\mathcal{P}_1$ with the elements $\eta_1/\sqrt{3}$ on the diagonal. The meson nonet, having a nonzero trace, is given by

$$\mathcal{P} \;=\; \mathcal{P}_8+\mathcal{P}_1 \;. \tag{4.3}$$

The physical mesons η and η' are superpositions of the octet and singlet mesons η_8 and η_1, usually written as

$$\begin{aligned}
\eta' &= \sin\theta\;\eta_8+\cos\theta\;\eta_1 \;, \\
\eta &= \cos\theta\;\eta_8-\sin\theta\;\eta_1 \;.
\end{aligned} \tag{4.4}$$

Similar expressions hold for the physical coupling constant of the η and η'. The octets and singlets for the scalar and vector mesons are defined in the same way and the expressions for the physical (ω,φ) and (σ, f_0) are analogous to (η',η). From these octets and nonets, $SU_f(3)$-invariant baryon-baryon-meson interaction Hamiltonians can be constructed, using the invariants $\mathrm{Tr}\left(\bar{\mathcal{B}}\mathcal{P}\mathcal{B}\right)$, $\mathrm{Tr}\left(\bar{\mathcal{B}}\mathcal{B}\mathcal{P}\right)$ and $\mathrm{Tr}\left(\bar{\mathcal{B}}\mathcal{B}\right)\mathrm{Tr}\left(\mathcal{P}\right)$. We take the antisymmetric (F) and symmetric (D) octet couplings and the singlet (S) coupling

$$\begin{aligned}
\left[\bar{\mathcal{B}}\mathcal{B}\mathcal{P}\right]_F &= \mathrm{Tr}\left(\bar{\mathcal{B}}\mathcal{P}\mathcal{B}\right)-\mathrm{Tr}\left(\bar{\mathcal{B}}\mathcal{B}\mathcal{P}\right)=\mathrm{Tr}\left(\bar{\mathcal{B}}\mathcal{P}_8\mathcal{B}\right)-\mathrm{Tr}\left(\bar{\mathcal{B}}\mathcal{B}\mathcal{P}_8\right) \;, \\
\left[\bar{\mathcal{B}}\mathcal{B}\mathcal{P}\right]_D &= \mathrm{Tr}\left(\bar{\mathcal{B}}\mathcal{P}\mathcal{B}\right)+\mathrm{Tr}\left(\bar{\mathcal{B}}\mathcal{B}\mathcal{P}\right)-\frac{2}{3}\mathrm{Tr}\left(\bar{\mathcal{B}}\mathcal{B}\right)\mathrm{Tr}\left(\mathcal{P}\right) \\
&= \mathrm{Tr}\left(\bar{\mathcal{B}}\mathcal{P}_8\mathcal{B}\right)+\mathrm{Tr}\left(\bar{\mathcal{B}}\mathcal{B}\mathcal{P}_8\right) \;, \\
\left[\bar{\mathcal{B}}\mathcal{B}\mathcal{P}\right]_S &= \mathrm{Tr}\left(\bar{\mathcal{B}}\mathcal{B}\right)\mathrm{Tr}\left(\mathcal{P}\right)=\mathrm{Tr}\left(\bar{\mathcal{B}}\mathcal{B}\right)\mathrm{Tr}\left(\mathcal{P}_1\right) \;.
\end{aligned} \tag{4.5}$$

The $SU_f(3)$-invariant baryon-baryon-meson interaction Hamiltonian is a linear combination of these quantities and defined according to [40]

$$m_{\pi^+}\mathcal{H} \;=\; f_8\sqrt{2}\left(\alpha\left[\bar{\mathcal{B}}\mathcal{B}\mathcal{P}\right]_F+(1-\alpha)\left[\bar{\mathcal{B}}\mathcal{B}\mathcal{P}\right]_D\right)+f_1\sqrt{\frac{1}{3}}\left[\bar{\mathcal{B}}\mathcal{B}\mathcal{P}\right]_S \;. \tag{4.6}$$

Here, α is the $F/(F+D)$-ratio. The most general interaction Hamiltonian that is invariant under isospin transformations is given by

$$\begin{aligned}
m_{\pi^+}\mathcal{H}_1 &= \left[f_{NN\eta_1}\left(\bar{N}N\right)+f_{\Lambda\Lambda\eta_1}\left(\bar{\Lambda}\Lambda\right)+f_{\Sigma\Sigma\eta_1}\left(\bar{\Sigma}\cdot\Sigma\right)+f_{\Xi\Xi\eta_1}\left(\bar{\Xi}\Xi\right)\right]\eta_1 \;, \\
m_{\pi^+}\mathcal{H}_8 &= f_{NN\pi}\left(\bar{N}\boldsymbol{\tau}N\right)\cdot\boldsymbol{\pi}-if_{\Sigma\Sigma\pi}\left(\bar{\Sigma}\times\bar{\Sigma}\right)\cdot\boldsymbol{\pi} \\
&\quad +f_{\Lambda\Sigma\pi}\left(\bar{\Lambda}\Sigma+\bar{\Sigma}\Lambda\right)\cdot\boldsymbol{\pi}+f_{\Xi\Xi\pi}\left(\bar{\Xi}\boldsymbol{\tau}\Xi\right)\cdot\boldsymbol{\pi} \\
&\quad +f_{\Lambda NK}\left[\left(\bar{N}K\right)\Lambda+\bar{\Lambda}\left(\bar{K}N\right)\right]+f_{\Xi\Lambda K}\left[\left(\bar{\Xi}K_c\right)\Lambda+\bar{\Lambda}\left(\bar{K}_c\Xi\right)\right] \\
&\quad +f_{\Sigma NK}\left[\bar{\Sigma}\cdot\left(\bar{K}\boldsymbol{\tau}N\right)+\left(\bar{N}\boldsymbol{\tau}K\right)\cdot\Sigma\right] \\
&\quad +f_{\Sigma\Xi K}\left[\bar{\Sigma}\cdot\left(\bar{K}_c\boldsymbol{\tau}\Xi\right)+\left(\bar{\Xi}\boldsymbol{\tau}K_c\right)\cdot\Sigma\right]+f_{NN\eta_8}\left(\bar{N}N\right)\eta_8 \\
&\quad +f_{\Lambda\Lambda\eta_8}\left(\bar{\Lambda}\Lambda\right)\eta_8+f_{\Sigma\Sigma\eta_8}\left(\bar{\Sigma}\cdot\Sigma\right)\eta_8+f_{\Xi\Xi\eta_8}\left(\bar{\Xi}\Xi\right)\eta_8 \;,
\end{aligned} \tag{4.7}$$

for the singlet and octet coupling respectively, and $f_{NN\pi}=f_8$ and $f_{NN\eta_1}=f_{\Lambda\Lambda\eta_1}=f_{\Sigma\Sigma\eta_1}=f_{\Xi\Xi\eta_1}=f_1$. We have introduced the isospin doublets

$$N = \begin{pmatrix} p \\ n \end{pmatrix}, \quad \Xi = \begin{pmatrix} \Xi^0 \\ \Xi^- \end{pmatrix}, \quad K = \begin{pmatrix} K^+ \\ K^0 \end{pmatrix}, \quad K = \begin{pmatrix} \bar{K}^0 \\ -K^- \end{pmatrix}, \tag{4.8}$$

the phases have been chosen according to [40], such that the inner product of the isovectors Σ and π is

$$\Sigma \cdot \pi = \Sigma^+\pi^- + \Sigma^0\pi^0 + \Sigma^-\pi^+ . \tag{4.9}$$

The interaction Hamiltonians in Eq. (4.7) are invariant under $SU_f(3)$ transformations if the coupling constants are expressed in terms of the octet coupling $f_8 \equiv f$ and α as, [40],

$$\begin{array}{llllll}
f_{NN\pi} = & f & f_{NN\eta_8} = & \frac{1}{\sqrt{3}}(4\alpha-1)f & f_{\Lambda NK} = & -\frac{1}{\sqrt{3}}(1+2\alpha)f \\
f_{\Xi\Xi\pi} = & -(1-2\alpha)f & f_{\Xi\Xi\eta_8} = & -\frac{1}{\sqrt{3}}(1+2\alpha)f & f_{\Xi\Lambda K} = & \frac{1}{\sqrt{3}}(4\alpha-1)f \\
f_{\Lambda\Sigma\pi} = & \frac{2}{\sqrt{3}}(1-\alpha)f & f_{\Sigma\Sigma\eta_8} = & \frac{2}{\sqrt{3}}(1-\alpha)f & f_{\Sigma NK} = & (1-2\alpha)f \\
f_{\Sigma\Sigma\pi} = & 2\alpha f & f_{\Lambda\Lambda\eta_8} = & -\frac{2}{\sqrt{3}}(1-\alpha)f & f_{\Xi\Sigma K} = & -f \ ,
\end{array} \tag{4.10}$$

and the singlet coupling f_1 as

$$f_{NN\eta_1} = f_{\Lambda\Lambda\eta_1} = f_{\Sigma\Sigma\eta_1} = f_{\Xi\Xi\eta_1} = f_1 . \tag{4.11}$$

The baryon-baryon-meson vertices are thus characterized by only four parameters if $SU_f(3)$-symmetry is assumed, the octet coupling constant f_8, the singlet coupling constant f_1, the $F/(F+D)$-ratio α and the mixing angle, which gives the relation between the physical and octet and singlet isoscalar mesons. The meson-meson-meson vertex as well as the Lorentz structure of the baryon-baryon-meson vertex is discussed in the next section.

We remark that the soft-core model the $SU_f(3)$-symmetry is broken dynamically, since we use the physical masses for the baryons and mesons. The $SU_f(3)$-symmetry for the coupling constants is not necessarily exact, in fact, we allow for a breaking in the soft-core kaon nucleon model, Chapter 7.

4.2 The interaction Hamiltonians

The potentials we use are obtained from the t-channel one-meson-exchange (OBE) and the u- and s-channel baryon-exchange Feynman diagrams. In the t-channel we consider the exchange of vector- and scalar-mesons and in the u- and s-channel we consider the exchange of $J^P = \frac{1}{2}^+$ and $\frac{3}{2}^+$-baryons. In this work we also include Pomeron exchange diagrams, where the physical nature of the Pomeron can be understood in the light of QCD as a two-gluon- exchange effect, see [20, 21]. The contribution of the Pomeron will almost completely cancel the contribution of the isoscalar scalar meson σ.

The OBE Feynman diagrams for meson-baryon interactions contain a meson-baryon-baryon vertex and a meson-meson-meson vertex. These vertices are determined by the effective local interaction Hamiltonian densities. The Lorentz structure of the local interaction densities for the meson-baryon-baryon (MBB) vertices we use are listed below [1]

[1]The couplings defined in this section are according to the 'Compilation of Coupling Constants and Low Energy Parameters', [41]

a. $J^{PC} = 0^{-+}$ Pseudoscalar-mesons:
For the pseudoscalar-mesons we use the pseudovector interaction Hamiltonian

$$\mathcal{H}_{PV} = \frac{f}{m_{\pi^+}}\, \bar{\psi}_f \gamma_5 \gamma_\mu \psi_i\, \partial^\mu \phi_P\ , \tag{4.12}$$

which is scaled with the charged-pion mass in order to have a dimensionless pseudovector coupling constant.

b. $J^{PC} = 1^{--}$ Vector-mesons:
The interaction Hamiltonian is given in terms of the electric and magnetic interaction

$$\mathcal{H}_V = g_V\ \bar{\psi}_f \gamma_\mu \psi_i\ \phi_V^\mu + \frac{f_V}{4\mathcal{M}} \bar{\psi}_f \sigma_{\mu\nu} \psi_i \left(\partial^\mu \phi_V^\nu - \partial^\nu \phi_V^\mu\right)\ , \tag{4.13}$$

where usually the proton mass is used for $\mathcal{M}$ to scale the magnetic part of the interaction Hamiltonian. The antisymmetric tensor operator used here, is defined as $\sigma_{\mu\nu} = \frac{i}{2}\left[\gamma_\mu, \gamma_\nu\right]$.

c. $J^{PC} = 0^{++}$ Scalar-mesons:

$$\mathcal{H}_S = g_S\ \bar{\psi}_f \psi_i\ \phi_S\ . \tag{4.14}$$

Since we include Pomeron exchange in the soft-core model, the scalar-meson exchange is canceled for the greater part, hence it is possible to satisfy the soft-pion theorem while including scalar-meson exchange.

d. $J^{PC} = 2^{++}$ Tensor-mesons:
For the tensor-mesons we use the interaction Hamiltonian

$$\mathcal{H}_T = \left[\frac{i}{4}\bar{\psi}_f \left(\gamma_\mu \overleftrightarrow{\partial_\nu} + \gamma_\nu \overleftrightarrow{\partial_\mu}\right) \psi_i \cdot F_1 - \frac{1}{4}\left(\bar{\psi}_f\ \overleftrightarrow{\partial^\mu}\overleftrightarrow{\partial^\nu}\ \psi_i\right) \cdot F_2\right] \cdot \phi_T^{\mu\nu}\ , \tag{4.15}$$

where the coupling constants F_1 and F_2 are related to the dimensionless Pauli coupling constants by $G_{T,1} = \mathcal{M} F_1$ and $G_{T,2} = \mathcal{M}^2 F_2$. Using the Gordon decomposition the Pauli coupling constants are related to the Dirac coupling constants by $g_T = G_{T,1} + G_{T,2}$ and $f_T = -G_{T,2}$.

e. $J^P = \frac{3}{2}^+$ Resonance-Baryon-Pseudoscalar-meson coupling:
The local interaction density for the $J^P = \frac{3}{2}^+$ Resonance -Nucleon-Pseudoscalar-meson $(Y^* N P)$ interaction is

$$\mathcal{H}_{Y^*NP} = -i\left(\frac{f^*_{Y^*NP}}{m_{\pi^+}}\right)\ \bar{\psi}_N\ \psi_{Y^*,\mu} \cdot \partial^\mu \phi_P\ , \tag{4.16}$$

where the charged-pion mass makes the coupling dimensionless. We use the Rarita-Schwinger formalism for the spin-3/2 resonances, see e.g. [26, 42].

f. $J^P = \frac{1}{2}^-$ Resonance-Baryon-Pseudoscalar-meson coupling:

The local interaction Hamiltionian for the $J^P = \frac{1}{2}^-$ Resonance-Nucleon-Pseudoscalar-meson (RNP) interaction is

$$\mathcal{H}_{RNP} = \frac{f^*_{RNP}}{m_{\pi^+}}\, \bar{\psi}_N \gamma_\mu \psi_R\, \partial^\mu \phi_P\ , \tag{4.17}$$

where ψ_R denotes the $J^P = \frac{1}{2}^-$ resonance, which has opposite parity to the nucleon. The $J^P = \frac{1}{2}^-$ resonances we consider in this work are the $S_{11}(1555)$ in the πN system and the $\Lambda(1405)$ in the KN system.

Here ϕ denotes the pseudoscalar-, vector-, scalar-, and tensor-meson fields respectively and ψ denotes the baryon fields. The Pomeron-baryon-baryon interaction density we use, has the same Lorentz structure as the scalar-mesons.

We note that, making use of the Dirac equation $\left(\gamma^\mu \partial_\mu + M\right)\psi = 0$, the pseudovector interaction Hamiltonian density in Eq. (4.12) is 'equivalent' to the pseudoscalar density $\mathcal{H}_{PS} = i\ g\ \bar{\psi}_f \gamma_5 \psi_i\ \phi_P$ for on-mass-shell particles. The coupling constants are then related according to $g/(M_{B_f} + M_{B_i}) = f/m_{\pi^+}$.

Analogous we find that the vector coupling Hamiltonian density in Eq. (4.17) is 'equivalent' to the scalar density $\mathcal{H}_{PS} = i\ g\ \bar{\psi}_f \psi_i\ \phi_P$ for on-mass-shell particles. The coupling constants are in this case related according to $g^*_{RNP}/(M_N - M_R) = f^*_{RNP}/m_{\pi^+}$.

Concerning the flavor structure of the interaction densities, we assume that the coupling constants are related via $SU_f(3)$ symmetry, as outlined in the previous section. However the potentials will break the $SU_f(3)$ symmetry dynamically, since we use the physical masses of the particles. The isospin factors are discussed in Appendix B and listed in Tables 6.1 and 7.1 for pion-nucleon and kaon-nucleon interactions respectively.

The $SU_f(3)$ invariant local interaction densities we use for the triple-meson (MMM) vertices are are given below.

(i) $J^{PC} = 1^{--}$ Vector-mesons:

$$\begin{aligned}
\mathcal{H}_{PPV} &= g'_{PPV}\, f_{abc}\, V^a_\mu\, P^b \overset{\leftrightarrow \mu}{\partial} P^c = \frac{-i g'_{PPV}}{\sqrt{2}}\, Tr\, \mathcal{P}\left(\partial_\mu \mathcal{P}\cdot \mathcal{V}^\mu - \mathcal{V}^\mu\, \partial_\mu \mathcal{P}\right) \\
&= g'_{PPV}\Big[\boldsymbol{\rho}_\mu \cdot \Big(\boldsymbol{\pi} \times \overset{\leftrightarrow \mu}{\partial} \boldsymbol{\pi} + i K^\dagger \boldsymbol{\tau} \overset{\leftrightarrow \mu}{\partial} K\Big) + \\
&\quad \Big(i K^{*\dagger}_\mu\, \boldsymbol{\tau} K \cdot \overset{\leftrightarrow \mu}{\partial} \boldsymbol{\pi} + H.c.\Big) + \sqrt{3}\Big(i K^{*\dagger}_\mu K \overset{\leftrightarrow \mu}{\partial} \eta + H.c.\Big) + \\
&\quad \sqrt{3}\, i \varphi_{8,\mu}\, K^\dagger \overset{\leftrightarrow \mu}{\partial} K\Big]\ ,
\end{aligned} \tag{4.18}$$

where $H.c.$ stands for the Hermitian conjugate of the preceding term, and we use the usual notation for the derivative $\overset{\leftrightarrow \mu}{\partial}$ acting on the pseudoscalar-mesons, $P^b \overset{\leftrightarrow \mu}{\partial} P^c \equiv$

$P^b\,(\partial^\mu P^c) - \left(\partial^\mu P^b\right)\cdot P^c$. The coupling of the vector-mesons to the pseudoscalar-mesons is $SU_f(3)$ antisymmetric, the symmetric coupling can be excluded by invoking a generalized Bose symmetry for the pseudoscalar-mesons, interchanging the two pseudoscalar-mesons leaves $\mathcal{H}_{PPV}$ invariant.

The coupling constant for the decay of a ρ-meson into two pions is defined as $g_{\pi\pi\rho} = 2\,g'_{PPV}$, which can be estimated using the decay width of the ρ-meson, see subsection 6.3.1.

(ii) $J^{PC} = 0^{++}$ Scalar-mesons:

$$
\begin{aligned}
\mathcal{H}_{PPS} &= g'_{PPS}\left[d_{abc}\, S^a\ P^b\ P^c\right] = \frac{g'_{PPS}}{\sqrt{2}} g_{PPS}\, Tr\,\mathcal{P}\left(\mathcal{P}\cdot\mathcal{S}+\mathcal{S}\cdot\mathcal{P}\right)\\
&= g'_{PPS}\left[\boldsymbol{a}_0\cdot\left(\boldsymbol{\pi}\eta+\frac{\sqrt{3}}{2}K^\dagger\boldsymbol{\tau}K\right)+\frac{\sqrt{3}}{2}\left(K_0^\dagger\boldsymbol{\tau}K\cdot\boldsymbol{\pi}+H.c.\right)\right.\\
&\left.\quad -\frac{1}{2}\left(K_0^\dagger K\eta+H.c.\right)+\frac{1}{2}f_0\left(\boldsymbol{\pi}\cdot\boldsymbol{\pi}-K^\dagger K-\eta\eta\right)\right].
\end{aligned} \tag{4.19}
$$

For the scalar-mesons we have a symmetric coupling. The dimensionless coupling constant for the decay of the σ-meson into two pions is defined as $g_{\pi\pi\sigma} = g'_{PPS}/m_{\pi^+}$, which can be estimated using the decay width of the σ-meson, see subsection 6.3.1.

(iii) $J^{PC} = 2^{++}$ Tensor-mesons:

$$
\begin{aligned}
\mathcal{H}_{PPT} &= 2g'_{PPT}/m_{\pi^+}\left[d_{abc}\, f^a_{\mu\nu}\left(\partial^\mu P^b\right)\cdot\left(\partial^\nu P^c\right)\right]\\
&= 2g_{PPT}/m_{\pi^+}\left[\boldsymbol{a}_2^{\mu\nu}\cdot\left(\partial_\mu\boldsymbol{\pi}\partial_\nu\eta+\frac{\sqrt{3}}{2}\partial_\mu K^\dagger\boldsymbol{\tau}\partial_\nu K\right)\right.\\
&\quad +\frac{\sqrt{3}}{2}\left(K_2^{\mu\nu\dagger}\boldsymbol{\tau}\partial_\mu K\cdot\partial_\nu\boldsymbol{\pi}+H.c.\right)-\frac{1}{2}\left(K_2^{\mu\nu\dagger}\partial_\mu K\partial_\nu\eta+H.c.\right)\\
&\left.\quad +\frac{1}{2}f_2^{\mu\nu}\left(\partial_\mu\boldsymbol{\pi}\cdot\partial_\nu\boldsymbol{\pi}-\partial_\mu K^\dagger\partial_\nu K-\partial_\mu\eta\partial_\nu\eta\right)\right].
\end{aligned} \tag{4.20}
$$

The coupling constant for the decay of the f_2-meson into two pions is given by $g_{\pi\pi f_2} = g_{PPT}$, which is estimated in subsection 6.3.1.

Some numerical values for the previous coupling constants are given by Nagels et al. [43].

4.3 The relativistic invariant amplitudes

Using the previously defined interaction Hamiltonians, we give, besides the isospin factors, the contributions to the relativistic invariant amplitudes $A(s,t,u)$ and $B(s,t,u)$ in Eq. (2.5) for the elastic (e.g. πN and KN) channels, i.e. $M_i = M_f \equiv M$, $m_i = m_f = m$, where M_f and M_I are the final and initial baryon masses and m_f and m_i are the final and initial pseudoscalar-meson masses respectively. A detailed derivation of these amplitudes for the general mass case is given in Appendix C.

4.3.1 Baryon-exchange amplitudes

For $J^P = \frac{1}{2}^+$ baryon-exchange the relativistic amplitudes are

$$
\begin{aligned}
A_{\mathrm{ps}}(s,t,u) &= -g_{14}^{(ps)}\, g_{23}^{(ps)}\, \frac{M_B - M}{u - M_B^2 + i\epsilon}\,, \\
B_{\mathrm{ps}}(s,t,u) &= -g_{14}^{(ps)}\, g_{23}^{(ps)}\, \frac{1}{u - M_B^2 + i\epsilon}\,, \\
A_{\mathrm{pv}}(s,t,u) &= -\frac{f_{14}^{(pv)} f_{23}^{(pv)}/m_{\pi^+}^2}{u - M_B^2 + i\epsilon}\left[u\,(M + M_B) - M^3 - M^2 M_B\right], \\
B_{\mathrm{pv}}(s,t,u) &= -\frac{f_{14}^{(pv)} f_{23}^{(pv)}/m_{\pi^+}^2}{u - M_B^2 + i\epsilon}\left[u + 2MM_B + M^2\right], \qquad (4.21)
\end{aligned}
$$

for pseudoscalar (ps) and pseudovector (pv) coupling respectively, M_B is the mass of the exchanged baryon. The $J^P = \frac{1}{2}^+$ baryon direct pole gives rise to the relativistic amplitudes

$$
\begin{aligned}
A_{\mathrm{ps}}(s,t,u) &= -g_{14}^{(ps)}\, g_{23}^{(ps)}\, \frac{M_B - M}{s - M_B^2 + i\epsilon}\,, \\
B_{\mathrm{ps}}(s,t,u) &= g_{14}^{(ps)}\, g_{23}^{(ps)}\, \frac{1}{s - M_B^2 + i\epsilon}\,, \\
A_{\mathrm{pv}}(s,t,u) &= -\frac{f_{14}^{(pv)} f_{23}^{(pv)}/m_{\pi^+}^2}{s - M_B^2 + i\epsilon}\left[s\,(M + M_B) - M^3 - M^2 M_B\right], \\
B_{\mathrm{pv}}(s,t,u) &= \frac{f_{14}^{(pv)} f_{23}^{(pv)}/m_{\pi^+}^2}{s - M_B^2 + i\epsilon}\left[s + 2MM_B + M^2\right], \qquad (4.22)
\end{aligned}
$$

for pseudoscalar and pseudovector coupling respectively. For $J^P = \frac{1}{2}^-$ baryon-exchange the relativistic amplitudes are

$$
\begin{aligned}
A_{\mathrm{s}}(s,t,u) &= g_{14}^{*(s)}\, g_{23}^{*(s)}\, \frac{M_B + M}{u - M_B^2 + i\epsilon}\,, \\
B_{\mathrm{s}}(s,t,u) &= -g_{14}^{*(s)}\, g_{23}^{*(s)}\, \frac{1}{u - M_B^2 + i\epsilon}\,, \\
A_{\mathrm{v}}(s,t,u) &= \frac{f_{14}^{*(v)} f_{23}^{*(v)}/m_{\pi^+}^2}{u - M_B^2 + i\epsilon}\left[u\,(-M + M_B) + M^3 - M^2 M_B\right], \\
B_{\mathrm{v}}(s,t,u) &= \frac{f_{14}^{*(v)} f_{23}^{*(v)}/m_{\pi^+}^2}{u - M_B^2 + i\epsilon}\left[-u + 2MM_B - M^2\right], \qquad (4.23)
\end{aligned}
$$

for scalar (s) and vector (v) coupling respectively, M_B is the mass of the exchanged baryon. The $J^P = \frac{1}{2}^-$ baryon direct pole gives rise to the relativistic amplitudes

$$
\begin{aligned}
A_{\rm s}(s,t,u) &= g_{14}^{*(s)}\, g_{23}^{*(s)}\, \frac{M_B+M}{s-M_B^2+i\epsilon}\ , \\
B_{\rm s}(s,t,u) &= g_{14}^{*(s)}\, g_{23}^{*(s)}\, \frac{1}{s-M_B^2+i\epsilon}\ , \\
A_{\rm v}(s,t,u) &= \frac{f_{14}^{*(v)} f_{23}^{*(v)}/m_{\pi^+}^2}{s-M_B^2+i\epsilon}\left[s\,(-M+M_B)+M^3-M^2M_B\right]\ , \\
B_{\rm v}(s,t,u) &= -\frac{f_{14}^{*(v)} f_{23}^{*(v)}/m_{\pi^+}^2}{s-M_B^2+i\epsilon}\left[-s+2MM_B-M^2\right]\ ,
\end{aligned}
\tag{4.24}
$$

for scalar and vector coupling respectively. The $J^P = \frac{3}{2}^+$ resonance-exchange relativistic amplitudes are more complicated

$$
\begin{aligned}
A_{Y^*}(s,t,u) &= \frac{f_{14}^*\, f_{23}^*}{m_{\pi^+}^2}\cdot\frac{1}{u-M_{Y^*}^2+i\epsilon}\cdot\left\{\frac{1}{2}\left[t-2m^2\right](M+M_{Y^*})+\frac{1}{3}M_{Y^*}\left[u-M^2\right]\right. \\
&\quad +\frac{1}{6M_{Y^*}}\left\{-u^2+2Mu\,(M+M_{Y^*})-2M^3M_{Y^*}-M^4+m^4\right\} \\
&\quad \left.+\frac{1}{6M_{Y^*}^2}\left[M^2-m^2-u\right]^2(M+M_{Y^*})\right\}\ , \\
B_{Y^*}(s,t,u) &= \frac{f_{14}^*\, f_{23}^*}{m_{\pi^+}^2}\cdot\frac{1}{u-M_{Y^*}^2+i\epsilon}\cdot\left\{-\frac{1}{2}\left[t-2m^2\right]\right. \\
&\quad +\frac{1}{3M_{Y^*}}\left\{(M+M_{Y^*})\left(2MM_{Y^*}-m^2\right)-uM+M^3\right\} \\
&\quad \left.-\frac{1}{6M_{Y^*}^2}\left[u-M^2+m^2\right]^2\right\}\ ,
\end{aligned}
\tag{4.25}
$$

where M_{Y^*} is the mass of the exchanged resonance. The $J^P = \frac{3}{2}^+$ resonance direct pole gives rise to the relativistic amplitudes

$$
\begin{aligned}
A_{Y^*}(s,t,u) &= \frac{f_{14}^*\, f_{23}^*}{m_{\pi^+}^2}\cdot\frac{1}{s-M_{Y^*}^2+i\epsilon}\cdot\left\{\frac{1}{2}\left[t-2m^2\right](M+M_{Y^*})+\frac{1}{3}M_{Y^*}\left[s-M^2\right]\right. \\
&\quad +\frac{1}{6M_{Y^*}}\left\{-s^2+2Ms\,(M+M_{Y^*})-2M^3M_{Y^*}-M^4+m^4\right\} \\
&\quad \left.+\frac{1}{6M_{Y^*}^2}\left[M^2-m^2-s\right]^2(M+M_{Y^*})\right\}\ , \\
B_{Y^*}(s,t,u) &= -\frac{f_{14}^*\, f_{23}^*}{m_{\pi^+}^2}\cdot\frac{1}{s-M_{Y^*}^2+i\epsilon}\cdot\left\{-\frac{1}{2}\left[t-2m^2\right]\right.
\end{aligned}
$$

$$
\begin{aligned}
&+\frac{1}{3M_{Y^*}}\left\{(M+M_{Y^*})\left(2MM_{Y^*}-m^2\right)-sM+M^3\right\}\\
&-\frac{1}{6M_{Y^*}^2}\left[s-M^2+m^2\right]^2\Bigg\} \ . \qquad (4.26)
\end{aligned}
$$

4.3.2 Meson- and Pomeron-exchange amplitudes

The relativistic amplitudes for the t-channel Pomeron-exchange, scalar-meson-exchange, vector-meson- and tensor-meson-exchange are

$$
\begin{aligned}
A_P(s,t,u) &= g_{PPP}\, g_P \frac{1}{\mathcal{M}} \ , \quad B_P(s,t,u)=0 \ ,\\
A_S(s,t,u) &= g_{PPS}\, g_S \cdot \frac{1}{t-m_S^2+i\epsilon} \ , \quad B_S(s,t,u)=0 \ ,\\
A_V(s,t,u) &= g_{PPV}\cdot \frac{1}{t-m_V^2+i\epsilon}\cdot\frac{f_V}{2\mathcal{M}}(s-u) \ ,\\
B_V(s,t,u) &= -2g_{PPV}\cdot\frac{1}{t-m_V^2+i\epsilon}\cdot\left(g_V+\frac{M}{\mathcal{M}}f_V\right) \ ,\\
A_T(s,t,u) &= \frac{g_{PPT}}{m_{\pi^+}}\cdot\frac{1}{t-m_T^2+i\epsilon}\cdot\left\{\frac{1}{4}(s-u)^2\ F_2\right.\\
&\left.-\frac{1}{6}\left[4m^2-t\right]\left[2MF_1+\frac{1}{2}\left(4M^2-t\right)F_2\right]\right\} \ ,\\
B_T(s,t,u) &= \frac{g_{PPT}}{m_{\pi^+}}\cdot\frac{1}{t-m_T^2+i\epsilon}\cdot(s-u)\ F_1 \ , \qquad (4.27)
\end{aligned}
$$

where m_S, m_V and m_T are the masses of the exchanged scalar-meson, vector-meson and tensor-meson respectively. The coupling constant g_{PPV} for the $KK\varphi$ vertex is $g_{PPV} = \sqrt{3}g'_{PPV}$, etc..

Here we notice that for the meson-exchange and Pomeron-exchange amplitudes an extra factor 2 must be added to the amplitudes if both the initial and final state contain a π or η, this is not the case for any other combination of pseudoscalar-mesons in the initial and final state. For elastic πN scattering for example, an extra factor 2 is added to the ρ-exchange, Pomeron-exchange and σ-exchange amplitudes.

4.4 Partial wave potentials

As discussed in Chapter 3 we solve the integral equation for the T-matrix on the partial wave basis, Eq. (3.17). And we fit the soft-core model to the πN partial wave analysis [1] and the KN partial wave analysis [2]. For this purpose we need to calculate the partial wave projection of the potentials, Eqs. (3.7) and (2.46). In our approximation, the potentials are given by the invariant amplitudes A and B, given by Eqs. (4.21)–(4.27), of the one-meson-exchange and one-baryon-exchange Feynman diagrams.

Until this point, we did not mention the need for form factors to regulate the high energy behavior, i.e. the short distance behavior, of the potentials, but in fact the kernel of the integral equation without form factors does not satisfy the Fredholm condition, $\int\int dp\, dk\ |K(p,k)|^2 < \infty$, in general.

Furthermore we have derived our one-meson-exchange and one-baryon-exchange potentials from Quantum Field Theory, which is in principle only valid for point particles, while mesons and baryons have an internal structure. Therefore we need to take into account the extended size of the mesons and baryons by means of a form factor. Since the ground state wave functions of the quarks are Gaussian, form factors of the Gaussian type are used in the soft-core model. For t-channel exchanges we multiply the potentials by the form factor

$$F(\Lambda) = e^{-(\mathbf{k}_f-\mathbf{k}_i)^2/\Lambda^2}\ , \tag{4.28}$$

where $\mathbf{k}_i$ and $\mathbf{k}_f$ are the CM three-momenta for the initial and final state respectively, i.e. at both vertices we have used the difference between the final and initial three-momenta. Λ is a cut-off mass, which will be determined in the fit to the experimental phases.

For u- and s-channel exchanges, the difference between the final and initial three-momenta of the baryon is used, giving the form factor

$$F(\Lambda) = e^{-(\mathbf{k}_f^2+\mathbf{k}_i^2)/2\Lambda^2}\ . \tag{4.29}$$

This form factor obviously does not depend on the scattering angle θ, which makes the partial wave projection easier. For the u- and t-channel we rewrite the denominators of the potentials in the form

$$\begin{aligned}\frac{1}{t-m^2} &= \frac{-1}{2p_f p_i}\frac{1}{z_t - x}\ ,\\ \frac{1}{u-m^2} &= \frac{-1}{2p_f p_i}\frac{1}{z_u + x}\ ,\end{aligned} \tag{4.30}$$

where $x = \cos(\theta)$ and θ is the angle between the final and initial three-momenta $\mathbf{k}_f$ and $\mathbf{k}_i$. Here we have defined the z_t and z_u factors

$$\begin{aligned} z_t &= \frac{1}{2p_f p_i}\left[m^2 + p_f^2 + p_i^2 - \frac{1}{4}\left[E_i - E_f - \omega_i + \omega_f\right]^2\right]\ ,\\ z_u &= \frac{1}{2p_f p_i}\left[m^2 + p_f^2 + p_i^2 - \frac{1}{4}\left[E_i + E_f - \omega_i - \omega_f\right]^2\right]\ ,\end{aligned} \tag{4.31}$$

where $E_{f,i}$ are the baryon energies, $\omega_{f,i}$ are the meson energies and m the mass of the exchanged particle. For positive and real momenta, i.e. for open channels, we have $z > 1$. Now it is clear that the potentials $V^{(\alpha)}$ of Eq. (2.37), where α stands for central or spin-orbit, can be expanded in x as [2]

$$
\begin{aligned}
V^{(\alpha)}(\mathbf{p}_f,\mathbf{p}_i) &= \frac{1}{2p_f p_i}\left(X^{(\alpha)}+xY^{(\alpha)}+x^2Z^{(\alpha)}\right)\frac{F(\Lambda_t)}{z_t-x}\,, \\
V^{(\alpha)}(\mathbf{p}_f,\mathbf{p}_i) &= \frac{1}{2p_f p_i}\left(X^{(\alpha)}+xY^{(\alpha)}+x^2Z^{(\alpha)}\right)\frac{F(\Lambda_u)}{z_u+x}\,, \\
V^{(\alpha)}(\mathbf{p}_f,\mathbf{p}_i) &= \left(X^{(\alpha)}+xY^{(\alpha)}\right)\frac{F(\Lambda_s)}{s-M_B^2}\,,
\end{aligned}
\tag{4.32}
$$

for t-, u- and s-channel exchanges respectively, for all particles that are exchanged. The coefficients $X^{(\alpha)}$, $Y^{(\alpha)}$ and $Z^{(\alpha)}$ can be found easily by writing out the x-dependence of the invariant amplitudes A and B, they are listed in Appendix D for each type of exchange.

The partial wave potentials $V_L^{(\alpha)}$ are found by inverting the partial wave expansion Eq. (A.3), giving

$$
V_L^{(\alpha)}(p_f,p_i) = \frac{1}{2}\int_{-1}^{1} dx\, P_L(x) V^{(\alpha)}(\mathbf{p}_f,\mathbf{p}_i)\,. \tag{4.33}
$$

The partial wave potentials now take the form

$$
\begin{aligned}
V_L^{(\alpha)}(p_f,p_i) &= \frac{1}{2p_f p_i}\Big[\left(X^{(\alpha)}+z_tY^{(\alpha)}+z_t^2Z^{(\alpha)}\right)U_L(\Lambda_t,z_t) \\
&\qquad -\left(Y^{(\alpha)}+z_tZ^{(\alpha)}\right)R_L(\Lambda_t,z_t)-Z^{(\alpha)}S_L(\Lambda_t,z_t)\Big]\,, \\
V_L^{(\alpha)}(p_f,p_i) &= \frac{(-1)^L}{2p_f p_i}\Big[\left(X^{(\alpha)}-z_uY^{(\alpha)}+z_u^2Z^{(\alpha)}\right)U_L(\Lambda_u,z_u) \\
&\qquad -\left(-Y^{(\alpha)}+z_uZ^{(\alpha)}\right)R_L(\Lambda_u,z_u)-Z^{(\alpha)}S_L(\Lambda_u,z_u)\Big]\,, \\
V_L^{(\alpha)}(p_f,p_i) &= \left(X^{(\alpha)}\frac{F(\Lambda_s)}{s-M_B^2}\delta_{L,0}+Y^{(\alpha)}\frac{F(\Lambda_s)}{s-M_B^2}\frac{1}{3}\delta_{L,1}\right)\,,
\end{aligned}
\tag{4.34}
$$

for t-, u-, and s-channel exchanges respectively. We have defined the basic partial wave projections U_L, R_L, S_L and T_L in terms of the Legendre polynomials $P_L(x)$ and the form factors

$$
\begin{aligned}
U_L(\Lambda,z) &= \frac{1}{2}\int_{-1}^{1} dx\,\frac{P_L(x)F(\Lambda)}{z-x}\,, \\
R_L(\Lambda,z) &= \frac{1}{2}\int_{-1}^{1} dx\,P_L(x)F(\Lambda)\,, \\
S_L(\Lambda,z) &= \frac{1}{2}\int_{-1}^{1} dx\,P_L(x)xF(\Lambda)\,,
\end{aligned}
$$

[2] In case of more complicated exchanges, e.g. $J^{PC}=\frac{3}{2}^+$-resonance, the expansions of the potentials have an additional term of higher order in x, for the t- and u-channel $x^3U^{(\alpha)}$, and for the s-channel $x^2Z^{(\alpha)}$.
We notice that a similar expansion for F and G instead of $V^{(C)}$ and $V^{(SO)}$ would be a little simpler. However we will use the central and spin-orbit potentials in light of a momentum space version of the soft-core model.

$$T_L(\Lambda,z) = \frac{1}{2}\int_{-1}^{1} dx\, P_L(x) x^2 F(\Lambda)\ . \tag{4.35}$$

The factor $(-)^L$ appearing in the u-channel partial wave potentials, which is the result of changing the integration variable $x \to -x$ in the Legendre polynomial, is typical for exchange forces. In this way it can be seen that the total partial wave potential is a linear combination of a direct and an exchange potential, $V^{(\pm)} = V_d \pm V_e$ and the corresponding T-matrix is $T^{(\pm)} = T_d \pm T_e$. The amplitude T_e itself does not satisfy an integral equation, but the two linear combinations $T^{(\pm)} = T_d \pm T_e$ do.

We notice that if the form factor does not depend on x (in case of u-channel potentials) or if we consider the limit $\Lambda \to \infty$, i.e. $F(\Lambda) \to 1$, the basic partial wave projections defined in Eq. (4.35) are proportional to the simple functions

$$\begin{aligned}
U_L(\Lambda,z) &\propto Q_L(z)\ ,\\
R_L(\Lambda,z) &\propto \delta_{L,0}\ ,\\
S_L(\Lambda,z) &\propto \frac{1}{3}\delta_{L,1}\ ,\\
T_L(\Lambda,z) &\propto \frac{1}{3}\delta_{L,0} + \frac{2}{15}\delta_{L,2}\ ,
\end{aligned} \tag{4.36}$$

where $Q_L(z)$ is the Legendre function of the second kind, which is an analytic function of its argument except for a cut on the real axis running from –1 to 1, as is clear from Eq. (4.35). In view of Eq. (4.31), the cut is entered only for on-energy-shell potentials below threshold, but we always calculate the on-energy-shell potentials above threshold, so we will never reach the cut.

In the soft-core model for the πN interaction we will include s-channel baryon-exchange diagrams, which are in principle separable diagrams, having the form

$$V\left(p_f, p_i\right) = \frac{\Gamma\left(p_f\right)\ \Gamma\left(p_i\right)}{\sqrt{s} \pm M_e}\ . \tag{4.37}$$

Writing out the partial wave potentials of Eq. (3.7) or (3.10), using Eq. (4.34), for example for the nucleon pole (P_{11}-wave), the delta resonance pole (P_{33}-wave) and the S_{11}-resonance pole (S_{11}-wave) explicitly

$$\begin{aligned}
V_{11} &= \frac{f^2}{m_{\pi^+}^2}\, 3\, \frac{p_f p_i}{\sqrt{\left(E_i+M_i\right)\left(E_f+M_f\right)}}\, \frac{\left(\sqrt{s}+M_f\right)\left(\sqrt{s}+M_i\right)}{\sqrt{s}-M_e}\ ,\\
V_{33} &= \frac{f_{\pi N\Delta}^2}{m_{\pi^+}^2}\, \frac{1}{3} \sqrt{\left(E_i+M_i\right)\left(E_f+M_f\right)}\ p_f p_i\, \frac{1}{\sqrt{s}-M_e}\ ,\\
V_{11} &= \frac{f_{\pi N S_{11}}^2}{m_{\pi^+}^2}\, 3\sqrt{\left(E_i+M_i\right)\left(E_f+M_f\right)}\, \frac{\left(\sqrt{s}-M_f\right)\left(\sqrt{s}-M_i\right)}{\sqrt{s}-M_e}\ ,
\end{aligned} \tag{4.38}$$

we see that these potentials are of the separable kind indeed and that they have a pole at the physical mass of the exchanged particle.

For the partial wave potentials we have used the notation $V_{2I,2J}$, where I is the total isospin and J is the total angular momentum. The first V_{11} in Eq. (4.38) is the P-wave nucleon pole potential, the second is the S-wave S_{11}-resonance pole potential with opposite parity. We note that the P-wave potentials are proportional to $p_f p_i$ as expected.

We need to be careful in including the s-channel diagrams in a model that has been renormalized, i.e. in which (renormalized) physical coupling constants and masses are used. It is not possible to simply add the s-channel diagrams to the other ones, because iterations of s-channel diagrams will give contributions to the vertex and self-energy.

The way these diagrams are included in the soft-core model is described in Chapter 5, here we show that bare masses and coupling constants should be used in the s-channel diagrams and that these bare parameters are determined by requiring that (i) the T-matrix has a pole at the physical mass $\sqrt{s} = M_e$, (ii) the residue at the pole is given by the physical coupling constant.

Chapter 5
Renormalization

The Lagrangians used are effective Lagrangians, expressed in terms of the physical coupling constants and masses. Then, in principle, counter-terms should be added to the Lagrangian and fixed by renormalization conditions. This is particularly to the point in channels where there occur bound-states and resonances. For example, the famous Δ_{33}-resonance at $M_\Delta = 1232$ MeV in the pion-nucleon system. The Δ_{33}-pole diagram gets "dressed" when it is iterated with other graph's upon insertion in an integral equation. Also, it appears that by using only u-channel and t-channel forces it is impossible to describe the experimental pion-nucleon phases above resonance in the P_{33}-wave. From the viewpoint of the quark-model this is natural, because here the Δ_{33}-resonance is, at least partly, a genuine three-quark state, and should not be described as a pure pion-nucleon resonance, but should be treated at the same footing as the nucleons. We take the same attitude to the other meson-baryon resonances as the $P_{11}(1440)$, the $S_{11}(1535)$, the $D_{13}(1700)$ etc. Therefore, we treat these resonances as follows. As we will see later, the resonance diagrams split nicely into a pole part, having a $(\sqrt{s} - M_B + i\epsilon)^{-1}$-factor, and a non-pole part having a $(\sqrt{s} + M_B - i\epsilon)^{-1}$-factor. Here, M_B is the so-called "bare" mass. As we will see in the following, the pole-position will move to $\sqrt{s} = M_R$, where M_R is the physical mass of the resonance. This determines the bare mass M_B.

To implement these ideas, we follow Haymaker [44]. We write the total potential V as a sum of a potential containing poles and a potential not containing poles $V(\mathbf{p}', \mathbf{p}) = V_s(\mathbf{p}', \mathbf{p}) + V_u(\mathbf{p}', \mathbf{p})$ [1], see Figure 5.1, where

$$V_s(\mathbf{p}', \mathbf{p}) = \sum_i \Gamma_i(\mathbf{p}')\ \Delta_i(P)\ \Gamma_i(\mathbf{p}) \tag{5.1}$$

is the pole part of the s-channel baryon exchanges. In Eq. (5.1) the right hand side is written in terms of the so-called 'bare' couplings and masses. We have $\Delta_i(P) = (\sqrt{s} - M_0 + i\epsilon)^{-1}$. (Here, and in the following, we denote the bare mass M_B by M_0.) The other part and the t-channel and u-channel exchanges are contained in $V_u(\mathbf{p}', \mathbf{p})$. In the following, we treat explicitly the cases when there is only one s-channel bound state or resonance present. It is easy to generalize this to the case with more s-channel poles. Following [44] we define two

[1] Note that in this chapter we have exclusively partial wave matrix elements. Notice also that in [44] the V- and T-matrices differ a (-)-sign with those used here.

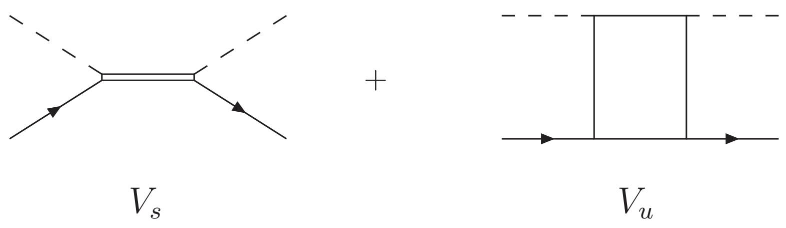

Figure 5.1: The pole potential V_s contains s-channel diagrams, the non-pole potential V_u contains t- and u-channel diagrams.

T-matrices T_j, $j = 1,2$ by

$$T_j = V_j + V_j\ G\ T\ ,\ T = T_1 + T_2\ , \tag{5.2}$$

where $V_1 := V_s$ and $V_2 := V_u$. The amplitude T_j is the sum of all graphs in the iteration of T in which‘ the potential V_j "acts last". Defining T_u as the T-matrix for the V_u interaction alone, i.e.

$$T_u = V_u + V_u\ G\ T_u\ , \tag{5.3}$$

it is shown in [44] that

$$T_1 = T_u + T_u\ G\ T_2\ ,\ T_2 = T_s + T_s\ G\ T_u\ , \tag{5.4}$$

with

$$T_s = V_s + V_s\ H_1\ T_s\ ,\ H_1 = G + G\ T_u\ G\ . \tag{5.5}$$

Taking together these results one obtains for the total T-matrix the expression

$$T = T_u + T_s + T_u\ G\ T_s + T_s\ G\ T_u + T_u\ G\ T_s\ G\ T_u\ . \tag{5.6}$$

Since V_s is a separable potential, the solution for T_s can be written as follows

$$T_s(\mathbf{p}',\mathbf{p}) = \frac{\Gamma(\mathbf{p}')\ \Gamma(\mathbf{p})}{\Delta(P)^{-1} - \Sigma(P)} \equiv \Gamma(\mathbf{p}')\ \Delta^*(P)\ \Gamma(\mathbf{p})\ , \tag{5.7}$$

where we introduced the shorthand $\Delta = \Delta_B$, and defined the self-energy Σ and the dressed propagator Δ^* by

$$\begin{aligned} \Sigma(P) &= \int \widetilde{dq'} \int \widetilde{dq''}\ \Gamma(\mathbf{q}')\ H_1(\mathbf{q}',\mathbf{q}'';P)\ \Gamma(\mathbf{q}'')\ , \\ \Delta^*(P) &= \frac{\Delta(P)}{1 - \Delta(P)\ \Sigma(P)} = \Delta(P) + \Delta(P)\ \Sigma(P)\ \Delta^*(P)\ , \end{aligned} \tag{5.8}$$

where $\widetilde{dq'} = d^3q'/(2\pi)^3$ etc.. Inserting Eqs. (5.7) and (5.8) in Eq. (5.6), and exploiting time-reversal and parity invariance which gives $T_u(\mathbf{p}',\mathbf{p}) = T_u(\mathbf{p},\mathbf{p}')$, one finds the expressions for the total amplitude, dressed vertex and self-energy

$$T(\mathbf{p}',\mathbf{p}) = T_u(\mathbf{p}',\mathbf{p}) + \Gamma^*(\mathbf{p}')\ \Delta^*(P)\ \Gamma^*(\mathbf{p})\ , \tag{5.9}$$

$$\Gamma^*(\mathbf{p}) = \Gamma(\mathbf{p}) + \int \widetilde{dq}\ \Gamma(\mathbf{q})\ G(q,P)\ T_u(\mathbf{q},\mathbf{p})\ , \tag{5.10}$$

$$\Sigma(P) = \int \widetilde{dq}\ \Gamma(\mathbf{q})\ G(q,P)\ \Gamma^*(\mathbf{q})\ , \tag{5.11}$$

where the dressed resonance propagator $\Delta^*(P)$ is given by

$$\Delta^*(P)^{-1} = \Delta(P)^{-1} - \Sigma(P)\ . \tag{5.12}$$

The equations above show that the complete T-matrix can be computed in a straightforward manner, using the full-off-shell T-matrix $T_u(p',p)$, defined in Eq. (5.3). The renormalized pole position $\sqrt{s} = M_R$ is determined by the condition

$$0 = \Delta^*(\sqrt{s} = M_R)^{-1} = \Delta(\sqrt{s} = M_R)^{-1} - \Sigma(\sqrt{s} = M_R)\ . \tag{5.13}$$

A diagrammatic representation of the previous derived equations for the meson-baryon amplitude, potential, dressed vertex and dressed propagator is given in Figure 5.2.

5.1 Partial wave analysis

The partial wave expansions for the vertex functions Γ and Γ^* read

$$\Gamma(\mathbf{p}) = \sqrt{4\pi}\sum_{L,M}\Gamma_L(p)\ Y_{L,M}(\hat{\mathbf{p}})\ ,\ \ \Gamma^*(\mathbf{p}) = \sqrt{4\pi}\sum_{L,M}\Gamma^*_L(p)\ Y_{L,M}(\hat{\mathbf{p}})\ , \tag{5.14}$$

and the partial wave expansions for the amplitude T reads

$$T(\mathbf{q},\mathbf{p}) = 4\pi\sum_{L,M} T_L(q,p)\ Y^*_{L,M}(\hat{\mathbf{q}})\ Y_{L,M}(\hat{\mathbf{p}})\ . \tag{5.15}$$

Then, the partial wave projection of the integrals in Eqs. (5.10) and (5.11) become

$$\begin{aligned} \Gamma^*_L(p) &= \Gamma_L(p) + \frac{1}{2\pi^2}\int q^2 dq\ \Gamma_L(q)\ G(q,P)\ T_{u,L}(q,p)\ , \\ \Sigma_L(P) &= \frac{1}{2\pi^2}\int q^2 dq\ \Gamma_L(q)\ G(q,P)\ \Gamma^*_L(q)\ . \end{aligned} \tag{5.16}$$

In the following subsections it is understood that we deal with the partial wave quantities. We suppress the angular momenta labels for notational convenience.

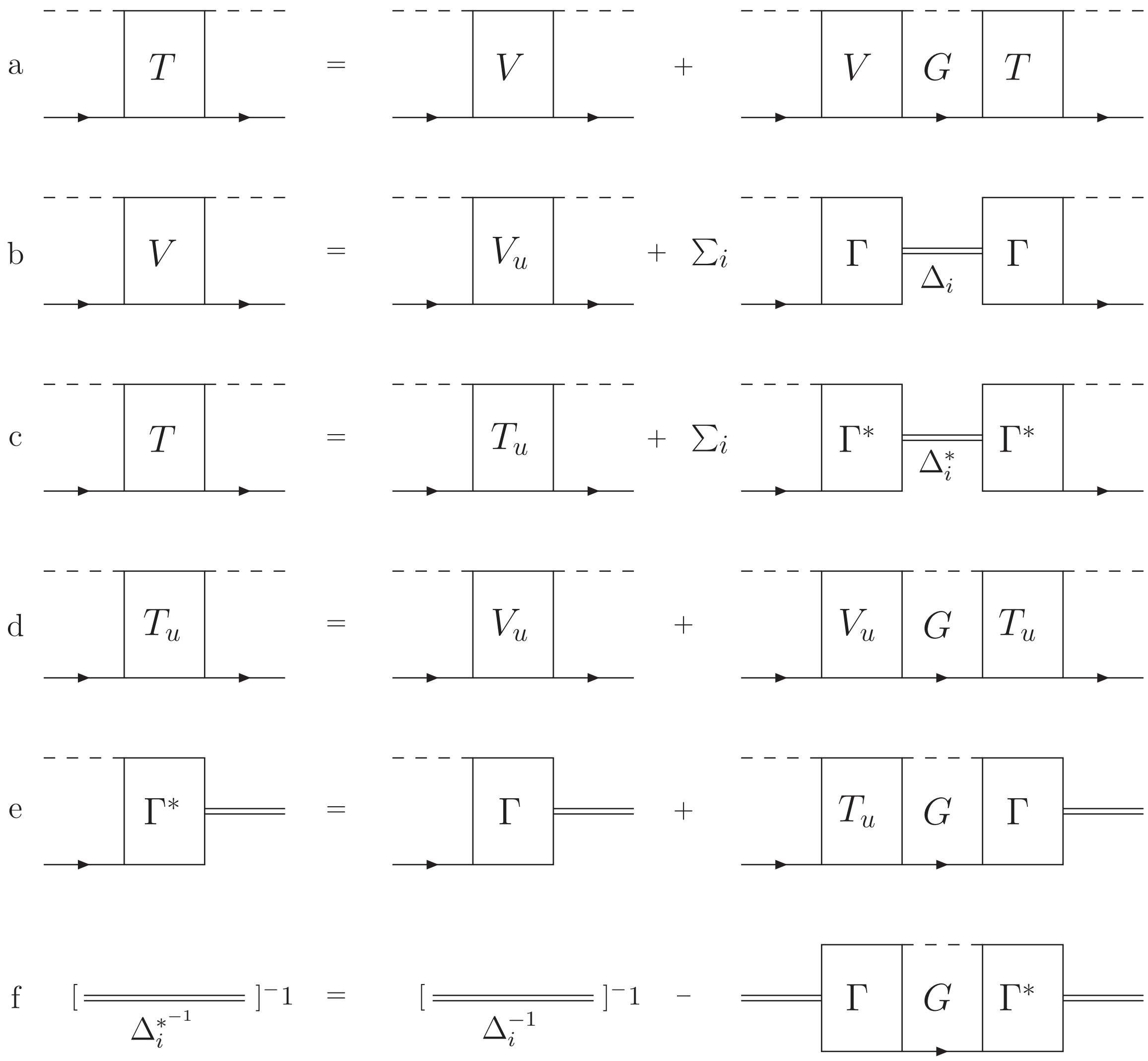

Figure 5.2: The integral equation for the amplitude in case of a non-pole and pole potential, a. integral equation for the amplitude Eq. (2.29), b. the potential in terms of the non-pole and pole potential, c. the amplitude in terms of the non-pole and pole amplitude Eq. (5.9), d. integral equation for the non-pole amplitude Eq. (5.3), e. equation for the dressed vertex Eq. (5.10), f. equation for the dressed propagator Eq. (5.12).

5.2 Multiplicative renormalization parameters

To start, in Eq. (5.9) the second part on the right hand side we consider to be given in terms of the bare resonance mass M_0 and the bare $\Delta N\pi$-coupling g_0. We consider only the wave function and $\Delta N\pi$-vertex renormalization for the resonance, and use the multiplicative renormalization method. Then, since the total Lagrangian is unchanged and hermitian, unitarity is preserved. The Z-transformation for the resonance field reads $\Psi_{0,\mu} = \sqrt{Z_2}\Psi_{r,\mu}$, and for the $\Delta N\pi$-coupling $g_0 = Z_g\ g_r$, where the subscripts r and 0 refer to respectively the 'renormalized, and 'bare' field. Applied to the $\Delta N\pi$ interaction this gives

$$\mathcal{L}_I \sim g_0\left[\bar{\Psi}_{0,\mu}\ \psi\right]\partial^\mu\phi = Z_g\sqrt{Z_2}\ g_r\left[\bar{\Psi}_{r,\mu}\ \psi\right]\partial^\mu\phi\ , \tag{5.17}$$

where $g_r = f_{\Delta N\pi}$ is the renormalized, i.e. the physical, and g_0 the unrenormalized, i.e. the bare coupling. Introducing the renormalization constant $Z_1 = Z_g\sqrt{Z_2}$, we have

$$\mathcal{L}_I \quad\sim\quad Z_1 g_r\left[\bar{\Psi}_{r,\mu}\ \psi\right]\partial^\mu\phi = g_r\left[\bar{\Psi}_{r,\mu}\ \psi\right]\partial^\mu\phi + (Z_1-1)g_r\left[\bar{\Psi}_{r,\mu}\ \psi\right]\partial^\mu\phi\ . \tag{5.18}$$

From the form of Eq. (5.10) it is useful at this stage to distinguish functions with the bare and physical couplings g_0 and g_r. Therefore, we introduce the vertex functions

$$\Gamma^*_{u,r}(p) = \Gamma_{u,r}(p) + \int \widetilde{dq}\ \Gamma_{u,r}(q)\ G(q)\ T_u(q,p)\ , \tag{5.19}$$

with the definitions

$$\Gamma_{u,r}(p) = g_{0,r}\ \bar{\Gamma}(p)\ ,\ \Gamma^*_{u,r}(p) = g_{0,r}\ \bar{\Gamma}^*(p)\ , \tag{5.20}$$

implying the relations

$$\Gamma_u(p) = Z_g\ \Gamma_r(p)\ ,\ \Gamma^*_u(p) = Z_g\ \Gamma^*_r(p)\ ,\ \Sigma_u(p) = Z_g^2\ \Sigma_r(p)\ . \tag{5.21}$$

(i) Resonance renormalization

Working out this renormalization scheme for the baryon resonances, we start, in Eq. (5.9) with the second part on the right hand side as given in terms of the bare resonance mass M_0 and bare $\Delta N\pi$-coupling g_0. We write this part of the amplitude as

$$T_{res}(p',p) = \Gamma^*_u(p')\frac{1}{\sqrt{s} - M_0 - \Sigma_u(\sqrt{s})}\ \Gamma^*_u(p)\ . \tag{5.22}$$

Next, we develop the denominator around the renormalized, i.e. the physical, resonance mass M_R and rearrange terms. We get

$$\begin{aligned}
T_{res}(p',p) \quad &= \quad \Gamma^*_u(p')\left\{\sqrt{s} - M_0 - \Sigma_u(M_R) - (\sqrt{s} - M_R)\frac{\partial\Sigma_u}{\partial\sqrt{s}}\ \ldots\right\}^{-1}\Gamma^*_u(p) \\
&= \quad \Gamma^*_u(p')\left\{(\sqrt{s} - M_R) - (\sqrt{s} - M_R)\frac{\partial\Sigma_u}{\partial\sqrt{s}}\ \ldots\right\}^{-1}\Gamma^*_u(p) \\
&= \quad \frac{\Gamma^*_u(p')\ Z_2\ \Gamma^*_u(p)}{(\sqrt{s} - M_R) - \frac{1}{2}(\sqrt{s} - M_R)^2\cdot Z_2\partial^2\Sigma_u/(\partial\sqrt{s})^2\ \ldots}\ .
\end{aligned} \tag{5.23}$$

Here, we have introduced the renormalization constant Z_2 defined by

$$Z_2 \equiv \left(1 - \left.\frac{\partial \Sigma_u}{\partial\sqrt{s}}\right|_{\sqrt{s}=M_R}\right)^{-1} = \left(1 - Z_g^2 \frac{\partial \Sigma_r}{\partial\sqrt{s}}\right)^{-1} = 1 + Z_1^2 \frac{\partial \Sigma_r}{\partial\sqrt{s}} \ . \tag{5.24}$$

Note that the derivatives in Eq. (5.23) w.r.t. $\sqrt{s}$ are evaluated at the point $\sqrt{s} = M_R$, as is indicated in Eq. (5.24).

Now we require that the residue at the resonance pole is given in terms of the physical coupling, i.e. g_r. In terms of the 'renormalized' quantities the amplitude T_{res} of Eq. (5.22) reads

$$T_{res}(p', p) = \Gamma^*_{ren}(p') \frac{1}{\sqrt{s} - M_R - \Sigma^{(2)}_{ren}(\sqrt{s})} \Gamma^*_{ren}(p) \ . \tag{5.25}$$

Here we have defined the 'renormalized' self-energy and the 'renormalized' dressed vertex

$$\Sigma^{(2)}_{ren} \equiv Z_2 \Sigma^{(2)}_u \ , \Gamma^*_{ren}(p) \equiv \sqrt{Z_2}\Gamma^*_u(p) \ . \tag{5.26}$$

The renormalized self-energy in the last expression in Eq. (5.23) and its first derivative are defined to be zero at the resonance position $\sqrt{s} = M_R$ and is given by

$$\begin{aligned} \Sigma^{(2)}_{ren}(\sqrt{s}) \ &\equiv \ \frac{1}{2}(\sqrt{s} - M_R)^2 \left.\frac{\partial^2 \Sigma_{ren}}{(\partial\sqrt{s})^2}\right|_{\sqrt{s}=M_R} + \ldots \\ &= \ \Sigma_{ren}(\sqrt{s}) - \Sigma_{ren}(M_R) - (\sqrt{s} - M_R) \left.\frac{\partial \Sigma_{ren}}{\partial\sqrt{s}}\right|_{\sqrt{s}=M_R} \ . \end{aligned} \tag{5.27}$$

We notice that the imaginary part of the self-energy is not changed by the wave function renormalization. It is straightforward to include $\Im\Sigma(\sqrt{s})$in the resonance mass M_R as well as in $\Sigma_{ren}(\sqrt{s})$.

The computation of the amplitude $T_{res}(p', p)$, Eq. (5.25), using renormalized quantities only runs as follows. From Eqs. (5.21) and (5.26) and the definition $Z_1 = Z_g\sqrt{Z_2}$ the renormalized vertex is given by

$$\Gamma^*_{ren}(p) = Z_1 \Gamma^*_r(p) \ . \tag{5.28}$$

Notice that $\Gamma^*_r(p_R) = \left|\Gamma^*_r(p_R)\right| exp(i\varphi^*_r(p_R))$*, and that this phase can be ignored when defining the effective decay Lagrangian in Eq. (5.18).* The renormalization condition for the vertex is that at the pole position ($\sqrt{s} = M_R$) the renormalized vertex is given in terms of the physical coupling constant

$$\left|\Gamma^*_{ren}(p = p_R)\right| = g_r \frac{p_R}{\sqrt{3}} \sqrt{E_R + M} = Z_1 \ \left|g_r \bar{\Gamma}^*(p = p_R)\right| \ , \tag{5.29}$$

which determines Z_1 and, by Eq. (5.24), Z_2 and Z_g, now the renormalized self-energy and the renormalized dressed vertex are known by Eq. (5.26). In passing we note that the coupling $g_r = f_{\Delta N\pi}/m_\pi$, and the other factors in the second expression of Eq. (5.29) are specific for a P_{33}-wave resonance.

As is clear from this section one can either express all quantities in terms of the bare parameters (M_0, g_0) or in terms of the renormalized parameters (M_R, g_r).

For the second part of this statement we now express the bare quantities in terms of the renormalized ones. From Eqs. (5.24) and (5.29) we know Z_g, thus

$$g_0^2 = Z_g^2 g_r^2 \; . \tag{5.30}$$

In the following, we denote the real part of the resonance mass by M_R. Also, we want to renormalize at a point which is experimentally accessible. Therefore, we choose for the renormalization point the real part of the resonance position, $\sqrt{s} = M_R$, so actually we consider the real part of the self energy, $\Re\Sigma$, in the previous derivations and from Eq. (5.23) we have

$$M_R = M_0 - g_0^2 \, \Re\bar{\Sigma}(M_R) \; , \tag{5.31}$$

giving the bare mass in terms of the renormalized quantities

$$M_0 = M_R - Z_g^2 g_r^2 \, \Re\bar{\Sigma}(M_R) \; . \tag{5.32}$$

This concludes the demonstration that one may start with the physical parameters and compute the bare parameters (g_0, M_0). Of course, in exploiting M_0 in order to force the pole position at the chosen $\sqrt{s} = M_R$ to be reasonable one must have $M_0 > 0$.

(ii) Nucleon pole renormalization

The renormalization of the nucleon pole is completely analogous to the resonance renormalization, except for the renormalization point, which is now the nucleon mass and thus below the pion-nucleon threshold. Here the Green function has no pole and is real. This implies that $\Re\Sigma(\sqrt{s_N}) = \Sigma(\sqrt{s_N})$, in contrast to the resonance case discussed above. All quantities in the expression for the self-energy, Eq. (5.11), are real at the nucleon pole.

The renormalization condition for the vertex, analogous to Eq. (5.29), is that at the nucleon pole position $(\sqrt{s} = M_N)$ the renormalized vertex is given in terms of the physical coupling constant

$$\left|\Gamma^*_{ren}(p = ip_N)\right| = \left| g_r \frac{\sqrt{3}\; i\; p_N}{\sqrt{E_N + M}} \right| = Z_1 \; \left| g_r \bar{\Gamma}^*(p = ip_N)\right| \; , \tag{5.33}$$

in case of ps-coupling and

$$\left|\Gamma^*_{ren}(p = ip_N)\right| = \left| \frac{f_r}{m_\pi} \frac{\sqrt{3}\; i\; p_N}{\sqrt{E_N + M}} (\sqrt{s} + M) \right| = Z_1 \; \left| g_r \bar{\Gamma}^*(p = ip_N)\right| \; , \tag{5.34}$$

in case of pv-coupling, which determines the renormalization constant Z_1. In passing we note that the factor in the second expression of Eqs. (5.33) and (5.34) is specific for a P_{11}-wave nucleon pole. Since the nucleon pole position lies below the pion-nucleon threshold, $\Gamma^*(ip_N)$ and in Eq. (5.10) $\Gamma(ip_N)$ and $T_u(q, ip_N)$ are imaginary.

5.3 Generalization to the multi-pole case

In case of multiple pole contributions we have the generalized expression for the pole potential Eq. (5.1)

$$V_s(\mathbf{p}', \mathbf{p}) = \sum_i \Gamma_i(\mathbf{p}')\ \Delta_i(P)\ \Gamma_i(\mathbf{p})\ . \tag{5.35}$$

From Eq. (5.5) one finds, using Eq. (5.35) that the pole amplitude T_s can be written as

$$T_s(\mathbf{p}', \mathbf{p}) = \sum_i \Gamma_i(\mathbf{p}')\ \Delta_i(P)\ A_i(\mathbf{p})\ . \tag{5.36}$$

Substituting this again in Eq. (5.5) one finds

$$\left[\Delta_i^{-1}(P)\delta_{ij} - \int\int \Gamma_i(\mathbf{p}'')\ H_1(\mathbf{p}'', \mathbf{p}')\ \Gamma_j(\mathbf{p}')\right]\Delta_j(P)A_j(\mathbf{p}) = \Gamma_i(\mathbf{p})\ , \tag{5.37}$$

which can be solved, and leads to the separable T_s-matrix

$$\begin{aligned} T_s(\mathbf{p}', \mathbf{p}) &= \sum_{ij} \Gamma_i(\mathbf{p}')\left(\Delta^{-1}(P) - \int\int \Gamma(\mathbf{p}'')\ H_1(\mathbf{p}'', \mathbf{p}')\ \Gamma(\mathbf{p}')\right)^{-1}_{ij} \Gamma_j(\mathbf{p}) \\ &\equiv \sum_{ij} \Gamma_i(\mathbf{p}')\left(\Delta^{-1}(P) - \Sigma(P)\right)^{-1}_{ij} \Gamma_j(\mathbf{p})\ , \end{aligned} \tag{5.38}$$

which obviously is a generalization of Eq. (5.7). In Eq. (5.38) the quantities $\Delta^{-1}(P)$, $\Gamma(\mathbf{p})$, and $H_1(\mathbf{p}', \mathbf{p})$ stand respectively for a diagonal matrix, a vector, and a constant in resonance-space. Above, we have introduced the generalized self-energy in resonance-space as

$$\Sigma_{ij}(P) = \int\int \Gamma_i(\mathbf{p}'')\ H_1(\mathbf{p}'', \mathbf{p}')\ \Gamma_j(\mathbf{p}')\ . \tag{5.39}$$

5.4 Baryon mixing

In this paragraph we consider the case of two different nucleon states, called N_1 and N_2. Apart from their masses they have identical quantum numbers. In particular, this applies to the ($I = \frac{1}{2}$, $J^P = \frac{1}{2}^+$)-states $N(940)$ and $N(1440)$, i.e. the P_{11}-wave. Obviously, the resonance-space is two-dimensional. Starting with the 'bare' states N_1 and N_2 these states will communicate with each other through the transition to the πN-states, and will themselves not be eigenstates of the strong Hamiltonian. The eigenstates of the strong Hamiltonian are identified with the physical states $N(940)$ and $N(1440)$, which are mixtures of N_1 and N_2. To perform the renormalization similarly to the case with only one resonance, we have in order to define the physical couplings at the physical states to diagonalize the propagator. This can be achieved using a complex orthogonal 2×2-matrix $\mathcal{O}$, $\mathcal{O}\widetilde{\mathcal{O}} = \widetilde{\mathcal{O}}\mathcal{O} = 1$. We can write, similar to Pascalutsa and Tjon [18],

$$\mathcal{O} = \begin{pmatrix} \cos\chi & \sin\chi \\ -\sin\chi & \cos\chi \end{pmatrix}\ , \tag{5.40}$$

where χ is the complex (N_1, N_2)-mixing angle. Now, since N_1 and N_2 have the same quantum numbers, apart from their couplings and masses, their πN-vertices are isomorphic. This implies that the self-energy matrix in Eq. (5.39) can be written as [2]

$$\begin{pmatrix} \Sigma_{11}(P) & \Sigma_{12}(P) \\ \Sigma_{21}(P) & \Sigma_{22}(P) \end{pmatrix}_u = \begin{pmatrix} g^2_{N_1N\pi} & g_{N_1N\pi}g_{N_2N\pi} \\ g_{N_1N\pi}g_{N_2N\pi} & g^2_{N_2N\pi} \end{pmatrix}_u \cdot \bar{\Sigma}(P)\,, \tag{5.41}$$

while for the vertices we have

$$\begin{pmatrix} \Gamma_{N_1} \\ \Gamma_{N_2} \end{pmatrix}_u = \begin{pmatrix} g_{N_1N\pi} \\ g_{N_2N\pi} \end{pmatrix}_u \cdot \bar{\Gamma}\,. \tag{5.42}$$

The propagator in Eq. (5.38) is diagonalized by the angle

$$\chi(P) \;=\; \frac{1}{2}\arctan\left\{2\left(\frac{g_{N_1N\pi}}{g_{N_2N\pi}} - \frac{g_{N_2N\pi}}{g_{N_1N\pi}} - \frac{M_{N_2}-M_{N_1}}{g_{N_1N\pi}g_{N_2N\pi}\,\Sigma(P)}\right)_u^{-1}\right\}. \tag{5.43}$$

We write $\Sigma = \Sigma_u$ in the following for notational convenience. The corresponding eigenvalues are

$$\begin{aligned} \Delta^*(P)^{-1}(\pm) \;&=\; \sqrt{s} - \frac{1}{2}(M_{0,1}+M_{0,2}) - \Sigma(\pm, P)\,, \\ \Sigma(\pm, P) \;&=\; \frac{1}{2}\left[(\Sigma_{11}+\Sigma_{22}) \pm \sqrt{\left(M_{0,2}-M_{0,1}+\Sigma_{22}-\Sigma_{11}\right)^2 + 4\Sigma_{12}^2}\,\right]. \end{aligned} \tag{5.44}$$

Here, we denoted the unrenormalized masses by $M_{0,1} = M_{N_1}$ for the nucleon, and by $M_{0,2} = M_{N_2}$ for the Roper-resonance. Likewise, the unrenormalized couplings are denoted as $g_{0,1} \equiv g_{N_1N\pi,u}$ and $g_{0,2} \equiv g_{N_2N\pi,u}$. Then, for example $\Sigma_{i,j}(P) = g_{0,i}g_{0,j}\bar{\Sigma}(P)$. The resonance amplitude T_{res} is a generalization of the second term in Eq. (5.9) and can be rewritten as follows

$$\begin{aligned} T_{res}(p', p) \;&=\; \sum_{ij} \Gamma_i^*(p')\;\Delta^*_{ij}(P)\Gamma_j^*(p) \\ &=\; \sum_i \left(\Gamma^*(p')\mathcal{O}\right)_i\;\left(\widetilde{\mathcal{O}}\Delta^*(P)\mathcal{O}\right)_{ij}\left(\widetilde{\mathcal{O}}\Gamma^*(p)\right)_j \\ &=\; \sum_{\alpha=\pm} \left(\Gamma^*(p')\mathcal{O}\right)_\alpha\; d_\alpha^{-1}(P)\;\left(\widetilde{\mathcal{O}}\Gamma^*(p)\right)_\alpha\,, \end{aligned} \tag{5.45}$$

where the diagonalized propagator is

$$d_\alpha(P) \;=\; \sqrt{s} - \frac{1}{2}(M_{0,1}+M_{0,2}) - \Sigma(\alpha, P)\,. \tag{5.46}$$

Unlike in [45] we renormalize the eigenstate $\alpha = (-)$ at the nucleon pole, and the eigenstate $\alpha = (+)$ at the Roper-resonance position. That is the reason why we formulate the procedure

[2] Notice that we distinguish the nucleon in the πN-state from $N_{1,2}$-states.

in terms of the 'bare' or unrenormalized parameters and not directly in terms of the physical parameters. This way we can utilize Eqs. (5.41) and (5.42). As we will see, we get four equations from the renormalization conditions on the masses and couplings, with the set of four unknowns $\left\{M_{0,1}, M_{0,2}, g_{0,1}, g_{0,2}\right\}$.

For both α-solutions we have, using $M_0 = (M_{0,1}+M_{0,2})/2$, that the resonance amplitude is

$$\begin{aligned}
T_{res}(\alpha) &= \Gamma^*_u(\alpha,p')\frac{1}{\sqrt{s}-M_0-\Sigma(\alpha,\sqrt{s})}\,\Gamma^*_u(\alpha,p) \\
&= \Gamma^*_u(\alpha,p')\left\{\sqrt{s}-M_0-\Sigma(\alpha,M_R(\alpha))-(\sqrt{s}-M_R(\alpha))\frac{\partial\Sigma(\alpha)}{\partial\sqrt{s}}\ldots\right\}^{-1}\Gamma^*_u(\alpha,p) \\
&= \Gamma^*_u(\alpha,p')\left\{(\sqrt{s}-M_R(\alpha))-(\sqrt{s}-M_R(\alpha))\frac{\partial\Sigma(\alpha)}{\partial\sqrt{s}}\ \ldots\right\}^{-1}\Gamma^*_u(\alpha,p) \\
&= \frac{\Gamma^*_u(\alpha,p')\ Z(\alpha)\ \Gamma^*_u(\alpha,p)}{(\sqrt{s}-M_R(\alpha)-\frac{1}{2}(\sqrt{s}-M_R(\alpha))^2\cdot Z(\alpha)\partial^2\Sigma(\alpha)/(\partial\sqrt{s})^2\ \ldots}\,, \qquad (5.47)
\end{aligned}$$

here we introduced the renormalization constants $Z(\alpha)$ defined by

$$Z(\alpha) \equiv \left(1-\left.\frac{\partial\Sigma(\alpha)}{\partial\sqrt{s}}\right|_{\sqrt{s}=M_R(\alpha)}\right)^{-1}. \qquad (5.48)$$

Also we can define $\Sigma_{ren}(\alpha,p) \equiv Z(\alpha)\Sigma(\alpha,p)$ similar to Eq. (5.26). Analogous to Eq. (5.27) we introduce the 'renormalized' self-energy by

$$\begin{aligned}
\Sigma^{(2)}_{ren}(\alpha,\sqrt{s}) &= \Sigma_{ren}(\alpha,\sqrt{s})-\Sigma_{ren}(\alpha,M_R(\alpha))-(\sqrt{s}-M_R(\alpha))\left.\frac{\partial\Sigma_{ren}(\alpha)}{\partial\sqrt{s}}\right|_{\sqrt{s}=M_R(\alpha)} \\
&= \frac{1}{2}(\sqrt{s}-M_R(\alpha))^2\left.\frac{\partial^2\Sigma_{ren}(\alpha)}{(\partial\sqrt{s})^2}\right|_{\sqrt{s}=M_R(\alpha)}+\ldots\,. \qquad (5.49)
\end{aligned}$$

The resonance amplitude $T_{res}(\alpha)$ in Eq. (5.47) in terms of the renormalized quantities reads

$$T_{res}(\alpha) = \Gamma^*_{ren}(\alpha,p')\frac{1}{\sqrt{s}-M_R(\alpha)-\Sigma^{(2)}_{ren}(\alpha,\sqrt{s})}\,\Gamma^*_{ren}(\alpha,p)\,, \qquad (5.50)$$

where the renormalized vertex is

$$\Gamma^*_{ren}(\alpha,p) \equiv \sqrt{Z(\alpha)}\ \Gamma^*_u(\alpha,p)\,. \qquad (5.51)$$

The renormalization is now performed by application of the following renormalization conditions:

(i) Mass-renormalization: The physical masses $M_R(\alpha)$ are given implicitly by

$$M_R(\alpha) = M_0+\Sigma\left(\alpha,\sqrt{s}=M_R(\alpha)\right)\,,\quad (\alpha=\pm)\,. \qquad (5.52)$$

(ii) Coupling-renormalization: The physical coupling constants $g_r(\alpha)$ are given by

$$\begin{aligned}\left|\lim_{\sqrt{s}\to M_R(\alpha)} \left(\sqrt{s}-M_R(\alpha)\right)\, T_{res}(\alpha)\right| &= \left|\Gamma^*_{ren}(\alpha,p_R)\right|^2 \\ &= Z(\alpha)\left|\Gamma^*_u(\alpha,p_R)\right|^2 \equiv \bar{g}^2_r(\alpha)\ . \end{aligned} \tag{5.53}$$

Eqs. (5.52) and (5.53) constitute four equations. These can be solved for the four bare parameters $\left\{M_{0,1}, M_{0,2}, g_{0,1}, g_{0,2}\right\}$ using as input the physical masses and coupling constants. We get

$$\begin{aligned} g_{0,1} &= g_{0,1}\left[g_r(+), g_r(-); M_R(+), M_R(-)\right]\ , \\ g_{0,2} &= g_{0,2}\left[g_r(+), g_r(-); M_R(+), M_R(-)\right]\ , \\ M_{0,1} &= M_{0,1}\left[g_r(+), g_r(-); M_R(+), M_R(-)\right]\ , \\ M_{0,2} &= M_{0,2}\left[g_r(+), g_r(-); M_R(+), M_R(-)\right]\ . \end{aligned} \tag{5.54}$$

From these we obtain the renormalization constants:

$$Z_g(-) \equiv g_{0,1}/g_r(-)\ \ ,\ \ Z_g(+) \equiv g_{0,2}/g_r(+)\ . \tag{5.55}$$

Notice that after the diagonalization of the propagator we have two uncoupled systems $\alpha = \pm$. Therefore, it is natural to define, in analogy with the single resonance case, the $Z_1(\alpha)$-factors by

$$\Gamma^*_{ren}(\alpha,p) = \sqrt{Z_2(\alpha)}\ \Gamma^*_u(\alpha,p) \equiv Z_1(\alpha)\ Z_g^{-1}(\alpha)\ \Gamma^*_u(\alpha,p) \equiv Z_1(\alpha)\ \Gamma^*_r(\alpha,p)\ , \tag{5.56}$$

where $Z_2(\alpha) \equiv Z(\alpha)$. Rotating back to the basis (N_1, N_2) we find the Z-transformation on the original basis before the diagonalization of the propagator. This Z-transformation on the unmixed fields is a 2×2-matrix. Note, that in Eqs. (5.55) and (5.56) we have defined several Z-factors suggestively. In order to find out how these constants are related to the Z-matrices alluded to above, we would have to work out this Z-transformation in detail. This we do not attempt, since it is not really necessary here.

From the input of the four physical parameters $\{M_R(\alpha), g_r(\alpha)\}$ one computes the bare parameters. Using the latter one computes $\Sigma_{ren}(\alpha,\sqrt{s})$ and $\Gamma^*_{ren}(\alpha,p)$. This defines the resonance part of the amplitudes unambiguously.

The four equations in Eqs. (5.52) and (5.53) can be solved numerically as follows. We write them schematically in the form

$$0 = a_i - f_i(x_1,x_2,x_3,x_4)\ \ (i = 1,2,3,4)\ , \tag{5.57}$$

where the x-components are the unrenormalized parameters, and the a-components the renormalized parameters. The solution of the equations is achieved by minimization of the squared distances $\chi_i^2 = (a_i - f_i(x))^2$. Variation of the unrenormalized parameters from a set of start initial values $x_0 = (x_1(0),\ldots,x_4(0)$ gives

$$\chi_i(x_0+\Delta x) \approx \chi_i(x_0) + \left.\frac{\partial\chi_i}{\partial x_p}\right|_{x=x_0} \Delta x_p\ . \tag{5.58}$$

Then the squared distance is

$$\chi^2(x_0+\Delta x) = \sum_i \chi_i^2(x_0+\Delta x) \approx \sum_i \chi_i^2(x_0) + 2\sum_i \chi_i(x_0)\sum_p \frac{\partial \chi_i}{\partial x_p}\Delta x_p + \sum_{p,q}\left(\sum_i \frac{\partial \chi_i}{\partial x_p}\frac{\partial \chi_i}{\partial x_q}\right)\Delta x_p \Delta x_q \; . \tag{5.59}$$

Searching for a minimum, we require $0 = \partial\chi^2/\partial\Delta x_k$, which gives the equations

$$0 = \sum_i \chi_i(x_0)\frac{\partial \chi_i}{\partial x_k} + \sum_q \sum_i \frac{\partial \chi_i}{\partial x_q}\frac{\partial \chi_i}{\partial x_k}\Delta x_q \; . \tag{5.60}$$

Introducing the matrix α by

$$\alpha_{k,q} = \sum_i \frac{\partial \chi_i}{\partial x_k}\frac{\partial \chi_i}{\partial x_q} \; , \tag{5.61}$$

we get an estimate for Δx_p by solving the linear equations

$$\Delta x_p = -\left(\alpha^{-1}\right)_{pq}\sum_i \chi_i(x_0)\frac{\partial \chi_i}{\partial x_q} \; . \tag{5.62}$$

Now one checks in the new point $x = x_0 + \Delta x$ the total χ^2. When this is not small enough one iterates further, until a minimum is reached.

Chapter 6

The πN interaction

In this chapter we show the results of the fit of the soft-core πN model to the most recent energy-dependent phase shift analysis (SM95) of Arndt et al. [1], which incorporates scattering data up to laboratory kinetic energy $T_{\rm lab} = 2.1$ GeV . We find a good agreement between the calculated and empirical phase shifts, up to $T_{\rm lab} = 600$ MeV for the lower partial waves.

The results of the fit to the Arndt phase shifts are shown in Figure 6.5. The soft-core πN model phase shifts are also compared with the Karlsruhe-Helsinki phase shift analysis (KH80), Koch and Pietarinen [46], in Figure 6.6. The fitted and fixed parameters of the soft-core model are given in Tables 6.3 and 6.4.

Some results of the renormalization procedure for the s-channel diagrams, discussed in Chapter 5, are given. The bare coupling constants and masses are listed in Table 6.4, and the energy dependence of the renormalized self energy of the nucleon and Δ are shown in Figure 6.4.

6.1 Introduction

The interaction between a pion and a nucleon has been investigated experimentally as well as theoretically for many years. For the early literature we would like to refer to Chew and Low [47], who presented one of the best early models that described the low energy P-wave scattering successfully, Hamilton [48] and the book of Bransden and Moorhouse [49].

Although the underlying dynamics of strong hadron interactions in general and the πN interaction specifically are believed to be given by quark-gluon interactions, it is in principle not possible to use these degrees of freedom to describe the low and intermediate energy strong interactions. This problem is related to the phase transition between low energy and high energy strong interactions and the nonperturbative nature of confinement. Instead an effective theory with meson and baryon degrees of freedom must be used to describe strong interaction phenomena at low and intermediate energies, at these energies the detailed quark-gluon structure of hadrons is expected to be unimportant.

In particular meson-exchange models have proven to be very successful in describing the low and intermediate energy baryon-baryon interactions for the NN and YN channels [50, 51, 52]. Similarly it is expected that this approach can also successfully be applied to the meson-baryon sector, i.e. πN, KN, $\bar{K}N$, etc...

The last decade the low and intermediate energy πN interaction has been studied theoretically, analogous to the NN interaction, in the framework of meson-exchange by several authors [53, 54, 55, 56, 57, 58, 18]. The KN interaction has been investigated in this framework only by the Jülich group [59, 19] and in this thesis. In the same way as the Nijmegen soft-core YN model was derived in the past as an $SU_f(3)$ extension of the Nijmegen soft-core NN model, we present a soft-core KN model which is an $SU_f(3)$ extension of the soft-core πN model given in this chapter. This will be discussed in the next chapter.

The above πN meson-exchange models have in common that besides the nucleon pole terms also the Δ pole terms are included explicitly, i.e. the Δ is not considered to be purely dynamically generated as a quasi-bound πN state, which might be possible if the πN potential is sufficiently attractive in the P_{33} wave. This possibility was investigated in the past by [60, 61]. From the quark model point of view the Δ resonance and other resonances are fundamental three-quark states and should be treated on the same footing as the nucleons.

We remark that the exact treatment of the propagator of the Δ and its coupling to πN is different in each model, Schütz et al [55]. use the same coupling and propagator for the Δ as we do.

The above πN models differ, however, in the treatment of the other resonances, $P_{11}(1440)$, $S_{11}(1535)$, etc... Gross and Surya [54] include the Roper resonance $P_{11}(1440)$ explicitly but the $S_{11}(1535)$ resonance is generated dynamically in their model, which gives a good description of the experimental data up to $T_{\rm lab} = 600$ MeV. Schütz et al. [55] do not include the Roper resonance explicitly but generate it dynamically. However their model describes the πN data only up to $T_{\rm lab} = 380$ MeV, and in this energy region the Roper is not expected to contribute much. Pascalutsa and Tjon [18] include the above resonances explicitly in their model in order to find a proper description of the experimental data up to $T_{\rm lab} = 600$ MeV.

The resonances that are relevant in the energy region we consider, the $\Delta(1232)$, $P_{11}(1440)$ and $S_{11}(1535)$, are included explicitly in the soft-core πN model, using the renormalization method described in Chapter 5.

Several other approaches to the πN interaction can be found in the literature, quark models have been used to describe πN scattering [62]. Also models in the framework of chiral perturbation theory exist, however, heavier degrees of freedom, such as vector mesons, are integrated out in this framework. We do not integrate out these degrees of freedom, but include them explicitly in the soft-core model.

For the πN interaction accurate experimental data exist over a wide range of energy and both energy-dependent and energy-independent phase shift analyses of that data have been made, [1, 46]. Several partial wave analyses for the πN interaction as well as for other interactions are available at http://gwdac.phys.gwu.edu/ (SAID).

6.2 The soft-core πN model

Our potential for the πN-interactions consists of the one-meson-exchange and one-baryon-exchange Feynman diagrams, derived from effective meson-baryon interaction Hamiltonians, see Chapter 4. The diagrams contributing to the πN potential are given in Figure 6.1. The partial wave potentials together with the pion-nucleon Green function constitute the kernel of the integral equation for the partial wave T-matrix, Eq. (3.17), which is solved numerically to find the observable quantities or the phase shifts. We solve the partial wave T-matrix by matrix inversion and we use the method introduced by Haftel and Tabakin [63] to deal numerically with singularities in the physical region in the Green function, for details we refer to Appendix E.

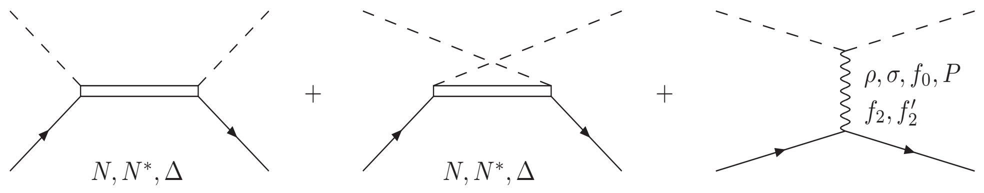

Figure 6.1: Contributions to the πN potential from the s-, u- and t-channel Feynman diagrams. The external dashed and solid lines are always the π and N respectively.

The interaction Hamiltonians from which the Feynman diagrams are derived, given in Chapter 4, are explicitly given below for the πN system. We use the pseudovector coupling for the $NN\pi$ vertex

$$\mathcal{H}_{NN\pi} = \frac{f_{NN\pi}}{m_{\pi^+}} \left(\bar{N}\gamma_5\gamma_\mu \boldsymbol{\tau} N\right) \cdot \partial^\mu \boldsymbol{\pi} , \tag{6.1}$$

the same structure is used for the Roper, and for the $S_{11}(1535)$ we use a similar coupling where the γ_5 is omitted. The $NN\pi$ coupling constant is quite well determined and is fixed in the fitting procedure. For the $N\Delta\pi$ vertex we use the conventional coupling

$$\mathcal{H}_{N\Delta\pi} = \frac{f_{N\Delta\pi}}{m_{\pi^+}} \left(\bar{N}\boldsymbol{T}\Delta_\mu\right) \cdot \partial^\mu \boldsymbol{\pi} + H.c. , \tag{6.2}$$

where $\boldsymbol{T}$ is the transition operator between isospin-$\frac{1}{2}$ isospin-$\frac{3}{2}$ states [42]. The only vector meson exchanged in πN scattering is the ρ. The $NN\rho$ and $\pi\pi\rho$ couplings we use are

$$\begin{aligned} \mathcal{H}_{NN\rho} &= g_{NN\rho}\left(\bar{N}\gamma_\mu \boldsymbol{\tau} N\right) \cdot \boldsymbol{\rho}^\mu + \frac{f_{NN\rho}}{4\mathcal{M}}\left(\bar{N}\sigma_{\mu\nu}\boldsymbol{\tau} N\right) \cdot \left(\partial^\mu \boldsymbol{\rho}^\nu - \partial^\nu \boldsymbol{\rho}^\mu\right) , \\ \mathcal{H}_{\pi\pi\rho} &= \frac{g_{\pi\pi\rho}}{2} \boldsymbol{\rho}_\mu \cdot \boldsymbol{\pi} \times \overset{\leftrightarrow\mu}{\partial} \boldsymbol{\pi} , \end{aligned} \tag{6.3}$$

we remark that the vector meson dominance model predicts the ratio of the tensor and vector coupling to be $\kappa_\rho = \frac{f_{NN\rho}}{g_{NN\rho}} = 3.7$, but in πN models it appears to be considerably lower [53, 57, 58, 18]. We also find a lower value for κ_ρ, see Table 6.3. The scalar meson couplings have the simple structure

$$\mathcal{H}_{NN\sigma} = g_{NN\sigma}\bar{N}N\sigma , \tag{6.4}$$

$$\mathcal{H}_{\pi\pi\sigma} = \frac{g_{\pi\pi\sigma}}{2} m_{\pi^+}\sigma\boldsymbol{\pi}\cdot\boldsymbol{\pi} . \tag{6.5}$$

In contrast with the other πN models, we consider the scalar mesons as genuine $SU_f(3)$ octet particles. Therefore not only the σ is exchanged but also the $f_0(975)$ having the same structure for the coupling, both giving an attractive contribution. The contribution of σ exchange is, however, much larger than the contribution of f_0 exchange. A repulsive contribution is obtained from Pomeron exchange, also having the same structure for the coupling. The contributions of the Pomeron and the scalar mesons cancel each other almost completely, as can be seen in the figures for the partial wave potentials, Figure 6.3. This cancellation is important in order to comply with the soft-pion theorems for low-energy pion-nucleon scattering [22, 23]. The σ and the ρ are treated as broad mesons, for details about the treatment we refer to [64].

The σ is not considered as an $SU_f(3)$ particle in the other πN models, but e.g. as an effective representation of correlated two-pion exchange [55, 56, 18], in that case its contribution may be repulsive in some partial waves.

We consider the exchange of the two isoscalar tensor mesons f_2 and f_2', the structure of the couplings we use is

$$\begin{aligned}
\mathcal{H}_{NNf_2} &= \left[\frac{iF_{1NNf_2}}{4}\bar{N}\left(\gamma_\mu \overset{\leftrightarrow}{\partial}_\nu + \gamma_\nu \overset{\leftrightarrow}{\partial}_\mu\right)N - \frac{F_{2NNf_2}}{4}\bar{N}\ \overset{\leftrightarrow}{\partial}{}^\mu \overset{\leftrightarrow}{\partial}{}^\nu\ N\right] f_2^{\mu\nu} , \\
\mathcal{H}_{\pi\pi f_2} &= \frac{g_{\pi\pi f_2}}{m_{\pi^+}}\ f_2^{\mu\nu}\left(\partial_\mu\boldsymbol{\pi}\cdot\partial_\nu\boldsymbol{\pi}\right) ,
\end{aligned} \tag{6.6}$$

and the coupling of f_2' is similar to the f_2 coupling. Similar as for the scalar mesons f_0 and σ, the f_2' contribution is very small compared to the f_2 contribution.

The spin-space structure of the amplitudes resulting from these interaction Hamiltonians is given in Chapter 4. The isospin structure results in the isospin factors for a given total isospin of the πN system, listed in Table 6.1, see also Appendix B for a derivation of the isospin factors. The spin-space amplitudes of Chapter 4 need to be multiplied by these isospin factors to find the complete πN amplitude. The masses, coupling constants and cut-off masses of the soft-core πN model that were fixed or fitted to the experimental data are given in Table 6.3.

Summarizing we consider in the t-channel the exchanges of the scalar mesons σ, f_0, the Pomeron, the vector meson ρ and the tensor mesons f_2 and f_2' , and in the u- and s-channel the exchanges of the baryons N, Δ, N^* (Roper) and S_{11}. The exchanges are given diagrammatically in Figure 6.1.

The latter two resonances were included in soft-core πN model to give a good description of the P_{11}- and S_{11}-wave phase shifts at higher energies, their contribution at lower energies is

Exchange	$I=\frac{1}{2}$	$I=\frac{3}{2}$
σ, f_0, f_2, f_2'	1	1
ρ	-2	1
$N(s-\text{channel})$	3	-
$N(u-\text{channel})$	-1	2
$\Delta(s-\text{channel})$	-	1
$\Delta(u-\text{channel})$	$\frac{4}{3}$	$\frac{1}{3}$

Table 6.1: The isospin factors for the various exchanges for a given total isospin I of the πN system, see Appendix B.

small. These resonances were also included in the model of Pascalutsa and Tjon [18].

It is instructive to examine the relative strength of the contributions of the various exchanges for each partial wave. The on shell partial wave potentials are given for each partial wave in Figure 6.3. The pole contributions for the Δ, Roper and S_{11} are omitted from the P_{33}-, P_{11}- and S_{11}-wave respectively to show the other contributions more clearly.

We remark that for the s-channel diagrams only the positive energy intermediate state develops a pole and is nonzero only in the partial wave having the same quantum numbers as the considered particle. The negative energy intermediate state (background contribution), which is also included in a Feynman diagram, see Figure 6.2, does not have a pole and may contribute to other waves having the same isospin. These background contributions from the nucleon and Δ pole to the S_{11}- and S_{31}-wave respectively are not small.

The Pomeron-σ cancellation is clearly seen in all partial waves. The nucleon exchange is quite strong in the P-waves, except for the P_{11}-wave where the nucleon pole is quite strong and gives a repulsive contribution, which causes the negative phase shifts at low energies in this wave. The change of sign of the phase shift in the P_{11}-wave is caused by the attractive ρ and Δ exchange.

The s-channel Δ exchange dominates the P_{33} -wave, but also a large contribution is present in the S_{31}-wave and a small contribution in the P_{31}-wave is seen. This contribution results from the spin-1/2 component of the Rarita-Schwinger propagator. The Δ exchange is present in all

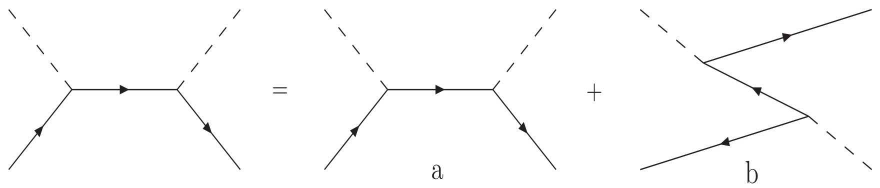

Figure 6.2: The two time-ordered contributions a and b to the s-channel Feynman graph. Graph a represents the positive energy intermediate state that develops a pole. Graph b represents the negative energy intermediate state.

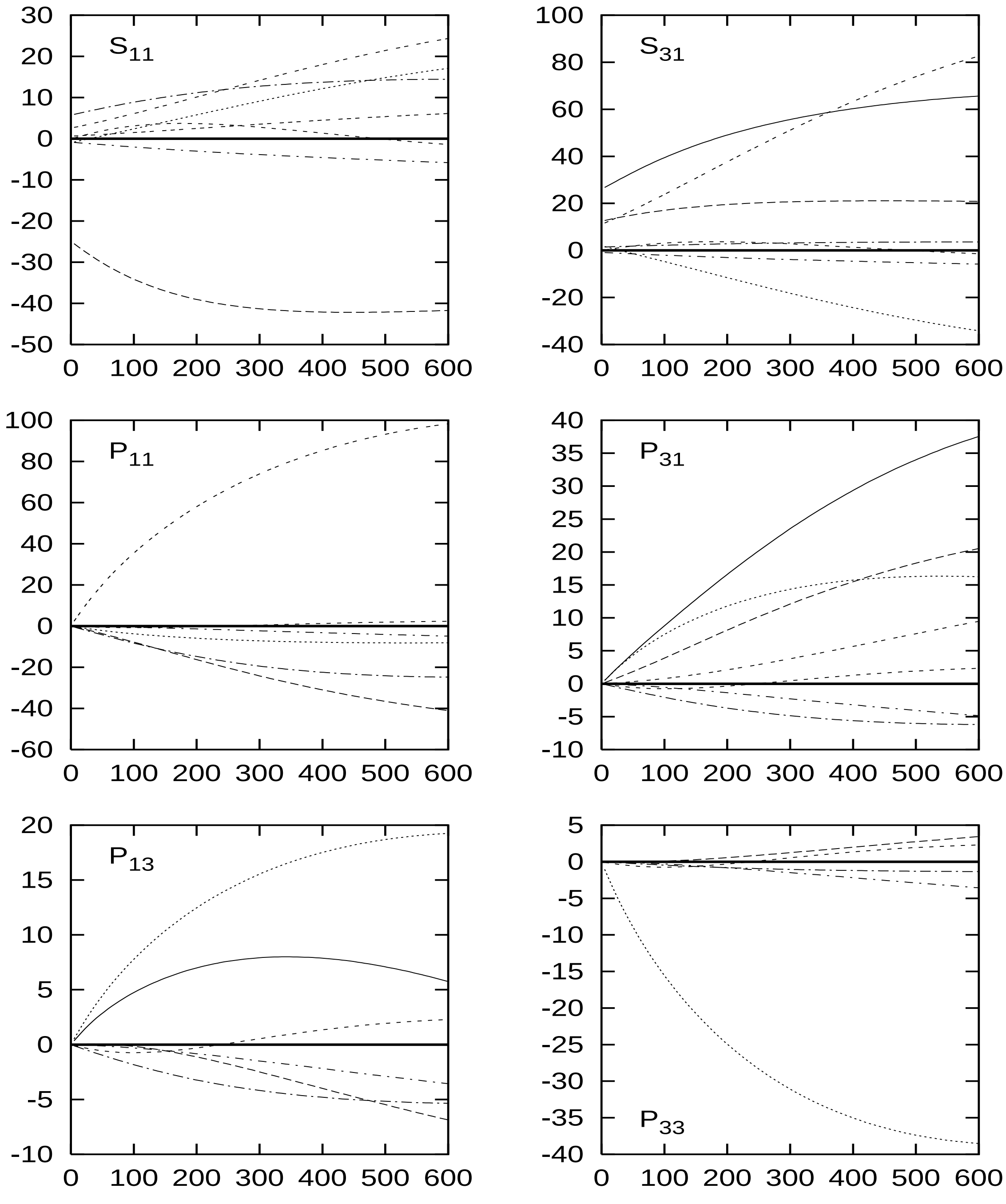

Figure 6.3: The total πN partial wave potentials V_L as a function of $T_{\rm lab}$ [MeV] are given by the solid line. For the S_{11}-, P_{11}- and P_{33}-wave the resonance pole and total contributions are omitted. The various contributions are a. the long dashed line: ρ, b. short dashed line: scalar mesons and Pomeron, c. the dotted line: nucleon exchange, d. the long dash-dotted line: Δ exchange, e. the short dash-dotted line: tensor mesons, f. the double dashed line: nucleon or Δ pole, g. the triple dashed line: Roper pole.

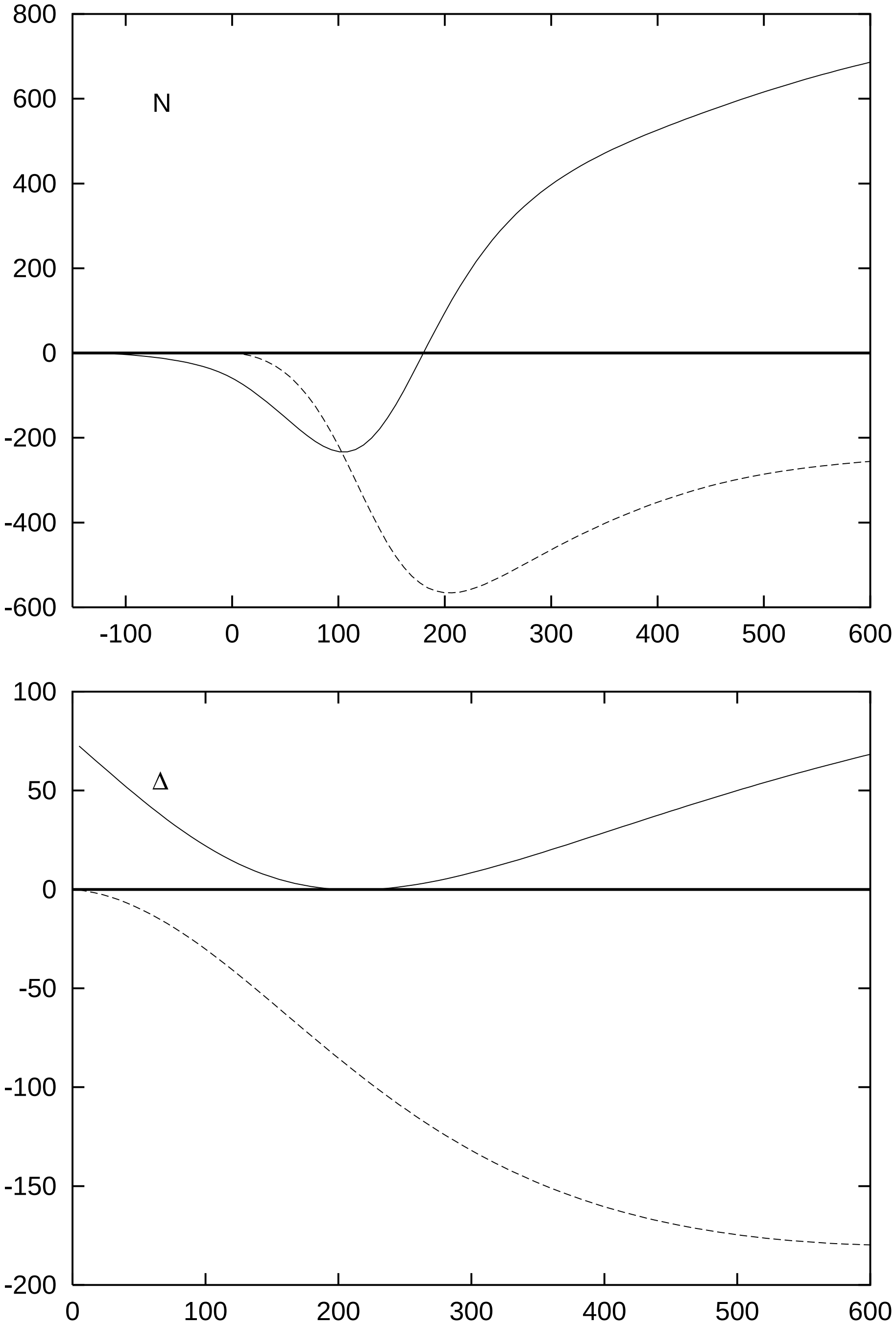

Figure 6.4: The renormalized self energy $\Sigma^{(2)}_{ren}$ [MeV] of Eqs. (5.49) and (5.27) for the nucleon and the Δ as a function of T_{lab} [MeV]. The real part is given by the solid line and the imaginary part is given by the dashed line.

partial waves. A significant contribution of ρ exchange is seen in all partial waves, except the P_{33}-wave, which is dominated by nucleon exchange and of course the Δ pole. A modest contribution from the tensor mesons is seen in all partial waves.

When solving the integral equation for the T-matrix, the propagator and vertices of the s-channel diagrams get dressed. The renormalization procedure, described in Chapter 5, determines the bare masses and coupling constants in terms of the physical parameters. The physical parameters and bare parameters obtained from the fitting procedure are given in Tables 6.3 and 6.4 respectively.

The self-energy of the baryons in the s-channel is renormalized, ensuring a pole at the physical mass of the baryons. For the nucleon and the Δ we show the energy dependence of the real and imaginary part of the renormalized self-energy in Figure 6.4. This figure clearly shows that the real part of the renormalized self-energy of the Δ and its derivative vanish at the Δ pole, by definition. This is of course also the case for the nucleon renormalized self-energy, however, the nucleon pole lies below the πN threshold.

6.3 Results and discussion for πN scattering

We have fitted the soft-core πN model to the energy dependent partial wave analysis of Arndt et al. [1] up to pion kinetic laboratory energy $T_{\text{lab}} = 600$ MeV. The results are shown in Figures 6.5 and 6.6, which show the calculated and empirical phase shift for the SM95 [1] and KH80 [46] phase shift analyses respectively. The calculated and empirical scattering lengths for the S- and P-waves, obtained from the partial wave analyses [1, 46], are listed in Table 6.2.

A good agreement between the soft-core πN model and the empirical phase shifts is found, but at higher energies some deviations are observed in some partial waves. These deviations may be caused by inelasticities, which become important at higher energies and have not been considered in this model. The scattering lengths have been reproduced quite well, except for the $I = \frac{1}{2}$ P-waves, here the soft-core model scattering lengths deviate a little from [1].

First we attempted to generate the Δ resonance in the P_{33}-wave dynamically, however, it was not possible to find the correct energy behavior for the P_{33} phase shift. Then we consid-

Scat. length	Model	SM95 [1]	KH80 [46]
S_{11}	0.171	0.172	0.173±0.003
S_{31}	-0.096	-0.097	-0.101±0.004
P_{11}	-0.060	-0.068	-0.081±0.002
P_{31}	-0.037	-0.040	-0.045±0.002
P_{13}	-0.031	-0.021	-0.030±0.002
P_{33}	0.213	0.209	0.214±0.002

Table 6.2: The calculated and empirical πN S-wave and P-wave scattering lengths in units of m_π^{-1} and m_π^{-3}.

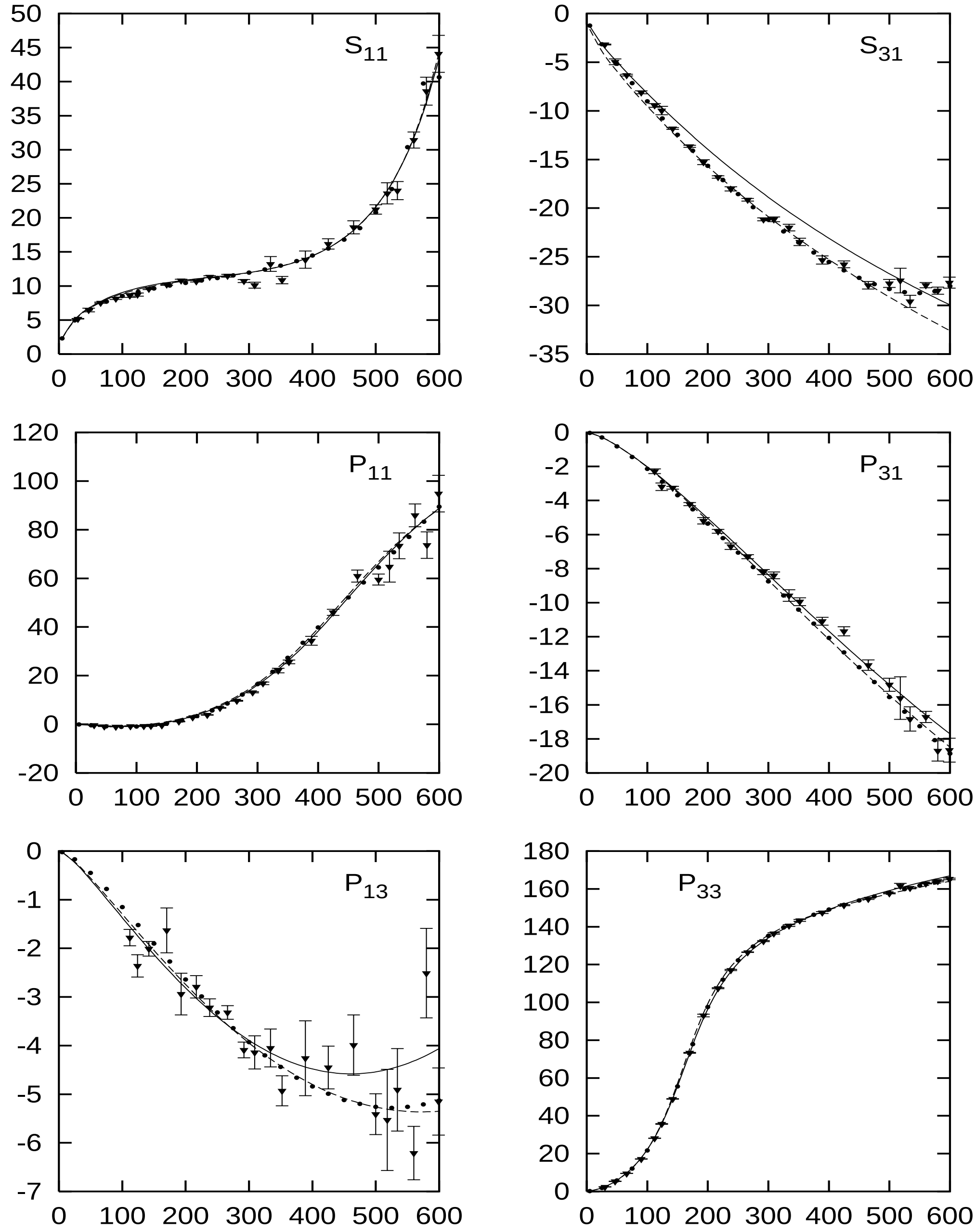

Figure 6.5: The S-wave and P-wave πN-phase shifts δ [degrees] as a function of $T_{\rm lab}$ [MeV]. The empirical phases are from the SM95 phase shift analysis, the dots are the multi energy phase shifts and the triangles with error bars are the single energy phase shifts. The soft-core πN model is given by the solid lines, the dashed line is the model without tensor mesons.

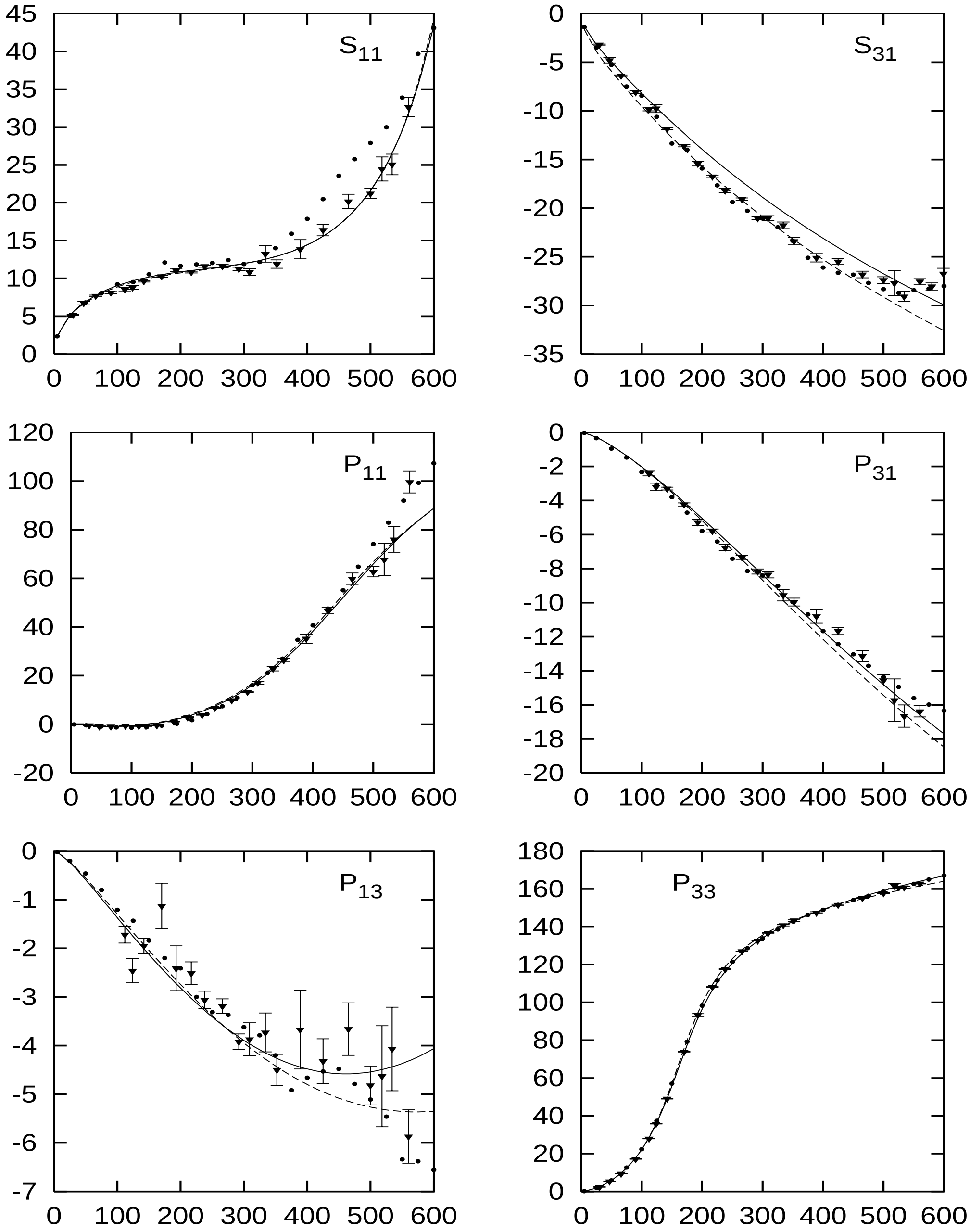

Figure 6.6: The S-wave and P-wave πN-phase shifts δ [degrees] as a function of T_{lab} [MeV]. The empirical phases are from the KH80 phase shift analysis, the dots are the multi energy phase shifts and the triangles with error bars are the single energy phase shifts. The soft-core πN model is given by the solid lines, the dashed line is the model without tensor mesons.

Exchange	Coupling Constants			Mass [MeV]	Λ [MeV]
ρ	$\frac{g_{NN\rho}g_{\pi\pi\rho}}{4\pi}$	$=$ 1.333	$\frac{f_{NN\rho}}{g_{NN\rho}} = 2.121$	770.00*	838.36
σ	$\frac{g_{NN\sigma}g_{\pi\pi\sigma}}{4\pi}$	$=$ 26.196*		760.00*	1126.46
f_0	$\frac{g_{NNf_0}g_{\pi\pi f_0}}{4\pi}$	$=$ -1.997*		975.00*	1126.46
f_2	$\frac{g_{NNf_2}g_{\pi\pi p_2}}{4\pi}$	$=$ 0.157*	$\frac{f_{NNf_2}}{g_{NNf_2}} = 0.382$*	1270.00*	411.94
f_2'	$\frac{g_{NNf_2'}g_{\pi\pi f_2'}}{4\pi}$	$=$ 0.003*	$\frac{f_{NNf_2'}}{g_{NNf_2'}} = 3.393$*	1525.00*	411.94
Pomeron	$\frac{g_{NNP}g_{\pi\pi P}}{4\pi}$	$=$ 4.135		315.32	
N	$\frac{f_{NN\pi}^2}{4\pi}$	$=$ 0.075*		938.27*	665.37
Δ	$\frac{f_{N\Delta\pi}^2}{4\pi}$	$=$ 0.478		1254.38	603.22
N^*	$\frac{f_{NN^*\pi}^2}{4\pi}$	$=$ 0.023		1439.68	665.37
S_{11}	$\frac{f_{NS_{11}\pi}^2}{4\pi}$	$=$ 0.003		1567.14	653.46

Table 6.3: Soft-core πN model parameters: the coupling constants, masses and cut-off masses of the exchanged particles. Numbers with an asterisk were fixed in the fitting procedure.

ered the Δ resonance, at least partially, as a three-quark state and included it explicitly in the potential, as is done in the modern pion-nucleon literature, and immediately found the correct energy behavior for the P_{33} phase shift. The other resonances have been treated in the same way.

We use six different cut off masses, which are free parameters in the fitting procedure. For the nucleon $N(938)$ and the Roper $N^*(1440)$ resonance we use the same cut off mass, for the two scalar mesons we use the same cut off mass and also for the two tensor mesons the same cut off mass is used. The masses of the mesons and the nucleon have been fixed in the fitting procedure, but the masses of the resonances are free parameters.

Table 6.3 shows that the pole positions of these resonances are not necessarily exactly the same as the resonance positions, due to the non-resonance part of the amplitude, see Eq. (5.9). The Δ and Roper resonate at respectively $\sqrt{s} = 1232$ MeV and $\sqrt{s} = 1440$ MeV while the poles are located at $\sqrt{s} = 1254$ MeV and $\sqrt{s} = 1440$ MeV respectively.

In order to obtain a good fit, we had to introduce an off-mass-shell damping for the u-channel Δ-exchange, we used the factor $e^{(u-M_\Delta^2)\gamma^2/M_\Delta^2}$, where γ was a free parameter in the fitting procedure and was found to be $\gamma = 1.18$.

Only the product of two coupling constants are determined in the fitting procedure. Therefore the triple-meson coupling constants are fixed at the value calculated from their decay width, see subsection 6.3.1, and the baryon-baryon-meson coupling constant is a free parameter in the fitting procedure. The resonance coupling constants are first calculated from their decay width, see subsection 6.3.1, but are also treated as free parameters. The fitted values deviate only a little from the calculated values.

The soft-core πN model has 17 free physical fit parameters; 3 meson and Pomeron coupling constants, 6 cut off masses, 4 masses, 3 decay coupling constants and γ. The values of the coupling constants, listed in Table 6.3, are in good agreement with the litera-

Exchange	Bare Coupling Constants	Bare Mass [MeV]
N	$\frac{f^2_{0NN\pi}}{4\pi} = 0.013$	1186.53
Δ	$\frac{f^2_{0N\Delta\pi}}{4\pi} = 0.167$	1399.12
N^*	$\frac{f^2_{0NN^*\pi}}{4\pi} = 0.015$	1831.21
S_{11}	$\frac{f^2_{0NS_{11}\pi}}{4\pi} = 0.018$	1774.38

Table 6.4: Renormalization parameters: bare masses and coupling constants. The renormalization conditions determine the bare parameters in terms of the model parameters of Table 6.3 .

ture; $g_{NN\rho} = 0.83$ and $g_{NN\sigma} = 2.57$. However, the tensor coupling constant for the ρ, $f_{NN\rho}/g_{NN\rho} = 2.12$ is small compared with values obtained in NN models and the vector dominance value of 3.7. Other πN models, [18, 53], also suffer from this problem. The $NN\pi$ coupling constant, which is quite well determined in the NN interaction, has been fixed in the soft-core πN model. We notice that for the tensor mesons we used the coupling constants $g_T = \mathcal{M}F_1 + \mathcal{M}^2 F_2$ and $f_T = -\mathcal{M}^2 F_2$ in Table 6.3.

The two conditions in the renormalization procedure for the pole contributions result in the two renormalization constants, listed in Table 6.4, the bare coupling constant and mass. These constants are determined by the soft-core model, via the renormalization conditions. We found the bare coupling constants to be smaller than the physical coupling constants except for the S_{11} resonance. The bare masses are larger then the physical masses for each type of exchange, the interaction shifts the bare mass down to the physical mass. Pascalutsa and Tjon [18] find a larger physical mass than bare mass for the Roper. This is probably caused by the choice of the renormalization point. They renormalize the Roper contribution at the nucleon pole, we think it is more natural to perform the renormalization at the Roper pole.

Besides the presented soft-core πN model, we also considered a model that does not contain tensor mesons. We fitted this model to the empirical phase shifts and the results of the fit are given by the dashed lines in Figures 6.5 and 6.6. We notice that in two partial waves a noticeable difference can be seen between the two models, the S_{11} partial wave is described better by this model than by the soft-core πN model. It is hard to say which model works better for the P_{13} partial wave, since the single energy phase shifts have large error bars and both models are in agreement with the P_{13} phase shifts. The tensor mesons are important for a good description of the KN data, this is shown in the next chapter. The πN scattering lengths are approximately the same for both models.

The parameters belonging to this model are listed in Table 6.5, and the bare masses and coupling constants are given in Table 6.6. The values of these parameters are essentially the same as the soft-core πN parameters.

Since the S-wave scattering lengths are reproduced well, the soft-pion theorems for low-energy pion-nucleon scattering [22, 23] are satisfied in the soft-core πN model, without the need for a derivative coupling for the $\pi\pi\sigma$-vertex, as was claimed by Pascalutsa and Tjon [18]. In view of chiral perturbation theory inspired models, the chiral c_1-, c_3- and c_4-terms are described implicitly by the soft-core πN model, since this model gives a good description of

Exchange	Coupling Constants			Mass	Λ
ρ	$\frac{g_{NN\rho}g_{\pi\pi\rho}}{4\pi}$	$=$ 1.282	$\frac{f_{NN\rho}}{g_{NN\rho}} = 1.730$	770.00*	716.82
σ	$\frac{g_{NN\sigma}g_{\pi\pi\sigma}}{4\pi}$	$=$ 26.196*		760.00*	864.22
f_0	$\frac{g_{NNf_0}g_{\pi\pi f_0}}{4\pi}$	$=$ -1.997*		975.00*	864.22
Pomeron	$\frac{g_{NNP}g_{\pi\pi P}}{4\pi}$	$=$ 4.453		295.73	
N	$\frac{f^2_{NN\pi}}{4\pi}$	$=$ 0.075*		938.27*	728.10
Δ	$\frac{f^2_{N\Delta\pi}}{4\pi}$	$=$ 0.470		1248.54	659.09
N^*	$\frac{f^2_{NN^*\pi}}{4\pi}$	$=$ 0.021		1440.71	728.10
S_{11}	$\frac{f_{NS^2_{11}\pi}}{4\pi}$	$=$ 0.003		1556.64	482.43

Table 6.5: Parameters of the soft-core πN model without tensor mesons: the coupling constants, masses and cut-off masses (in MeV) of the exchanged particles. Numbers with an asterisk were fixed in the fitting procedure.

Exchange	Bare Coupling Constants	Bare Mass
N	$\frac{f^2_{0NN\pi}}{4\pi} = 0.011$	1203.40
Δ	$\frac{f^2_{0N\Delta\pi}}{4\pi} = 0.159$	1417.22
N^*	$\frac{f^2_{0NN^*\pi}}{4\pi} = 0.022$	1943.64
S_{11}	$\frac{f_{0NS^2_{11}\pi}}{4\pi} = 0.016$	1601.58

Table 6.6: Renormalization parameters of the soft-core πN model without tensor mesons: bare masses (in MeV) and coupling constants. The renormalization conditions determine the bare parameters in terms of the model parameters of Table 6.3.

the empirical phase shifts.

6.3.1 Decay coupling constants

The physical coupling constants of the resonances included in the soft-core πN model can be estimated by relating the width of the resonance to the T-matrix element of its decay into two particles, in this case πN. This relation for the two-particle decay is derived in [26], the two-particle width is

$$\Gamma(p) \;=\; \frac{p}{4M^2}\int \frac{d\cos\theta}{4\pi}\sum_\sigma |T|^2, \tag{6.7}$$

where M is the resonance mass and the absolute square of the T-matrix is summed over the nucleon spin. The decay processes $\Delta \to \pi N$, $N^* \to \pi N$ and $S_{11} \to \pi N$ is considered in order to find an estimate for the coupling constants $f_{\pi N\Delta}$, $g_{\pi NN^*}$ and $g_{\pi NS_{11}}$ respectively. The T-matrix elements of the various decays in lowest order can be calculated using the interaction Hamiltonians defined in Chapter 4 and Eq. (6.7) gives us the estimates for the coupling constants

$$
\begin{aligned}
\frac{f^2_{\pi N\Delta}}{4\pi} &= 3\frac{M_\Delta}{E+M}\frac{m^2_{\pi^+}\Gamma}{p^3} \simeq 0.39\,, \\
\frac{f^2_{\pi NN^*}}{4\pi} &= \frac{2}{3}\frac{m^2_{\pi^+}}{\left(M_{R_{11}}+M\right)^2}\frac{(E+M)M_{R_{11}}\Gamma}{p^3} \simeq 0.023\,, \\
\frac{f^2_{\pi NS_{11}}}{4\pi} &= \frac{2}{3}\frac{m^2_{\pi^+}}{\left(M_{S_{11}}-M\right)^2}\frac{M_{S_{11}}}{E+M}\frac{\Gamma}{p} \simeq 0.004\,.
\end{aligned}
\tag{6.8}
$$

The numerical values are obtained by using the Breit-Wigner masses and widths from the Particle Data Group. In fitting the data, the fitted values for the resonance masses and coupling constants should not differ too much from the values above.

The coupling constant for the decay of the ρ, σ and f_2 into two pions can be estimated in the same way using the triple meson interaction Hamiltonians defined in Chapter 4, we find

$$
\begin{aligned}
\frac{g^2_{\pi\pi\rho}}{\sqrt{4\pi}} &= \frac{3}{2}m^2_\rho\frac{\Gamma}{p^3} \simeq 1.70\,, \\
\frac{g^2_{\pi\pi\sigma}}{\sqrt{4\pi}} &= 2\frac{m^2_\sigma}{m^2_{\pi^+}}\frac{\Gamma}{p} \simeq 10.6\,, \\
\frac{g^2_{\pi\pi f_2}}{\sqrt{4\pi}} &= \frac{15}{16}m^2_{f_2}m^2_{\pi^+}\frac{\Gamma}{p^5} \simeq 0.224\,.
\end{aligned}
\tag{6.9}
$$

Chapter 7

The K^+N interaction

In this chapter we present the soft-core kaon-nucleon (KN) model, which is obtained by an $SU_f(3)$ extension of the soft-core πN model. With kaons we mean the positive strangeness kaons $K^+ = u\bar{s}$ and $K^0 = d\bar{s}$. The negative strangeness kaons $K^- = \bar{u}s$ and $\bar{K}^0 = \bar{d}s$ are referred to as antikaons, and are not considered in this thesis.

We show the results of the fit of the soft-core KN model to the energy-dependent phase shift analysis (SP92) of Hyslop et al. [2], which incorporates scattering data up to laboratory kinetic energy $T_{\text{lab}} = 2.65$ GeV. The soft-core model phase shifts are also compared with the single energy phase shift analyses of Hashimoto [65] and Watts et al. [66]. We find a fair agreement between the calculated and empirical phase shifts, up to $T_{\text{lab}} = 600$ MeV for the lower partial waves. The results of the fit are shown in Figures 7.4 and 7.5 and the fitted and fixed parameters of the soft-core KN model are given in Table 7.3.

Since the various phase shift analyses [2, 65, 66] are not always consistent and have quite large error bars, we also give a comparison between the experimental observables (total cross sections, differential cross sections and polarizations) and their model predictions. The total elastic cross sections for both the isospin $I = 0$ and $I = 1$ channel up to T_{lab}=600 MeV are shown in Figure 7.6. The differential cross sections for the elastic processes $K^+p \to K^+p$ and $K^+n \to K^+n$ at various values of T_{lab} can be found in Figures 7.7 and 7.8. For the same elastic processes, the polarizations at various values of T_{lab} are shown in Figure 7.9.

7.1 Introduction

Contrary to pions, the kaon (K) and antikaon ($\bar{K}$) interaction with the nucleons is completely different. This is due to the difference in strangeness, which is conserved in strong interactions. Kaons have strangeness $S = 1$, meaning that they contain an $\bar{s}$-quark and a u- or d-quark in case of K^+ and K^0 respectively. Antikaons have strangeness $s = -1$, meaning that they contain an s-quark and a $\bar{u}$- or $\bar{d}$-quark in case of K^- and $\bar{K}^0$ respectively. Since the $\bar{u}$- or $\bar{d}$-quark of the antikaon can annihilate with a u- or d-quark of the nucleon, the $\bar{K}N$ interaction is strong because low-lying resonances can be produced, giving a large cross section. This situation can be compared with the Δ-resonance in πN interactions.

The $\bar{s}$-quark of the kaon can not annihilate with one of the quarks of the nucleon in strong interactions, therefore three-quark resonances can not be produced, only heavy exotic five-quark ($qqqq\bar{q}$) resonances (referred to as Z^* in the old literature or the pentaquark Θ^+ in the new literature) can be formed, so the KN interaction is weak at energies below the energy of Z^*. The cross sections are not large and the S-wave phase shifts are repulsive.

However, in four recent photo-production experiments [3, 67, 68, 69] indications are found for the existence of a narrow exotic $S = 1$ light resonance in the $I = 0$ KN system with $\sqrt{s} \simeq 1540$ MeV and $\Gamma \leq 25$ MeV. The existence of such an exotic resonance was predicted by Diakonov et al. [70], they predicted the exotic resonance to have a mass of about 1530 MeV and a width of less than 15 MeV and spin-parity $J^P = \frac{1}{2}^+$.

The existing KN scattering data, which we use to fit the soft-core KN model, does, however, not show this low-lying exotic resonance. On the other hand, this exotic resonance has not been searched for at low energies in the scattering experiments. At these energies not much scattering data exists and a narrow resonance could have escaped detection.

For the early literature on the K^+N interaction we would like to refer to the review article by Dover and Walker [71]. The K^+N interaction has been studied a few years ago by the Jülich group, they presented a model in the meson-exchange framework, Bütgen et al. [59] and Hoffmann et al. [19], in analogy to the Bonn NN model [72].

In [59] a reasonable description of the empirical phase shifts is obtained, here not only single particle exchanges, (σ,ρ,ω,Λ,Σ,Y^*), are included in the KN model, also fourth-order processes with N, Δ, K and K^* intermediate states are included in analogy to the Bonn NN model, in which σ-exchange effectively represents correlated two-pion-exchange. Coupling constants involving strange particles are obtained from the known $NN\pi$ and $\pi\pi\rho$ coupling constants assuming $SU(6)$ symmetry.

However an exception had to be made for the ω-coupling, which had to be increased by 60% in order to find enough short-range repulsion and to obtain a reasonable description of the S-wave phase shifts, model A. But this also caused too much repulsion in the higher partial waves and it was concluded that the necessary repulsion had to be of much shorter range. In model B the ω coupling was kept at its symmetry value and a phenomenological short-ranged repulsive σ_0 with a mass of 1200 MeV was introduced, which led to a more satisfactory description of the empirical phase shifts.

In [19] the model of [59] is extended by replacing the σ- and ρ-exchange by the correlated two-pion-exchange. A satisfactory description of the experimental observables up to $T_{\rm lab}$=600 MeV, having the same quality as in [59], is achieved. Just as in [59] the phenomenological short ranged σ_0 was needed in this model in order to keep the ω coupling at its symmetry value. Bütgen et al. suggest that this short ranged σ_0 might be seen as a real scalar meson or perhaps as a real quark-gluon effect.

The most recent quark models for the KN interaction are from Barnes and Swanson [73], Silvestre-Brac et al. [74, 75] and Lemaire et al. [76, 77]. The agreement of these quark models with the experimental data is not good. The results of [74]- [77] show that there is enough repulsion in the S-waves, but the other waves can not be described well.

Recently a hybrid model for the KN interaction was published by Hadjimichef et al. [78]. They used the Jülich model extended by the inclusion of the isovector scalar meson $a_0(980)$ exchange, which was taken into account in the Bonn NN model [72], but not in the Jülich KN models [59, 19]. The short ranged phenomenological σ_0 exchange was replaced by quark-gluon exchange. A nonrelativistic quark model, in which one-gluon-exchange and the interchange of the quarks is considered, was used. This quark-gluon exchange is, contrary to the σ_0 exchange, isospin dependent. A satisfactory description of the empirical phase shifts, having the same quality as [19], was obtained. However Hadjimichef et al. conjecture that the short ranged quark-gluon dynamics they include could perhaps be replaced by the exchange of heavier vector mesons.

Another approach for the KN interaction is given by Lutz and Kolmeitsev [79]. Meson-baryon interactions in general and KN interactions specifically are studied by means of chiral Lagrangians in this work. A reasonable description of the KN differential cross sections and phase shifts was achieved, but only up to $T_{\rm lab} = 360$ MeV.

The basis of our KN model is the soft-core πN model, which is a more natural basis than the NN model [72] in case of the Jülich KN models [59, 19].

7.2 The soft-core KN model

The soft-core model for the KN-interactions is an $SU_f(3)$ extension of the soft-core πN model and consists analogously of the one-meson-exchange and one-baryon-exchange Feynman diagrams, derived from effective meson-baryon interaction Hamiltonians, see Chapter 4. The various diagrams contributing to the KN potential are given in Figure 7.1.

The interaction Hamiltonians from which the Feynman diagrams for the KN system are derived, are explicitly given below. We use the pseudovector coupling for the $N\Lambda K$ and $N\Sigma K$ vertex

$$\begin{aligned} \mathcal{H}_{N\Lambda K} &= \frac{f_{N\Lambda K}}{m_{\pi^+}}\left(\bar{N}\gamma_5\gamma_\mu\partial^\mu K\right)\Lambda + H.c.\,, \\ \mathcal{H}_{N\Sigma K} &= \frac{f_{N\Sigma K}}{m_{\pi^+}}\left(\bar{N}\gamma_5\gamma_\mu\boldsymbol{\tau}\partial^\mu K\right)\cdot\Sigma + H.c.\,, \end{aligned} \tag{7.1}$$

the coupling constants are determined by the $NN\pi$ coupling constant and the $F/(F+D)$-ratio, α_{ps}. For the $N\Sigma^*K$ vertex we use, just as for the $N\Delta\pi$ vertex, the conventional coupling

$$\mathcal{H}_{N\Sigma^*K} = \frac{f_{N\Sigma^*K}}{m_{\pi^+}}\left(\bar{N}\boldsymbol{\tau}\partial^\mu K\right)\cdot\Sigma^*_\mu + H.c.\,. \tag{7.2}$$

Since the $SU_f(3)$ decuplet occurs only once in the direct product of two octets, there is no mixing parameter α for this coupling. The $N\Sigma^*K$ coupling constant is determined by $SU_f(3)$ to be $f^2_{N\Sigma^*K} = f^2_{N\Delta\pi}/3$. Besides the ρ also the isoscalar vector mesons ω and φ are exchanged in the KN system. The following vector meson couplings are used

$$\begin{aligned} \mathcal{H}_{NN\rho} &= g_{NN\rho}\left(\bar{N}\gamma_\mu\boldsymbol{\tau}N\right)\cdot\boldsymbol{\rho}^\mu + \frac{f_{NN\rho}}{4\mathcal{M}}\left(\bar{N}\sigma_{\mu\nu}\boldsymbol{\tau}N\right)\cdot\left(\partial^\mu\boldsymbol{\rho}^\nu - \partial^\nu\boldsymbol{\rho}^\mu\right)\,, \\ \mathcal{H}_{NN\omega} &= g_{NN\omega}\bar{N}\gamma_\mu N\omega^\mu + \frac{f_{NN\omega}}{4\mathcal{M}}\bar{N}\sigma_{\mu\nu}N\left(\partial^\mu\omega^\nu - \partial^\nu\omega^\mu\right)\,, \end{aligned} \tag{7.3}$$

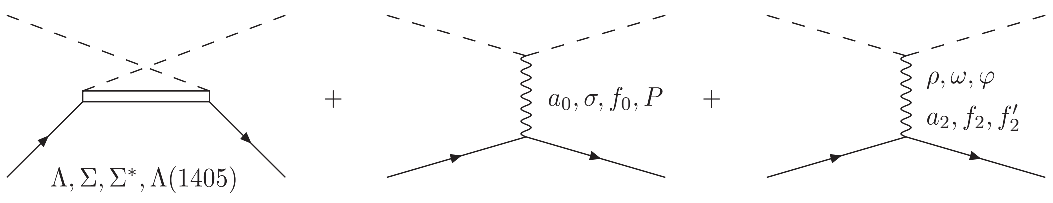

Figure 7.1: Contributions to the KN potential from the u- and t-channel Feynman diagrams. The external dashed and solid lines are always the K and N respectively.

$$
\begin{aligned}
\mathcal{H}_{KK\rho} &= g_{KK\rho}\boldsymbol{\rho}_\mu \cdot \left(iK^\dagger \boldsymbol{\tau} \overleftrightarrow{\partial}^\mu K \right) , \\
\mathcal{H}_{KK\omega} &= g_{KK\omega}\omega_\mu \left(iK^\dagger \overleftrightarrow{\partial}^\mu K \right) .
\end{aligned}
\tag{7.4}
$$

The coupling of φ is similar to the ω coupling. Although we include φ exchange its contribution is negligible compared to ω exchange. The coupling constants $g_{KK\omega}$ and $g_{KK\varphi}$ are fixed by $SU_f(3)$ in terms of $g_{\pi\pi\rho}$ and θ_V. The $NN\omega$ coupling constant is a free parameter and the $NN\varphi$ coupling constant depends on θ_V, α_V and the other two coupling constants. In addition to σ and f_0 exchange, also the isovector scalar meson a_0 is exchanged in the KN system, contrary to the πN system, the following scalar meson couplings are used

$$
\begin{aligned}
\mathcal{H}_{NNa_0} &= g_{NNa_0} \left(\bar{N} \boldsymbol{\tau} N \right) \cdot \boldsymbol{a_0} , \\
\mathcal{H}_{NN\sigma} &= g_{NN\sigma} \bar{N} N \sigma ,
\end{aligned}
\tag{7.5}
$$

$$
\begin{aligned}
\mathcal{H}_{KKa_0} &= g_{KKa_0} m_{\pi^+} \boldsymbol{a_0} \cdot \left(K^\dagger \boldsymbol{\tau} K \right) , \\
\mathcal{H}_{KK\sigma} &= g_{\pi\pi\sigma} m_{\pi^+} \sigma K^\dagger K .
\end{aligned}
\tag{7.6}
$$

The structure of the f_0 coupling is the same as the structure of the σ coupling. Concerning the tensor mesons, besides the exchange of the f_2 and the f_2' also the isovector tensor meson a_2 is exchanged in the KN system. The following tensor meson couplings are used

$$
\begin{aligned}
\mathcal{H}_{NNa_2} &= \left[\frac{iF_{1NNa_2}}{4} \bar{N} \left(\gamma_\mu \overleftrightarrow{\partial}_\nu + \gamma_\nu \overleftrightarrow{\partial}_\mu \right) \boldsymbol{\tau} N - \frac{F_{2NNa_2}}{4} \bar{N} \; \overleftrightarrow{\partial}^\mu \overleftrightarrow{\partial}^\nu \boldsymbol{\tau} N \right] \cdot \boldsymbol{a}_2^{\mu\nu} , \\
\mathcal{H}_{NNf_2} &= \left[\frac{iF_{1NNf_2}}{4} \bar{N} \left(\gamma_\mu \overleftrightarrow{\partial}_\nu + \gamma_\nu \overleftrightarrow{\partial}_\mu \right) N - \frac{F_{2NNf_2}}{4} \bar{N} \; \overleftrightarrow{\partial}^\mu \overleftrightarrow{\partial}^\nu N \right] f_2^{\mu\nu} ,
\end{aligned}
\tag{7.7}
$$

$$
\begin{aligned}
\mathcal{H}_{KKa_2} &= \frac{g_{KKa_2}}{m_{\pi^+}} \boldsymbol{a}_2^{\mu\nu} \cdot \left(\partial_\mu K^\dagger \boldsymbol{\tau} \partial_\nu K \right) , \\
\mathcal{H}_{KKf_2} &= \frac{g_{KKf_2}}{m_{\pi^+}} f_2^{\mu\nu} \left(\partial_\mu K^\dagger \partial_\nu K \right) .
\end{aligned}
\tag{7.8}
$$

Exchange	$I=0$	$I=1$
σ, f_0, ω, φ, f_2, f_2'	1	1
a_0, ρ, a_2	-3	1
Λ	-1	1
Σ	3	1

Table 7.1: The isospin factors for the various exchanges for a given total isospin I of the KN system, see Appendix B.

The coupling of f_2' is similar to the f_2 coupling. A repulsive contribution is obtained from Pomeron exchange, which is assumed to couple as a singlet and the value of its coupling constant is determined in the πN system.

The spin-space structure of the amplitudes resulting from these interaction Hamiltonians is given in Chapter 4. The isospin structure gives the isospin factors for the KN system, listed in Table 7.1 for the various exchanges, see also Appendix B. The spin-space amplitudes of Chapter 4 need to be multiplied by these isospin factors to find the complete KN amplitude. The masses, coupling constants and cut-off masses of the soft-core KN model that were fixed or fitted to the experimental data are given in Table 7.3.

Summarizing we consider in the t-channel the exchanges of the scalar mesons σ, f_0 and a_0, the Pomeron, the vector mesons ω, φ and ρ and the tensor mesons a_2, f_2 and f_2', and in the u-channel the exchanges of the baryons Λ, Σ, Σ^* and $\Lambda(1405)$. The exchanges are given diagrammatically in Figure 7.1.

The Coulomb interaction is neglected in the soft-core πN and KN models. Its contribution to the partial wave phase shifts is in principle relevant at very low energies. However, for the KN interaction we will not only investigate the phase shifts, but also some scattering observables. The differential cross section and polarization in the $K^+p \to K^+p$ channel as a function of the scattering angle clearly show the effect of the Coulomb peak at forward angles, the differential cross sections blow up and the polarizations go to zero. For the description of these scattering observables we correct for the Coulomb interaction by replacing the spin-nonflip and spin-flip scattering amplitudes $\tilde{f}$ and $\tilde{g}$ in Eq. (3.28) by [49, 65]

$$
\begin{aligned}
\tilde{f} &= \sum_L \left[(L+1)\,F_{L_+,J} + L F_{L_-,J}\right] e^{2i\phi_L} P_L(\cos\theta) + f_C \,, \\
\tilde{g} &= \sum_L \left[F_{L_+,J} - F_{L_-,J}\right] e^{2i\phi_L} \sin\theta \, \frac{dP_L(\cos\theta)}{d\cos\theta} \,.
\end{aligned}
\tag{7.9}
$$

Here f_C is the Coulomb amplitude and ϕ_L are the Coulomb phase shifts, defined respectively as

$$
\begin{aligned}
f_C &= -\frac{\alpha}{2kv\sin^2(\theta/2)} e^{-i\frac{\alpha}{v}\ln\left(\sin^2(\theta/2)\right)} \,, \\
\phi_L &= \sum_{n=1}^{L} \arctan\left(\frac{\alpha}{nv}\right) \,,
\end{aligned}
\tag{7.10}
$$

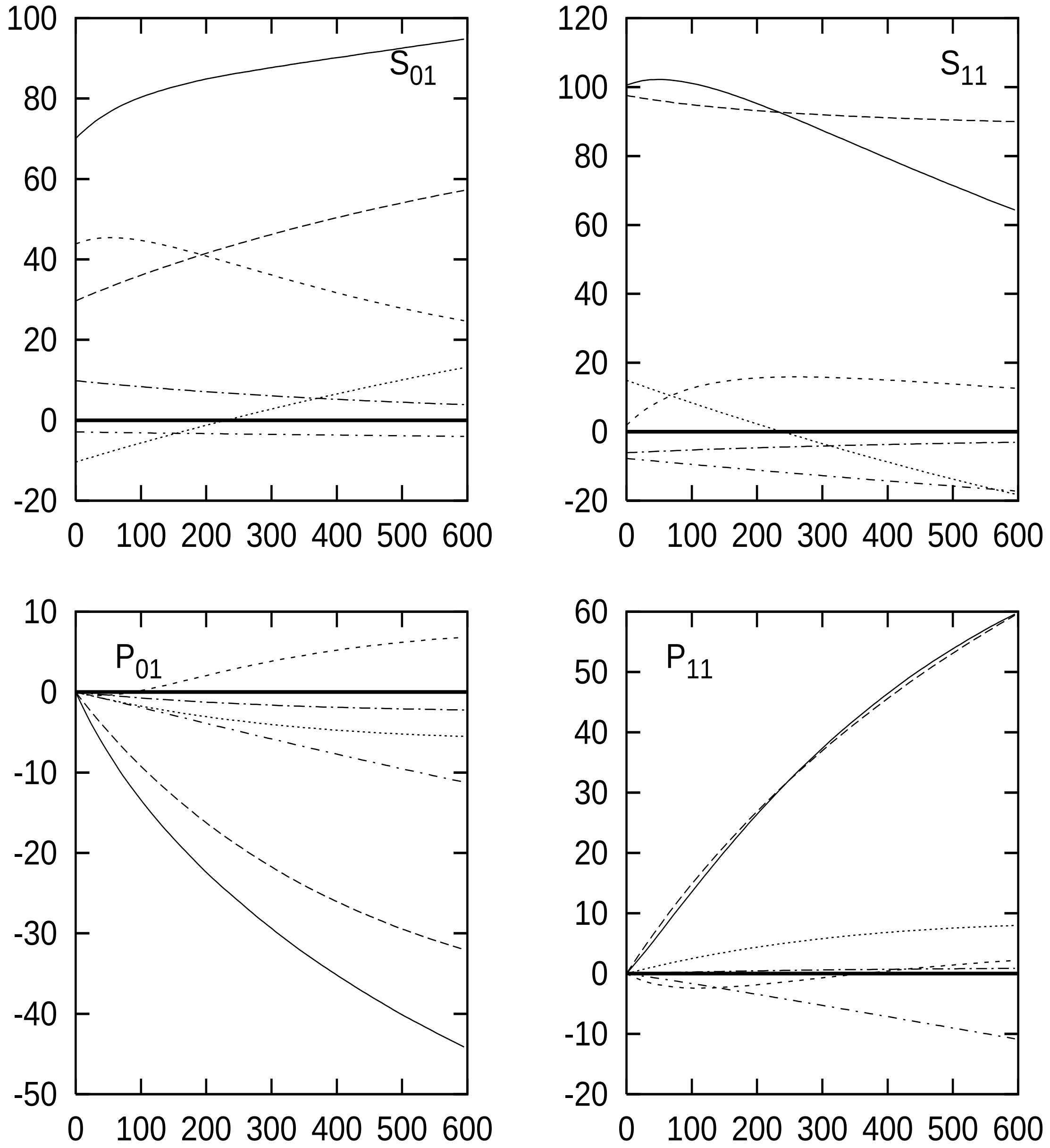

Figure 7.2: The K^+N partial wave potentials V_L as a function of T_{lab} [MeV] for the S and P partial waves are given by the solid line. The various contributions are a. the long dashed line: vector mesons, b. short dashed line: scalar mesons and Pomeron, c. the dotted line: Λ and Σ, d. the long dash-dotted line: $\Sigma(1385)$ and $\Lambda(1405)$, e. the short dash-dotted line: tensor mesons.

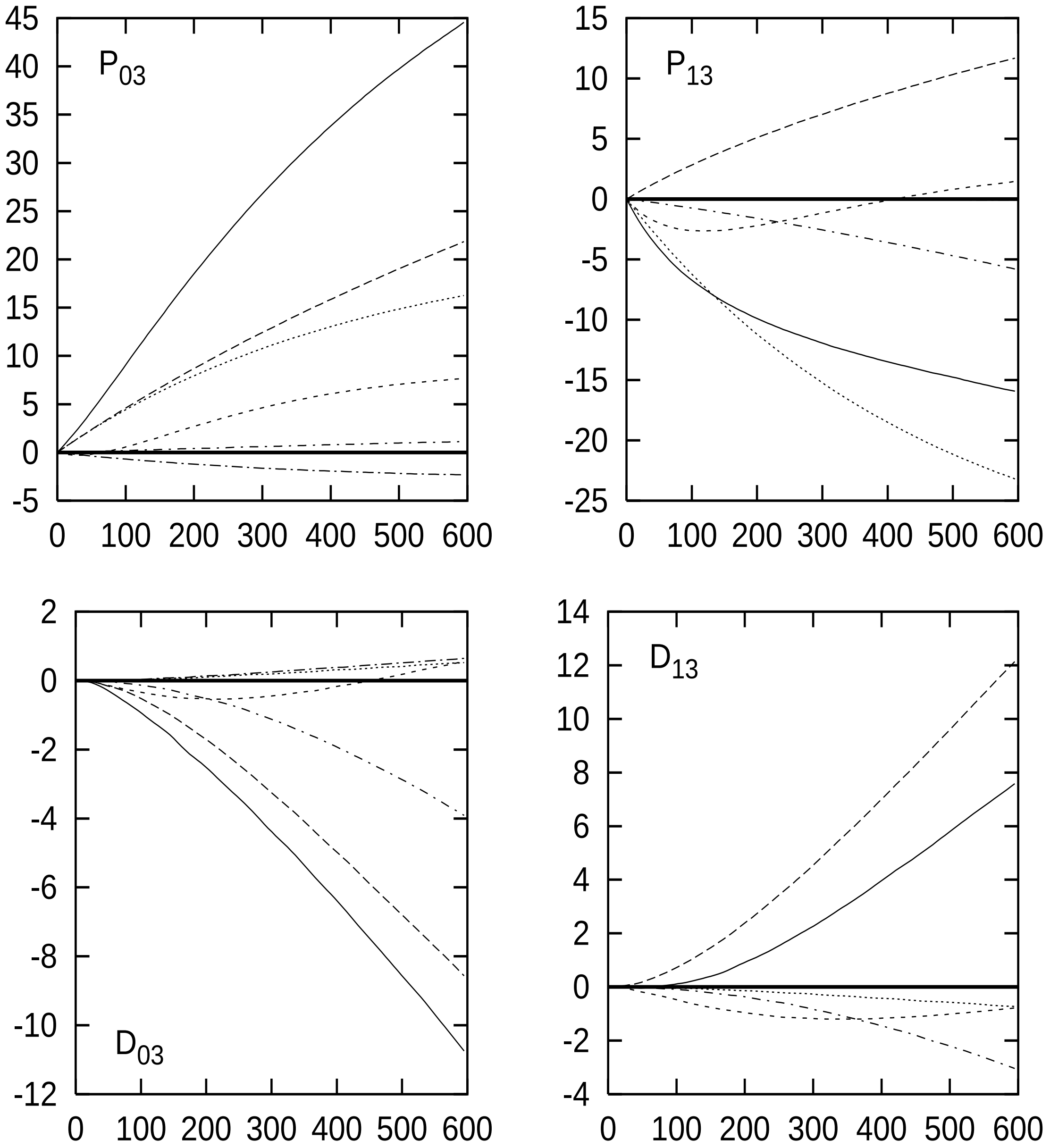

Figure 7.3: The K^+N partial wave potentials V_L as a function of $T_{\rm lab}$ [MeV] for the P and D partial waves are given by the solid line. The various contributions are a. the long dashed line: vector mesons, b. short dashed line: scalar mesons and Pomeron, c. the dotted line: Λ and Σ, d. the long dash-dotted line: $\Sigma(1385)$ and $\Lambda(1405)$, e. the short dash-dotted line: tensor mesons.

where k is the CM momentum, v is the relative velocity of the particles in the CM system, θ is the CM scattering angle and α is the fine structure constant. We remark that the Coulomb interaction can in principle be taken into account exactly in momentum space calculations, using the boundary-matching method originally introduced by Vincent and Phatak [80].

It is instructive to examine the relative strength of the different exchanges, given diagrammatically in Figure 7.1, that contribute to the partial wave KN potentials. The on-shell partial wave potentials are given by the solid line in Figures 7.2 and 7.3 for the S, P and D partial waves.

The largest contribution to the partial wave potentials comes from vector meson exchange, ω-exchange gives the largest contribution and the isospin splitting of the vector mesons is caused by ρ-exchange. Especially the S_{11}, P_{01} and P_{11} partial waves are dominated by vector meson exchange.

The cancellation between the scalar mesons and the Pomeron in the KN interaction is less than in the πN interaction, so the scalar mesons and the Pomeron give a relevant contribution. Specifically a large repulsive contribution is seen in the S partial waves.

The contribution from Λ- and Σ-exchange is large in the $J = \frac{3}{2}$ P-waves, in the other partial waves it is smaller. This exchange plays in particular an important role in describing the rise of the P_{13} phase shift. The contribution of the strange resonances $\Sigma(1385)$ and $\Lambda(1405)$ is practically negligible over the whole energy range in all partial waves.

The tensor mesons give a relevant contribution in most partial waves, especially at higher energies. The inclusion of tensor meson exchange in the KN potential improved the description of the partial wave phase shifts at higher energies.

7.3 Results and discussion for KN scattering

We have fitted the soft-core KN model, an $SU_f(3)$ extension of the soft-core πN model, to the partial wave analysis of Hyslop et al. [2] up to kaon kinetic laboratory energy $T_{\rm lab} = 600$ MeV. The results of the fit are shown in Figures 7.4 and 7.5, which show the calculated and empirical phase shift for S, P and D partial waves, and in Table 7.2, which shows the calculated and empirical scattering lengths for the S and P partial waves.

Scat. length	Model	SP92 [2]	[81]	[71]
S_{01}	-0.09	0.00	-0.04	0.03± 0.15
S_{11}	-0.28	-0.33	-0.32	-0.30± 0.03
P_{01}	0.137	0.08	0.086	
P_{11}	-0.035	-0.16	-0.032	
P_{03}	-0.020	-0.13	-0.019	
P_{13}	0.059	0.07	0.021	

Table 7.2: The calculated and empirical KN S-wave and P-wave scattering lengths in units of fm and fm^3.

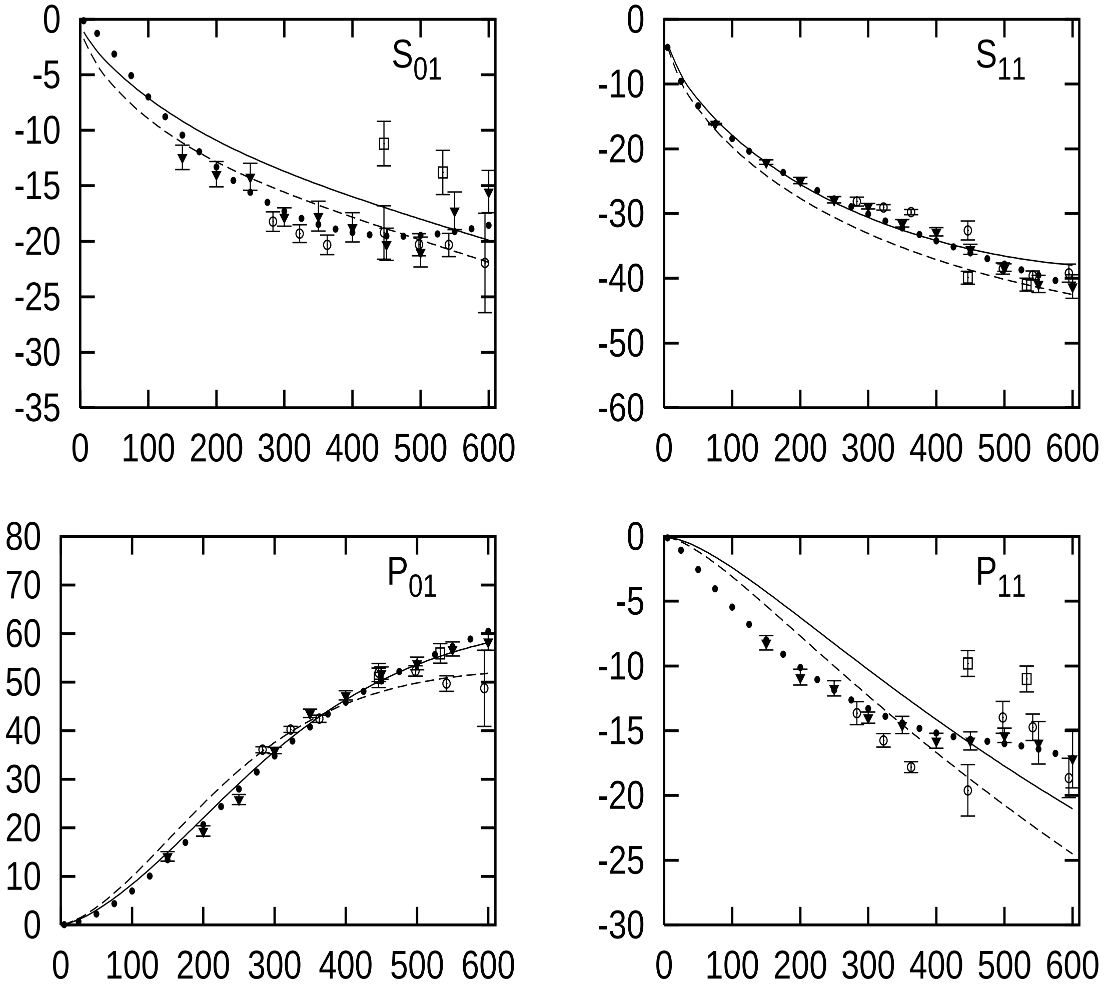

Figure 7.4: The S-wave and P-wave K^+N-phase shifts δ [degrees] as a function of T_{lab} [MeV]. The empirical phases are from the SP92 phase shift analysis: multi energy phase shifts (dots) single energy phase shifts (filled triangles), [65] single energy phase shifts (open circles), [66] single energy phase shifts (open squares). The soft-core KN model is given by the solid line, the dashed line is the model without tensor mesons.

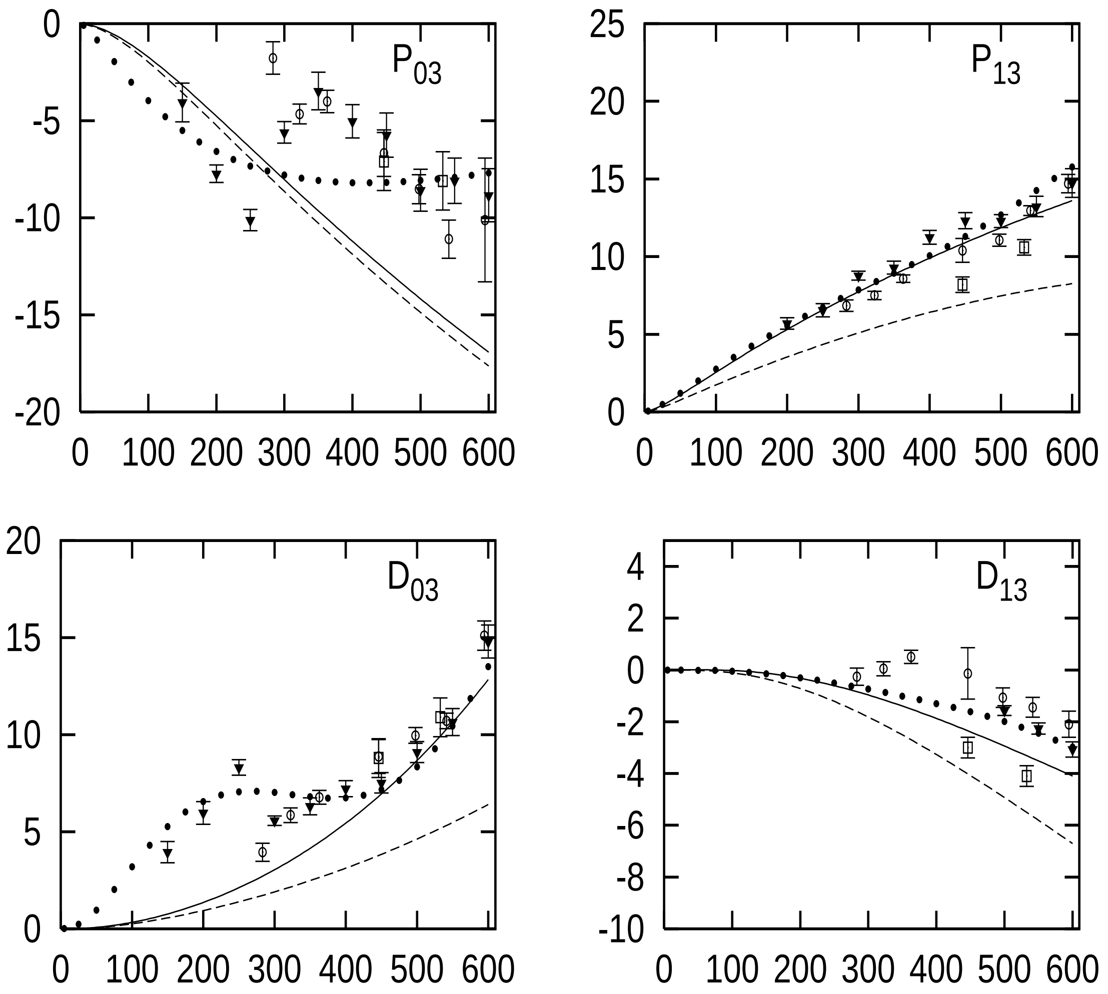

Figure 7.5: The P-wave and D-wave K^+N-phase shifts δ [degrees] as a function of T_{lab} [MeV]. The empirical phases are from the SP92 phase shift analysis: multi energy phase shifts (dots) single energy phase shifts (filled triangles), [65] single energy phase shifts (open circles), [66] single energy phase shifts (open squares). The soft-core KN model is given by the solid lines, the dashed line is the model without tensor mesons.

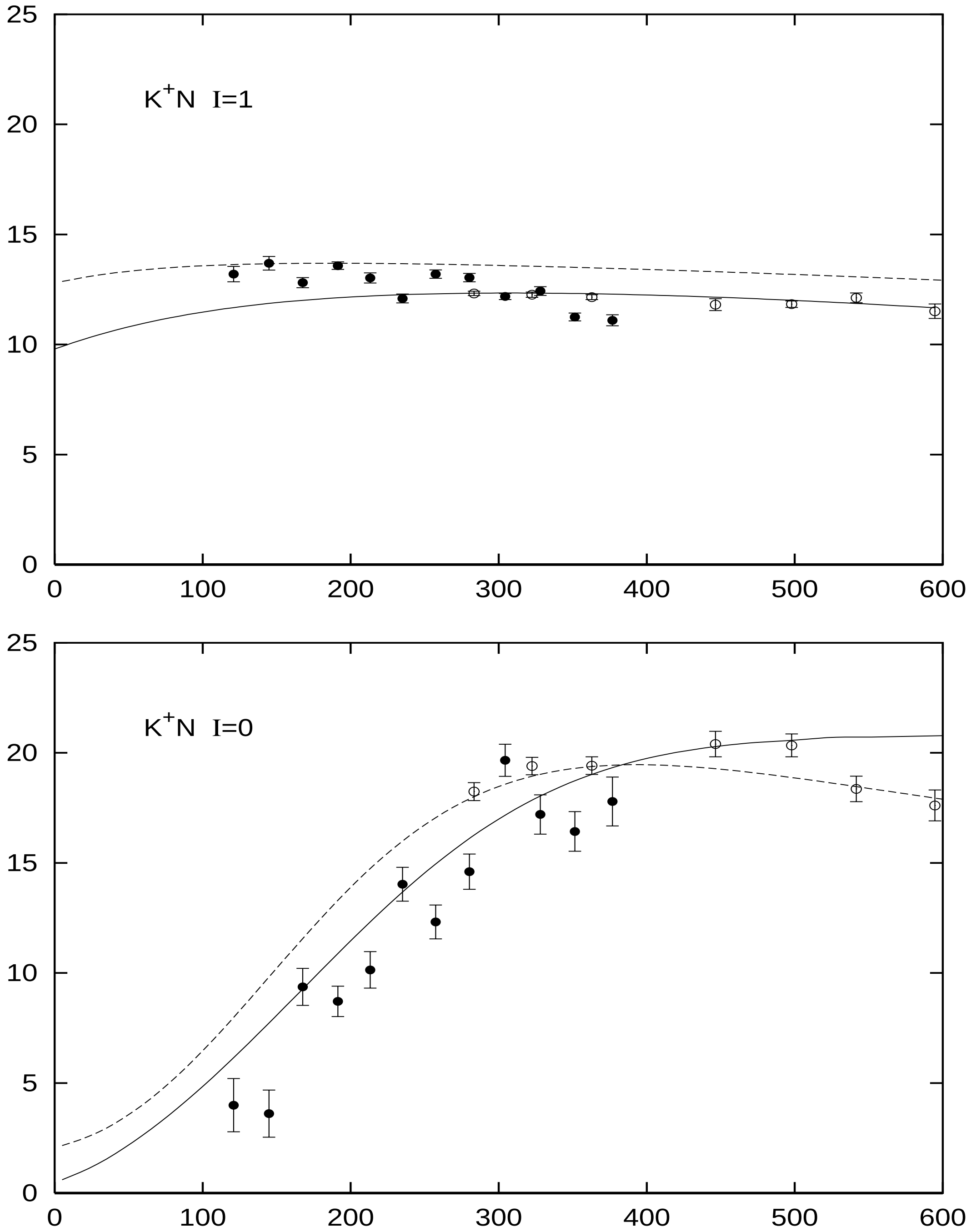

Figure 7.6: The total elastic K^+N cross section σ [mb] as a function of T_{lab} [MeV] for both isospin channels. The experimental cross sections are given by [82] (full circles) and [65] (empty circles). The soft-core KN model is given by the solid lines, the dashed line is the model without tensor mesons.

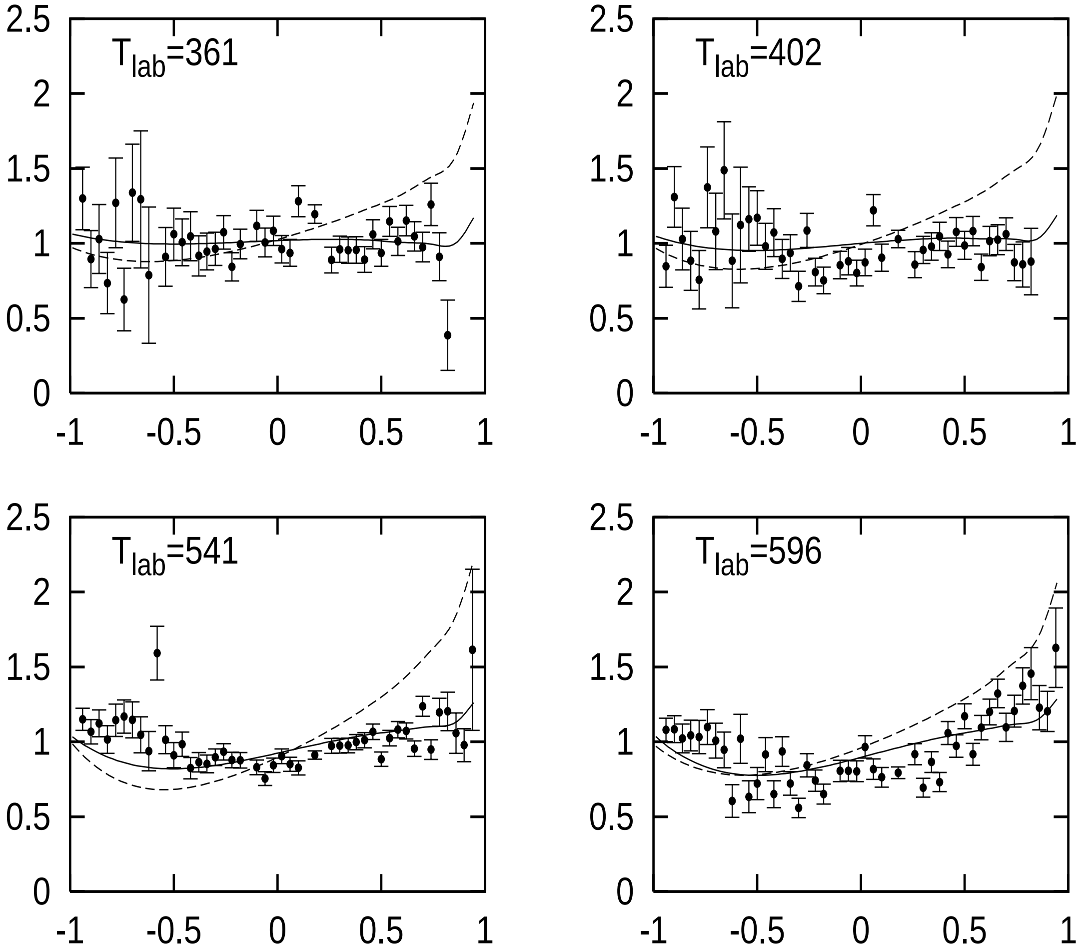

Figure 7.7: The $K^+p \to K^+p$ differential cross section $d\sigma/d\Omega$ [mb/sr] as a function of $\cos\theta$, where θ is the CM scattering angle, at various values of $T_{\rm lab}$ [MeV]. The experimental differential cross sections are given by [83]. The soft-core KN model is given by the solid lines, the dashed line is the model without tensor mesons.

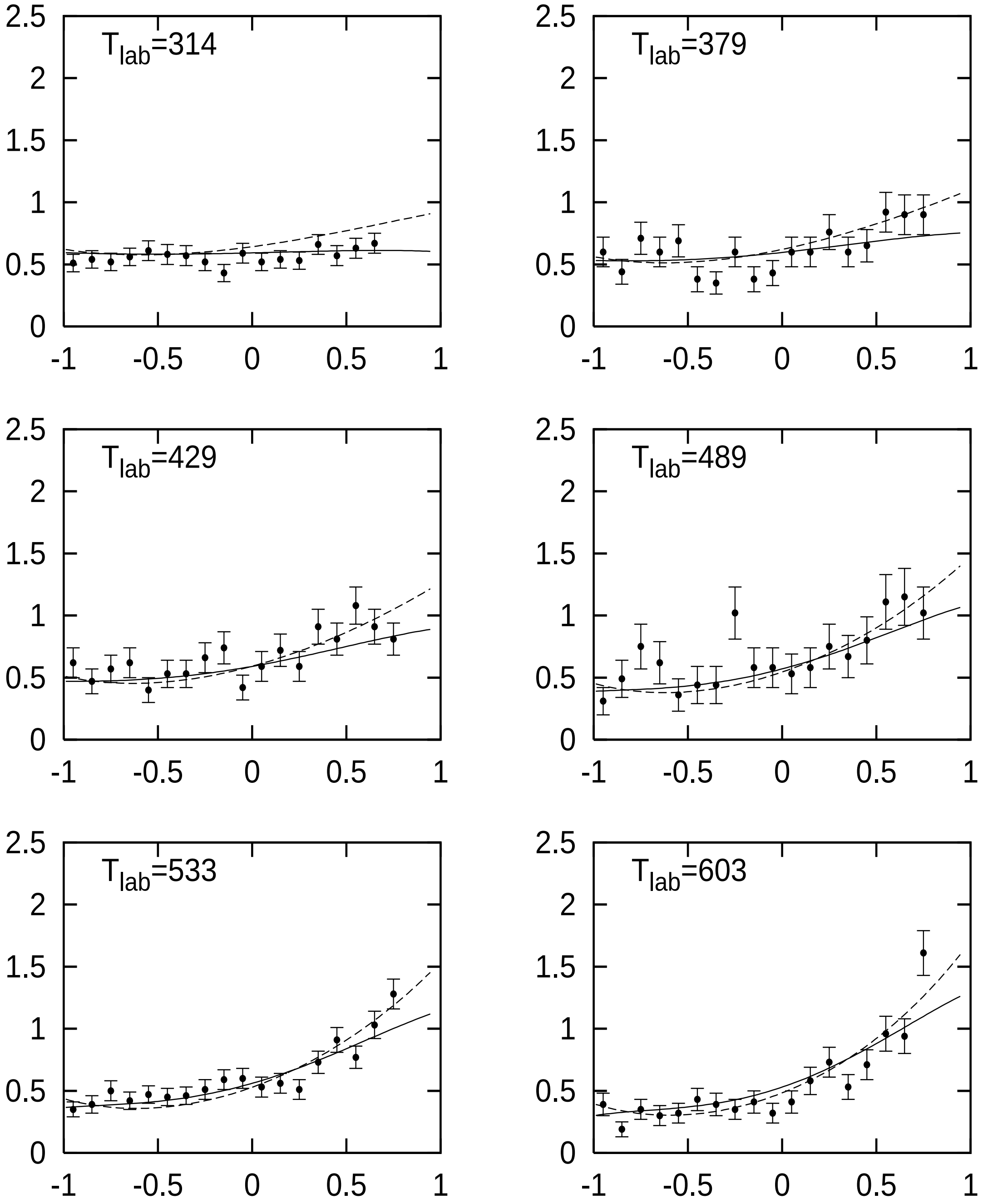

Figure 7.8: The $K^+n \to K^+n$ differential cross section $d\sigma/d\Omega$ [mb/sr] as a function of $\cos\theta$, where θ is the CM scattering angle, at various values of $T_{\rm lab}$ [MeV]. The experimental differential cross sections are given by [84]. The soft-core KN model is given by the solid lines, the dashed line is the model without tensor mesons.

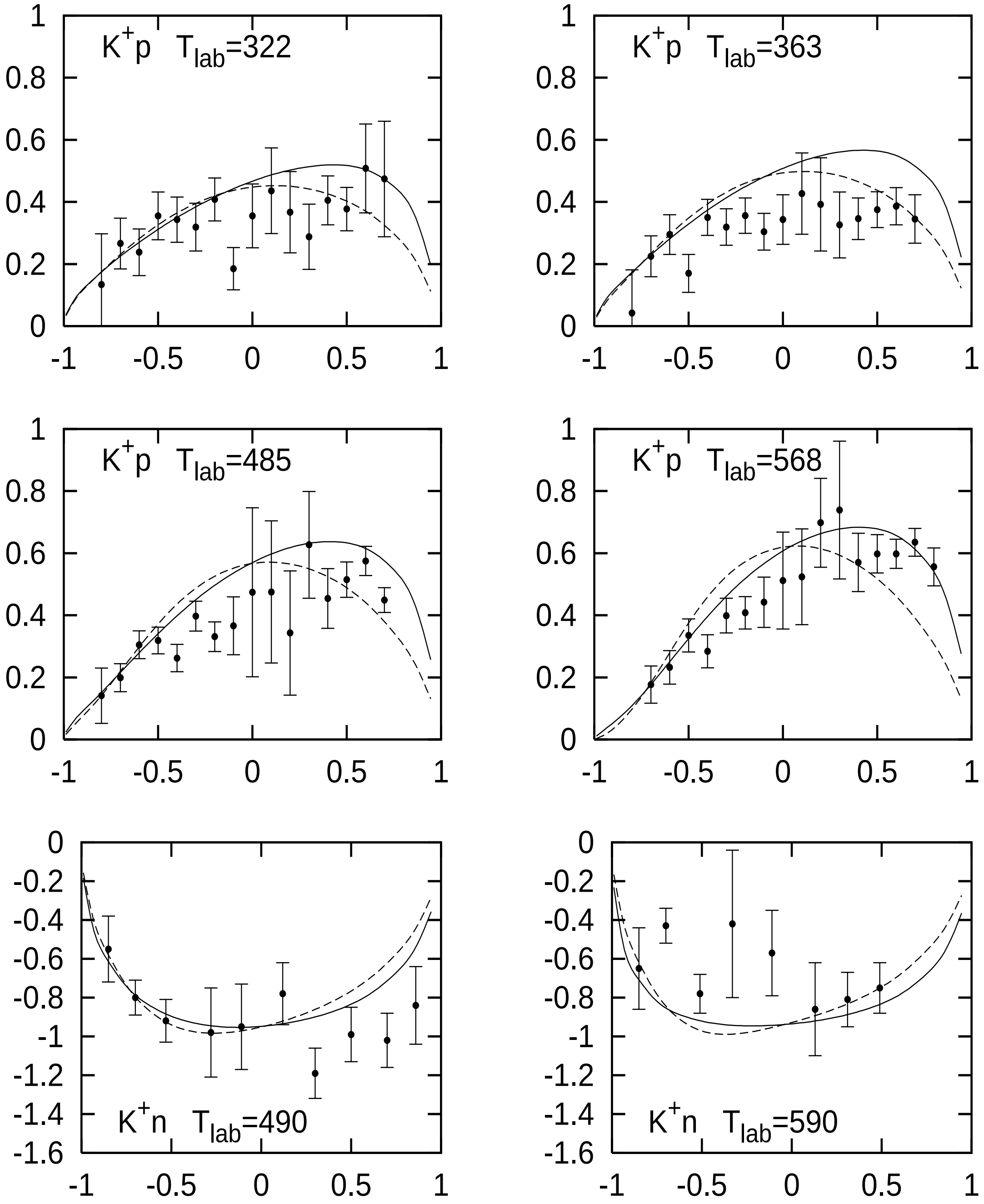

Figure 7.9: The $K^+p \to K^+p$ and $K^+n \to K^+n$ polarizations P as a function of $\cos\theta$, where θ is the CM scattering angle, at various values of T_{lab} [MeV]. The experimental polarizations are given by [85, 86]. The soft-core KN model is given by the solid line, the dashed line is the model without tensor mesons.

A reasonable agreement between the soft-core KN model and the empirical phase shifts up to $T_{\rm lab} = 600$ MeV is obtained, but the energy behavior of the empirical multi energy phase shifts in the P_{11}, P_{03} and D_{03} partial waves is not reproduced well by the soft-core KN model. This, however, is also the case for the Jülich KN models [19, 78]. The various phase shift analyses are not very consistent in these partial waves, in particular the behavior of the SP92 multi energy P_{03} and D_{03} phase shifts deviate much from the different single energy phase shifts. The low-energy structure of the multi energy D_{03} phase shift is not expected, and one should wonder if this strange structure causes problems for other partial waves in the phase shift analysis.

The S-wave scattering lengths for both isospin zero and one, listed in Table 7.2, are reproduced well. For the P-waves the situation is less clear, the empirical P-wave scattering lengths found in the two partial wave analyses [2] and [81] are contradictory. The model P_{13} partial wave scattering length is in reasonable in agreement with [2]. The P_{11} and P_{03} scattering lengths are in agreement with [81].

Since the various phase shift analyses do not always give consistent results and one should wonder how well the multi energy SP92 phase shifts represent the experimental data, we also compared the soft-core KN model with the experimental scattering observables directly. The total elastic cross section for the isospin zero and one channels as a function of $T_{\rm lab}$ are shown in Figure 7.6, the experimental isospin one (K^+p) total elastic cross sections are known quite accurately, the isospin zero total elastic cross sections are known to less accuracy. The soft-core KN model reproduces both total elastic cross sections quite well. The differential cross sections for the channels $K^+p \to K^+p$ and $K^+n \to K^+n$, having quite large error bars, are shown in Figures 7.7 and 7.8 as a function of the scattering angle at various values of $T_{\rm lab}$, they are described well by the soft-core KN model. Finally the polarizations, also having large error bars, are given in Figure 7.9 for the same channels as a function of the scattering angle at various values of $T_{\rm lab}$, again a good agreement between the model prediction and the experimental values is seen.

Although the empirical phase shifts are not in all partial waves described very well by the soft-core KN model, the scattering observables as well as the S-wave scattering lengths (proportional to the total cross sections at threshold) are. We remark that the description of the experimental scattering data and the phase shifts by the soft-core KN model, containing only one-particle-exchange processes, is as least as good as that of the Jülich models [19, 78], these models, however, used two-particle-exchanges to describe the experimental data.

The parameters of the soft-core KN model, coupling constants, meson and baryon masses and cut off masses, searched and fixed in the fitting procedure are listed in Table 7.3.

The soft-core KN model has six different cut off masses, which are free parameters in the fitting procedure. For the three scalar mesons we use the same cut off masses, for the vector mesons we use the same cut off mass for the ρ and φ, but allow for a different value for the ω in order to find a better description of the S_{11} and P_{01} partial waves at higher energies. For the three tensor mesons, necessary to fit the S_{11} P_{01} and P_{13} partial waves simultaneously, we also use the same cut off mass. For the Pomeron mass we take the value found for the soft-core πN model, the meson and baryon masses have been fixed in the fitting procedure.

Exchange	Coupling Constants				Mass	Λ
ρ	$\frac{g_{NN\rho}g_{KK\rho}}{4\pi}$	=	0.667*	$\frac{f_{NN\rho}}{g_{NN\rho}} = 5.285$	770.00	1563.11
ω	$\frac{g_{NN\omega}g_{KK\omega}}{4\pi}$	=	2.572	$\frac{f_{NN\omega}}{g_{NN\omega}} = 0.345$	783.00	1804.88
φ	$\frac{g_{NN\varphi}g_{KK\varphi}}{4\pi}$	=	−0.573*	$\frac{f_{NN\varphi}}{g_{NN\varphi}} = 0.932^*$	1020.00	1563.11
a_0	$\frac{g_{NNa_0}g_{KKa_0}}{4\pi}$	=	3.461		980.00	712.27
σ	$\frac{g_{NN\sigma}g_{KK\sigma}}{4\pi}$	=	20.676*		760.00	712.27
f_0	$\frac{g_{NNf_0}g_{KKf_0}}{4\pi}$	=	4.203*		975.00	712.27
a_2	$\frac{g_{NNa_2}g_{KKa_2}}{4\pi}$	=	0.019	$\frac{f_{NNa_2}}{g_{NNa_2}} = -3.161$	1320.00	853.98
f_2	$\frac{g_{NNf_2}g_{KKf_2}}{4\pi}$	=	0.080	$\frac{f_{NNf_2}}{g_{NNf_2}} = 0.382$	1270.00	853.98
f_2'	$\frac{g_{NNf_2'}g_{KKf_2'}}{4\pi}$	=	0.022*	$\frac{f_{NNf_2'}}{g_{NNf_2'}} = 3.393^*$	1525.00	853.98
Pomeron	$\frac{g_{NNP}g_{KKP}}{4\pi}$	=	4.135*		315.32*	
Λ	$\frac{f^2_{\Lambda NK}}{4\pi}$	=	0.074*		1116.00	1029.49
Σ	$\frac{f^2_{\Sigma NK}}{4\pi}$	=	0.006*		1189.00	1029.49
$\Sigma^*(1385)$	$\frac{f^2_{\Sigma^* NK}}{4\pi}$	=	0.147*		1385.00	1051.82
$\Lambda(1405)$	$\frac{f_{\Lambda(1405)NK}}{4\pi}$	=	0.710*		1405.00	1051.82

Table 7.3: Soft-core KN model parameters: the coupling constants, masses and cut-off masses (in MeV) of the exchanged particles. Coupling constants with an asterisk were not searched in the fitting procedure, but constrained via $SU_f(3)$ or simply put to some value used in previous work. An $SU_f(3)$-breaking factor λ is allowed for the vector and scalar mesons. For the vector mesons we find $\lambda_v = 0.764$ and for the scalar mesons we find $\lambda_s = 0.899$.

Ideal mixing is assumed for the vector mesons, so $\theta_V = 35,26^\circ$, the $F/(F+D)$ ratios are fixed to the values in [7], $\alpha_V^e = 1.0$ and $\alpha_V^m = 0.275$, this fixes the PPV coupling constants in terms of the empirical determined $f_{\pi\pi\rho}$ and leaves $g_{NN\omega}$ and $f_{NN\omega}$ as fit parameters, the fitted values are in agreement with the literature. The $NN\rho$ tensor coupling $f_{NN\rho}$ is in principle determined in the soft-core πN model, but since its value was determined to be very low we also fit this parameter in the soft-core KN model and we found a larger value than in the soft-core πN model. We remark that the exchange of the vector meson φ is considered for consistency, but its contribution is negligible. For the scalar mesons $g_{NN\sigma}$ and g_{NNf_0} are determined in the soft-core πN model, we use g_{NNa_0} and θ_S as fit parameters, all scalar meson coupling constants are then determined. For the tensor mesons we use the $F/(F+D)$ ratios $\alpha_T^e = 1.0$ and $\alpha_T^m = 0.4$ and an almost ideal mixing angle $\theta_T = 37.50$, this fixes the PPT coupling constants in terms of $f_{\pi\pi f_2}$. We notice that the tensor meson coupling constants $g_T = \mathcal{M}F_1 + \mathcal{M}^2F_2$ and $f_T = -\mathcal{M}^2F_2$ are used in Table 7.3.

The ΛNK and ΣNK coupling constants are determined by $f_{NN\pi}$ and fixing α_P at the value in [7] $\alpha_P = 0.355$. The Pomeron is considered as an $SU_f(3)$-singlet and its coupling to the KN system is determined in the soft-core πN model and by $SU_f(3)$, the $\Sigma^*(1385)$ coupling constant is fixed by $SU_f(3)$ at the value $f_{\Sigma^* NK} = f_{N\Delta\pi}/\sqrt{3}$, where the $N\Delta\pi$ cou-

Exchange	Coupling Constants				Mass	Λ
ρ	$\frac{g_{NN\rho}g_{KK\rho}}{4\pi}$	=	0.641*	$\frac{f_{NN\rho}}{g_{NN\rho}} = 5.443$	770.00	1547.49
ω	$\frac{g_{NN\omega}g_{KK\omega}}{4\pi}$	=	2.215	$\frac{f_{NN\omega}}{g_{NN\omega}} = 0.345$	783.00	1704.33
φ	$\frac{g_{NN\varphi}g_{KK\varphi}}{4\pi}$	=	−0.243*	$\frac{f_{NN\varphi}}{g_{NN\varphi}} = 1.842^*$	1020.00	1547.49
a_0	$\frac{g_{NNa_0}g_{KKa_0}}{4\pi}$	=	3.806		980.00	909.18
σ	$\frac{g_{NN\sigma}g_{KK\sigma}}{4\pi}$	=	26.068*		760.00	909.18
f_0	$\frac{g_{NNf_0}g_{KKf_0}}{4\pi}$	=	1.168*		975.00	909.18
Pomeron	$\frac{g_{NNP}g_{KKP}}{4\pi}$	=	4.453*		295.73*	
Λ	$\frac{f^2_{\Lambda NK}}{4\pi}$	=	0.074*		1116.00	1041.33
Σ	$\frac{f^2_{\Sigma NK}}{4\pi}$	=	0.006*		1189.00	1041.33
$\Sigma^*(1385)$	$\frac{f^2_{\Sigma^* NK}}{4\pi}$	=	0.147*		1385.00	629.49
$\Lambda(1405)$	$\frac{f_{\Lambda(1405)NK}}{4\pi}$	=	0.710*		1405.00	629.49

Table 7.4: Parameters of the soft-core KN model without tensor mesons: the coupling constants, masses and cut-off masses (in MeV) of the exchanged particles. Coupling constants with an asterisk were not searched in the fitting procedure, but constrained via $SU_f(3)$ or simply put to some value used in previous work. An $SU_f(3)$-breaking factor λ is allowed for the vector and scalar mesons. For the vector mesons we find $\lambda_v = 0.918$ and for the scalar mesons we find $\lambda_s = 0.900$.

pling is determined in the soft-core πN model. For the $\Lambda(1405)$ coupling constant we take an average value from [43]. In the fitting procedure we found that it was desirable to allow for an $SU_f(3)$-breaking for the scalar- and vector-meson couplings, the breaking factors we found are $\lambda_S = 0.899$ and $\lambda_V = 0.764$ respectively.

The soft-core KN model has 17 free physical parameters; 8 coupling constants, 1 mixing angle, 6 cut off masses and 2 $SU_f(3)$ breaking parameters. From the πN fit we have $g_{NN\rho} = 0.78$ and $g_{NN\sigma} = 2.57$, from the KN fit we have $g_{NN\omega} = 3.03$ and $g_{NNa_0} = 0.78$.

Besides the presented soft-core KN model, we also considered a model that does not contain tensor mesons. We fitted this model to the empirical phase shifts and the results of the fit are given by the dashed lines in Figures 7.4 and 7.5. The parameters of this model are listed in Table 7.4. We remark that in the P_{13} and D_{03} partial waves a noticeable difference can be seen between the two models, these partial waves as well as the S_{11} and P_{01} partial waves are described better by the soft-core KN model, i. e. the model including the tensor mesons. The total cross sections and $K^+p \to K^+p$ differential cross sections are described better by the soft-core KN model, while the $K^+n \to K^+n$ differential cross sections and the polarizations are described equally well.

Summarizing, the soft-core KN model gives a reasonable description of the empirical partial wave phase shifts and also the S-wave scattering lengths are reproduced well. The scattering observables: total elastic cross sections, differential cross sections and polarizations, which are investigated because the various phase shift analyses are not always consistent, are described satisfactory by this model.

7.4 Exotic resonances

Evidence for the existence of a resonance structure in the isospin zero KN system at low energies has recently been found in various measurements from SPring-8, ITEP, Jefferson Lab and ELSA [3, 67, 68, 69]. The exotic resonance, a $qqqq\bar{q}$-state, was called Z^* but is now renamed as Θ^+. The experimental values for its mass and decay width are $\sqrt{s} \simeq 1540$ MeV and $\Gamma_{\Theta^+} \leq 25$ MeV respectively, which is in good agreement with the theoretical predictions of Diakonov et al. [70] based on the chiral quark-soliton model, giving $\sqrt{s} \simeq 1530$ MeV and $\Gamma_{\Theta^+} \simeq 15$ MeV, isospin $I = 0$ and spin-parity $J^P = \frac{1}{2}^+$.

The present KN scattering data does not explicitly show this resonance structure, but some fluctuations in the isospin zero scattering data around $\sqrt{s} = 1540$ MeV are present, however the decay width of the Θ^+ is expected to be quite small. Arndt et al. [87] have reanalyzed the KN scattering database and investigated the possibility of a resonance structure in their KN phase shift analysis, since their last phase shift analysis [2] no new scattering data has become available. Arndt et al. concluded that the Θ^+ decay width must indeed be quite small in view of the present scattering data, they concluded that Γ_{Θ^+} is not much larger than a few MeV's.

In this section the soft-core KN model, describing the experimental data well far beyond the Θ^+ resonance region, is used to examine the influence of including this resonance explicitly on the total elastic isospin zero KN cross section. The Θ^+ resonance is assumed to be present in the P_{01} partial wave. The procedure for including the Θ^+ resonance explicitly in the KN system is completely the same as for the $\Delta(1232)$ resonance in the πN system, this renormalization procedure, giving a good description of the πN P_{33} partial wave, is described in detail in Chapter 5.

A pole diagram for the Θ^+ resonance with bare mass and coupling constant M_0 and g_0 is added to the KN potential, iteration in the integral equation dresses the vertex and self-energy. The renormalization procedure ensures a pole at the physical Θ^+ mass and the vanishing of the self-energy and its first derivative at the pole position. The bare mass and coupling constant are in the renormalization procedure determined in terms of the physical parameters. The physical $KN\Theta^+$ coupling constant is calculated using the decay width and Eq. (6.8). We mention that we did not fit the model which includes the Θ^+ resonance to the scattering data, but simply used the soft-core KN model and added the Θ^+ pole diagram and observed the change in the cross section.

The total elastic cross sections in the isospin one and zero channels, predicted by the soft-core KN model, are given in Figure 7.10 by the solid line. Inclusion of the Θ^+ resonance leaves of course the isospin one cross section unchanged, but in the isospin zero cross section a peak appears around $\sqrt{s} = 1540$ MeV or $T_{\text{lab}} = 171$ MeV. We calculated the influence of the inclusion of the Θ^+ resonance on the isospin zero cross section for two values of its decay width, $\Gamma_{\Theta^+} = 10$ and 25 MeV, respectively corresponding to the short and long dashed curves in Figure 7.10.

Far away from the resonance position the dashed curves coincide with the solid soft-core KN curve. It is clear that the smaller the Θ^+ decay width the narrower the peak and the more the dashed curve coincides with the solid soft-core KN curve. It is hard to reconcile the present isospin zero KN scattering data with a Θ^+ resonance with a decay width larger than

10 MeV, unless the Θ^+ resonance lies much closer to threshold, where no scattering data is available. In both cases new and accurate scattering experiments, especially at low energies and around $\sqrt{s} = 1540$ MeV, would be desirable.

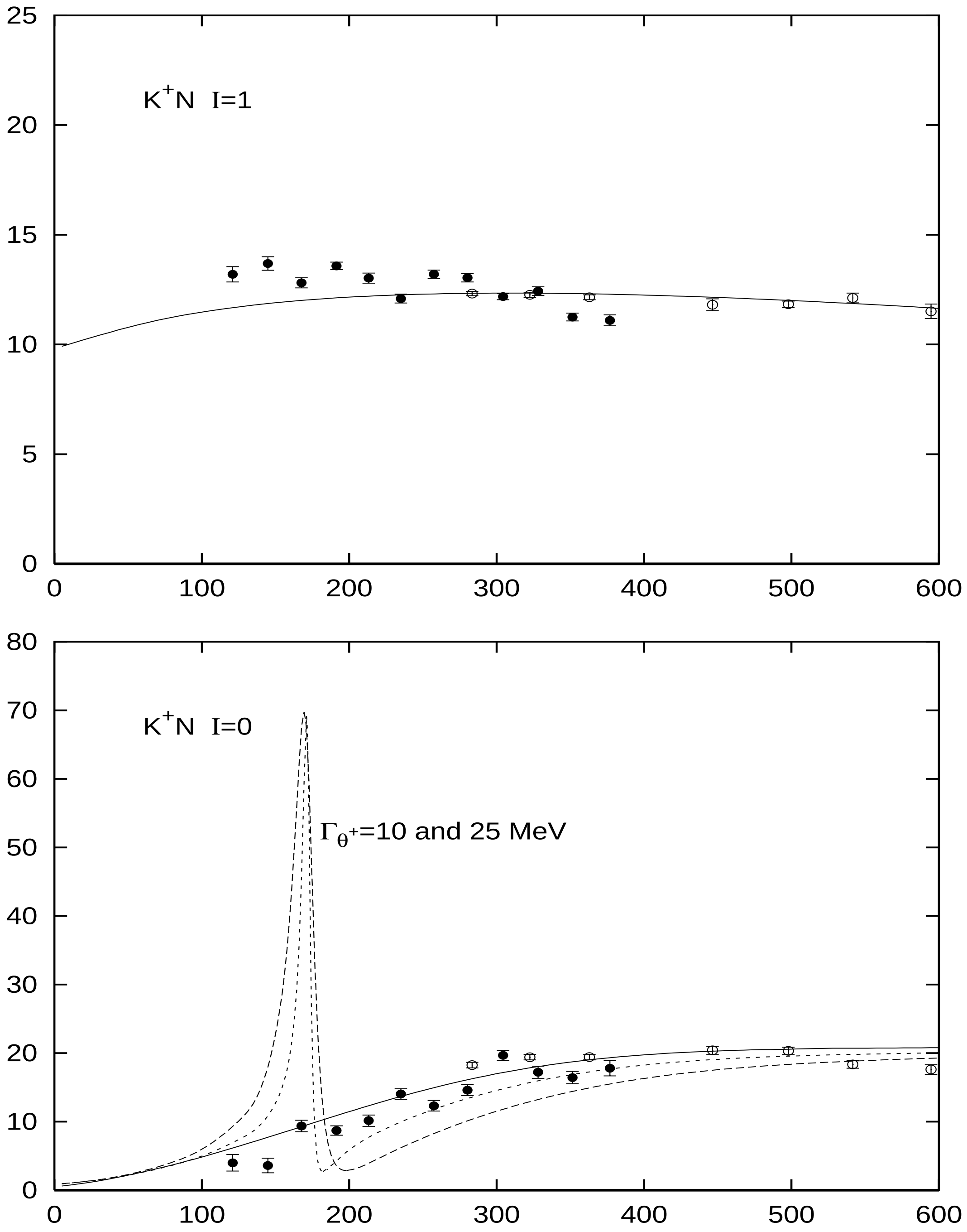

Figure 7.10: The $\Theta^+(1540)$ resonance included in the soft-core KN model. The total elastic K^+N cross section σ [mb] is given as a function of T_{lab} [MeV] for both isospin channels. The experimental cross sections are given by [82] (full circles) and [65] (empty circles). The soft-core KN model is given by the solid lines.

Chapter 8

Summary

This thesis, entitled *"Strong Meson-Baryon Interactions"*, investigates the strong interaction between mesons and baryons at low and intermediate energies, giving a contribution to the detailed understanding of hadron-hadron interactions in general. The strong meson-baryon interaction is investigated experimentally by scattering a meson beam of a nuclear target, and the measured observable quantities are used to construct theoretical models.

In particular the pion-nucleon interaction has been investigated for more than forty years. High intensity pion beams are available and scattering experiments have been performed at various laboratories and a very rich scattering data base is now available. The situation for the kaon-nucleon interaction is, however, different. The scattering experiments have been performed in the seventies and the beginning of the eighties using kaon beams having a lower intensity than the pion beams. The kaon-nucleon scattering observables are thus known to less accuracy, especially at lower energies. More and accurate kaon-nucleon scattering data are to be expected in the near future, the presently constructed *K-factory* at the Japan Proton Accelerator Research Complex (J-PARC) will have at disposal a kaon beam having a much higher intensity (ca. ten times) than any kaon beam before. New kaon-nucleon scattering data is also to be expected from the DAΦNE facility in Italy.

In the past and present meson-exchange models have proven to be very successful in describing the nucleon-nucleon (NN) interaction and the hyperon-nucleon (YN) interaction quantitatively. In this thesis a similar approach is applied to the pion-nucleon (πN) interaction, being mainly a natural basis for an $SU_f(3)$-symmetry extension to the kaon-nucleon (KN) interaction. These interactions are, however, different from the NN and YN interactions in the sense that not only meson-exchanges occur, but also baryon-exchanges in the s- and u-channel occur. We have derived a soft-core meson- and baryon-exchange model for the πN and KN interaction analogous to the Nijmegen soft-core one-boson-exchange nucleon-nucleon and hyperon-nucleon models.

The meson-baryon potentials in the context of a relativistic two-particle equation, the Bethe-Salpeter equation, are defined in Chapter 2. The potentials consist of one-meson and one-baryon exchange Feynman diagrams. The Bethe-Salpeter equation is approximated by assuming "dynamical pair-suppression", hence neglecting the propagation of negative energy states, and by integrating over the time variable, giving a three-dimensional integral equation for the scattering amplitude, which is a generalization of the Lippmann-Schwinger equation.

A transformation of this equation on the plane wave basis to the partial wave (LSJ) basis is described in Chapter 3. A one-dimensional integral equation for the partial wave scattering amplitude is derived, which is decoupled for each partial wave, because of parity conservation in strong interactions.

The soft-core πN model presented in this thesis shows that the soft-core approach of the Nijmegen group not only gives a good description of the NN and YN data, but also the πN data are described well in this approach. The soft-core πN model serves as a solid basis for the soft-core KN model, assumed to be connected via $SU_f(3)$-symmetry. For completeness the definitions of the octet irreducible representation (irrep) for the $J^P = \frac{1}{2}^+$ baryons and the octet and singlet irreps for the mesons as well as the invariant interaction Hamiltonians are given in Chapter 4. Using these interaction Hamiltonians the one-baryon exchange and one-meson exchange invariant amplitudes have been derived, these amplitudes define the partial wave potentials used in the calculations.

In the πN cross section some resonances are present at low and intermediate energies, e.g. the $\Delta(1232)$ and the Roper(1440). It turned out that these resonances can not be described by using only a πN potential, i.e. they could not be generated dynamically. This confirms the quark-model picture. We consider these resonances as, at least partially, genuine three-quark states and we treat them in the same way as the nucleon. Therefore we have included s-channel diagrams for these resonances in the soft-core πN model. However, this is done carefully in a renormalized procedure, i.e. a procedure in which physical coupling constants and masses are used, since iterations of s-channel diagrams give contributions to the vertex and self-energy. The renormalization procedure used to include s-channel diagrams is described in detail in Chapter 5. We have described the method for partial waves which contain one resonance, e.g. the $\Delta(1232)$ in the P_{33}-wave, and partial waves in which multiple s-channel diagrams play a role, e.g. the P_{11}-wave (nucleon and Roper(1440)).

The soft-core πN model and the fit to the experimental data are presented in Chapter 6. The model contains the exchanges of the baryons N, Δ, Roper and S_{11} and the scalar mesons σ and f_0, vector meson ρ and tensor mesons f_2 and f_2'. An excellent fit to the empirical S- and P- wave phase shifts up to pion laboratory energy 600 MeV has been found, with normal values for the coupling constants and cut-off masses, except for a low value of $f_{NN\rho}/g_{NN\rho}$, which is also a problem in other πN models. The scattering lengths have been reproduced well. The soft-pion theorems for low-energy πN scattering are satisfied, since the S-wave scattering lengths are described well. The c_1-, c_2-, c_3- and c_4-terms in chiral perturbation theory are described implicitly by the soft-core πN model, higher derivative terms in chiral perturbation theory are effectively described by the propagators and Gaussian form factors in the soft-core πN model.

The soft-core KN model, an $SU_f(3)$ extension of the soft-core πN model, and the fit to the experimental data are presented in Chapter 7. The model contains the exchanges of the baryons Λ, Σ, $\Sigma^*(1385)$ and $\Lambda(1405)$, the scalar mesons a_0, σ and f_0, the vector mesons ρ, ω and φ and the tensor mesons a_2, f_2 and f_2'. The quality of the fit to the empirical phase shifts up to kaon laboratory energy 600 MeV is not as good as for the soft-core πN model, but the soft-core KN model presented here certainly reflects the present state of the art. The scattering observables themselves, i.e. the total and differential cross sections and polarizations as well as the S-wave scattering lengths are reproduced well.

Low energy (exotic) resonances have never been seen in the present KN scattering data, however, recently indications for the existence of a narrow resonance in the isospin zero KN system have been found in several photo-production experiments. We have included this resonance $\Theta^+(1540)$ in the soft-core KN model, in the same way as we included resonances in the soft-core πN models, and investigated its influence as a function of its decay width on the total cross section. We concluded that, in view of the present scattering data, its decay width must be smaller than 10 MeV.

The present soft-core πN and KN models, in which one-particle exchanges are included in the potentials, could be improved by adding two-particle exchange processes to the πN and KN potentials, similar to the extended soft-core NN and YN models. Also, the Coulomb interaction, which in principle plays a role at very low energies, has not been considered here.

Finally this thesis provides the basis for the extension of the soft-core approach to the antikaon-nucleon ($\bar{K}N$) interaction, and to meson-baryon interactions in general. The $\bar{K}N$ system is already at threshold coupled to the $\Lambda\pi$ and $\Sigma\pi$ channels. The coupled channels treatment for this system is similar to that of the YN system.

Appendix A

Matrix elements on the LSJ-basis

A.1 Partial wave amplitudes

Here we derive the central and non-central potential matrix elements on the LSJ-basis in Eqs. (3.4) and (3.5)

1. *Central* $P_1 = 1$:

$$\begin{aligned}\left(q_f; L'J'M'|F(\mathbf{q}_f,\mathbf{q}_i)|q_i; LJM\right) &= \sum_{s_f,s_i}\int\frac{d^3q'_f}{(2\pi)^3}\int\frac{d^3q'_i}{(2\pi)^3}\\ &\times\left(q_f; L'J'M'|\mathbf{q}'_f, s_f\right)\left(\mathbf{q}'_f, s_f|F_{op}|\mathbf{q}'_i, s_i\right)\,\left(\mathbf{q}'_i, s_i|q_i, LJM\right). \end{aligned}\tag{A.1}$$

We now use the matrix element

$$\left(\mathbf{q}'_f, s_f|F_{op}|\mathbf{q}'_i, s_i\right) = F(\mathbf{q}'_f,\mathbf{q}'_i)\delta_{s_f,s_i}\ ,\tag{A.2}$$

with the partial wave expansion for the amplitude $F(\mathbf{q}'_f,\mathbf{q}'_i)$

$$\begin{aligned}F(\mathbf{q}'_f,\mathbf{q}'_i) &= \sum_{l=0}^{\infty}(2l+1)\ F_l(q'_f,q'_i)\ P_l\left(\hat{\mathbf{q}}'_f\cdot\hat{\mathbf{q}}'_i\right)\\ &= \sum_{l=0}^{\infty}(2l+1)\ F_l(q'_f,q'_i)\cdot\sum_{n=-l}^{l}\frac{4\pi}{2l+1}\ Y^l_n(\hat{\mathbf{q}}'_f)Y^l_n(\hat{\mathbf{q}}'_i)^*\ ,\end{aligned}\tag{A.3}$$

and

$$\left(\mathbf{q}', s|q, LJM\right) = (2\pi)^3\,\frac{\delta(q'-q)}{q^2}\ \mathcal{Y}^M_{L\ J}(\hat{\mathbf{q}}', s)\ ,\tag{A.4}$$

see Appendix A.2. Then, substituting Eqs. (A.2)–(A.4) into Eq. (A.1) and performing the momentum and angular integrals, we find

$$\left(q_f; L'J'M'|F(\mathbf{q}_f,\mathbf{q}_i)|q_i; LJM\right) = 4\pi\sum_{s_f,s_i,m',m}\delta_{s_f,s_i}\sum_l F_l\left(q_f,q_i\right)\cdot\sum_{n=-l}^{l}$$

$$
\begin{aligned}
& \times C^{L'\ 1/2\ J'}_{m'\ s_f\ M'}\ C^{L\ 1/2\ J}_{m\ s_i\ M} \cdot \delta_{L',l}\ \delta_{m',n}\ \delta_{l,L}\ \delta_{n,m} \\
= \;& 4\pi\, F_L\left(q_f, q_i\right) \cdot \sum_{n,s} C^{L\ 1/2\ J'}_{n\ s\ M'}\ C^{L\ 1/2\ J}_{n\ s\ M}\ \delta_{L'L} \\
= \;& 4\pi\, F_L\left(q_f, q_i\right)\ \delta_{L'L}\delta_{J',J}\ \delta_{M',M}\ . \qquad \text{(A.5)}
\end{aligned}
$$

2. *Non-central* $P_2' = (\boldsymbol{\sigma}\cdot\hat{\mathbf{q}}_f)(\boldsymbol{\sigma}\cdot\hat{\mathbf{q}}_i)$:

$$
\begin{aligned}
\left(q_f; L'J'M'|G(\mathbf{q}_f, \mathbf{q}_i)|q_i; LJM\right) = & \sum_{s_f, s_i} \int \frac{d^3q'_f}{(2\pi)^3} \int \frac{d^3q'_i}{(2\pi)^3} \\
& \times \left(q'_f; L'J'M'|\mathbf{q}_f, s_f\right) \left(\mathbf{q}'_f, s_f|G_{op}|\mathbf{q}'_i, s_i\right)\ \left(\mathbf{q}'_i, s_i|q_i, LJM\right)\ , \qquad \text{(A.6)}
\end{aligned}
$$

where

$$
\left(\mathbf{q}'_f, s_f|G_{op}|\mathbf{q}'_i, s_i\right) = G(\mathbf{q}'_f, \mathbf{q}'_i) \cdot \sum_s \langle s_f|(\boldsymbol{\sigma}\cdot\hat{\mathbf{q}}'_f)|s\rangle\ \langle s|(\boldsymbol{\sigma}\cdot\hat{\mathbf{q}}'_i)|s_i\rangle\ , \qquad \text{(A.7)}
$$

with, analogously to Eq. (A.3),

$$
G(\mathbf{q}'_f, \mathbf{q}'_i) \;=\; 4\pi \sum_{l=0}^{\infty} G_l(q'_f, q'_i) \cdot \sum_{n=-l}^{l} Y^l_n(\hat{\mathbf{q}}'_f) Y^l_n(\hat{\mathbf{q}}'_i)^*\ . \qquad \text{(A.8)}
$$

Using Eq. (A.4) and substituting Eqs. (A.7) and (A.8) into Eq. (A.6), and performing the momentum and angular integrals, we find

$$
\begin{aligned}
\left(q_f; L'J'M'|G_{op}|q_i; LJM\right) = 4\pi & \sum_{s_f, s_i, s} \int d^3q'_f \int d^3q'_i\ \frac{\delta(q'_f - q_f)}{q_f^2} \frac{\delta(q'_i - q_i)}{q_i^2} \\
& \times \Bigg[\mathcal{Y}^{M'}_{L_f, J'}(\hat{\mathbf{q}}_f, s_f)^*\ (s_f|\left(\boldsymbol{\sigma}\cdot\hat{\mathbf{q}}'_f\right)|s)\ \sum_l G_l\left(q'_f, q'_i\right) \\
& \times \sum_{n=-l}^{l} Y^l_n(\hat{\mathbf{q}}'_f) Y^l_n(\hat{\mathbf{q}}'_i)^* (s|\left(\boldsymbol{\sigma}\cdot\hat{\mathbf{q}}'_i\right)|s_i)\ \mathcal{Y}^M_{L_i, J}(\hat{\mathbf{q}}_i, s_i) \Bigg] \\
= 4\pi & \sum_{s_f, s_i, s} \sum_l G_l\left(q_f, q_i\right) \cdot \sum_{n=-l}^{l} \\
& \times \Bigg[\int d\hat{\Omega}_{q_f}\ \mathcal{Y}^{M'}_{L_f, J'}(\hat{\mathbf{q}}_f, s_f)^* (s_f|\left(\boldsymbol{\sigma}\cdot\hat{\mathbf{q}}_f\right)|s)\ Y^l_n(\hat{\mathbf{q}}_f) \\
& \times \int d\hat{\Omega}_{q_i}\ Y^l_n(\hat{\mathbf{q}}_i)^* (s|\left(\boldsymbol{\sigma}\cdot\hat{\mathbf{q}}_i\right)|s_i)\ \mathcal{Y}^M_{L_i, J}(\hat{\mathbf{q}}_i, s_i) \Bigg]\ . \qquad \text{(A.9)}
\end{aligned}
$$

In the two-dimensional $L = J \mp \frac{1}{2}$-space, the $(\boldsymbol{\sigma}\cdot\hat{\mathbf{q}})$-operator has the matrix elements, see Appendix A.2,

$$
\sum_{s'} (s|\left(\boldsymbol{\sigma}\cdot\hat{\mathbf{q}}\right)|s')\ \mathcal{Y}^M_{L,J}(\hat{\mathbf{q}}, s') = \sum_{L'} \mathcal{Y}^M_{L',J}(\hat{\mathbf{q}}, s)\ a_{L',L}\ \text{ where } a_{L',L} = \begin{pmatrix} 0 & -1 \\ -1 & 0 \end{pmatrix}\ , \qquad \text{(A.10)}
$$

i.e. $a_{J\mp\frac{1}{2},J\mp\frac{1}{2}}=0$, and $a_{J\mp\frac{1}{2},J\pm\frac{1}{2}}=-1$. The angular integrals in Eq. (A.9) can now be performed easily, and one finds

$$\sum_{s_i}\int d\hat{\Omega}_{q_i}\ Y_n^l(\hat{\mathbf{q}}_i)^*(s|\left(\boldsymbol{\sigma}\cdot\hat{\mathbf{q}}_i\right)|s_i)\mathcal{Y}^M_{L_i,J}(\hat{\mathbf{q}}_i,s_i)=$$
$$\sum_{L',m',\mu} a_{L',L_i}\ C^{L'\ 1/2\ J}_{m'\ \ \mu\ \ M}\ \chi^{(1/2)}_\mu(s)\ \delta_{l,L'}\delta_{n,m'}\ ,$$
$$\sum_{s_f}\int d\hat{\Omega}_{q_f}\ \mathcal{Y}^{M'}_{L_f,J'}(\hat{\mathbf{q}}_f,s_f)^*(s_f|\left(\boldsymbol{\sigma}\cdot\hat{\mathbf{q}}_f\right)|s)\ Y_n^l(\hat{\mathbf{q}}_f)=$$
$$\sum_{L'',m'',\nu} a_{L_f,L''}\ C^{L''\ 1/2\ J'}_{m''\ \ \nu\ \ M'}\ \chi^{(1/2)*}_\nu(s)\ \delta_{l,L''}\delta_{n,m''}\ . \tag{A.11}$$

Then, the result for the non-central amplitude is

$$\begin{aligned}\left(q_f;L_fJ'M'|G|q_i;L_iJM\right)&=4\pi\sum_l G_l\left(q_f,q_i\right)\cdot\sum_s\sum_{n=-l}^{l}\\ \times\sum_{L'',L',m'',m'} a_{L_f,L''}\ C^{L''\ 1/2\ J'}_{m''\ s\ M'}\ \delta_{l,L''}\delta_{n,m''}&\cdot a_{L_i,L'}\ C^{L'\ 1/2\ J}_{m'\ s\ M}\ \delta_{l,L'}\delta_{n,m'}\\ =4\pi\sum_l\sum_{m,s}C^{l\ 1/2\ J'}_{m\ s\ M'}\ C^{l\ 1/2\ J}_{m\ s\ M}&\cdot\left[a_{L_f,l}G_l\left(q_f,q_i\right)\ a_{l,L_i}\right]\\ =4\pi\sum_{L'} a_{L_f,L'}G_{L'}\left(q_f,q_i\right)\ a_{L',L_i}\delta_{J',J}\delta_{M',M}&\ .\end{aligned} \tag{A.12}$$

A.2 LSJ-matrix elements

In this appendix we derive Eq. (A.10). The spherical wave functions in momentum space with quantum numbers J, L, S, are for spin-0 spin-1/2 given by [88]

$$\mathcal{Y}^M_{LJ}(\hat{\mathbf{p}},s)=\sum_{m,\mu}C^{J\ \ L\ \ \frac{1}{2}}_{M\ m\ \mu}Y^L_m(\hat{\mathbf{p}})\chi^{(1/2)}_\mu(s)\ , \tag{A.13}$$

where χ is the baryon spin wave function.

$$\sum_s(s'|\left(\boldsymbol{\sigma}\cdot\hat{\mathbf{p}}\right)|s)\ \mathcal{Y}^M_{L,J}(\hat{\mathbf{p}},s)=\mathcal{Y}^M_{L',J}(\hat{\mathbf{p}},s')\ a_{L',L}\ \text{ where } a_{L',L}=\begin{pmatrix}0&-1\\-1&0\end{pmatrix}. \tag{A.14}$$

Using the definition for $\mathcal{Y}^M_{L,J}$, Eq. (A.13), we have

$$\begin{aligned}\sum_s(s'|\left(\boldsymbol{\sigma}\cdot\hat{\mathbf{p}}\right)|s)\ \mathcal{Y}^M_{L,J}(\hat{\mathbf{p}},s)&=(-)^m\hat{\mathbf{p}}_m\ (s'|\sigma_{-m}|s)\ C^{L\ 1/2\ J}_{m_l\ \mu\ M}\ Y^L_{m_l}(\hat{\mathbf{p}})\chi^{(1/2)}_\mu(s)\\ &=(-)^m\hat{\mathbf{p}}_m\ (s'|\sigma_{-m}|s)\ C^{L\ 1/2\ J}_{m_l\ s\ M}\ Y^L_{m_l}(\hat{\mathbf{p}})\ ,\end{aligned} \tag{A.15}$$

where we used the convention of summation over repeated indices, and quantization along the z-axis, which defines the spin variables s, s'.

Now, we use the expressions

$$\begin{aligned}
\hat{\mathbf{p}}_m \, Y^L_{m_l}(\hat{\mathbf{p}}) &= \sqrt{\frac{4\pi}{3}} Y^1_m(\hat{\mathbf{p}}) \, Y^L_{m_l}(\hat{\mathbf{p}}) \\
&= \sqrt{\frac{4\pi}{3}} \left[\frac{3(2L+1)}{4\pi(2L'+1)}\right]^{1/2} C^{L\ 1\ L'}_{0\ 0\ 0} \cdot C^{L\ \ 1\ L'}_{m_l\ m\ m'_L} \ Y^{L'}_{m'_l}(\hat{\mathbf{p}}) \,, \\
(s'|\sigma_{-m}|s) &= \sqrt{3}\, C^{1/2\ 1\ 1/2}_{s\ -m\ s'} \,.
\end{aligned} \tag{A.16}$$

Furthermore, we note that $(-)^m = -\sqrt{3}\, C^{1\ \ 1\ \ 0}_{m\ -m\ 0}$. These formulas give for Eq. (A.15) the result

$$\begin{aligned}
&\sum_s (s'|\left(\boldsymbol{\sigma}\cdot\hat{\mathbf{p}}\right)|s)\, \mathcal{Y}^M_{L,J}(\hat{\mathbf{p}},s) = -3\left[\frac{(2L+1)}{(2L'+1)}\right]^{1/2} C^{L\ 1\ L'}_{0\ \ 0\ 0} \\
&\times \sum_{all\ m\neq M'} C^{L\ 1/2\ J}_{m_l\ s\ M}\, C^{1\ \ \ 1\ 0}_{m\ -m\ 0}\, C^{L'\ 1/2\ J'}_{m'_l\ \ s'\ M'} C^{L\ \ \ 1\ L'}_{m_l\ m\ m'_l}\, C^{1/2\ 1\ 1/2}_{s\ -m\ s'}\, \mathcal{Y}^M_{L'J}(\hat{\mathbf{p}}) \,.
\end{aligned}$$

From the definition of the $9j$-coefficient [89], we can write the expression above as

$$\begin{aligned}
\sum_s (s'|\left(\boldsymbol{\sigma}\cdot\hat{\mathbf{p}}\right)|s)\, \mathcal{Y}^M_{L,J}(\hat{\mathbf{p}},s) &= -3\left[\frac{(2L+1)}{(2L'+1)}\right]^{1/2} C^{L\ 1\ L'}_{0\ \ 0\ 0} \cdot \begin{bmatrix} L & \frac{1}{2} & J \\ 1 & 1 & 0 \\ L' & \frac{1}{2} & J' \end{bmatrix} \\
&\quad \times \mathcal{Y}^M_{L'J}(\hat{\mathbf{p}}) \,.
\end{aligned} \tag{A.17}$$

$$C^{L\ 1\ L'}_{0\ 0\ 0} = -\sqrt{\frac{L}{2L+1}}\,\delta_{L',L-1} + \sqrt{\frac{L+1}{2L+1}}\,\delta_{L',L+1} \,. \tag{A.18}$$

Since, for a given J, there are only possible $L = J \mp \frac{1}{2}$, we have in view of Eq. (A.18) the following cases with a matrix element $\neq 0$:

a. $J = L - \frac{1}{2}, L = J + \frac{1}{2}, L' = L - 1$: The 9j-coefficient becomes, see [90],

$$\begin{bmatrix} L & \frac{1}{2} & L-1/2 \\ 1 & 1 & 0 \\ L-1 & \frac{1}{2} & L-1/2 \end{bmatrix} = -\frac{1}{3}\sqrt{\frac{2L-1}{L}} \,, \tag{A.19}$$

b. $J = L + \frac{1}{2}, L = J - \frac{1}{2}, L' = L + 1$: The 9j-coefficient becomes

$$\begin{bmatrix} L & \frac{1}{2} & L+1/2 \\ 1 & 1 & 0 \\ L+1 & \frac{1}{2} & L+1/2 \end{bmatrix} = \frac{1}{3}\sqrt{\frac{2L+3}{L+1}} \,. \tag{A.20}$$

Combining the results Eqs. (A.17)-(A.20), one finds for the matrix a in Eq. (A.14)

$$a = \begin{pmatrix} 0 & -1 \\ -1 & 0 \end{pmatrix} \,. \tag{A.21}$$

This result can be checked by observing the following:

(i) We have $(\boldsymbol{\sigma}\cdot\hat{\mathbf{p}})^2 = 1$, and $(\boldsymbol{\sigma}\cdot\hat{\mathbf{p}})^\dagger = \boldsymbol{\sigma}\cdot\hat{\mathbf{p}}$. Furthermore, in $L = J \mp \frac{1}{2}$-space $\boldsymbol{\sigma}\cdot\hat{\mathbf{p}}$ is a purely off-diagonal operator. as a result of these properties, $a_{J\pm 1/2,J\pm 1/2} = 0$, and $a_{J+1/2,J-1/2} = a^*_{J-1/2,J+1/2} \equiv \alpha$.

(ii) To determine α, we choose $\hat{\mathbf{p}} = (0,0,1) = \hat{\mathbf{e}}_3$, which gives $\boldsymbol{\sigma}\cdot\hat{\mathbf{p}} \Rightarrow \sigma_3$, and the spherical functions

$$Y^L_m(\hat{\mathbf{e}}_3) = \delta_{m0}\sqrt{\frac{2L+1}{4\pi}} \; . \tag{A.22}$$

(iii) Employing now the Clebsch-Gordan coefficients,

$$C^{L\ 1/2\ L-1/2}_{0\ 1/2\ \ 1/2} = \sqrt{\frac{L}{2L+1}} \;,\; C^{L\ 1/2\ L+1/2}_{0\ 1/2\ \ 1/2} = -\sqrt{\frac{L+1}{2L+1}} \;, \tag{A.23}$$

one easily verifies that $\alpha = -1$.

(i) Normalization of states

The normalization of the states and wave function we use is given by

$$\begin{aligned} (\mathbf{r}'|\mathbf{r}) &= \delta^3(\mathbf{r}'-\mathbf{r}) \;, \\ (\mathbf{p}'|\mathbf{p}) &= (2\pi)^3\delta^3(\mathbf{p}'-\mathbf{p}) \;, \\ (\mathbf{r}|\mathbf{p}) &= e^{i\mathbf{p}\cdot\mathbf{r}} \;. \end{aligned} \tag{A.24}$$

In the case of a spinless particle the state with momentum p and orbital angular momentum l is given by

$$|plm) = \int d\Omega_{\hat{\mathbf{p}}} Y_{lm}(\hat{\mathbf{p}})|\mathbf{p}) \;, \tag{A.25}$$

this state is an eigenstate of the angular momentum operator L. From this equation we can also find

$$|\mathbf{p}) = \sum_{lm} Y^*_{lm}(\hat{\mathbf{p}})|plm) \;. \tag{A.26}$$

Using the previous definitions we can calculate the matrix elements

$$\begin{aligned} (\mathbf{r}|plm) &= \int d\Omega_{\hat{\mathbf{p}}} Y_{lm}(\hat{\mathbf{p}}) 4\pi \sum_{l'm'} i^{l'} j_l(kr) Y^*_{l'm'}(\hat{\mathbf{p}}) Y_{l'm'}(\hat{\mathbf{r}}) \\ &= 4\pi i^l j_l(kr) Y_{lm}(\hat{\mathbf{r}}) \;, \\ (p'l'm'|\mathbf{p}) &= \int d\Omega_{\hat{\mathbf{p}}'} Y^*_{l'm'}(\hat{\mathbf{p}}')(2\pi)^3\delta^3(\mathbf{p}'-\mathbf{P}) \\ &= (2\pi)^3\frac{\delta(p'-p)}{p^2} Y^*_{l'm'}(\hat{\mathbf{p}}) \;. \end{aligned} \tag{A.27}$$

The extension of this last matrix element to the case in which spin is included is straightforward, we find

$$(\mathbf{p}'s'|p, LJM) \;=\; (2\pi)^3 \frac{\delta(p'-p)}{p^2} \mathcal{Y}^M_{LJ}(\hat{\mathbf{p}}', s') \,, \tag{A.28}$$

where $\mathcal{Y}^M_{LJ}(\hat{\mathbf{p}}', s')$ is given by

$$\mathcal{Y}^M_{LJ}(\hat{\mathbf{p}}', s') = \sum_{m,\mu} C^{J\;L\;\frac{1}{2}}_{M\;m\;\mu} Y^L_m(\hat{\mathbf{p}}') \chi^{(1/2)}_\mu(s') \,. \tag{A.29}$$

Appendix B

OBE and baryon-exchange isospin factors

We outline the calculation of the isospin factors for the meson-baryon interactions, making use of the Wigner 6-j and 9-j symbols, see for example Edmonds [90], this reference also gives relations for interchanging the labels of Clebsch-Gordan coefficients. An example for the pion-nucleon and for the kaon-nucleon interaction is given.

(i) Baryon exchange in pion-nucleon interactions:

The isospin matrix element for a given total final and initial isospin in the πN system reads

$$\langle I_f\ M_f|\mathcal{H}|I_i\ M_i\rangle \quad = \quad C^{1\ \frac{1}{2}\ I_f}_{m'\ n'\ M_f}\ C^{1\ \frac{1}{2}\ I_i}_{m\ n\ M_i}\ \langle \pi_{m'}\ N_{n'}|\mathcal{H}|\pi_m\ N_n\rangle\ , \tag{B.1}$$

where I is the total isospin of the system and M its z-component, m is the z-component of the pions isospin and n is the z-component of the nucleons isospin, see Figure B.1. We can rewrite the first Clebsch-Gordan coefficient in Eq. (B.1), [90],

$$C^{1\ \frac{1}{2}\ I_f}_{m'\ n'\ M_f} \quad = \quad (-)^{\frac{3}{2}-I_f}\ C^{\frac{1}{2}\ 1\ I_f}_{n'\ m'\ M_f}\ . \tag{B.2}$$

For baryon exchange the isospin interaction Hamiltonian $\mathcal{H}$ for either the $NN\pi$ or the $N\Delta\pi$

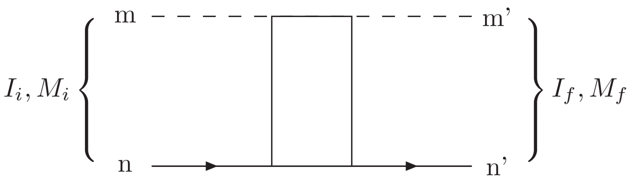

Figure B.1: The matrix element for the total isospin, m is the z-component of the pion isospin and n is the z-component of the nucleon isospin.

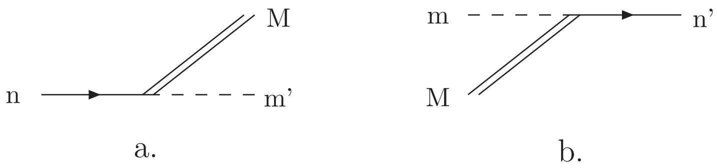

Figure B.2: Figure a. shows the baryon emission vertex and figure b. shows the baryon absorption vertex.

vertex is of the form

$$\mathcal{H} \;\sim\; g\left[C^{1\,\frac{1}{2}\,i}_{m\,n\,M}\;\psi^*_M N_n \pi_m + C^{1\,\frac{1}{2}\,i}_{m\,n\,M}\;N^*_n \psi_M \pi^*_m\right], \tag{B.3}$$

where ψ_M denotes either the nucleon with $i=\frac{1}{2}$ or the Δ with $i=\frac{3}{2}$. Here $\pi_{+1} = -(\pi_1 + i\pi_2)/\sqrt{2}$, $\pi_{-1} = (\pi_1 - i\pi_2)/\sqrt{2}$ and $\pi_0 = \pi_3$, we note that $\pi_m = (-)^m \pi^*_{-m}$. The baryon emission vertex shown in Figure B.2 gives the factor

$$\begin{aligned}(-)^{-m'}\,C^{1\,\frac{1}{2}\,i}_{-m'\,n\,M} &= (-)^{-m'}(-)^{\frac{1}{2}+n}\sqrt{\frac{2i+1}{3}}\,C^{\frac{1}{2}\,i\,1}_{-n\,M\,-m'} \\ &= (-)^{-m'}(-)^{n+i}\sqrt{\frac{2i+1}{3}}\,C^{\frac{1}{2}\,i\,1}_{n\,-M\,m'}\,. \end{aligned}\tag{B.4}$$

The baryon absorption vertex shown in Figure B.2 gives the factor

$$\begin{aligned}(-)^{-m}\,C^{1\,\frac{1}{2}\,i}_{-m\,n'\,M} &= (-)^{-m}(-)^{1+m}\sqrt{\frac{2i+1}{2}}\,C^{1\,i\,\frac{1}{2}}_{-m\,-M\,-n'} \\ &= (-)^{-m}(-)^{m+i-\frac{1}{2}}\sqrt{\frac{2i+1}{2}}\,C^{1\,i\,\frac{1}{2}}_{m\,M\,n'}\,. \end{aligned}\tag{B.5}$$

Using Eqs. (B.2), (B.4) and (B.5) we find for the total isospin matrix element of Eq. (B.1)

$$\begin{aligned}\langle I_f\;M_f|\mathcal{H}|I_i\;M_i\rangle &= g^2\,(-)^{1+3i-I_f+(i-M)}\,\frac{2i+1}{\sqrt{6}}\times \\ &\qquad C^{\frac{1}{2}\,1\,I_f}_{n'\,m'\,M_f}\,C^{1\,\frac{1}{2}\,I_i}_{m\,n\,M_i}\,C^{\frac{1}{2}\,i\,1}_{n\,-M\,m'}\,C^{1\,i\,\frac{1}{2}}_{m\,M\,n'}\,, \end{aligned}\tag{B.6}$$

applying the identity $(-)^{i-M} = \sqrt{2i+1}C^{i\,1\,0}_{M\,-M\,0}$, we find

$$\begin{aligned}\langle I_f\;M_f|\mathcal{H}|I_i\;M_i\rangle &= g^2\,(-)^{1+3i-I_f}\sqrt{2i+1}\,\frac{2i+1}{\sqrt{6}}\begin{bmatrix}1 & i & \frac{1}{2}\\ \frac{1}{2} & i & 1\\ I & 0 & I\end{bmatrix} \\ &= -g^2\,(2i+1)\begin{Bmatrix}\frac{1}{2} & 1 & i\\ \frac{1}{2} & 1 & I\end{Bmatrix}, \end{aligned}\tag{B.7}$$

here we have used the conservation of isospin $I_f = I_i = I$. The isospin factors we find for nucleon and Δ exchange, using the interaction Hamiltonians of Eqs. (6.1) and (6.2),

$$\mathcal{H}_{NN\pi} = \frac{f_{NN\pi}}{m_{\pi^+}} \left(\bar{N}\gamma_5\gamma_\mu \boldsymbol{\tau} N\right)\cdot\partial^\mu \boldsymbol{\pi} \,, \tag{B.8}$$

$$\mathcal{H}_{N\Delta\pi} = \frac{f_{N\Delta\pi}}{m_{\pi^+}} \left(\bar{N}\boldsymbol{T}\Delta_\mu\right)\cdot\partial^\mu \boldsymbol{\pi} + H.c. \,, \tag{B.9}$$

are equal to Eq. (B.7) multiplied with the reduced matrix elements squared. For nucleon exchange the reduced matrix element is $\langle\frac{1}{2}\|\boldsymbol{\tau}\|\frac{1}{2}\rangle = \sqrt{3}$ and for Δ exchange it is $\langle\frac{1}{2}\|\boldsymbol{T}\|\frac{1}{2}\rangle = 1$. The 6-j symbols are tabulated in Edmonds [90], we find for the isospin factors the results given in Table B.1.

Exchange	$I=\frac{1}{2}$	$I=\frac{3}{2}$
N	-1	2
Δ	$\frac{4}{3}$	$\frac{1}{3}$

Table B.1: The isospin factors for nucleon and Δ exchange for a given total isospin I of the πN system.

(ii) ρ exchange in kaon-nucleon interactions:

The isospin matrix element for a given total final and initial isospin in the KN system reads

$$\langle I_f\ M_f|\mathcal{H}|I_i\ M_i\rangle = C^{\frac{1}{2}\ \frac{1}{2}\ I_f}_{m'\ n'\ M_f}\, C^{\frac{1}{2}\ \frac{1}{2}\ I_i}_{m\ n\ M_i}\, \langle K_{m'}\ N_{n'}|\mathcal{H}|K_m\ N_n\rangle \,, \tag{B.10}$$

where I is the total isospin of the system and M its z-component, m is the z-component of the kaon isospin and n is the z-component of the nucleon isospin. For ρ exchange the isospin interaction Hamiltonians $\mathcal{H}$ for the $NN\rho$ and $KK\rho$ vertex are of the form

$$\begin{aligned} \mathcal{H}_{NN\rho} &\sim g_{NN\rho}\, C^{\frac{1}{2}\ 1\ \frac{1}{2}}_{n\ M\ n'}\, N^*_{n'} N_n \rho_M \,, \\ \mathcal{H}_{KK\rho} &\sim g_{KK\rho}\, C^{\frac{1}{2}\ 1\ \frac{1}{2}}_{m\ M\ m'}\, K^*_{m'} K_m \rho_M \,, \end{aligned} \tag{B.11}$$

we note that $\rho_m = (-)^m \rho^*_{-m}$. The ρ emission vertex shown in Figure B.3 gives the factor

$$(-)^{-M}\, C^{\frac{1}{2}\ 1\ \frac{1}{2}}_{n\ -M\ n'} \,. \tag{B.12}$$

The ρ absorption vertex shown in Figure B.3 gives the factor

$$C^{\frac{1}{2}\ 1\ \frac{1}{2}}_{m\ M\ m'} \,. \tag{B.13}$$

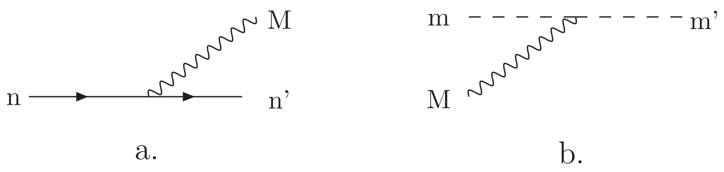

Figure B.3: Figure a. shows the ρ emission vertex and figure b. shows the ρ absorption vertex.

Using Eqs. (B.11), (B.12) and (B.13) we find for the total isospin matrix element of Eq. (B.10)

$$\langle I_f\ M_f|\mathcal{H}|I_i\ M_i\rangle \;=\; g_{NN\rho}g_{KK\rho}\,(-)^{-M}C^{\frac{1}{2}\,\frac{1}{2}\,I_f}_{m'\,n'\,M_f}\,C^{\frac{1}{2}\,\frac{1}{2}\,I_i}_{m\,n\,M_i}\,C^{\frac{1}{2}\,1\,\frac{1}{2}}_{n\,-M\,n'}\,C^{\frac{1}{2}\,1\,\frac{1}{2}}_{m\,M\,m'}\,, \tag{B.14}$$

applying the identity $(-)^{-M} = -\sqrt{3}C^{1\,1\,0}_{-M\,M\,0}$, we find

$$\begin{aligned}\langle I_f\ M_f|\mathcal{H}|I_i\ M_i\rangle &= -g_{NN\rho}g_{KK\rho}\,\sqrt{3}\begin{bmatrix}\frac{1}{2} & i & \frac{1}{2}\\ \frac{1}{2} & i & \frac{1}{2}\\ I & 0 & I\end{bmatrix}\\ &= g_{NN\rho}g_{KK\rho}\,\frac{1}{3}\,[2I\,(I+1)-3]\;,\end{aligned} \tag{B.15}$$

here we have used the conservation of isospin $I_f = I_i = I$. The isospin factors we find for ρ exchange, using the interaction Hamiltonians of Eqs. (7.3) and (7.4), are equal to Eq. (B.14) multiplied with the reduced matrix element squared. For ρ exchange it is $\langle\frac{1}{2}\|\boldsymbol{\tau}\|\frac{1}{2}\rangle = \sqrt{3}$. So for $I = 0$ we find an isospin factor of -3 and for $I = 1$ a factor 1.

Other isospin factors can be calculated in the same way, all relevant isospin factors for the pion-nucleon and kaon-nucleon interaction are listed in Tables 6.1 and 7.1 respectively.

Appendix C

Relativistic invariant amplitudes

In this appendix the contributions from the various Feynman diagrams to the relativistic invariant amplitudes $A(s,t,u)$ and $B(s,t,u)$, defined in Eq. (2.5), are derived in detail from the Feynman rules in [27] and the local interaction Hamiltonians defined in Eqs. (4.12)–(4.19). We derive the Lorentz structure of the amplitudes, so the isospin structure is omitted here . We notice that the invariant amplitude M_{fi} we use is defined differently, according to Eq. (2.2).

In the derivation we use the assumption that the intermediate particles are on-mass-shell, see subsection 2.3.1. Since we distinguish between initial and final masses, the results are valid for elastic as well as inelastic reactions.

C.1 Momentum space baryon-exchange diagrams

(i) $J^P = \frac{1}{2}^+$ baryon-exchange

(i) pseudoscalar coupling:
The S-matrix element for the baryon-exchange diagram is given by

$$\begin{aligned} S_{fi} &= g_{14}^{(ps)} g_{23}^{(ps)} \int \frac{d^4 p_u}{(2\pi)^4}\, \bar{u}(\mathbf{p}_f, s_f) \left[\gamma_5 \frac{i}{\not{p}_u - M_B + i\epsilon} \gamma_5 \right] u(\mathbf{p}_i, s_i) \\ &\quad \times (2\pi)^4 \delta^4(p - p_u - q')\, (2\pi)^4 \delta^4(p' - q - p_u) \\ &= (2\pi)^4\, i\, \delta^4(p' + q' - p - q)\, g_{14}^{(ps)} g_{23}^{(ps)} \\ &\quad \times \bar{u}(\mathbf{p}_f, s_f) \left[\gamma_5 \frac{1}{(\not{p} - \not{q}') - M_B + i\epsilon} \gamma_5 \right] u(\mathbf{p}_i, s_i)\ . \end{aligned} \tag{C.1}$$

The corresponding M-matrix element is therefore

$$\begin{aligned} M_{fi} &= -g_{14}^{(ps)} g_{23}^{(ps)}\, \bar{u}(\mathbf{p}_f, s_f) \left[\gamma_5 \frac{1}{(\not{p} - \not{q}') - M_B + i\epsilon} \gamma_5 \right] u(\mathbf{p}_i, s_i) \\ &= -g_{14}^{(ps)} g_{23}^{(ps)}\, \bar{u}(\mathbf{p}_f, s_f) \frac{-(\not{p} - \not{q}') + M_B}{u - M_B^2 + i\epsilon} u(\mathbf{p}_i, s_i)\ . \end{aligned} \tag{C.2}$$

Now, since implicitly in Eq. (C.2) $p - q' = p' - q$, we can write

$$\not{p}_u = \not{p} - \not{q}' = \frac{1}{2}(\not{p}' + \not{p}) - \frac{1}{2}(\not{q}' + \not{q}) \,. \tag{C.3}$$

Then, using the Dirac equation and the fact that particles are on-mass-shell, we can rewrite the right-hand side of Eq. (C.2) as

$$M_{fi} = -\frac{g_{14}^{(ps)}\, g_{23}^{(ps)}}{u - M_B^2 + i\epsilon}\, \bar{u}(\mathbf{p}_f, s_f) \left[\left\{ -\frac{1}{2}(M_f + M_i) + M_B \right\} + \not{Q} \right] u(\mathbf{p}_i, s_i) \,, \tag{C.4}$$

where $Q = \frac{1}{2}\left(q' + q\right)$. From Eq. (C.4), we can readily obtain the contribution to the invariant amplitudes $A_{fi}(s,t,u)$ and $B_{fi}(s,t,u)$ defined in Eq. (2.5). We get

$$\begin{aligned} A_{fi}(PS) &= -\frac{g_{14}^{(ps)}\, g_{23}^{(ps)}}{u - M_B^2 + i\epsilon} \left\{ -\frac{1}{2}(M_f + M_i) + M_B \right\} \,, \\ B_{fi}(PS) &= -\frac{g_{14}^{(ps)}\, g_{23}^{(ps)}}{u - M_B^2 + i\epsilon} \,. \end{aligned} \tag{C.5}$$

(ii) pseudovector coupling:
From the interaction Hamiltonian density in Eq. (4.12), the interaction vertex is given by the matrix element

$$\begin{aligned} &(2\pi)^4 \delta(p' - p - q) \left[\bar{u}(\mathbf{p}', s')\, \Gamma_{PV}(p', p)\, u(\mathbf{p}, s) \right] \equiv \langle p' | -i \int d^4x \mathcal{H}_{pv}(x) | p, q \rangle \\ &= -i\; (2\pi)^4 \delta(p' - p - q) \cdot \frac{f_{pv}}{m_{\pi^+}} \cdot \bar{u}(\mathbf{p}', s') \gamma_5 \gamma_\mu\, u(\mathbf{p}, s) \cdot -i q^\mu \\ &= -\frac{f_{pv}}{m_{\pi^+}}\, (2\pi)^4 \delta(p' - p - q)\; \left[\bar{u}(\mathbf{p}', s') \gamma_5 \gamma \cdot q\; u(\mathbf{p}, s) \right] \,. \end{aligned} \tag{C.6}$$

It is clear that for a vertex with an outgoing pseudoscalar-meson we have to replace in Eq. (C.6) q by $-q$. It follows that irrespectively whether the meson is absorbed or created at the vertex, the vertex-function $\Gamma_{PV}(p', p)$ is given by

$$\Gamma_{PV}(p', p) = -\frac{f_{pv}}{m_{\pi^+}}\; \left[\gamma_5 \gamma \cdot (p' - p) \right] \,. \tag{C.7}$$

The S-matrix element for the pseudovector coupling baryon-exchange diagram is now given by

$$\begin{aligned} S_{fi} &= \frac{f_{14}^{(pv)}\, f_{23}^{(pv)}}{m_{\pi^+}^2} \int \frac{d^4 p_u}{(2\pi)^4}\, \bar{u}(\mathbf{p}_f, s_f) \left[(-\gamma_5\, \not{q}) \, \frac{i}{\not{p}_u - M_B + i\epsilon}\, (+\gamma_5\, \not{q}') \right] u(\mathbf{p}_i, s_i) \\ &\quad \times (2\pi)^4 \delta^4(p - p_u - q')\; (2\pi)^4 \delta^4(p' - q - p_u) \\ &= (2\pi)^4\; i\; \delta^4(p' + q' - p - q)\; \frac{f_{14}^{(pv)}\, f_{23}^{(pv)}}{m_{\pi^+}^2} \\ &\quad \times \bar{u}(\mathbf{p}_f, s_f) \left[\not{q}\; \gamma_5\, \frac{1}{(\not{p} - \not{q}') - M_B + i\epsilon}\, \gamma_5\;\; \not{q}' \right] u(\mathbf{p}_i, s_i) \,. \end{aligned} \tag{C.8}$$

The corresponding M-matrix element is given by

$$M_{fi} = -\frac{f_{14}^{(pv)} f_{23}^{(pv)}}{m_{\pi^+}^2} \bar{u}(\mathbf{p}_f, s_f) \left[\not{q} \frac{-(\not{p} - \not{q}') + M_B}{(p' - q)^2 - M_B^2 + i\epsilon} \not{q}' \right] u(\mathbf{p}_i, s_i) \,. \qquad \text{(C.9)}$$

Using Eq. (C.3), the M-matrix element can be written as

$$\begin{aligned} M_{fi} = & -\frac{f_{14}^{(pv)} f_{23}^{(pv)}/m_{\pi^+}^2}{u - M_B^2 + i\epsilon} \bar{u}(\mathbf{p}_f, s_f) \Big[u \left\{ \frac{1}{2} \left(M_f + M_i \right) + M_B \right\} \\ & - \frac{1}{2} \left(M_f + M_i \right)^2 M_B + M_f M_i \left\{ -\frac{1}{2} \left(M_f + M_i \right) + M_B \right\} \\ & + \left\{ u + \left(M_f + M_i \right) M_B + M_f M_i \right\} \not{Q} \Big] u(\mathbf{p}_i, s_i) \,, \end{aligned} \qquad \text{(C.10)}$$

where $u = p_u^2$. We can readily find from Eq. (C.10) the contribution to the invariant amplitudes $A_{fi}(s,t,u)$ and $B_{fi}(s,t,u)$,

$$\begin{aligned} A_{fi}(PV) = & -\frac{f_{14}^{(pv)} f_{23}^{(pv)}/m_{\pi^+}^2}{u - M_B^2 + i\epsilon} \Big[u \left\{ \frac{1}{2} \left(M_f + M_i \right) + M_B \right\} \\ & - \frac{1}{2}(M_f + M_i) M_f M_i - \frac{1}{2} \left(M_f^2 + M_i^2 \right) M_B \Big] \,, \\ B_{fi}(PV) = & -\frac{f_{14}^{(pv)} f_{23}^{(pv)}/m_{\pi^+}^2}{u - M_B^2 + i\epsilon} \left[u + \left(M_f + M_i \right) M_B + M_f M_i \right] \,. \end{aligned} \qquad \text{(C.11)}$$

(ii) $J^P = \frac{1}{2}^+$ pole diagram

Using crossing symmetry [91], we can cross the results of the u-channel baryon-exchange into the s-channel and obtain the invariant amplitudes $A_{fi}(s,t,u)$ and $B_{fi}(s,t,u)$ for the pole diagram. We have to replace $q \to -q'$ and $q' \to -q$, which means that we have to make the substitutions $u \leftrightarrow s$, $m_f^2 \leftrightarrow m_i^2$ and add a minus sign to the amplitude B because of Eq. (2.5). The $J^P = \frac{1}{2}^+$ pole amplitudes are

(i) pseudoscalar coupling:

$$\begin{aligned} A_{fi}(PS) = & -\frac{g_{14}^{(ps)} g_{23}^{(ps)}}{s - M_B^2 + i\epsilon} \left\{ -\frac{1}{2}(M_f + M_i) + M_B \right\} \,, \\ B_{fi}(PS) = & \frac{g_{14}^{(ps)} g_{23}^{(ps)}}{s - M_B^2 + i\epsilon} \,. \end{aligned} \qquad \text{(C.12)}$$

(ii) pseudovector coupling:

$$
\begin{aligned}
A_{fi}(PV) &= -\frac{f_{14}^{(pv)} f_{23}^{(pv)}/m_{\pi^+}^2}{s-M_B^2+i\epsilon}\left[s\left\{\frac{1}{2}\left(M_f+M_i\right)+M_B\right\}\right. \\
&\quad \left. -\frac{1}{2}(M_f+M_i)M_f M_i - \frac{1}{2}\left(M_f^2+M_i^2\right)M_B\right] , \\
B_{fi}(PV) &= \frac{f_{14}^{(pv)} f_{23}^{(pv)}/m_{\pi^+}^2}{s-M_B^2+i\epsilon}\left[s+\left(M_f+M_i\right)M_B+M_f M_i\right] .
\end{aligned}
\tag{C.13}
$$

(iii) $J^P = \frac{1}{2}^-$ baryon-exchange

(i) scalar coupling:
The S-matrix element for the baryon-exchange diagram is given by

$$
\begin{aligned}
S_{fi} &= -g_{14}^{(s)} g_{23}^{(s)} \int \frac{d^4 p_u}{(2\pi)^4}\, \bar{u}(\mathbf{p}_f, s_f)\left[\frac{i}{\not{p}_u - M_B + i\epsilon}\right] u(\mathbf{p}_i, s_i) \\
&\quad \times (2\pi)^4 \delta^4(p-p_u-q')\,(2\pi)^4\delta^4(p'-q-p_u) \\
&= -(2\pi)^4\, i\, \delta^4(p'+q'-p-q)\, g_{14}^{(s)} g_{23}^{(s)} \\
&\quad \times \bar{u}(\mathbf{p}_f, s_f)\left[\frac{1}{(\not{p}-\not{q}')-M_B+i\epsilon}\right] u(\mathbf{p}_i, s_i) .
\end{aligned}
\tag{C.14}
$$

The corresponding M-matrix element is therefore

$$
\begin{aligned}
M_{fi} &= g_{14}^{(s)} g_{23}^{(s)}\, \bar{u}(\mathbf{p}_f, s_f)\left[\frac{1}{(\not{p}-\not{q}')-M_B+i\epsilon}\right] u(\mathbf{p}_i, s_i) \\
&= g_{14}^{(s)} g_{23}^{(s)}\, \bar{u}(\mathbf{p}_f, s_f)\frac{(\not{p}-\not{q}')+M_B}{u-M_B^2+i\epsilon} u(\mathbf{p}_i, s_i) .
\end{aligned}
\tag{C.15}
$$

Now, since implicitly in Eq. (C.15) $p-q'=p'-q$, we can write

$$
\not{p}_u = \not{p}-\not{q}' = \frac{1}{2}(\not{p}'+\not{p}) - \frac{1}{2}(\not{q}'+\not{q}) . \tag{C.16}
$$

Then, using the Dirac equation and the fact that particles are on-mass-shell, we can rewrite the right-hand side of Eq. (C.15) as

$$
M_{fi} = \frac{g_{14}^{(s)} g_{23}^{(s)}}{u-M_B^2+i\epsilon}\, \bar{u}(\mathbf{p}_f, s_f)\left[\left\{\frac{1}{2}(M_f+M_i)+M_B\right\} - \not{Q}\right] u(\mathbf{p}_i, s_i) , \tag{C.17}
$$

where $Q = \frac{1}{2}\left(q'+q\right)$. From Eq. (C.17), we can readily obtain the contribution to the invariant amplitudes $A_{fi}(s,t,u)$ and $B_{fi}(s,t,u)$ defined in Eq. (2.5). We get

$$
\begin{aligned}
A_{fi}(S) &= -\frac{g_{14}^{(s)} g_{23}^{(s)}}{u-M_B^2+i\epsilon}\left\{-\frac{1}{2}(M_f+M_i)-M_B\right\} , \\
B_{fi}(S) &= -\frac{g_{14}^{(s)} g_{23}^{(s)}}{u-M_B^2+i\epsilon} .
\end{aligned}
\tag{C.18}
$$

(ii) vector coupling:
From the interaction Hamiltonian density in Eq. (4.17), the interaction vertex is given by the matrix element

$$(2\pi)^4\delta(p'-p-q)\left[\bar{u}(\mathbf{p}',s')\;\Gamma_V(p',p)\;u(\mathbf{p},s)\right]\equiv\langle p'|-i\int d^4x\mathcal{H}_v(x)|p,q\rangle$$
$$=-i\;(2\pi)^4\delta(p'-p-q)\cdot\frac{f_v}{m_{\pi^+}}\cdot\bar{u}(\mathbf{p}',s')\gamma_\mu\;u(\mathbf{p},s)\cdot -iq^\mu$$
$$=-\frac{f_v}{m_{\pi^+}}\;(2\pi)^4\delta(p'-p-q)\;\left[\bar{u}(\mathbf{p}',s')\gamma\cdot q\;u(\mathbf{p},s)\right]\;. \tag{C.19}$$

It is clear that for a vertex with an outgoing pseudoscalar-meson we have to replace in Eq. (C.19) q by $-q$. It follows that irrespectively whether the meson is absorbed or created at the vertex, the vertex-function $\Gamma_V(p',p)$ is given by

$$\Gamma_V(p',p)=-\frac{f_v}{m_{\pi^+}}\;\left[\gamma\cdot\left(p'-p\right)\right]\;. \tag{C.20}$$

The S-matrix element for the pseudovector coupling baryon-exchange diagram is now given by

$$\begin{aligned}
S_{fi} &= \frac{f_{14}^{(v)}f_{23}^{(v)}}{m^2_{\pi^+}}\int\frac{d^4p_u}{(2\pi)^4}\,\bar{u}(\mathbf{p}_f,s_f)\left[(-\,\not{q})\;\frac{i}{\not{p}_u-M_B+i\epsilon}\;(+\,\not{q}')\right]u(\mathbf{p}_i,s_i)\\
&\quad\times(2\pi)^4\delta^4(p-p_u-q')\;(2\pi)^4\delta^4(p'-q-p_u)\\
&= -(2\pi)^4\;i\;\delta^4(p'+q'-p-q)\;\frac{f_{14}^{(v)}f_{23}^{(v)}}{m^2_{\pi^+}}\\
&\quad\times\bar{u}(\mathbf{p}_f,s_f)\left[\not{q}\;\frac{1}{(\not{p}-\not{q}')-M_B+i\epsilon}\;\not{q}'\right]u(\mathbf{p}_i,s_i)\;.
\end{aligned} \tag{C.21}$$

The corresponding M-matrix element is given by

$$M_{fi}\;=\;\frac{f_{14}^{(v)}f_{23}^{(v)}}{m^2_{\pi^+}}\;\bar{u}(\mathbf{p}_f,s_f)\left[\not{q}\;\frac{(\not{p}-\not{q}')+M_B}{(p'-q)^2-M_B^2+i\epsilon}\;\not{q}'\right]u(\mathbf{p}_i,s_i)\;. \tag{C.22}$$

Using Eq. (C.16), the M-matrix element can be written as

$$\begin{aligned}
M_{fi} &= \frac{f_{14}^{(v)}f_{23}^{(v)}/m^2_{\pi^+}}{u-M_B^2+i\epsilon}\bar{u}(\mathbf{p}_f,s_f)\left[u\left\{-\frac{1}{2}\left(M_f+M_i\right)+M_B\right\}\right.\\
&\quad -\frac{1}{2}\left(M_f+M_i\right)^2M_B+M_fM_i\left\{\frac{1}{2}\left(M_f+M_i\right)+M_B\right\}\\
&\quad \left.+\left\{-u+\left(M_f+M_i\right)M_B-M_fM_i\right\}\;\not{Q}\right]u(\mathbf{p}_i,s_i)\;,
\end{aligned} \tag{C.23}$$

where $u = p_u^2$. We can readily find from Eq. (C.23) the contribution to the invariant amplitudes $A_{fi}(s,t,u)$ and $B_{fi}(s,t,u)$,

$$\begin{aligned} A_{fi}(V) &= -\frac{f_{14}^{(v)} f_{23}^{(v)}/m_{\pi^+}^2}{u - M_B^2 + i\epsilon} \left[u \left\{ \frac{1}{2}\left(M_f + M_i\right) - M_B \right\} \right. \\ &\quad \left. -\frac{1}{2}(M_f + M_i) M_f M_i + \frac{1}{2}\left(M_f^2 + M_i^2\right) M_B \right] , \\ B_{fi}(V) &= -\frac{f_{14}^{(v)} f_{23}^{(v)}/m_{\pi^+}^2}{u - M_B^2 + i\epsilon} \left[u - \left(M_f + M_i\right) M_B + M_f M_i \right] . \end{aligned} \tag{C.24}$$

(iii) $J^P = \frac{1}{2}^-$ pole diagram

Applying crossing symmetry again we find, similar to the $J^P = \frac{1}{2}^+$ baryon pole diagram, the invariant amplitudes for the $J^P = \frac{1}{2}^-$ baryon pole diagram.

(i) scalar coupling:

$$\begin{aligned} A_{fi}(S) &= -\frac{g_{14}^{(s)} g_{23}^{(s)}}{s - M_B^2 + i\epsilon} \left\{ -\frac{1}{2}(M_f + M_i) - M_B \right\} , \\ B_{fi}(S) &= \frac{g_{14}^{(s)} g_{23}^{(s)}}{s - M_B^2 + i\epsilon} . \end{aligned} \tag{C.25}$$

(ii) vector coupling:

$$\begin{aligned} A_{fi}(V) &= -\frac{f_{14}^{(v)} f_{23}^{(v)}/m_{\pi^+}^2}{s - M_B^2 + i\epsilon} \left[s \left\{ \frac{1}{2}\left(M_f + M_i\right) - M_B \right\} \right. \\ &\quad \left. -\frac{1}{2}(M_f + M_i) M_f M_i + \frac{1}{2}\left(M_f^2 + M_i^2\right) M_B \right] , \\ B_{fi}(V) &= \frac{f_{14}^{(v)} f_{23}^{(v)}/m_{\pi^+}^2}{s - M_B^2 + i\epsilon} \left[s - \left(M_f + M_i\right) M_B + M_f M_i \right] . \end{aligned} \tag{C.26}$$

(v) $J^P = \frac{3}{2}^+$ baryon-exchange

From the interaction Hamiltonian density Eq. (4.16), the resonance-baryon-pseudoscalar-meson interaction vertex is given by the matrix element

$$\begin{aligned} &\langle P | \int d^4x \mathcal{H}_{Y^*NP}(x) | p, q \rangle = (2\pi)^4 \delta(P - p - q) \cdot \frac{f_{Y^*NP}}{m_{\pi^+}} \cdot \bar{u}_\mu^*(\mathbf{P}, s') u(\mathbf{p}, s) \cdot q^\mu \\ &\equiv (2\pi)^4 \delta(P - p - q) \left[\bar{u}_\mu^*(\mathbf{P}, s')\, \Gamma_{Y^*NP}^\mu(P; p, q)\, u(\mathbf{p}, s) \right] , \end{aligned} \tag{C.27}$$

which gives for the vertex

$$\Gamma^{\mu}_{Y^*NP}(P;p,q) = \frac{f^*_{Y^*NP}}{m_{\pi^+}}\, q^{\mu}\ . \tag{C.28}$$

Here, the $J^P = \frac{3}{2}^+$-resonances, are described by the Rarita-Schwinger Dirac spinors [26, 42], which satisfy the equations

$$(\not{P} - M_Y)\ u^{\mu}_Y(P) = 0\ \ ,\ \ \gamma_{\mu} u^{\mu}_Y(P) = P_{\mu} u^{\mu}_Y(P) = 0\ . \tag{C.29}$$

The resonance propagator is

$$P_{\mu\nu}(p) = \frac{U_{\mu\nu}(p)}{p^2 - M_Y^2 + i\epsilon}\quad , \tag{C.30}$$

where the spin projector $U_{\mu\nu}(p)$ reads explicitly

$$\begin{aligned} U_{\mu\nu}(p) \ &=\ \sum_{\sigma=-3/2}^{+3/2} u_{\mu}(p,\sigma)\bar{u}_{\nu}(p,\sigma) \qquad\qquad (C.31)\\ &=\ (\not{p} + M_{Y^*})\left(-g_{\mu\nu} + \frac{1}{3}\,\gamma_{\mu}\gamma_{\nu} + \frac{1}{3M_{Y^*}}\left(\gamma_{\mu}p_{\nu} - \gamma_{\nu}p_{\mu}\right) + \frac{2}{3M_{Y^*}^2}\ p_{\mu}p_{\nu}\right)\ . \end{aligned}$$

The S-matrix element is given by

$$\begin{aligned} S_{fi} \ &=\ \frac{f^*_{14}f^*_{23}}{m^2_{\pi^+}}\,(-i)^2 \int \frac{d^4P_u}{(2\pi)^4}\ \bar{u}(\mathbf{p}_f,s_f)\left[(-q^{\mu})\frac{i\ U_{\mu\nu}(P_u)}{P_u^2 - M_{Y^*}^2 + i\epsilon}\,(-q'^{\nu})\right] u(\mathbf{p}_i,s_i)\\ &\quad \times(2\pi)^4\delta^4(p - P_u - q')\ (2\pi)^4\delta^4(p' - q - P_u)\\ &=\ -(2\pi)^4\ i\ \delta^4(p' + q' - p - q)\ \left(f^*_{14}f^*_{23}/m^2_{\pi^+}\right)\\ &\quad \times\bar{u}(\mathbf{p}_f,s_f)\left[\frac{\left[q^{\mu}U_{\mu\nu}(P_u)q'^{\nu}\right]}{u - M^2_{Y^*} + i\epsilon}\right] u(\mathbf{p}_i,s_i)\ . \end{aligned} \tag{C.32}$$

The corresponding M-matrix element is therefore

$$M_{fi} \ =\ f^*_{14}f^*_{23}/m^2_{\pi^+}\ \bar{u}(\mathbf{p}_f,s_f)\left[\frac{q^{\mu}U_{\mu\nu}(P_u)q'^{\nu}}{u - M^2_{Y^*} + i\epsilon}\right] u(\mathbf{p}_i,s_i)\ . \tag{C.33}$$

Writing out the denominator term by term by using identities like $P_u \cdot q' = \left(M_i^2 - m_f^2 - u\right)/2$ and $P_u \cdot p' = \left(M_f^2 - m_i^2 + u\right)/2$ gives us the invariant amplitudes $A_{fi}(s,t,u)$ and $B_{fi}(s,t,u)$

$$\begin{aligned} A_{fi} \ &=\ \frac{f^*_{14}f^*_{23}}{m^2_{\pi^+}}\cdot\frac{1}{u - M^2_{Y^*} + i\epsilon}\cdot\left\{\frac{1}{2}\left[t - m_f^2 - m_i^2\right]\left[\frac{1}{2}\left(M_f + M_i\right) + M_{Y^*}\right]\right.\\ &\quad +\frac{1}{6M^2_{Y^*}}\left[M_f^2 - m_i^2 - u\right]\left[M_i^2 - m_f^2 - u\right]\left[\frac{1}{2}\left(M_f + M_i\right)\right] \end{aligned}$$

$$
\begin{aligned}
&+\frac{1}{3}M_{Y^*}\left[u-\frac{1}{2}\left(M_f^2+M_i^2\right)\right] \\
&+\frac{1}{3}\left[\frac{1}{2}(M_f+M_i)u-\frac{1}{4}(M_f^2+M_i^2)(M_f+M_i)+\frac{1}{4}(m_i^2-m_f^2)(M_f-M_i)\right] \\
&+\frac{1}{6M_{Y^*}}\left[(M_f^2-m_i^2-u)(\frac{M_i}{2}(M_i-M_f)-m_f^2)-\right. \\
&\left.\left.(M_i^2-m_f^2-u)(\frac{M_f}{2}(M_i-M_f)+m_i^2)\right]\right\}\ , \qquad (C.34)
\end{aligned}
$$

$$
\begin{aligned}
B_{fi} &= \frac{f_{14}^*f_{23}^*}{m_{\pi^+}^2}\cdot\frac{1}{u-M_{Y^*}^2+i\epsilon}\cdot\left\{-\frac{1}{2}\left[t-m_f^2-m_i^2\right]-\frac{1}{6M_{Y^*}^2}\left[u-M_f^2+m_i^2\right]\right. \\
&\times\left[u-M_i^2+m_f^2\right]+\frac{M_{Y^*}}{3}(M_f+M_i)-\frac{1}{6}[m_f^2+m_i^2-(M_f+M_i)^2] \\
&\left.\frac{1}{6M_{Y^*}}\left[M_f(M_i^2-m_f^2-u)+M_i(M_f^2-m_i^2-u)\right]\right\}\ . \qquad (C.35)
\end{aligned}
$$

(vi) $J^P=\frac{3}{2}^+$ pole diagram

Applying crossing symmetry again we find, similar to the $J^P=\frac{1}{2}^+$ baryon pole diagram, the invariant amplitudes for the $J^P=\frac{3}{2}^+$ baryon pole diagram

$$
\begin{aligned}
A_{fi} &= \frac{f_{14}^*f_{23}^*}{m_{\pi^+}^2}\cdot\frac{1}{s-M_{Y^*}^2+i\epsilon}\cdot\left\{\frac{1}{2}\left[t-m_f^2-m_i^2\right]\left[\frac{1}{2}\left(M_f+M_i\right)+M_{Y^*}\right]\right. \\
&+\frac{1}{6M_{Y^*}^2}\left[M_f^2-m_f^2-s\right]\left[M_i^2-m_i^2-s\right]\left[\frac{1}{2}\left(M_f+M_i\right)\right] \\
&+\frac{1}{3}M_{Y^*}\left[s-\frac{1}{2}\left(M_f^2+M_i^2\right)\right] \\
&+\frac{1}{3}\left[\frac{1}{2}(M_f+M_i)s-\frac{1}{4}(M_f^2+M_i^2)(M_f+M_i)+\frac{1}{4}(m_f^2-m_i^2)(M_f-M_i)\right] \\
&+\frac{1}{6M_{Y^*}}\left[(M_f^2-m_f^2-s)(\frac{M_i}{2}(M_i-M_f)-m_i^2)-\right. \\
&\left.\left.(M_i^2-m_i^2-s)(\frac{M_f}{2}(M_i-M_f)+m_f^2)\right]\right\}\ , \qquad (C.36)
\end{aligned}
$$

$$
\begin{aligned}
B_{fi} &= -\frac{f_{14}^*f_{23}^*}{m_{\pi^+}^2}\cdot\frac{1}{s-M_{Y^*}^2+i\epsilon}\cdot\left\{-\frac{1}{2}\left[t-m_f^2-m_i^2\right]-\frac{1}{6M_Y^2}\left[s-M_f^2+m_f^2\right]\right. \\
&\times\left[s-M_i^2+m_i^2\right]+\frac{M_{Y^*}}{3}(M_f+M_i)-\frac{1}{6}[m_f^2+m_i^2-(M_f+M_i)^2] \\
&\left.\frac{1}{6M_{Y^*}}\left[M_f(M_i^2-m_i^2-s)+M_i(M_f^2-m_f^2-s)\right]\right\}\ . \qquad (C.37)
\end{aligned}
$$

C.2 Momentum space meson-exchange diagrams

(i) $J^P = 0^{++}$ scalar-meson-exchange

The S-matrix element is given by

$$\begin{aligned} S_{fi} &= -g_{13}^{(s)} g_{24}^{(s)} \int \frac{d^4 p_u}{(2\pi)^4} \left[\bar{u}(\mathbf{p}_f, s_f)\, u(\mathbf{p}_i, s_i)\right] \frac{i}{(p'-p)^2 - m^2 + i\epsilon} \\ &\quad \times (2\pi)^4 \delta(q' - q - p_u)(2\pi)^4 \delta(p - p' - p_u) \\ &= -(2\pi)^4\, i\, \delta^4(p' + q' - p - q)\, \frac{g_{13}^{(s)} g_{24}^{(s)}}{(p'-p)^2 - m^2 + i\epsilon} \left[\bar{u}(\mathbf{p}_f, s_f)\, u(\mathbf{p}_i, s_i)\right] . \end{aligned} \tag{C.38}$$

From the right-hand side of Eq. (C.38) the M_{fi}-amplitude can immediately be read off. The contribution to the invariant amplitudes $A_{fi}(s,t,u)$ and $B_{fi}(s,t,u)$ defined in Eq. (2.5) is

$$\begin{aligned} A_{fi} &= \frac{g_{13}^{(s)} g_{24}^{(s)}}{t - m^2 + i\epsilon} , \\ B_{fi} &= 0 , \end{aligned} \tag{C.39}$$

where t is the Mandelstam variable $t = (p' - p)^2 = (q - q')^2$.

(ii) $J^P = 1^{--}$ vector-meson-exchange

a) The triple-meson interaction density is given in Eq. (4.18). The PPV-vertex is given by the matrix element [1]

$$\begin{aligned} \langle q'| \int d^4x \mathcal{H}_{PPV}(x) |q, \Delta\rangle &= (2\pi)^4 \delta(q' - q - \Delta) \cdot g_{PPV} \left(q'_\mu + q_\mu\right) \varepsilon^\mu(\lambda) \\ &\equiv (2\pi)^4 \delta(p - p' - \Delta) \varepsilon_\mu(\lambda) \Gamma^\mu_{PPV}(q', q) . \end{aligned} \tag{C.40}$$

Here, $\Delta = q' - q = p - p'$. The triple-meson vertex function from Eq. (C.40) is

$$\Gamma^\mu_{PPV}(q', q) = g_{PPV} \left(q' + q\right)^\mu . \tag{C.41}$$

b) From the interaction Hamiltonian density Eq. (4.13), the BBV-vertex is given by the matrix element

$$\begin{aligned} &\langle p', \Delta| \int d^4x \mathcal{H}_V(x) |p\rangle = (2\pi)^4 \delta(p' - p + \Delta) \left[g_V\, \bar{u}(\mathbf{p}', s') \gamma^\mu u_i(\mathbf{p})\, \varepsilon^*_\mu(\lambda) \right. \\ &\left. + \frac{i\, f_V}{4\mathcal{M}} \left[\bar{u}_f(\mathbf{p}')\, \sigma^{\mu\nu}\, u_i(\mathbf{p})\right] \left(\Delta_\mu \varepsilon^*_\nu - \Delta_\nu \varepsilon^*_\mu\right) \right] \\ &= (2\pi)^4 \delta(p' - p + \Delta)\, \bar{u}_f(\mathbf{p}') \left[g_V \gamma^\mu - \frac{i\, f_V}{2\mathcal{M}} \sigma^{\mu\nu} \Delta_\nu \right] u_i(\mathbf{p}) \cdot \varepsilon^*_\mu(\lambda) \\ &\equiv (2\pi)^4 \delta(p' - p + \Delta)\, \varepsilon^*_\mu(\lambda) \left[\bar{u}(\mathbf{p}', s')\, \Gamma^\mu_{BBV}(p', p)\, u(\mathbf{p}, s)\right] . \end{aligned} \tag{C.42}$$

[1] The vertex function $\Gamma(p', p)$ is defined such that the Feynman rule gives a factor $-i\Gamma(p', p)$ for any interaction vertex of this kind.

To go from the first to the second line we used that $\sigma_{\mu\nu} = \frac{1}{2}\left(\sigma_{\mu\nu} - \sigma_{\nu\mu}\right)$. The BBV-vertex function from Eq. (C.40) is

$$\Gamma^{\mu}_{BBV}(p', p) = \left[g_V \gamma^{\mu} - \frac{i\, f_V}{2\mathcal{M}} \sigma^{\mu\nu} \Delta_\nu\right] . \tag{C.43}$$

The S-matrix element for vector-meson exchange is given by

$$\begin{aligned} S_{fi} \;&=\; \sum_\lambda \int \frac{d^4\Delta}{(2\pi)^4} \cdot -i\; g_{PPV}\; (q'+q)_\nu \varepsilon^\nu(\lambda) \\ &\times (2\pi)^4 \delta(q'-q-\Delta) \cdot \frac{i}{\Delta^2 - m^2 + i\epsilon} \\ &\times (2\pi)^4 \delta(p - p' - \Delta)\; -i\varepsilon^\mu(\lambda)^* \\ &\times \bar{u}_f(\mathbf{p}') \left[g_V \gamma_\mu - i \frac{f_V}{2\mathcal{M}} \sigma_{\mu\kappa} \Delta^\kappa\right] u_i(\mathbf{p}) \,. \end{aligned} \tag{C.44}$$

Now,

$$\sum_\lambda \varepsilon^*_\mu(\Delta,\lambda) \varepsilon_\nu(\Delta,\lambda) = -g_{\mu\nu} + \frac{\Delta_\mu \Delta_\nu}{m^2} \,,$$

which is substituted in Eq. (C.44). For the M_{fi}-amplitude this leads to the contribution

$$\begin{aligned} M_{fi} \;&=\; g_{PPV}\; (q'+q)_\nu \cdot \frac{-g^{\mu\nu} + \Delta^\mu \Delta^\nu / m^2}{\Delta^2 - m^2 + i\epsilon} \cdot \bar{u}_f(\mathbf{p}') \left[g_V \gamma_\mu - \frac{i\, f_V}{2\mathcal{M}} \sigma_{\mu\kappa} \Delta^\kappa\right] u_i(\mathbf{p}) \\ &\equiv\; M^{(1)}_{fi} + M^{(2)}_{fi} \,, \end{aligned} \tag{C.45}$$

where the first term refers to the contribution due to the $g_{\mu\nu}$-term and the second one to that from $\Delta_\mu \Delta_\nu$ in the vector meson propagator.
(i) $-g^{\mu\nu}$ term: The contribution is

$$M^{(1)}_{fi} \;=\; -2 g_{PPV} \cdot \frac{1}{\Delta^2 - m^2 + i\epsilon} \cdot \bar{u}_f(\mathbf{p}') \left[g_V\; \not{Q} - \frac{i f_V}{2\mathcal{M}} \cdot \sigma_{\mu\kappa} Q^\mu \Delta^\kappa\right] u_i(\mathbf{p}) \,. \tag{C.46}$$

The anomalous magnetic term in Eq. (C.46) can be rewritten using

$$\sigma_{\mu\kappa} Q^\mu \Delta^\kappa \;=\; i\left\{\left(M_f + M_i\right) \not{Q} - \frac{1}{2}(s-u)\right\} .$$

This result leads to the expression

$$\begin{aligned} M^{(1)}_{fi} \;&=\; -2 g_{PPV} \cdot \frac{1}{\Delta^2 - m^2 + i\epsilon} \cdot \bar{u}_f(\mathbf{p}') \left[\left(g_V + + f_V \frac{M_f + M_i}{2\mathcal{M}}\right) \not{Q} \right. \\ &\left. - \frac{s-u}{4\mathcal{M}} f_V \right] u_i(\mathbf{p}) \,. \end{aligned} \tag{C.47}$$

(ii) $\Delta^\mu \Delta^\nu$ term: The contribution is

$$M_{fi}^{(2)} = g_{PPV}\, g_V \cdot \frac{1}{\Delta^2 - m^2 + i\epsilon} \cdot \frac{m_f^2 - m_i^2}{m^2} \left(M_i - M_f\right) \left[\bar{u}_f(\mathbf{p}') u_i(\mathbf{p})\right] . \quad \text{(C.48)}$$

The contributions to the invariant amplitudes $A_{fi}(s,t,u)$ and $B_{fi}(s,t,u)$ are

$$\begin{aligned} A_{fi} &= g_{PPV} \cdot \frac{1}{t - m^2 + i\epsilon} \cdot \left[g_V \frac{m_f^2 - m_i^2}{m^2} \left(M_i - M_f\right) + \frac{s-u}{2\mathcal{M}} f_V \right] , \\ B_{fi} &= -2 g_{PPV} \cdot \frac{1}{t - m^2 + i\epsilon} \cdot \left(g_V + f_V \frac{M_f + M_i}{2\mathcal{M}} \right) . \end{aligned} \quad \text{(C.49)}$$

(iii) $J^P = 2^{++}$ tensor-meson-exchange

a) The triple-meson interaction density is given by Eq. (4.20). The PPT-vertex is given by the matrix element

$$\begin{aligned} &\langle q' | \int d^4x \mathcal{H}_{PPT}(x) | q, \Delta\rangle \\ &= (2\pi)^4 \delta(q' - q - \Delta) \cdot \frac{g_{PPT}}{m_{\pi^+}} \left(q'_\mu + q_\mu\right) \left(q'_\nu + q_\nu\right) \cdot \varepsilon^{\mu\nu}(\lambda) \\ &\equiv (2\pi)^4 \delta(p' - p + \Delta) \varepsilon_{\mu\nu}(\lambda) \Gamma^{\mu\nu}_{PPT}(q', q) . \end{aligned} \quad \text{(C.50)}$$

Where we used that $2\left(q_\mu q'_\nu + q'_\mu q_\nu\right) = 4 Q_\mu Q_\nu - \Delta\mu \Delta_\nu = \left(q'_\mu + q_\mu\right)\left(q'_\nu + q_\nu\right)$, since later on $\Delta \cdot P = 0$. The triple-meson vertex function from Eq. (C.50) is

$$\Gamma^{\mu\nu}_{PPT}(q', q) = \frac{g_{PPT}}{m_{\pi^+}} \left(q' + q\right)^\mu \left(q' + q\right)^\nu . \quad \text{(C.51)}$$

b) From the interaction Hamiltonian density Eq. (4.15), the BBT-vertex is given by the matrix element

$$\begin{aligned} &\langle p', \Delta | \int d^4x \mathcal{H}_T(x) | p\rangle \\ &= (2\pi)^4 \delta(p' - p - q) \frac{1}{2} \left(p' + p\right)^\nu \bar{u}_f(\mathbf{p}') \left[\gamma^\mu F_1 + \frac{1}{2}\left(p' + p\right)^\mu F_2\right] u_i(\mathbf{p}) \cdot \varepsilon^*_{\mu\nu}(\lambda) \\ &\equiv (2\pi)^4 \delta(p' - p + \Delta)\, \varepsilon^*_{\mu\nu}(\lambda) \left[\bar{u}(\mathbf{p}', s')\, \Gamma^{\mu\nu}_{BBT}(p', p)\, u(\mathbf{p}, s)\right] . \end{aligned} \quad \text{(C.52)}$$

The BBT-vertex function from Eq. (C.52) is

$$\Gamma^{\mu\nu}_{BBT}(p', p) = \frac{1}{2}\left(p' + p\right)^\nu \left[\gamma^\mu F_1 + \frac{1}{2}\left(p' + p\right)^\mu F_2\right] . \quad \text{(C.53)}$$

The S-matrix element for tensor-meson exchange is given by

$$S_{fi} = \sum_\lambda \int \frac{d^4\Delta}{(2\pi)^4} \frac{g_{PPT}}{m_{\pi^+}} (q' + q)^\mu (q' + q)^\nu \varepsilon_{\mu\nu}(\lambda)$$

$$
\begin{aligned}
&\times -i(2\pi)^4 \delta(q' - q - \Delta) \cdot \frac{i}{\Delta^2 - m^2 + i\epsilon} \cdot \\
&\times -i(2\pi)^4 \delta(p - p' - \Delta)\ \varepsilon_{\kappa\rho}(\lambda)^* \\
&\times \frac{1}{2}(p' + p)^\kappa\ \bar{u}_f(\mathbf{p}') \left[\gamma^\rho\ F_1 + \frac{1}{2}\left(p' + p\right)^\rho\ F_2 \right] u_i(\mathbf{p})\ .
\end{aligned} \tag{C.54}
$$

Now,

$$
P_{\kappa\rho;\mu\nu} \equiv \sum_\lambda \varepsilon^*_{\kappa\rho}(\Delta,\lambda)\varepsilon_{\mu\nu}(\Delta,\lambda) = \frac{1}{2}\left(P_{\kappa\mu}P_{\rho\nu} + P_{\kappa\nu}P_{\rho\mu}\right) - \frac{1}{3}P_{\kappa\rho}P_{\mu\nu}\ , \tag{C.55}
$$

where $P_{\mu\nu} = -g_{\mu\nu} + \Delta_\mu \Delta_\nu / m^2$. Substituted in Eq. (C.54), this gives for the M_{fi}-amplitude the contribution

$$
\begin{aligned}
M_{fi} &= \frac{g_{PPT}}{m_{\pi^+}}\ (q' + q)^\mu (q' + q)^\nu \cdot \frac{P_{\mu\nu;\kappa\rho}(\Delta)}{\Delta^2 - m^2 + i\epsilon} \cdot \\
&\quad \times \frac{1}{2}(p' + p)^\kappa\ \bar{u}_f(\mathbf{p}') \left[\gamma^\rho\ F_1 + \frac{1}{2}\left(p' + p\right)^\rho\ F_2 \right] u_i(\mathbf{p}) \\
&\equiv M^{(1)}_{fi} + M^{(2)}_{fi} + M^{(3)}_{fi}\ ,
\end{aligned} \tag{C.56}
$$

where the three terms correspond to the contributions of the three terms on the right-hand side of Eq. (C.55).
(i) $\frac{1}{2}P_{\kappa\mu}P_{\rho\nu}$-term:

$$
\begin{aligned}
M^{(1)}_{fi} &= \frac{g_{PPT}/m_{\pi^+}}{\Delta^2 - m^2 + i\epsilon} \\
&\quad \times \left\{ Q^\mu Q^\nu \left(-g_{\kappa\mu} + \frac{\Delta_\kappa \Delta_\mu}{m^2} \right) \left(-g_{\rho\nu} + \frac{\Delta_\rho \Delta_\nu}{m^2} \right) \right. \\
&\quad \left. \times\ (p' + p)^\kappa\ \bar{u}_f(\mathbf{p}') \left[\gamma^\rho\ F_1 + \frac{1}{2}\left(p' + p\right)^\rho\ F_2 \right] u_i(\mathbf{p}) \right\}\ .
\end{aligned} \tag{C.57}
$$

Using the identities

$$
\begin{aligned}
&Q \cdot \Delta = \frac{1}{2}(q' + q) \cdot (q' - q) = \frac{1}{2}(m_f^2 - m_i^2)\ , \\
&(p' + p) \cdot \Delta = (p' + p) \cdot (p - p') = M_i^2 - M_f^2\ , \\
&Q \cdot (p' + p) = \frac{1}{2}(q' + q) \cdot (p' + p) = \frac{1}{2}(s - u)\ ,
\end{aligned} \tag{C.58}
$$

one obtains

$$
\begin{aligned}
M_{fi} &= \frac{g_{PPT}/m_{\pi^+}}{\Delta^2 - m^2 + i\epsilon} \times \bar{u}_f(\mathbf{p}') \left\{ \frac{1}{2}(s - u)\ \left[\not{Q} F_1 + \frac{1}{4}(s - u) F_2 \right] \right. \\
&\quad - \frac{(m_f^2 - m_i^2)(s - u)}{4m^2}\ \left[(M_i - M_f) F_1 + \frac{1}{2}(M_i^2 - M_f^2) F_2 \right]
\end{aligned} \tag{C.59}
$$

$$-\frac{(m_f^2-m_i^2)(M_i^2-M_f^2)}{2m^2}\left[\not{Q}F_1+\frac{1}{4}(s-u)F_2\right]$$
$$\left.+\frac{(m_f^2-m_i^2)^2(M_i^2-M_f^2)}{4m^4}\left[(M_i-M_f)F_1+\frac{1}{2}(M_i^2-M_f^2)F_2\right]u_i\right\}u_i(\mathbf{p})\ .$$

(ii) $\frac{1}{2}P_{\kappa\nu}P_{\rho\mu}$-term: Since $Q^\mu Q^\nu\ P_{\kappa\nu}\ P_{\rho\mu}=Q^\mu\ Q^\nu\ P_{\kappa\mu}\ P_{\rho\nu}$, this gives the same contribution as the first term, which is evaluted above.
(iii) $-\frac{1}{3}P_{\kappa\rho}P_{\mu\nu}$-term: In this case the matrix element factorizes into a factor from the triple-meson vertex and a factor from the meson-baryon-baryon vertex. One has:
a. MMM-factor:

$$4Q^\mu\ Q^\nu\ P_{\mu\nu}=4Q^\mu\ Q^\nu\left(-g_{\mu\nu}+\frac{\Delta_\mu\Delta_\nu}{m^2}\right)=4\left[-Q^2+\frac{(m_f^2-m_i^2)^2}{4m^2}\right]=$$
$$4\left[-\left(\frac{1}{2}(m_f^2+m_i^2)-\frac{1}{4}t\right)+\frac{(m_f^2-m_i^2)^2}{4m^2}\right]\ . \tag{C.60}$$

b. BBM-factor:

$$P_{\kappa\rho}\cdot\frac{1}{2}(p'+p)^\kappa\ \bar{u}_f\left[\gamma^\rho\ F_1+\frac{1}{2}\left(p'+p\right)^\rho\ F_2\right]u_i=$$
$$-\frac{1}{2}\bar{u}_f\left[(M_f+M_i)F_1+\frac{1}{2}(p'+p)^2F_2\right]u_i$$
$$+\frac{(M_i^2-M_f^2)}{2m^2}\bar{u}_f\left[(M_i-M_f)F_1+\frac{1}{2}(M_i^2-M_f^2)F_2\right]u_i\ . \tag{C.61}$$

Collecting all results above, one obtains for the invariant amplitudes Eq. (2.5)

$$\begin{aligned}
A_{fi}\ &=\ \frac{g_{PPT}}{m_{\pi^+}}\frac{1}{\Delta^2-m^2+i\epsilon}\left\{\frac{1}{4}(s-u)^2\ F_2\right.\\
&-\frac{1}{2m^2}(m_f^2-m_i^2)(s-u)\left[(M_i-M_f)\ F_1+(M_i^2-M_f^2)\ F_2\right]\\
&+\frac{1}{2m^4}(m_f^2-m_i^2)^2(M_i^2-M_f^2)\left[(M_i-M_f)F_1+\frac{1}{2}(M_i^2-M_f^2)F_2\right]\\
&-\frac{4}{3}\left[-Q^2+\frac{(m_f^2-m_i^2)^2}{4m^2}\right]\cdot\left[-\frac{1}{2}\left\{(M_f+M_i)F_1+\frac{1}{2}(p'+p)^2F_2\right\}\right.\\
&\left.\left.+\frac{M_i^2-M_f^2}{2m^2}\left\{(M_i-M_f)F_1+\frac{1}{2}(M_i^2-M_f^2)F_2\right\}\right]\right\}\ ,\\
B_{fi}\ &=\ \frac{g_{PPT}}{m_{\pi^+}}\frac{1}{\Delta^2-m^2+i\epsilon}\cdot\left\{(s-u)\ F_1-\frac{(m_f^2-m_i^2)(M_i^2-M_f^2)}{m^2}\ F_1\right\}\ .
\end{aligned} \tag{C.62}$$

C.3 Momentum space Pomeron-exchange

The contribution to the invariant amplitudes $A_{fi}(s,t,u)$ and $B_{fi}(s,t,u)$ is

$$\begin{aligned} A_{fi} &= \frac{g_{13}\, g_{24}}{M_s}\,, \\ B_{fi} &= \frac{g_{13}\, g_{24}}{M_s}\,. \end{aligned} \tag{C.63}$$

Appendix D

X,Y,Z-coefficients

Here we list the explicit expressions for the expansion coefficients $X^{(\alpha)}$, $Y^{(\alpha)}$, $Z^{(\alpha)}$ and $U^{(\alpha)}$ of the partial wave potentials, Eq. (4.34), for each type of exchange in the s-, u- and t-channel.

D.1 Baryon-exchange

(i) $J^P = \frac{1}{2}^+$ baryon-exchange

(i) pseudoscalar coupling:

$$
\begin{aligned}
X_B^{(C)} &= g_{14}g_{23}\sqrt{(E_f+M_f)(E_i+M_i)}\left[M_B+\frac{1}{2}\left(W_f+W_i\right)-M_f-M_i\right], \qquad \text{(D.1)}\\
Y_B^{(C)} &= g_{14}g_{23}\sqrt{(E_f-M_f)(E_i-M_i)}\left[-M_B+\frac{1}{2}\left(W_f+W_i\right)+M_f+M_i\right],\\
X_B^{(SO)} &= -g_{14}g_{23}\sqrt{(E_f-M_f)(E_i-M_i)}\left[-M_B+\frac{1}{2}\left(W_f+W_i\right)+M_f+M_i\right].
\end{aligned}
$$

(ii) pseudovector coupling:

$$
\begin{aligned}
X_B^{(C)} &= -\frac{f_{14}f_{23}}{m_{\pi^+}^2}\sqrt{(E_f+M_f)(E_i+M_i)}\left[\left(-\frac{M_f+M_i}{2}-M_B\right)\right.\\
&\times\left(\frac{1}{4}\left(E_f+E_i-\omega_f-\omega_i\right)^2-p_f^2-p_i^2\right)+\frac{1}{2}\left(M_f+M_i\right)M_fM_i\\
&+\frac{1}{2}\left(M_f^2+M_i^2\right)M_B-\frac{1}{2}\left(W_f+W_i-M_f-M_i\right)\left(\frac{1}{4}\left(E_f+E_i-\omega_f-\omega_i\right)^2\right.\\
&\left.\left.-p_f^2-p_i^2+\left(M_f+M_i\right)M_B+M_fM_i\right)\right],\\
Y_B^{(C)} &= -\frac{f_{14}f_{23}}{m_{\pi^+}^2}\left[\sqrt{(E_f+M_f)(E_i+M_i)}\left[-\left(-\frac{M_f+M_i}{2}-M_B\right)\right.\right.
\end{aligned}
$$

$$
\begin{aligned}
& +\frac{1}{2}\left(W_f+W_i-M_f-M_i\right)\Big] 2 p_f p_i+\sqrt{(E_f-M_f)(E_i-M_i)}\, \times \\
& \left[-\left(-\frac{M_f+M_i}{2}-M_B\right)\left(\frac{1}{4}\left(E_f+E_i-\omega_f-\omega_i\right)^2-p_f^2-p_i^2\right)\right. \\
& -\frac{1}{2}\left(M_f+M_i\right) M_f M_i-\frac{1}{2}\left(M_f^2+M_i^2\right) M_B-\frac{1}{2}\left(W_f+W_i+M_f+M_i\right) \\
& \left.\left.\times\left(\frac{1}{4}\left(E_f+E_i-\omega_f-\omega_i\right)^2-p_f^2-p_i^2+\left(M_f+M_i\right) M_B+M_f M_i\right)\right]\right] , \\
Z_B^{(C)} = & -\frac{f_{14} f_{23}}{m_{\pi^+}^2} \sqrt{(E_f-M_f)(E_i-M_i)}\Big[-\frac{M_f+M_i}{2}-M_B+\frac{1}{2}\big(W_f+W_i \\
& +M_f+M_i\big)\Big] 2 p_f p_i\ , \\
X_B^{(SO)} = & \frac{f_{14} f_{23}}{m_{\pi^+}^2} \sqrt{(E_f-M_f)(E_i-M_i)}\left[-\left(-\frac{M_f+M_i}{2}-M_B\right)\right. \\
& \times\left(\frac{1}{4}\left(E_f+E_i-\omega_f-\omega_i\right)^2-p_f^2-p_i^2\right)-\frac{1}{2}\left(M_f+M_i\right) M_f M_i \\
& -\frac{1}{2}\left(M_f^2+M_i^2\right) M_B\ -\frac{1}{2}\left(W_f+W_i+M_f+M_i\right)\left(\frac{1}{4}\left(E_f+E_i-\omega_f-\omega_i\right)^2\right. \\
& \left.\left.-p_f^2-p_i^2\ +\left(M_f+M_i\right) M_B+M_f M_i\right)\right] , \\
Y_B^{(SO)} = & \frac{f_{14} f_{23}}{m_{\pi^+}^2} \sqrt{(E_f-M_f)(E_i-M_i)}\Big[-\frac{M_f+M_i}{2}-M_B+\frac{1}{2}\big(W_f+W_i \\
& +M_f+M_i\big)\Big] 2 p_f p_i\ .
\end{aligned}
\tag{D.2}
$$

(ii) $J^P = \frac{1}{2}^+$ pole term

(i) pseudoscalar coupling:

$$
\begin{aligned}
X_B^{(C)} &= -g_{14} g_{23} \sqrt{(E_f+M_f)(E_i+M_i)}\left[M_B-\frac{1}{2}\left(W_f+W_i\right)\right] , \\
Y_B^{(C)} &= g_{14} g_{23} \sqrt{(E_f-M_f)(E_i-M_i)}\left[M_B+\frac{1}{2}\left(W_f+W_i\right)\right] , \\
X_B^{(SO)} &= -g_{14} g_{23} \sqrt{(E_f-M_f)(E_i-M_i)}\left[M_B+\frac{1}{2}\left(W_f+W_i\right)\right] .
\end{aligned}
\tag{D.3}
$$

(ii) pseudovector coupling:

$$
\begin{aligned}
X_B^{(C)} = & \frac{f_{14} f_{23}}{m_{\pi^+}^2} \sqrt{(E_f+M_f)(E_i+M_i)}\Big[\left(-\frac{1}{2}\left(M_f+M_i\right)-M_B\right) s \\
& +\frac{1}{2}\left(M_f+M_i\right) M_f M_i+\frac{1}{2}\left(W_f+W_i-M_f-M_i\right)\big(s+\left(M_f+M_i\right) M_B
\end{aligned}
$$

$$
\begin{aligned}
& \left. +M_f M_i\right) + \frac{1}{2}\left(M_f^2+M_i^2\right) M_B \Big] , \\
Y_B^{(C)} &= \frac{f_{14} f_{23}}{m_{\pi^+}^2} \sqrt{(E_f-M_f)(E_i-M_i)} \Big[-\left(-\frac{1}{2}\left(M_f+M_i\right)-M_B\right) s \\
& -\frac{1}{2}\left(M_f+M_i\right) M_f M_i + \frac{1}{2}\left(W_f+W_i-M_f-M_i\right)\left(s+\left(M_f+M_i\right) M_B\right. \\
& \left. +M_f M_i\right) - \frac{1}{2}\left(M_f^2+M_i^2\right) M_B \Big] , \\
X_B^{(SO)} &= -\frac{f_{14} f_{23}}{m_{\pi^+}^2} \sqrt{(E_f-M_f)(E_i-M_i)} \Big[-\left(-\frac{1}{2}\left(M_f+M_i\right)-M_B\right) s \\
& -\frac{1}{2}\left(M_f+M_i\right) M_f M_i + \frac{1}{2}\left(W_f+W_i-M_f-M_i\right)\left(s+\left(M_f+M_i\right) M_B\right. \\
& \left. +M_f M_i\right) - \frac{1}{2}\left(M_f^2+M_i^2\right) M_B \Big] . \qquad \text{(D.4)}
\end{aligned}
$$

(iii) $J^P = \frac{1}{2}^-$ baryon-exchange

(i) scalar coupling:

$$
\begin{aligned}
X_B^{(C)} &= g_{14}^* g_{23}^* \sqrt{(E_f+M_f)(E_i+M_i)} \left[-M_B + \frac{1}{2}\left(W_f+W_i\right) - M_f - M_i \right] , \\
Y_B^{(C)} &= g_{14}^* g_{23}^* \sqrt{(E_f-M_f)(E_i-M_i)} \left[M_B + \frac{1}{2}\left(W_f+W_i\right) + M_f + M_i \right] , \\
X_B^{(SO)} &= -g_{14}^* g_{23}^* \sqrt{(E_f-M_f)(E_i-M_i)} \left[M_B + \frac{1}{2}\left(W_f+W_i\right) + M_f + M_i \right] . \qquad \text{(D.5)}
\end{aligned}
$$

(ii) vector coupling:

$$
\begin{aligned}
X_B^{(C)} &= -\frac{f_{14}^* f_{23}^*}{m_{\pi^+}^2} \sqrt{(E_f+M_f)(E_i+M_i)} \Big[\left(-\frac{M_f+M_i}{2}+M_B\right) \\
& \times \left(\frac{1}{4}\left(E_f+E_i-\omega_f-\omega_i\right)^2 - p_f^2 - p_i^2\right) + \frac{1}{2}\left(M_f+M_i\right) M_f M_i \\
& -\frac{1}{2}\left(M_f^2+M_i^2\right) M_B - \frac{1}{2}\left(W_f+W_i-M_f-M_i\right)\Big(\frac{1}{4}\left(E_f+E_i-\omega_f-\omega_i\right)^2 \\
& -p_f^2 - p_i^2 - \left(M_f+M_i\right) M_B + M_f M_i\Big)\Big] , \\
Y_B^{(C)} &= -\frac{f_{14}^* f_{23}^*}{m_{\pi^+}^2} \Big[\sqrt{(E_f+M_f)(E_i+M_i)} \Big[-\left(-\frac{M_f+M_i}{2}+M_B\right) \\
& +\frac{1}{2}\left(W_f+W_i-M_f-M_i\right)\Big] 2 p_f p_i + \sqrt{(E_f-M_f)(E_i-M_i)} \times
\end{aligned}
$$

$$
\begin{aligned}
& \Big[-\Big(-\frac{M_f+M_i}{2}+M_B\Big)\Big(\frac{1}{4}\left(E_f+E_i-\omega_f-\omega_i\right)^2-p_f^2-p_i^2\Big) \\
& -\frac{1}{2}\left(M_f+M_i\right)M_fM_i+\frac{1}{2}\left(M_f^2+M_i^2\right)M_B-\frac{1}{2}\left(W_f+W_i+M_f+M_i\right) \\
& \times\Big(\frac{1}{4}\left(E_f+E_i-\omega_f-\omega_i\right)^2-p_f^2-p_i^2-\left(M_f+M_i\right)M_B+M_fM_i\Big)\Big]\Big]\ , \\
Z_B^{(C)} \ = \ & -\frac{f_{14}^* f_{23}^*}{m_{\pi^+}^2}\sqrt{(E_f-M_f)(E_i-M_i)}\Big[-\frac{M_f+M_i}{2}+M_B+\frac{1}{2}\left(W_f+W_i\right. \\
& \left.+M_f+M_i\right)\Big]2p_fp_i\ , \\
X_B^{(SO)} \ = \ & \frac{f_{14}^* f_{23}^*}{m_{\pi^+}^2}\sqrt{(E_f-M_f)(E_i-M_i)}\Big[-\Big(-\frac{M_f+M_i}{2}+M_B\Big) \\
& \times\Big(\frac{1}{4}\left(E_f+E_i-\omega_f-\omega_i\right)^2-p_f^2-p_i^2\Big)-\frac{1}{2}\left(M_f+M_i\right)M_fM_i \\
& +\frac{1}{2}\left(M_f^2+M_i^2\right)M_B\ -\frac{1}{2}\left(W_f+W_i+M_f+M_i\right)\Big(\frac{1}{4}\left(E_f+E_i-\omega_f-\omega_i\right)^2 \\
& -p_f^2-p_i^2-\left(M_f+M_i\right)M_B+M_fM_i\Big)\Big]\ , \\
Y_B^{(SO)} \ = \ & \frac{f_{14}^* f_{23}^*}{m_{\pi^+}^2}\sqrt{(E_f-M_f)(E_i-M_i)}\Big[-\frac{M_f+M_i}{2}+M_B+\frac{1}{2}\left(W_f+W_i\right. \\
& \left.+M_f+M_i\right)\Big]2p_fp_i\ .
\end{aligned}
\tag{D.6}
$$

(iv) $J^P = \frac{1}{2}^-$ pole term

(i) <u>scalar coupling:</u>

$$
\begin{aligned}
X_B^{(C)} \ &= \ g_{14}^* g_{23}^*\sqrt{(E_f+M_f)(E_i+M_i)}\Big[M_B+\frac{1}{2}\left(W_f+W_i\right)\Big]\ , \\
Y_B^{(C)} \ &= \ g_{14}^* g_{23}^*\sqrt{(E_f-M_f)(E_i-M_i)}\Big[-M_B+\frac{1}{2}\left(W_f+W_i\right)\Big]\ , \\
X_B^{(SO)} \ &= \ -g_{14}^* g_{23}^*\sqrt{(E_f-M_f)(E_i-M_i)}\Big[-M_B+\frac{1}{2}\left(W_f+W_i\right)\Big]\ .
\end{aligned}
\tag{D.7}
$$

(ii) <u>vector coupling:</u>

$$
\begin{aligned}
X_B^{(C)} \ = \ & \frac{f_{14}^* f_{23}^*}{m_{\pi^+}^2}\sqrt{(E_f+M_f)(E_i+M_i)}\Big[\Big(-\frac{1}{2}\left(M_f+M_i\right)+M_B\Big)s \\
& +\frac{1}{2}\left(M_f+M_i\right)M_fM_i+\frac{1}{2}\left(W_f+W_i-M_f-M_i\right)\left(s-\left(M_f+M_i\right)M_B\right. \\
& \left.+M_fM_i\right)-\frac{1}{2}\left(M_f^2+M_i^2\right)M_B\Big]\ ,
\end{aligned}
$$

$$
\begin{aligned}
Y_B^{(C)} &= \frac{f_{14}^* f_{23}^*}{m_{\pi^+}^2} \sqrt{(E_f - M_f)(E_i - M_i)} \Big[-\Big(-\frac{1}{2} \left(M_f + M_i \right) + M_B \Big) s \\
&\quad -\frac{1}{2} \left(M_f + M_i \right) M_f M_i + \frac{1}{2} \left(W_f + W_i - M_f - M_i \right) \left(s - \left(M_f + M_i \right) M_B \right. \\
&\quad \left. + M_f M_i \right) + \frac{1}{2} \left(M_f^2 + M_i^2 \right) M_B \Big] , \\
X_B^{(SO)} &= -\frac{f_{14}^* f_{23}^*}{m_{\pi^+}^2} \sqrt{(E_f - M_f)(E_i - M_i)} \Big[-\Big(-\frac{1}{2} \left(M_f + M_i \right) + M_B \Big) s \\
&\quad -\frac{1}{2} \left(M_f + M_i \right) M_f M_i + \frac{1}{2} \left(W_f + W_i - M_f - M_i \right) \left(s - \left(M_f + M_i \right) M_B \right. \\
&\quad \left. + M_f M_i \right) + \frac{1}{2} \left(M_f^2 + M_i^2 \right) M_B \Big] . \qquad \text{(D.8)}
\end{aligned}
$$

(v) $J^P = \frac{3}{2}^+$ baryon-exchange

$$
\begin{aligned}
X_{Y^*}^{(C)} &= -\frac{f_{14}^* f_{23}^*}{m_{\pi^+}^2} \sqrt{(E_i + M_i)(E_f + M_f)} \left[A_0 + \frac{B_0}{2} \left(W_f + W_i - M_i - M_f \right) \right] , \\
Y_{Y^*}^{(C)} &= -\frac{f_{14}^* f_{23}^*}{m_{\pi^+}^2} \Big\{ \sqrt{(E_i + M_i)(E_f + M_f)} \left[A_1 + \frac{B_1}{2} \left(W_f + W_i - M_f - M_i \right) \right] \\
&\quad + \sqrt{(E_i - M_i)(E_f - M_f)} \left[-A_0 + \frac{B_0}{2} \left(W_f + W_i + M_f + M_i \right) \right] \Big\} , \\
Z_{Y^*}^{(C)} &= -\frac{f_{14}^* f_{23}^*}{m_{\pi^+}^2} \Big\{ \sqrt{(E_i + M_i)(E_f + M_f)} \left[A_2 + \frac{B_2}{2} \left(W_f + W_i - M_f - M_i \right) \right] \\
&\quad + \sqrt{(E_i - M_i)(E_f - M_f)} \left[-A_1 + \frac{B_1}{2} \left(W_f + W_i + M_f + M_i \right) \right] \Big\} , \\
U_{Y^*}^{(C)} &= \frac{f_{14}^* f_{23}^*}{m_{\pi^+}^2} \sqrt{(E_i - M_i)(E_f - M_f)} \left[-A_2 + \frac{B_2}{2} \left(W_f + W_i + M_f + M_i \right) \right] , \\
X_{Y^*}^{(SO)} &= \frac{f_{14}^* f_{23}^*}{m_{\pi^+}^2} \sqrt{(E_i - M_i)(E_f - M_f)} \left[-A_0 + \frac{B_0}{2} \left(W_f + W_i + M_i + M_f \right) \right] , \\
Y_{Y^*}^{(SO)} &= \frac{f_{14}^* f_{23}^*}{m_{\pi^+}^2} \sqrt{(E_i - M_i)(E_f - M_f)} \left[-A_1 + \frac{B_1}{2} \left(W_f + W_i + M_i + M_f \right) \right] , \\
Z_{Y^*}^{(SO)} &= \frac{f_{14}^* f_{23}^*}{m_{\pi^+}^2} \sqrt{(E_i - M_i)(E_f - M_f)} \left[-A_2 + \frac{B_0}{2} \left(W_f + W_i - M_f - M_i \right) \right] . \qquad \text{(D.9)}
\end{aligned}
$$

Where A_0, A_1, A_2, B_0, B_1 and B_2 depend on the mass and momentum of the particles as follows.

$$
A_0 = \frac{1}{12 M_{Y^*}^2} \left(M_f + M_i \right) \left(-2 p_f p_i z_u + M_{Y^*}^2 \right)^2
$$

$$
\begin{aligned}
&+\Bigg(-\frac{1}{6M_{Y^*}^2}\left(M_f^2+M_i^2-m_f^2-m_i^2\right)\frac{1}{2}\left(M_f+M_i\right)+\frac{M_{Y^*}}{3}+\frac{1}{6}\left(M_f+M_i\right)\\
&-\frac{1}{6M_{Y^*}}\left(\frac{M_i}{2}\left(M_i-M_f\right)-m_f^2+\frac{M_f}{2}\left(M_f-M_i\right)-m_i^2\right)\Bigg)\left(-2p_f p_i z_u+M_{Y^*}^2\right)\\
&+\frac{1}{2}\left(\frac{1}{2}\left(M_f+M_i\right)+M_{Y^*}\right)\left(\frac{1}{2}\left\{\left(E_f-E_i\right)^2+\left(\omega_f-\omega_i\right)^2\right\}-p_f^2-p_i^2\right)\\
&-\frac{1}{2}\left(m_f^2+m_i^2\right)\left[\frac{1}{2}\left(M_f+M_i\right)+M_{Y^*}\right]+\frac{1}{12M_{Y^*}^2}\left(M_f+M_i\right)\left(M_f^2-m_i^2\right)\times\\
&\left(M_i^2-m_f^2\right)-\frac{M_{Y^*}}{6}\left(M_f^2+M_i^2\right)+\frac{1}{12}\left[\left(m_i^2-m_f^2\right)\left(M_f-M_i\right)-\left(M_f^2+M_i^2\right)\times\right.\\
&\left.\left(M_f+M_i\right)\right]+\frac{1}{6M_{Y^*}}\left[\left(M_f^2-m_i^2\right)\left(\frac{M_i}{2}\left(M_i-M_f\right)-m_f^2\right)+\left(M_i^2-m_f^2\right)\times\right.\\
&\left.\left(\frac{M_f}{2}\left(M_f-M_i\right)-m_i^2\right)\right]\;,
\end{aligned}
$$

$$
\begin{aligned}
A_1 &= \Bigg[-\frac{1}{12M_{Y^*}^2}\left(M_f+M_i\right)2\left(-2p_f p_i z_u+M_{Y^*}^2\right)\\
&\quad+\frac{1}{6M_{Y^*}^2}\left(M_f^2+M_i^2-m_f^2-m_i^2\right)\frac{1}{2}\left(M_f+M_i\right)-\frac{M_{Y^*}}{3}-\frac{1}{6}\left(M_f+M_i\right)\\
&\quad+\frac{1}{6M_{Y^*}}\left(\frac{M_i}{2}\left(M_i-M_f\right)-m_f^2+\frac{M_f}{2}\left(M_f-M_i\right)-m_i^2\right)\\
&\quad+\frac{1}{2}\left(\frac{1}{2}\left(M_f+M_i\right)+M_{Y^*}\right)\Bigg]2p_f p_i\;,\\
A_2 &= \frac{1}{12M_{Y^*}^2}\left(M_f+M_i\right)\left(2p_f p_i\right)^2\;,\\
B_0 &= \frac{1}{2}\left(m_f^2+m_i^2\right)-\frac{1}{6M_{Y^*}^2}\left(M_f^2-m_i^2\right)\left(M_i^2-m_f^2\right)+\frac{M_{Y^*}}{3}\left(M_f+M_i\right)\\
&\quad-\frac{1}{6}\left[m_f^2+m_i^2-\left(M_f+M_i\right)^2\right]+\frac{1}{6M_{Y^*}}\left(M_f\left(M_i^2-m_f^2\right)+M_i\left(M_f^2-m_i^2\right)\right)\\
&\quad-\frac{1}{2}\left[\frac{1}{2}\left\{\left(E_f-E_i\right)^2+\left(\omega_f-\omega_i\right)^2\right\}-p_f^2-p_i^2\right]-\frac{1}{6M_{Y^*}^2}\left(-2p_f p_i z_u+M_{Y^*}^2\right)^2\\
&\quad+\left(\frac{1}{6M_{Y^*}^2}\left[M_f^2+M_i^2-m_f^2-m_i^2\right]-\frac{1}{6M_{Y^*}}\left(M_f+M_i\right)\right)\left(-2p_f p_i z_u+M_{Y^*}^2\right)\;,\\
B_1 &= \Bigg[\frac{1}{3M_{Y^*}^2}\left(-2p_f p_i z_u+M_{Y^*}^2\right)\\
&\quad-\frac{1}{6M_{Y^*}}\left(\frac{1}{M_{Y^*}}\left[M_f^2+M_i^2-m_f^2-m_i^2\right]-\left[M_f+M_i\right]\right)-\frac{1}{2}\Bigg]2p_f p_i\;,
\end{aligned}
$$

$$B_2 = -\frac{1}{6M_{Y*}^2}\left(2p_f p_i\right)^2 . \tag{D.10}$$

(vi) $J^P = \frac{3}{2}^+$ pole term

$$\begin{aligned}
X_{Y*}^{(C)} &= \frac{f_{14}^* f_{23}^*}{m_{\pi^+}^2}\sqrt{(E_i+M_i)(E_f+M_f)}\left[A_0+\frac{B_0}{2}\left(W_f+W_i-M_i-M_f\right)\right] , \\
Y_{Y*}^{(C)} &= \frac{f_{14}^* f_{23}^*}{m_{\pi^+}^2}\left\{\sqrt{(E_i+M_i)(E_f+M_f)}\left[A_1+\frac{B_1}{2}\left(W_f+W_i-M_f-M_i\right)\right]\right. \\
&\quad \left. +\sqrt{(E_i-M_i)(E_f-M_f)}\left[-A_0+\frac{B_0}{2}\left(W_f+W_i+M_f+M_i\right)\right]\right\} , \\
Z_{Y*}^{(C)} &= \frac{f_{14}^* f_{23}^*}{m_{\pi^+}^2}\sqrt{(E_i-M_i)(E_f-M_f)}\left[-A_1+\frac{B_1}{2}\left(W_f+W_i+M_f+M_i\right)\right] , \\
X_{Y*}^{(SO)} &= -\frac{f_{14}^* f_{23}^*}{m_{\pi^+}^2}\sqrt{(E_i-M_i)(E_f-M_f)}\left[-A_0+\frac{B_0}{2}\left(W_f+W_i+M_i+M_f\right)\right] , \\
Y_{Y*}^{(SO)} &= -\frac{f_{14}^* f_{23}^*}{m_{\pi^+}^2}\sqrt{(E_i-M_i)(E_f-M_f)}\left[-A_1+\frac{B_1}{2}\left(W_f+W_i+M_i+M_f\right)\right] .
\end{aligned} \tag{D.11}$$

Where A_0, A_1, B_0 and B_1 depend on the mass and momentum of the particles as follows.

$$\begin{aligned}
A_0 &= \frac{1}{2}\left[\frac{1}{2}\left\{\left(E_f-E_i\right)^2+\left(\omega_f-\omega_i\right)^2\right\}-p_f^2-p_i^2-m_f^2-m_i^2\right]\left[\frac{1}{2}\left(M_f+M_i\right)+M_{Y*}\right] \\
&\quad +\frac{1}{6M_{Y*}^2}\left[M_f^2-m_f^2-s\right]\left[M_i^2-m_i^2-s\right]\left[\frac{M_f+M_i}{2}\right]+\frac{1}{3M_{Y*}}\left[s-\frac{1}{2}\left(M_f^2\right.\right. \\
&\quad \left.\left.+M_i^2\right)\right]+\frac{1}{3}\left[\frac{1}{2}(M_f+M_i)s-\frac{1}{4}(M_f^2+M_i^2)(M_f+M_i)+\frac{1}{4}(m_f^2-m_i^2)\right. \\
&\quad \left.(M_f-M_i)\right]+\frac{1}{6M_{Y*}}\left[(M_f^2-m_f^2-s)(\frac{M_i}{2}(M_i-M_f)-m_i^2)-(M_i^2-m_i^2-s)\right. \\
&\quad \left.(\frac{M_f}{2}(M_i-M_f)+m_f^2)\right] , \\
A_1 &= \frac{1}{2}\left[\frac{1}{2}\left(M_f+M_i\right)+M_{Y*}\right]2p_f p_i , \\
B_0 &= \frac{1}{2}\left[\frac{1}{2}\left\{\left(E_f-E_i\right)^2+\left(\omega_f-\omega_i\right)^2\right\}-p_f^2-p_i^2-m_f^2-m_i^2\right]\frac{1}{6M_{Y*}^2}\left[s-M_f^2+m_f^2\right] \\
&\quad \left[s-M_i^2+m_i^2\right]-\frac{M_{Y*}}{3}(M_f+M_i)+\frac{1}{6}[m_f^2+m_i^2-(M_f+M_i)^2]-\frac{1}{6M_{Y*}}\times \\
&\quad \left[M_f(M_i^2-m_i^2-s)+M_i(M_f^2-m_f^2-s)\right] , \\
B_1 &= p_f p_i .
\end{aligned} \tag{D.12}$$

D.2 Meson-exchange

(i) $J^P = 0^{++}$ scalar-meson-exchange

$$
\begin{aligned}
X_S^{(C)} &= -g_{13}^{(s)} g_{24}^{(s)} \sqrt{(E_f + M_f)(E_i + M_i)}\,, \\
Y_S^{(C)} &= g_{13}^{(s)} g_{24}^{(s)} \sqrt{(E_f - M_f)(E_i - M_i)}\,, \\
X_S^{(SO)} &= -g_{13}^{(s)} g_{24}^{(s)} \sqrt{(E_f - M_f)(E_i - M_i)}\,.
\end{aligned} \tag{D.13}
$$

(ii) $J^P = 1^{--}$ vector-meson-exchange

$$
\begin{aligned}
X_V^{(C)} &= -g_{PPV} g_V \sqrt{(E_i + M_i)(E_f + M_f)} \Bigg[\frac{\left(m_f^2 - m_i^2\right)\left(M_i - M_f\right)}{m_V^2} - \big(W_f + W_i \\
&\quad - M_i - M_f\big)\Bigg] - g_{PPV} f_V \sqrt{(E_i + M_i)(E_f + M_f)} \Bigg[-\frac{M_f + M_i}{2M_S} \big(W_f + W_i \\
&\quad - M_i - M_f\big) + \frac{\left(\omega_f + \omega_i\right)\left(E_f + E_i\right) + p_f^2 + p_i^2}{2M_S} \Bigg]\,, \\
Y_V^{(C)} &= -g_{PPV} g_V \sqrt{(E_i - M_i)(E_f - M_f)} \Bigg[-\frac{(m_f^2 - m_i^2)(M_i - M_f)}{m_V^2} - \big(W_f + W_i \\
&\quad + M_i + M_f\big)\Bigg] - g_{PPV} f_V \Bigg[\sqrt{(E_i + M_i)(E_f + M_f)}\, \frac{p_f p_i}{M_S} \\
&\quad + \sqrt{(E_i - M_i)(E_f - M_f)} \Bigg[-\frac{M_f + M_i}{2M_S} \big(W_f + W_i + M_i + M_f\big) \\
&\quad - \frac{\left(\omega_f + \omega_i\right)\left(E_f + E_i\right) + p_f^2 + p_i^2}{2M_S} \Bigg]\Bigg]\,, \\
Z_V^{(C)} &= g_{PPV} f_V \sqrt{(E_i - M_i)(E_f - M_f)}\, \frac{p_f p_i}{M_s}\,, \\
X_V^{(SO)} &= g_{PPV} g_V \sqrt{(E_i - M_i)(E_f - M_f)} \Bigg[-\frac{(m_f^2 - m_i^2)(M_i - M_f)}{m_V^2} - \big(W_f + W_i \\
&\quad + M_f + M_i\big)\Bigg] + g_{PPV} f_V \sqrt{(E_i - M_i)(E_f - M_f)} \Bigg[-\frac{M_f + M_i}{2M_S} \big(W_f + W_i \\
&\quad + M_f + M_i\big) - \frac{\left(\omega_f + \omega_i\right)\left(E_f + E_i\right) + p_f^2 + p_i^2}{2M_S} \Bigg]\,, \\
Y_V^{(SO)} &= -g_{PPV} f_V \sqrt{(E_i - M_i)(E_f - M_f)}\, \frac{p_f p_i}{M_s}\,.
\end{aligned} \tag{D.14}
$$

(iii) $J^P = 2^{++}$ tensor-meson-exchange

$$
\begin{aligned}
X_T^{(C)} &= -\frac{g_{PPT}F_1}{m_{\pi^+}}\sqrt{(E_i+M_i)(E_f+M_f)}\left[A_0+\frac{1}{2}B_0\left(W_f+W_i-M_i-M_f\right)\right] , \\
Y_T^{(C)} &= -\frac{g_{PPT}F_1}{m_{\pi^+}}\left\{\sqrt{(E_i+M_i)(E_f+M_f)}\left[A_1+\frac{1}{2}B_1\left(W_f+W_i-M_f-M_i\right)\right]\right. \\
&\quad \left.+\sqrt{(E_i-M_i)(E_f-M_f)}\left[-A_0+\frac{1}{2}B_0\left(W_f+W_i+M_f+M_i\right)\right]\right\} , \\
Z_T^{(C)} &= -\frac{g_{PPT}F_1}{m_{\pi^+}}\left\{\sqrt{(E_i+M_i)(E_f+M_f)}A_2\right. \\
&\quad \left.+\sqrt{(E_i-M_i)(E_f-M_f)}\left[-A_1+\frac{1}{2}B_1\left(W_f+W_i+M_f+M_i\right)\right]\right\} , \\
U_T^{(C)} &= \frac{g_{PPT}F_1}{m_{\pi^+}}\sqrt{(E_i-M_i)(E_f-M_f)}A_2 , \\
X_T^{(SO)} &= \frac{g_{PPT}F_1}{m_{\pi^+}}\sqrt{(E_i-M_i)(E_f-M_f)}\left[-A_0+\frac{1}{2}B_0\left(W_f+W_i+M_i+M_f\right)\right] , \\
Y_T^{(SO)} &= \frac{g_{PPT}F_1}{m_{\pi^+}}\sqrt{(E_i-M_i)(E_f-M_f)}\left[-A_1+\frac{1}{2}B_1\left(W_f+W_i+M_i+M_f\right)\right] , \\
Z_T^{(SO)} &= -\frac{g_{PPT}F_1}{m_{\pi^+}}\sqrt{(E_i-M_i)(E_f-M_f)}A_2 . \qquad \text{(D.15)}
\end{aligned}
$$

Where A_0, A_1, A_2, B_0 and B_1 depend on the mass and momentum of the particles as follows.

$$
\begin{aligned}
A_0 &= \frac{F_2}{F_1}\left\{\frac{1}{4}\left(\left(\omega_i+\omega_f\right)\left(E_f+E_i\right)+p_f^2+p_i^2\right)^2+\frac{1}{4m_T^4}\left(m_f^2-m_i^2\right)^2\left(M_i^2-M_f^2\right)^2\right. \\
&\quad -\frac{\left(\omega_i+\omega_f\right)\left(E_f+E_i\right)+p_f^2+p_i^2}{2m_T^2}\left(m_f^2-m_i^2\right)\left(M_i^2-M_f^2\right)-\frac{1}{3}\times \\
&\quad \left(-2\left(m_f^2+m_i^2\right)+\frac{\left(m_f^2-m_i^2\right)^2}{m_T^2}+\frac{1}{2}\left[\left(E_f-E_i\right)^2+\left(\omega_f-\omega_i\right)^2\right]-p_f^2-p_i^2\right)\times \\
&\quad \left.\left(\frac{\left(M_i^2-M_f^2\right)^2}{4m_T^2}-\frac{M_f^2+M_i^2}{2}+\frac{1}{4}\left(\frac{1}{2}\left[\left(E_f-E_i\right)^2+\left(\omega_f-\omega_i\right)^2\right]-p_f^2-p_i^2\right)\right)\right\} \\
&\quad +\left\{-\frac{\left(\omega_i+\omega_f\right)\left(E_f+E_i\right)+p_f^2+p_i^2}{2m_T^2}\left(m_f^2-m_i^2\right)\left(M_i-M_f\right)\right. \\
&\quad +\frac{1}{2m_T^4}\left(m_f^2-m_i^2\right)^2\left(M_i^2-M_f^2\right)\left(M_i-M_f\right)
\end{aligned}
$$

$$
\begin{aligned}
& -\frac{1}{3}\left(-2\left[m_f^2+m_i^2\right]+\frac{\left(m_f^2-m_i^2\right)^2}{m_T^2}+\frac{1}{2}\left[\left(E_f-E_i\right)^2+\left(\omega_f-\omega_i\right)^2\right]-p_f^2-p_i^2\right) \\
& \times\left(\frac{\left(M_i^2-M_f^2\right)}{2m_T^2}\left(M_i-M_f\right)-\frac{1}{2}\left(M_f+M_i\right)\right)\Bigg\} \;, \\
A_1 \;=\;& \frac{F_2}{F_1}\left\{\left(\omega_i+\omega_f\right)\left(E_f+E_i\right)+p_f^2+p_i^2-\frac{\left(m_f^2-m_i^2\right)\left(M_i^2-M_f^2\right)}{m_T^2}\right. \\
& -\frac{1}{6}\left(-2\left(m_f^2+m_i^2\right)+\frac{\left(m_f^2-m_i^2\right)^2}{m_T^2}+\frac{1}{2}\left[\left(E_f-E_i\right)^2+\left(\omega_f-\omega_i\right)^2\right]-p_f^2-p_i^2\right) \\
& -\frac{\left(M_i^2-M_f^2\right)^2 2}{6m_T^2}+\frac{1}{3}\left(M_f^2+M_i^2\right)-\frac{1}{6}\left(\frac{1}{2}\left[\left(E_f-E_i\right)^2+\left(\omega_f-\omega_i\right)^2\right]-p_f^2\right. \\
& \left.\left.-p_i^2\right)\right\} p_f p_i+\left\{-\frac{\left(m_f^2-m_i^2\right)\left(M_i-M_f\right)}{m_T^2}-\frac{\left(M_i^2-M_f^2\right)\left(M_i-M_f\right)}{3m_T^2}+\right. \\
& \left.\frac{1}{3}\left(M_f+M_i\right)\right\} p_f p_i \;, \\
A_2 \;=\;& -\frac{1}{3}p_f^2 p_i^2\frac{F_2}{F_1} \;, \\
B_0 \;=\;& \left(\omega_i+\omega_f\right)\left(E_f+E_i\right)+p_f^2+p_i^2-\frac{\left(m_f^2-m_i^2\right)\left(M_i^2-M_f^2\right)}{m_T^2} \;, \\
B_1 \;=\;& 2p_f p_i \;.
\end{aligned}
\tag{D.16}
$$

D.3 Pomeron-exchange

$$
\begin{aligned}
X_P^{(C)} &= g_{13}^P g_{24}^P\sqrt{(E_f+M_f)(E_i+M_i)} \;, \\
Y_P^{(C)} &= -g_{13}^P g_{24}^P\sqrt{(E_f-M_f)(E_i-M_i)} \;, \\
X_P^{(SO)} &= g_{13}^P g_{24}^P\sqrt{(E_f-M_f)(E_i-M_i)} \;.
\end{aligned}
\tag{D.17}
$$

Appendix E

Haftel-Tabakin matrix-inversion method

The integral equation for the scattering amplitude, Eq. (3.17), has a singularity in the Green function G_0, the method we use to deal with this singularity, originally introduced by Haftel and Tabakin [63], is described in detail in this appendix. The on-shell, half off-shell as well as the full off-shell amplitude is found using this method.

The integral equation for the amplitude to be solved numerically is typically of the form

$$T(p',p) \;=\; V(p',p)+\mathcal{P}\int\frac{dk}{2\pi^2}V(p',k)\frac{1}{4E(k)\mathcal{E}(k)}\frac{k^2}{\sqrt{s}-E(k)-\mathcal{E}(k)}T(k,p)\;. \tag{E.1}$$

Here we have defined the on-shell energy $\sqrt{s}=E(q)+\mathcal{E}(q)$, where q is the on-shell momentum. Now we subtract a term which is equal to zero, having the same pole and residue as the integrand. The integrand now becomes smooth and the principal-value integral in Eq. (E.1) can be replaced by an ordinary integral, giving

$$\begin{aligned} T(p',p) \;=\; V(p',p)+\int\frac{dk}{2\pi^2}V(p',k)\Bigg[&\frac{1}{4E(k)\mathcal{E}(k)}\frac{k^2}{\sqrt{s}-E(k)-\mathcal{E}(k)}T(k,p)\\ &-\frac{1}{2\sqrt{s}}\frac{q^2}{q^2-k^2}T(q,p)\Bigg]\;. \end{aligned} \tag{E.2}$$

Rearranging the terms leads to

$$\begin{aligned} T(p',p) \;-\; \int\frac{dk}{2\pi^2}V(p',k)\Bigg[&\frac{1}{4E(k)\mathcal{E}(k)}\frac{k^2}{\sqrt{s}-E(k)-\mathcal{E}(k)}T(k,p)\\ &-\frac{1}{2\sqrt{s}}\frac{q^2}{q^2-k^2}T(q,p)\Bigg]=V(p',p)\;. \end{aligned} \tag{E.3}$$

To make this equation discrete for its numerical evaluation, we use N grid points. We use the Gaussian integration grid points (x_j) and weights (w_j), however, these grid points are in the interval [-1,..,1] while the integration momenta run from 0 to ∞. We have to perform a mapping of the interval [-1,..1] to the interval [0,..,∞], the mapping we use is

$$\begin{aligned} p_j &= p_{\rm cut}\,\tan\left[\frac{\pi}{4}\left(x_j+1\right)\right] , \\ s_j &= p_{\rm cut}\frac{\pi}{4}\frac{w_j}{\cos^2\left[\frac{\pi}{4}\left(x_j+1\right)\right]} , \end{aligned} \tag{E.4}$$

where p_j and s_j are the momentum integration grid points and weights and we have chosen $p_{\rm cut} = 1000$ MeV. The integral now becomes a summation over N off-shell momenta, labeled by j,

$$\begin{aligned} T(p_i,p_l) \;-\; \sum_{j=1}^{N}\frac{s_j}{2\pi^2}V(p_i,p_j)\Bigg[\frac{1}{4E(p_j)\mathcal{E}(p_j)}\frac{p_j^2}{\sqrt{s}-E(p_j)-\mathcal{E}(p_j)}T(p_j,p_l) \\ -\frac{1}{2\sqrt{s}}\frac{q^2}{q^2-p_j^2}T(q,p_l)\Bigg] = V(p_i,p_l) \end{aligned} \tag{E.5}$$

where s_j are the integration weights. We introduce the definitions for the function u_j and the on-shell momentum q,

$$\begin{aligned} u_j &= \frac{1}{4E(p_j)\mathcal{E}(p_j)}\frac{p_j^2}{E(p_j)+\mathcal{E}(p_j)-\sqrt{s}}\frac{s_j}{2\pi^2} \quad , j=1,..,N , \\ u_{N+1} &= \sum_{n=1}^{N}\frac{1}{2\sqrt{s}}\frac{q^2}{q^2-p_n^2}\frac{s_n}{2\pi^2} , \\ q &= p_{N+1} , \end{aligned} \tag{E.6}$$

where all the integration grid points p_j need to be distinct from the on-shell momentum q. We find that Eq. (E.5) can be written in the compact form

$$\begin{aligned} & T(p_i,p_l)+\sum_{j=1}^{N}u_jV(p_i,p_j)T(p_j,p_l)+u_{N+1}V(p_i,p_{N+1})T(p_{N+1},p_l) = V(p_i,p_l) , \\ & \sum_{j=1}^{N+1}\left(\delta_{ij}+u_jV(p_i,p_j)\right)T(p_j,p_l) = V(p_i,p_l) , \\ & \sum_{j=1}^{N+1}A_{ij}T(p_j,p_l) \equiv V(p_i,p_l) . \end{aligned} \tag{E.7}$$

Here, also i and l run from $i,l = 1,..,N$ for off-shell momenta and $i,j = N+1$ for on-shell momenta. The integral equation with a singularity in the Green function, Eq. (E.1), has been reduced to a simple matrix-inversion problem for an $(N+1)\times(N+1)$ matrix . The full off-shell matrix elements are given by $i,l = 1,..,N$, the left off-shell by $i = 1,..,N$ and $l = N+1$, the right off-shell by $i = N+1$ and $l = 1,..,N$ and the on-shell by $i,l = N+1$. We notice that this method is easily extended for a coupled channels problem.

References

[1] R. A. Arndt, I. I. Strakovsky, and R. L. Workman, Phys. Rev. C **52**, 2120 (1995). 3, 33, 51, 52, 58

[2] J. S. Hyslop, R. A. Arndt, L. D. Roper, and R. L. Workman, Phys. Rev. D **46**, 961 (1992). 3, 33, 65, 72, 79, 82

[3] T. Nakano et al., Phys. Rev. Lett. **91**, 012002 (2003). 3, 66, 82

[4] L. Maiani, G. Pancheri, and N. Pavers, *The Second DAΦNE Physics Handbook*, Frascati, 1995. 4

[5] Y. Akaishi and T. Yamazaki, Phys. Rev. C **65**, 044005 (2002). 4

[6] M. M. Nagels, T. A. Rijken, and J. J. de Swart, Phys. Rev. D **17**, 768 (1978). 4

[7] P. M. M. Maessen, T. A. Rijken, and J. J. de Swart, Phys. Rev. C **40**, 2226 (1989). 4, 80

[8] S. Weinberg, Physica A **96**, 327 (1979). 4

[9] A. Manohar and H. Georgi, Nucl. Phys. **B234**, 189 (1984). 4

[10] H. Georgi, Annu. Rev. Nucl. Sci. **43**, 209 (1993). 4

[11] J. Wheeler, Phys. Rev. **52**, 1083 (1937). 4

[12] J. Wheeler, Phys. Rev. **52**, 1107 (1937). 4

[13] D. Liberman, Phys. Rev. D **16**, 1542 (1977). 4

[14] J. E. F. T. Ribeiro, Z. Phys. C **5**, 27 (1980). 4

[15] Y. Fujiwara, C. Nakamoto, and Y. Suzuki, Phys. Rev. C **54**, 2180 (1996). 4

[16] J. Polchinsky, Nucl. Phys. **B231**, 269 (1984). 4

[17] E. E. Salpeter and H. A. Bethe, Phys. Rev. **84**, 1232 (1951). 6

[18] V. Pascalutsa and J. A. Tjon, Phys. Rev. C **61**, 054003 (2000). 6, 46, 52, 54, 55, 62

[19] M. Hoffmann, J. W. Durso, K. Holinde, B. C. Pearce, and J. Speth, Nucl. Phys. **A593**, 341 (1995). 6, 52, 66, 67, 79

[20] F. E. Low, Phys. Rev. D **12**, 163 (1975). 6, 27

[21] S. Nussinov, Phys. Rev. Lett. **34**, 1286 (1975). 6, 27

[22] S. Weinberg, Phys. Rev. Lett. **17**, 616 (1966). 6, 54, 62

[23] S. L. Adler, Phys. Rev. **137**, B 1022 (1965). 6, 54, 62

[24] H. P. Stapp, T. Ypsilantis, and M. Metropolis, Phys. Rev. **105**, 311 ((1957). 7, 129

[25] P. D. B. Collins and E. J. Squires, Springer Tracts in Modern Physics **45** (1968). 9

[26] H. Pilkuhn, *The Interaction of Hadrons*, North-Holland Publishing Company, Amsterdam, 1967. 9, 28, 63, 105

[27] J. D. Bjorken and S. D. Drell, *Relativistic Quantum Fields*, McGraw-Hill Inc., New York, 1965.
We follow the conventions of this reference except for two things. First, we use Dirac spinors with the normalization $u^\dagger(\mathbf{p})\, u(p) = 2E(\mathbf{p})$, in accordance with the normalization Eq. (2.17). Secondly, we have a $(-)$-sign in the definition Eq. (2.2) of the M-matrix. 11, 17, 99

[28] M. M. Nagels, T. A. Rijken, and J. J. de Swart, Phys. Rev. D **15**, 2547 (1977). 13, 16

[29] A. A. Logunov and A. N. Tavkhelidze, Nuovo Cimento **29**, 380 (1963). 13

[30] R. Blankenbecler and R. Sugar, Phys. Rev. **142**, 1051 (1966). 13

[31] M. H. Partovi and E. L. Lomon, Phys. Rev. D **2**, 1999 (1970). 13

[32] R. H. Thompson, Phys. Rev. D **1**, 110 (1970). 13

[33] A. Gersten, P. A. Verhoeven, and J. J. de Swart, Nuovo Cimento **A26**, 375 (1975). 13

[34] P. A. Verhoeven, *Off-shell baryon-baryon scattering*, PhD thesis, University of Nijmegen, 1976, unpublished. 13, 14, 22

[35] T. A. Rijken, Ann. Phys. **164**, 1 and 23 (1985). 13

[36] V. G. Kadyshevsky, Sov. Phys. JETP **19**, 443 and 597 (1964). 14

[37] V. G. Kadyshevsky, Nucl. Phys. **B6**, 125 (1968). 14

[38] V. G. Kadyshevsky, Nuovo Cimento **A55**, 275 (1968). 14

[39] C. Itzykson, V. G. Kadyshevski, and N. D. Mattev, Phys. Rev. D **1**, 2823 (1970). 14

[40] J. J. de Swart, Rev. Mod. Phys. **35**, 916 (1963). 25, 26, 27

[41] O. D. et al, Nucl. Phys. **B216**, 277 (1983). 27

[42] P. A. Carruthers, *Spin and Isospin in Particle Physics*, Gordon and breach Science Publishers, Inc., New York, 1971.
The isospin-$\frac{1}{2}$ isospin-$\frac{3}{2}$ transition operator we use is equal to $1/\sqrt{2}$ times the operator defined in this reference. 28, 53, 105

[43] M. M. Nagels, T. A. Rijken, and J. J. de Swart, Nucl. Phys. **B147**, 557 (1979). 30, 81

[44] R. W. Haymaker, Phys. Rev. **181**, 2040 (1969). 39, 40

[45] V. Pascalutsa, *Covariant Description of Pion-Nucleon Dynamics*, PhD thesis, University of Utrecht, 1998, unpublished. 47

[46] R. Koch and E. Pietarinen, Nucl. Phys. **A336**, 331 (1980). 51, 52, 58

[47] G. F. Chew and F. E. Low, Phys. Rev. **101**, 1570 (1956). 51

[48] E. H. S. Burhop, *High Energy Physics*, Academic Press Inc., New York, 1967,
J. Hamilton, *Pion-Nucleon Interactions*. 51

[49] B. H. Bransden and R. G. Moorhouse, *The Pion-Nucleon System*, Princeton University Press, Princeton, New Jersey, 1973. 51, 69

[50] T. A. Rijken, H. Polinder, and J. Nagata, Phys. Rev. C **66**, 044008 (2002). 52

[51] T. A. Rijken, H. Polinder, and J. Nagata, Phys. Rev. C **66**, 044009 (2002). 52

[52] T. A. Rijken, V. G. J. Stoks, and Y. Yamamoto, Phys. Rev. C **59**, 21 (1999). 52

[53] B. C. Pearce and B. K. Jennings, Nucl. Phys. **A528**, 655 (1990). 52, 54, 62

[54] F. Gross and Y. Surya, Phys. Rev. C **47**, 703 (1993). 52

[55] G. Schütz, J. W. Durso, K. Holinde, and J. Speth, Phys. Rev. C **49**, 2671 (1994). 52, 54

[56] G. Schütz et al., Phys. Rev. C **51**, 1374 (1995). 52, 54

[57] T. Sato and T. S. H. Lee, Phys. Rev. C **54**, 2660 (1996). 52, 54

[58] A. D. Lahiff and I. R. Afnan, Phys. Rev. C **60**, 024608 (1999). 52, 54

[59] R. Büttgen, K. Holinde, A. Müller-Groeling, J. Speth, and P. Wyborny, Nucl. Phys. **A506**, 586 (1990). 52, 66, 67

[60] H. M. Nieland and J. A. Tjon, Phys. Lett. **27B**, 309 (1968). 52

[61] H. M. Nieland, *Some off-shell calculations for πN scattering*, PhD thesis, University of Nijmegen, 1971, unpublished. 52

[62] D. Lu, S. C. Phatak, and R. H. Landau, Phys. Rev. C **51**, 2207 (1995). 52

[63] M. I. Haftel and F. Tabakin, Nucl. Phys. **A158**, 1 (1970). 53, 123

[64] M. M. Nagels, T. A. Rijken, and J. J. de Swart, Phys. Rev. D **12**, 744 (1975). 54

[65] K. Hashimoto, Phys. Rev. C **29**, 1377 (1983). 65, 69, 73, 74, 75, 84

[66] S. J. Watts et al., Phys. Lett. **95B**, 323 (1980). 65, 73, 74

[67] V. Barmin et al., arXiv:hep-ex/0304040 . 66, 82

[68] S. Stepanyan et al., arXiv:hep-ex/0307018 . 66, 82

[69] J. Barth et al., arXiv:hep-ex/0307083 . 66, 82

[70] D. Diakonov, V. Petrov, and M. Polyakov, Z. Phys. **A359**, 305 (1997), arXiv:hep-ph/9703373. 66, 82

[71] C. B. Dover and G. E. Walker, Phys. Reports **89**, 1 (1982). 66, 72

[72] R. Machleidt, K. Holinde, and C. Elster, Phys. Reports **149**, 1 (1987). 66, 67

[73] T. Barnes and E. S. Swanson, Phys. Rev. C **49**, 1166 (1994). 66

[74] B. Silvestre-Brac, J. Leandri, and J. Labarsouque, Nucl. Phys. **A589**, 585 (1995). 66

[75] B. Silvestre-Brac, J. Labarsouque, and J. Leandri, Nucl. Phys. **A613**, 342 (1997). 66

[76] S. Lemaire, J. Labarsouque, and B. Silvestre-Brac, Nucl. Phys. **A696**, 497 (2001). 66

[77] S. Lemaire, J. Labarsouque, and B. Silvestre-Brac, Nucl. Phys. **A700**, 330 (2002). 66

[78] D. Hadjimichef, J. Haidenbauer, and G. Krein, Phys. Rev. C **66**, 055214 (2002). 66, 79

[79] M. F. M. Lutz and E. E. Kolomeitsev, Nucl. Phys. **A700**, 193 (2002). 67

[80] C. M. Vincent and S. C. Phatak, Phys. Rev. C **10**, 391 (1974). 72

[81] B. R. Martin, Nucl. Phys. **B94**, 413 (1975). 72, 79

[82] T. Bowen et al., Phys. Rev. D **2**, 2599 (1970). 75, 84

[83] B. J. Charles et al., Nucl. Phys. **B131**, 7 (1977). 76

[84] G. Giacomelli et al., Nucl. Phys. **B56**, 346 (1973). 77

[85] B. R. Lovett et al., Phys. Rev. D **23**, 1924 (1981). 78

[86] A. W. Robertson et al., Phys. Lett. **91B**, 465 (1980). 78

[87] R. A. Arndt, I. I. Strakovsky, and R. L. Workman, arXiv:nucl-th/0308012 . 82

[88] J. R. Taylor, *Scattering Theory: The Quantum Theory on Nonrelativistic Collisions*, John Wiley & Sons, Inc., New York, 1972.
In the SYM-convention [24] the configuration space basic JLS-states are $\mathcal{Y}^M_{JLS}(\hat{\mathbf{r}}) = C^{J\ L\ S}_{M\ m\ \mu} Y^L_m(\hat{\mathbf{r}}) \chi^S_\mu$. Transformation to momentum space gives Eq. (A.13). 91

[89] P. A. Carruthers, *Encyclopedia of Mathematics and its Applications*, Addison-Wesley Publishing Company, 1981,
L. C. Biedenharn and J. D. Louck, *The Racah-Wigner Algebra in Quantum Theory*. 92

[90] A. R. Edmonds, *Angular Momentum in Quantum Mechanics*, Princeton University Press, Princeton, 1957.
The explicit relation between our $9j$-symbols and those of this reference Eq. (6.4.4) is

$$\begin{bmatrix} j_{11} & j_{12} & j_{13} \\ j_{21} & j_{22} & j_{23} \\ j_{31} & j_{32} & j_{33} \end{bmatrix} = \left[(2j_{13}+1)(2j_{31}+1)(2j_{23}+1)(2j_{32}+1)\right]^{1/2} \times \begin{Bmatrix} j_{11} & j_{12} & j_{13} \\ j_{21} & j_{22} & j_{23} \\ j_{31} & j_{32} & j_{33} \end{Bmatrix}$$

. 92, 95, 97

[91] S. Gasiorowicz, *Elementary particle physics*, John Wiley & Sons, New York, 1966. 101

Samenvatting

Dit proefschrift, getiteld *"Sterke Meson-Baryon wisselwerkingen"*, onderzoekt de sterke wisselwerking tussen mesonen en baryonen bij lage en intermediaire energieën, en levert een bijdrage aan het gedetailleerde begrip van hadron-hadron wisselwerkingen in het algemeen. De sterke meson-baryon wisselwerking wordt experimenteel onderzocht middels het verstrooien van een meson bundel aan een nucleair doelwit. De gemeten grootheden (observabelen) worden gebruikt bij het construeren van theoretische modellen.

De pion-nucleon wisselwerking in het bijzonder wordt al meer dan veertig jaar onderzocht. Pion bundels met hoge intensiteit zijn beschikbaar en bij verschillende laboratoria zijn verstrooiingsexperimenten gedaan. Een zeer rijke verstrooiingsdatabank is nu beschikbaar. De situatie voor de kaon-nucleon wisselwerking is echter anders. De verstrooiingsexperimenten zijn verricht in de jaren zeventig en begin jaren tachtig, gebruik makende van kaon bundels die een veel lagere intensiteit hebben dan de pion bundels. De kaon-nucleon verstrooiingsobservabelen zijn dus veel minder nauwkeurig bekend, vooral bij lagere energiën. Meer en nauwkeurige kaon-nucleon verstrooiingsdata wordt binnenkort verwacht, de *K-fabriek* die op dit moment gebouwd wordt bij de Japan Proton Accelerator Research Complex (J-PARC) zal beschikken over een kaon bundel met een veel hogere intensiteit (ca. tien maal) dan welke kaon bundel voorheen. Nieuwe kaon-nucleon verstrooiingsdata worden ook verwacht van de DAΦNE faciliteit in Italië.

In het verleden en in het heden zijn meson-uitwisselings modellen zeer succesvol gebleken in het kwantitatief beschrijven van de nucleon-nucleon (NN) wisselwerking en de hyperon-nucleon (YN) wisselwerking. In dit proefschrift wordt een soortgelijke benadering toegepast op de pion-nucleon (πN) wisselwerking, voornamelijk dienend als een natuurlijke basis voor een $SU_f(3)$-symmetrische uitbreiding naar de kaon-nucleon (KN) wisselwerking. Deze wisselwerking onderscheidt zich echter van de NN en YN wisselwerkingen doordat niet alleen meson-uitwisselingen plaatsvinden, maar ook baryon-uitwisselingen in het s- en u-kanaal. We hebben een "soft-core" meson- en baryon-uitwisselings model voor de πN en KN wisselwerking afgeleid, overeenkomstig de Nijmegen soft-core één-boson-uitwisselings NN en YN modellen.

De meson-baryon potentialen in de samenhang met een relativistische twee-deeltjes vergelijking, de Bethe-Salpeter vergelijking, zijn gedefinieerd in Hoofdstuk 2. De potentialen bestaan uit één-meson- en één-baryon-uitwisselings Feynman diagrammen. De Bethe-Salpeter vergelijking wordt benaderd door "dynamische paar-onderdrukking" aan te nemen, en daarom het verwaarlozen van de voortplanting van negatieve energie toestanden, en door te integreren over de tijd variabele. Dit resulteert in een drie-dimensionale integraal vergelijking voor de verstrooiingsamplitude, welke een generalisatie van de Lippmann-Schwinger vergelijking is.

Een transformatie van deze vergelijking op de vlakke golf basis naar de partiële golf (LSJ) basis wordt beschreven in Hoofdstuk 3. Een één-dimensionale integraal vergelijking voor de partiële golf verstrooiingsamplitude wordt afgeleid. Deze is voor elke partiële golf ontkoppeld vanwege pariteit behoud in sterke wisselwerkingen.

Het soft-core πN model dat in dit proefschrift wordt beschreven, toont aan dat de soft-core benadering van de Nijmegen groep niet alleen een goede beschrijving van de NN en YN data geeft, maar dat ook de πN en KN data goed worden beschreven met deze benadering. Het soft-core πN model dient als een solide basis voor het soft-core KN model onder de aanname dat deze aan elkaar gerelateerd zijn door $SU_f(3)$-symmetrie. Voor de volledigheid worden de definities van de octet irreducibele representatie (irrep) voor de $J^P = \frac{1}{2}^+$ baryonen en de octet en singlet irreps voor de mesonen alsmede de invariante wisselwerkings Hamiltonianen gegeven in Hoofdstuk 4. Deze Hamiltonianen zijn gebruikt om de één-baryon- en één-meson-uitwisselings invariante amplitudes af te leiden. Deze amplitudes definiëren de partiële golf potentialen die we gebruiken in de berekeningen.

In de πN werkzame doorsnede zijn enkele resonanties aanwezig bij lage en intermediaire energieën, bijvoorbeeld de $\Delta(1232)$ en de Roper(1440). Het is gebleken dat deze resonanties niet beschreven konden worden door alleen een πN potentiaal te gebruiken; ze konden niet dynamisch gegenereerd worden. Dit bevestigt het idee van het quark-model. We beschouwen deze resonanties, op zijn minst gedeeltelijk, als echte drie-quark toestanden en behandelen ze op dezelfde manier als het nucleon. Daarom hebben we s-kanaal diagrammen voor deze resonanties opgenomen in het soft-core πN model. Dit dient echter zorgvuldig gedaan te worden in een gerenormaliseerd schema, d.w.z. een schema waarin fysische koppeling constantes en massa's worden gebruikt, omdat iteraties van s-kanaal diagrammen bijdragen leveren aan het vertex en de zelf-energie. De renormalisatie procedure die we gebruiken om s-kanaal diagrammen op te nemen in een gerenormaliseerd model wordt in detail beschreven in Hoofdstuk 5. We beschrijven de methode voor partiële golven die één resonantie bevatten, bijvoorbeeld de $\Delta(1232)$ in de P_{33}-golf, en voor partiële golven waarin meerdere s-kanaal diagrammen een rol spelen, met name in de P_{11}-golf (nucleon en Roper(1440)).

Het soft-core πN model en de fit aan de experimentele data worden gepresenteerd in Hoofdstuk 6. Het model bevat de uitwisselingen van de baryonen N, Δ, Roper and S_{11}, de scalaire mesonen σ en f_0, het vector meson ρ en de tensor mesonen f_2 en f_2'. Een uitstekende fit aan de empirische S- en P-golf faseverschuivingen voor een pion kinetische energie tot 600 MeV is bereikt. De gevonden waarden voor de koppeling constantes en vormfactor massa's zijn goed, behalve de te lage waarde voor $f_{NN\rho}/g_{NN\rho}$, Dit is ook een probleem in andere πN modellen. De verstrooiingslengtes worden goed gereproduceerd. Aan de "soft-pion" theorema's voor lage energie πN verstrooiing wordt voldaan, aangezien de S-golf verstrooiingslengtes goed beschreven worden. De c_1-, c_2-, c_3- and c_4-termen in chirale storingstheorie worden impliciet beschreven door het soft-core πN model; hogere afgeleide termen in chirale storingstheorie worden effectief beschreven door de propagatoren en Gaussische vormfactoren in het soft-core πN model.

In Hoofdstuk 7 worden het soft-core KN model, een $SU_f(3)$ uitbreiding van het soft-core πN model, en de fit aan de experimentele data gepresenteerd. Het model bevat de uitwisselingen van de baryonen Λ, Σ, $\Sigma^*(1385)$ en $\Lambda(1405)$, de scalaire mesonen a_0, σ en f_0, de vector mesonen ρ, ω en φ en de tensor mesonen a_2, f_2 and f_2'. De kwaliteit van de fit aan de empirische faseverschuivingen voor een kaon kinetische energie tot 600 MeV is niet zo goed als die van het soft-core πN model, maar het in dit proefschrift gepresenteerde soft-core KN model vertegenwoordigt zeker de huidige stand van de theorie. De verstrooiingsobservabelen zelf: de totale en differentiële werkzame doorsneden en polarizaties, alsmede de S-golf verstrooiingslengtes worden goed gereproduceerd.

Lage energie (exotische) resonanties zijn nooit waargenomen in de K^+n-verstrooiingsdata. Recentelijk zijn in verschillende photo-productie experimenten aanwijzingen gevonden voor het bestaan van een smalle resonantie in het isospin nul KN systeem. We hebben deze resonantie $\Theta^+(1540)$ opgenomen in het soft-core KN model, op dezelfde manier als we resonanties in het soft-core πN model hebben opgenomen. Haar invloed op de totale werkzame doorsnede als functie van de vervalsbreedte hebben we onderzocht. We concluderen dat, gezien de hedendaagse verstrooiingsdata, de vervalsbreedte kleiner moet zijn dan 10 MeV.

De soft-core πN en KN modellen, waarin één-deeltje-uitwisselingen zijn opgenomen in de potentialen, zouden verbeterd kunnen worden door twee-deeltjes-uitwisselings processen toe te voegen aan de πN en KN potentialen, gelijk aan de "extended soft-core" NN en YN modellen. Ook de Coulomb wisselwerking, die in principe een rol speelt bij heel lage energieën, is hier buiten beschouwing gelaten.

Ten slotte, dit proefschrift geeft de basis voor de uitbreiding van de soft-core benadering naar de antikaon-nucleon ($\bar{K}N$) wisselwerking, en naar meson-baryon wisselwerkingen in het algemeen. Het $\bar{K}N$ systeem is op de drempel al gekoppeld aan de $\pi\Lambda$ en $\pi\Sigma$ kanalen. De gekoppelde kanalen behandeling voor dit systeem is gelijk aan dat van het YN systeem.

Curriculum Vitae

Henk Polinder werd op 29 juli 1975 geboren te Harderwijk. Na in 1994 het VWO eindexamen behaald te hebben aan het Lambert Franckens College te Elburg, begon hij aan de studie natuurkunde aan de Rijksuniversiteit Groningen. Het propedeutisch examen werd behaald op 31-08-1995. Na zijn afstudeeronderzoek onder begeleiding van Dr. R. G. E. Timmermans bij het Kernfysisich Versneller Instituut (KVI) te Groningen werd op 25-03-1999 het doctoraal examen theoretische natuurkunde afgelegd.

Van 1 mei 1999 tot 31 oktober 2003 was hij werkzaam als assistent-in-opleiding bij de afdeling Theoretische Hoge-Enegiefysica aan de Katholieke Universiteit Nijmegen. Het onderzoek dat tot dit proefschrift heeft geleid, werd verricht onder leiding van Dr. Th. A. Rijken. Tevens assisteerde hij, in het kader van zijn onderwijstaak, bij de werkcolleges van Advanced Mathematics, Quantummechanica II en Groepentheorie.